~~THE~~ ELECTRICAL PROPERTIES OF THIN METAL FILMS

by

John Garth Swanson, B.Sc.(Eng.), A.C.G.I.

A thesis submitted for the

Degree of Doctor of Philosophy

in the University of London.

Department of Electrical
Engineering,

Imperial College,

February, 1967.

ABSTRACT

A more complete understanding of conduction processes in thin metal films has become necessary owing to their use in micro-electronic circuits. Conduction in both continuous and discontinuous structures needs to be studied.

For continuous films formulae have been derived independently for the effect of surface scattering on the temperature coefficient of resistance (T.C.R.). These were found to be identical to ones derived by Savornin[55]. Several series of annealed gold films deposited on Bi_2O_3 were prepared to compare the predicted formulae with experiment. Unfortunately, these experiments were unsuccessful owing to weak binding between the Bi_2O_3 underlayer and the gold films causing agglomeration. It is thought that this was due to exposing the underlayer to air before depositing the metal films. This would be consistent with the suggestion of March[91] that free bismuth must be present to produce strong adhesion.

The theory of conduction in discontinuous thin metal films proposed by Neugebauer and Webb[19] has been amplified taking into account electron transfer between charged island species other than charged to neutral island transfers. The effect on the resistivity has been shown to be slight but the predicted values of T.C.R. agree more closely with experiment. However, exact correspondence cannot be claimed owing to the difficulties involved in measuring island

sizes and separations accurately.

Studies have been made of both continuous and discontinuous nichrome films. Work by Campbell and Hendry[42] on flash evaporated nichrome alloy films has been repeated and extended to lower preparation pressures. This has resulted in the identification of maxima in the T.C.R. of 80% Ni 20% Cr films at a thickness of $\sim$120A$^{\circ}$. This is believed to be due to an alloy segregation effect at the substrate film interface which causes the films to become nickel rich in the early stages of growth.

ACKNOWLEDGEMENTS

I would like to record my sincere appreciation for the help and encouragement throughout this research of Professor J.C. Anderson who also provided the laboratory facilities. I am particularly indebted to Mr. D.S. Campbell for his help and guidance, and especially for proposing the study of nichrome thin films.

My gratitude is due to the members of the Materials Laboratory for their cooperation, discussions and technical assistance. I would also like to thank the staff of the Engineering Workshop for their care and advice.

This work would not have been possible without the provision of a Research Studentship by the Science Research Council and a Bursary awarded by the Worshipful Company of Clothworkers, for which I am extremely grateful.

I would like to thank members of the Allen Clarke Research Centre, Caswell, for many illuminating discussions, Miss Christine Lloyd for typing this thesis and lastly, but not least, my wife for her patience and understanding.

CONTENTS

	Page
ABSTRACT	(ii)
ACKNOWLEDGEMENTS	(iv)
CHAPTER I INTRODUCTION	
1.1 Introduction	1
1.2 Early work	1
1.3 The growth of thin films	4
1.4 Studies of continuous films	7
1.5 Work on aggregated structures	10
1.6 Some applications of metal films	11
1.6.1 Heating elements	13
1.6.2 Discrete thin film resistors	14
1.6.3 Microminiaturisation	15
1.7 Thin film resistor materials	19
1.7.1 Requirements	19
1.7.2 Chromium films	20
1.7.3 Tantalum films	21
1.7.4 Cermets	22
1.7.5 Alloys	22
1.8 Review of work on nichrome thin films	23
1.9 Objects of this work	29
1.9.1 Continuous films	29
1.9.2 Discontinuous films	29

CONTENTS (Continued)

		Page
CHAPTER II	CONDUCTION MECHANISMS IN THIN METAL FILMS	
2.1	Introduction	31
2.2	Electrical conduction in bulk metals	31
2.2.1	The perfect lattice and the effects of non periodicity	31
2.2.2	The relaxation time and Matthiesen's Rule	34
2.2.3	Scattering mechanisms in real lattices	36
2.2.4	The temperature coefficient of resistivity of metals and alloys	43
2.3	Size effects	47
2.3.1	The electron mean free path	47
2.3.2	Surface scattering of electrons	47
2.3.3	Thomson's model	50
2.3.4	The Fuchs Sondheimer model	52
2.3.5	The effect of size on the temperature coefficient of resistance of a film	58
2.3.6	Discussion of mean free path effects	59
2.4	Conduction in discontinuous thin films	66
2.4.1	The conduction mechanism	66
2.4.2	A general expression for conduction through a potential barrier	70
2.4.3	Thermodynamic equilibrium	72

CONTENTS (Continued)

	Page
2.4 (continued)	
2.4.4 The four types of electron transition	74
2.4.5 The electron flux	80
2.4.6 Calculation of the sheet resistivity and T.C.R. of a discontinuous film	84
2.4.7 Real potential barriers	91
2.5 Summary	96
CHAPTER III EXPERIMENTAL APPARATUS AND TECHNIQUES	
3.1 Introduction	99
3.2 Nichrome and nickel films	99
3.2.1 Introduction	99
3.2.2 The vacuum system	101
3.2.3 The mass spectrometer	105
3.2.4 Evaporation sources	106
3.2.5 The substrate jig	113
3.2.6 Substrates	120
3.2.7 Measurements	126
3.3 Continuous gold films	137
3.3.1 Introduction	137
3.3.1.1 Method of formation	137
3.3.1.2 The preparation of the films	138
3.3.1.3 Measurements	143

CONTENTS (Continued)

	Page
CHAPTER IV EXPERIMENTS AND RESULTS	
4.1 Introduction	147
4.2 Nichrome and nickel films	147
4.2.1 Vacuum conditions	147
4.2.2 Deposition conditions	153
4.2.3 Summary of films prepared	154
4.3 Gold films	188
4.3.1 Preparation conditions	188
4.3.2 Annealing and measurement	188
CHAPTER V DISCUSSIONS AND CONCLUSIONS	
5.1 Introduction	194
5.2 Structural considerations	194
5.3 Nickel films	196
5.3.1 Films prepared at 10^{-5} torr.	196
5.3.2 Films prepared at 7×10^{-7} torr.	203
5.4 Nichrome films	207
5.4.1 Films prepared at 2×10^{-5} torr.	207
5.4.2 Films prepared at 7×10^{-7} torr.	209
5.4.3 Oxidation of nickel chromium alloys	211
5.4.4 A model of the structure of thin nichrome films	212
5.4.5 Comparison of the model with experiment	214

CONTENTS (continued)

	Page
5.4 (continued)	
5.4.6 The oxidising agent	217
5.4.7 Electron diffraction evidence	218
5.4.8 Comparison with previous work	225
5.5 Discussion of the results on gold films	230
5.6 Conclusions	234
Appendix A	237
Appendix B	240
References	244

CHAPTER 1

INTRODUCTION

1.1 Introduction

The work described in this thesis is concerned with the preparation and properties of thin metal films, mainly of michrome or gold. This first chapter is therefore devoted to a broad survey of development in the knowledge of thin film resistor properties in order to show how the aims of the present work are derived.

Early interest in thin conducting layers arose from a need for stable high resistors which were necessary to extend the measuring range of the Wheatstone bridge. Until 1900 high value resistances were made from fire clay rods dipped into sugar solution and fired at a high temperature to form a thin carbon layer. These were unstable and required frequent recalibration. Longden[1] was one of the first to prepare thin metal layers for this purpose, by sputtering bismuth and platinum films on to flat glass sheets. Thin metal films are still used today as resistive elements and conductors in microelectronic circuits.

1.2 Early Work

Though Longden was not able to measure the thickness of his thinner films directly, he obtained relative thicknesses by comparing deposition times. He noticed that by reducing the film thickness

ten times and then one hundred times he could increase the resistance from a few hundred ohms to several hundreds and then to millions of ohms. These high resistance films possessed negative temperature coefficients of resistance (T.C.R.)

At about the same time Thomson[2] proposed a "corpuscular" theory of electrical conduction in metals. He suggested that there existed within metals a gas-like assembly of particles which carried negative charges. He likened these particles to "cathode rays". They were in random thermal motion and suffered collisions with each other which limited their mean free path. An applied electric field would produce a net drift velocity in the field direction causing an observed current. This was the basis of the free electron theory.

The very sharp increase observed in film resistance as thickness decreased suggested itself to Thomson[3] as a way of determining the mean free path of electrons. He proposed that as a conductor became thinner the electrons would suffer an increased proportion of collisions with the surfaces. He related the reduced mean free path l' to the film thickness d and the bulk mean free path l and obtained:-

$$l' = d\left(\frac{3}{4} + \frac{1}{2}\log\frac{l}{d}\right) \qquad (1.1)$$

It was possible therefore to deduce l by relating the increased film resistance or l' to the film thickness.

The form of this relationship was confirmed qualitatively by Longden and Patterson using sputtered bismuth films. Whilst Thomson's

explanation accounted qualitatively at least for the increased resistivity it did not attempt to explain the accompanying negative temperature coefficients of resistance.

Two or three years later Beilby[4] and Wood[5] who were intrigued by the colours of thin films attempted to account for their anomalous optical absorption. Beilby found that colour changes occurred when gold and silver films were annealed at 300°C. Optical microscopy, x500, revealed that the film had broken up, or agglomerated, into globules. Resistance measurements on aggregated films showed them to be either open circuit or to have very high resistances. Eventually Maxwell-Garnett[6] successfully explained the anomalous absorption in terms of the aggregated structure.

In trying to account for the high resistivities and negative temperature coefficients of resistance of thin films Swann[7] (1914) independently deduced that the film structure was aggregated. He believed that films were formed by the impingement of clusters of atoms which were initially unconnected. As the film grew thicker the clusters joined to give low resistance films.

Swann sputtered platinum films and measured their electrical resistivity and temperature coefficients of resistance. He pointed out that the increased resistivity of thicker films was three or four orders of magnitude higher than Thomson's surface scattering model could account for. If Thomson's model were true, then on cooling films the sudden increase of resistivity should occur in

thicker films because of the increased electron mean free path. He found that this was not so.

Swann suggested that the clusters of atoms on the substrate were not pressed into intimate contact and only electrons which possessed more than a minimum velocity could travel from one cluster to the next. This necessary velocity depended on the closeness of packing and decreased as the film grew so that the clusters became closer. Effectively Swann suggested that conduction in an aggregated film is activated and that the activation energy decreased as the film thickness increased. In this way he qualitatively accounted for the negative temperature coefficient of resistance of thin films.

Plate 1.1 is an electron micrograph showing the stages of growth of a gold film, and it can be seen that Swann had correctly deduced the structure of thin metal films. Though his explanation has since been refined it is still essentially true.

1.3 The growth of thin films

The next stage in the understanding of thin metal films came about due to investigations of the nucleation and growth of thin deposits so as to put Swann's understanding on a less imaginative basis. Work by Wood[8] in 1915 had already shown that the probability of an impinging atom sticking to the substrate was not unity and depended on the substrate temperature. In 1924 Frenkel[9] published his classical theory of condensation and it is appropriate at this

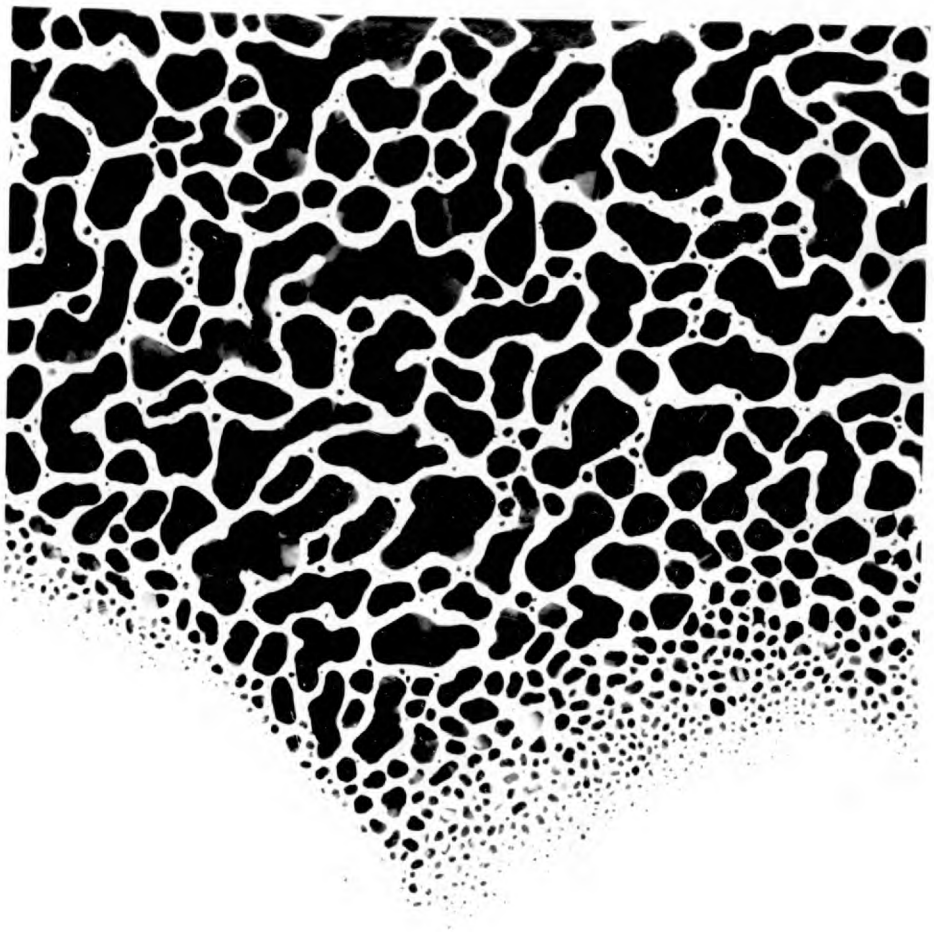

Plate(1.1)

The different stages in the growth of a thin film illustrated by a film edge

stage to describe his concepts of the growth of a thin film from a vapour.

When atoms land on a substrate they are free to move over the surface and have a finite lifetime before they re-evaporate from the substrate. This lifetime depends on the magnitude of the forces binding the atom to the substrate and on the substrate temperature. If during this period the atom collides with another condensed atom it may form a pair which has a longer lifetime because of the increased total binding energy. The pair will behave as a nucleus for other colliding atoms and this may eventually lead to the formation of large aggregates of atoms.

The free energy of a nucleus reaches a maximum at a particular radius known as the critical radius.

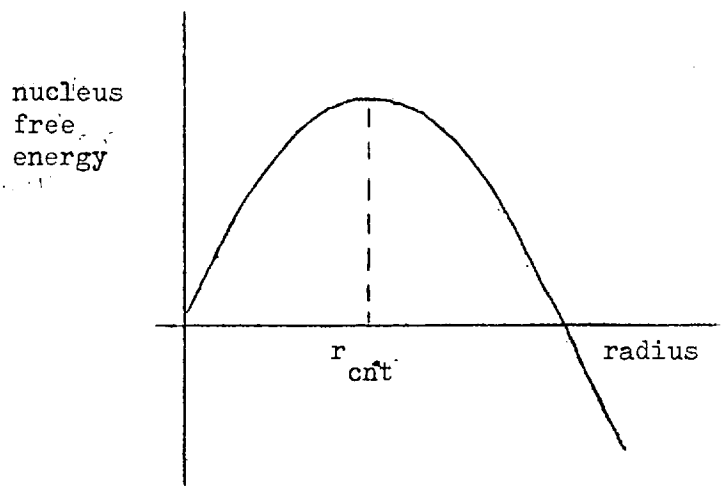

The variation of nucleus free energy with size

Below this critical size the free energy of the nucleus tends to increase as another atom impinges on it and growth is not favoured thermodynamically. Above the critical radius a decrease of free energy occurs and growth is favoured. The rate of formation of critical nuclei depends on the vapour incidence rate and on the substrate temperature. Frenkel suggested that there existed particular incidence rates and substrate temperatures below and above which nucleation would not occur; these rates and temperatures being mutually dependent. Cockcroft was one of the first to demonstrate this experimentally[10]. Since Frenkel, workers have expanded and refined nucleation theory considerably[11],[12] but without altering the basic concepts, i.e. that nucleation begins at various random points on the surface from which the growth of clusters proceeds. The clusters will eventually join and form continuous sheets. This is illustrated by plate 1.1.

1.4 Studies of continuous films

By the 1930's workers were well aware that the thinner films they studied were by no means thin plane laminae. Electron diffraction provided further evidence for this. Improved knowledge concerning the mechanisms of condensation led Lovell and Appleyard[13],[14] to take a fresh interest in the idea of surface scattering of electrons originally conceived by Thomson.

Lovell was able to prepare metal films only 40^{o}A thick which did not possess a very large resistivity due to aggregation effects.

He did this by evaporating metal onto very smooth, clean Pyrex substrates held at liquid air temperatures during deposition. The vacua he used were between 10^{-7} and 10^{-8} torr. and provided a much cleaner environment than had previously been possible using sputtering.

The surface mobility of atoms impinging on a substrate is reduced when the substrate is cooled. One can almost imagine atoms remaining at the site at which they collide with the substrate, so that a continuous film is produced using a smaller mass of condensate. By this means Lovell was able to reduce the aggregation effects experienced at normal temperatures.

Films of rubidium, potassium and caesium were prepared using this method. Alkali metals were chosen because of their simple electronic structure. A 40^{o}A film of rubidium possessed a resistivity only ten times that of the bulk material, whilst previously a similar film would have been a thousand times more resistive.

Lovell developed a simple theory of surface scattering to account for this which provided the relationship

$$l' = d\left(1 + \log \frac{l_{(\theta)}}{d}\right) \qquad (1.2)$$

where $l_{(\theta)}$ is the electron mean free path in bulk material at temperature θ. In spite of the simplicity of his theory his experimental results agreed quantitatively with this theory for films as thin as 40^{o}A. Below this thickness the deviation increased

owing to aggregation effects. This theory will be discussed in more detail in Chapter II.

In the following year Fuchs[15] published a more rigorous theory using the Boltzmann transport equation. The refinements he made were:

(i) the consideration of all the electrons at a given instant in assessing the mean free path;

(ii) the consideration of partially elastic surface scattering.

The exact relationship is complicated, (see Chapter II); however, approximations have been made by Sondheimer[16] in his review entitled "The mean free path of electrons in metals". These are:

$$l' = \frac{l_o}{1 + \frac{3}{8}\frac{l}{d}(1 - p)} \qquad \frac{d}{l} \gg 1 \qquad (1.3)$$

$$l' = \frac{3}{4}\frac{l_o (1 + p)}{(1 - p)}\frac{d}{l}\log\left(\frac{l}{d}\right) \qquad \frac{d}{l} \ll 1 \qquad (1.4)$$

where p is the proportion of elastic reflections at the film surface. Using essentially the same approach as Fuchs, Lucas[17] considered the case of a film having different surface "roughnesses". He assumed a proportion p of specular reflections with one surface and q with the other and computed the effect on the resistivity for various combinations of p and q.

1.5 Work on aggregated structures

The results of studies of discontinuous thin films before 1951 have been reviewed by Mostevich and Vodar[18]. Experiments had shown an exponential dependence of conductivity on temperature from which activation energies of conduction could be deduced. In general these decreased as the film thickness increased. Workers were not able to account for this behaviour quantitatively but suggested that the electrons were excited over the potential barriers between the aggregates. This, however, did not explain the discrepance between the measured activation energies of $\sim$ 0.02eV and the values of $\sim$4eV due to the work function of the metal.

Neugebauer and Webb[19](1962) performed similar experiments and were able to relate the activation energies observed to the aggregate dimensions. It was concluded that the energy required was equal to the energy necessary to charge an aggregate, i.e. to free an electron for conduction. This assumed that the electrons were only partially activated over the potential barrier between the islands of metal and conduction proceeded by quantum mechanical tunnelling through the remaining barrier.

In the following year, Hartman[20] developed an idea suggested by Mostevich and Vodar that the electron states within the metal aggregates were quantised owing to their atomic dimensions. This led to energy level separations being dependent on the island dimensions. He proposed that it might be necessary for electrons to

be excited into adjacent levels for tunnelling to occur; this was likely because tunnelling can only occur between states having the same energy. In this way he was able to relate the island diameters to the observed activation energies using the data of heugebauer and Webb.

More recently, Hill[21] has suggested that transport occurs via electron states in the substrate and not through the intermediate vacuum space. A similar process has been described by Hermann and Rhodin who have also noted the dependence of activation energies on island size. They have likened this process to impurity band conduction in semiconductors.

In summary, two types of conduction process have been established:

(i) conduction in continuous lamellae;

(ii) conduction in discontinuous aggregated films.

Their regions of influence are illustrated in Fig. 1.1. These mechanisms are considered in more detail in Chapter II.

1.6 Some applications of metal films

Until the Second World War most work on thin metal films had been performed to gain fundamental knowledge concerning electrical conduction in metals. Thin films provided a means of studying processes in bulk materials. The increase in scientific activity associated with the war produced practical applications for metal films. Since then interest has been mainly technological. The

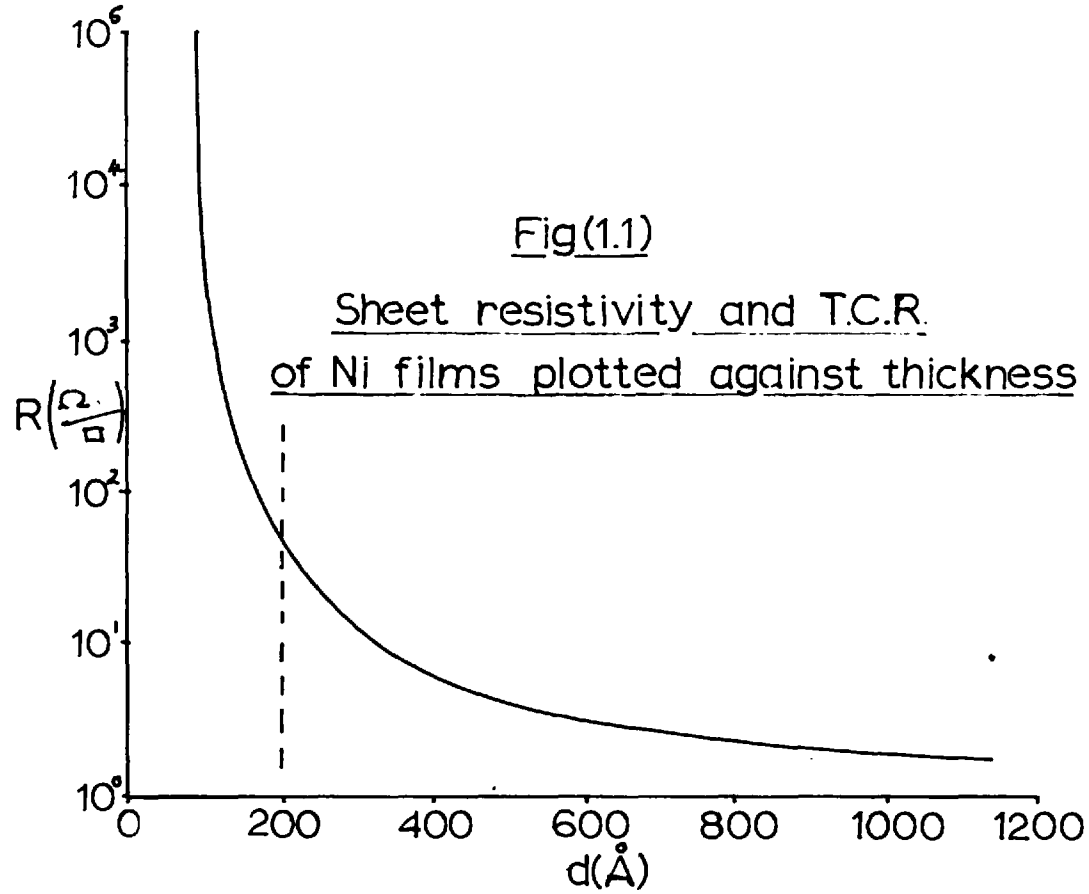

Fig(1.1)

Sheet resistivity and T.C.R. of Ni films plotted against thickness

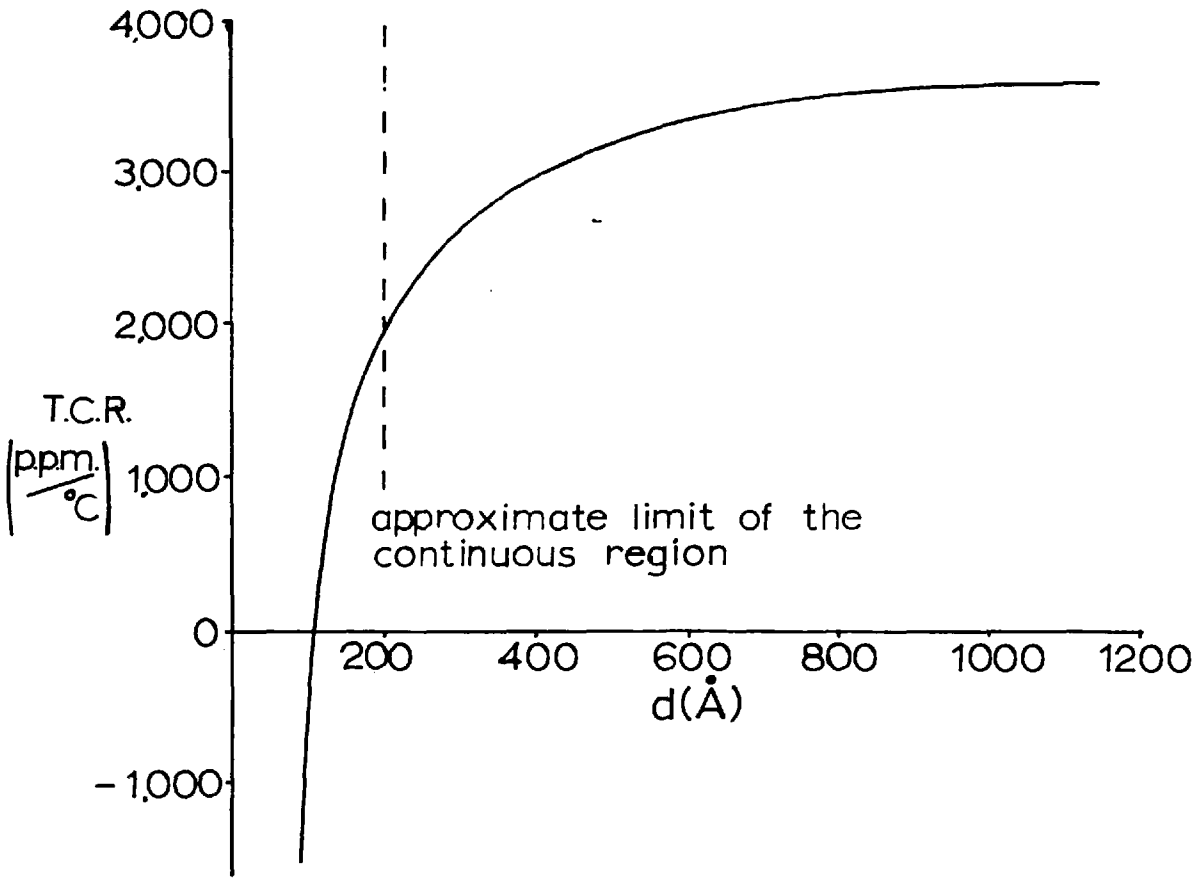

improvements in the understanding of conduction processes in metal films which have occurred since then have arisen from the constant desire to produce better devices. This section will describe some of the more important applications of the metal films.

1.6.1 Heating elements

Icing up of windscreens was a problem which accompanied the development of aircraft which flew at high altitudes. In the early 1950's several workers[23,24,25] investigated the use of thin films as windscreen heating elements. The requirements were:

(i) optical transmission of at least 75%;

(ii) power dissipation of 1 KW./sq.ft.;

(iii) a sheet resistivity to give a heater which could be driven from low tension voltage supplies used in aeroplanes.

Requirements (i) and (ii) conflicted because gold films evaporated onto glass which were transparent enough possessed a sheet resistivity of several thousand ohms per square. A value of $10\Omega/\square$ was considered acceptable. The problem of preparing thin continuous films was the problem Lovell had solved by growing the films on low temperature substrates.

Another means of reducing the mobility of the condensing atoms was required which gave structurally stable films on heating.

The solution was discovered by Preston and Gillham[23]. They

suggested that the thin film heater should be condensed onto a substrate which exhibited a high binding energy between the film atoms and the substrate. This could be achieved by coating the glass first with an oxide layer. Several materials were tried including cadmium oxide, zinc oxide and bismuth oxide. The material most frequently used is bismuth oxide which is prepared by sputtering. Extremely low resistivities could be achieved by putting another layer of bismuth oxide on top of the gold and annealing to about 400°C. This annealed out imperfections and improved the smoothness of the gold film. Preston and Gilham deduced that approximately 90% of electron collisions with surfaces of thin film were elastic, i.e. $p = 0.9$. In films prepared without these precautions p is usually in the range 0.1 to zero. In this application the temperature coefficient of resistivity was of little importance.

1.6.2 Discrete thin film resistors

Discrete thin film resistors have been available for several years. They can take the form of a ceramic cylinder coated with a thin metal layer. The wire terminations are usually soldered to the metallised ends of the cylinder. In order to obtain high values of resistance it is necessary to increase the film length by cutting spiral grooves in the cylinder to produce a spiralled track. This also provides a means of accurately trimming the resistance to a desired value and resistors of this kind are available commercially.

It is possible to achieve resistance values between 1 Ω and 2MΩ with a tolerance of $\pm$ 0.1% and a T.C.R. of less than $\pm$ 150 p.p.m./^{o}C.

1.6.3 Microminiaturisation

(a) Thin film circuits

In large complex electronic systems reliability is extremely important. Studies have shown that very often the weakest points in a circuit, both electrically and mechanically, are the interconnections between components. This led to the development of thin film microelectronic circuits in which there are very few discrete components.

Resistors and capacitors can be formed by depositing layers of metals and dielectric materials through accurately shaped masks. The circuit interconnections are made by using thicker overlapping films formed in another deposition process. This method of fabricating microelectronic circuits has various disadvantages. The main one is that it is not easy to make thin film active devices which are reliable, cheap, easy to make and reproducible. It has been necessary to attach individual silicon chip transistors to the main circuit, so introducing unwanted connections. Also, geometrical reasons preclude the formation of inductors of more than a few microhenries. To some extent this difficulty has been avoided by ingenious circuit design though this difficulty will always be present in microelectronic techniques. Thin film circuits are usually produced on substrate panels which are

stacked close to each other in the final assembly. The panel interconnections have to be made by conventional means.

(b) Semiconductor integrated circuitry

It is useful here to describe another means of making microelectronic circuits which has been developed concurrently with the thin film approach. A wafer of single crystal silicon approximately 0.006" thick forms the starting point in the fabrication of this kind of circuit. An epitaxial film about 15μ thick having a controlled resistivity is then grown onto this. It is then possible to locally diffuse p or n type impurities into it by etching "windows" in a protective silicon oxide layer, which can be formed by thermal oxidation of the silicon. The windows are etched selectively using a photo resist technique. By successive oxidation, etching and diffusing processes pn, pnp, or pnpn structures can be formed.

In one production cycle as many as a thousand identical circuits can be produced on each wafer of silicon which is finally diced and encapsulated. As far as component interconnections are concerned, this kind of circuit is inherently more reliable because of the greater number of circuit functions per module which itself is more rugged than a thin film circuit. The main advantage of this technique is that it overcomes the problem of using discrete active devices as in thin film circuits.

Resistors can be formed by diffusing in impurities to produce a given resistivity semiconducting path, its geometry being con-

trolled by the oxide etch technique. In this process, the host silicon chip has been doped with an opposite type of impurity to form the resistor so forming a pn junction. One important consideration is that the resistor potential must be maintained so as to reverse bias the junction to provide isolation between the resistor and the rest of the circuit. Capacitors can be formed too by employing reverse biased pn junctions to store charge, this has the disadvantage of producing a voltage dependent capacitance. However, this can be put to good use if a variable capacitor is required in the circuit. Clearly when components are formed using these techniques it becomes difficult to isolate resistance and capacitance.

(c) Comparison of diffused and thin film resistive elements

The main disadvantage of the diffused type of resistor used in integrated circuits is its large temperature coefficient of resistance. In heavily doped semiconductors the change of resistance with temperature is mainly due to a change of carrier mobility associated with lattice scattering. This produces values of T.C.R. in the range + 1000 to + 5000 p.p.m./^{o}C. These are much greater than values for thin film resistors which are typically less than + 100 p.p.m./^{o}C, In some applications this disadvantage can be circumvented by designing circuits to depend on the ratios of values rather than absolute values.

The maximum sheet resistivity that can be achieved with diffused resistors is about 200$\Omega/\square$ In practice line widths of 0.001" can

be formed with an accuracy of $\pm$ 10% and with great care $\pm$ 5% is possible. Since the linear dimensions of the silicon circuit fix the maximum length of a resistor at around 0.1" aspect ratios are limited to approximately 100:1. These factors limit the maximum possible value of resistance to about 50,000Ω. This range of resistance is suitable for most digital transistor circuits but linear circuits often require values in the region of one megohm.

The tolerance of a diffused resistor is governed by the geometrical tolerance and the accuracy of the diffusion process. Unlike thin film resistors their value cannot be adjusted after formation. Practical tolerances are between 15 and 20% compared with 0.1% for thin film elements after adjustment.

Another disadvantage of diffused resistors is the shunt capacitance of the element which is an order of magnitude greater than that of a comparable thin film resistor. This arises because of the relatively large volume which a diffused element occupies.

In practice, an attractive feature of the thin film element is that they can be employed with semiconductor integrated circuits. This is possible by either direct deposition onto the silicon surface or by attaching the integrated circuit modules to substrates carrying the precision thin film components. Various combinations of these techniques are employed to form circuits known as "hybrids".

1.7 Thin film resistor materials

Thin metal films are thus used for separate resistors and for resistive elements in thin film circuits, often in various forms of hybrid circuits. This section will go on to consider the materials which are used to fabricate them.

1.7.1 Requirements

The main requirements of a resistor are that its value should be stable with temperature and time. It is therefore necessary for the resistor material to possess a low temperature coefficient of resistance and to be structurally and chemically stable.

The familiar plot of film resistance against thickness exhibits a very sharp rise in resistance when the thickness is small (see Fig. 1.1.) In this region small changes of thickness produce large resistance changes owing to the agglomerated nature of the film. It is undesirable to use films with this structure because of their greater sensitivity to oxidation and structural change. For the same reason it is very difficult to manufacture films having reproducible electrical properties in this region. These factors make it desirable to use films with a continuous structure which unfortunately exhibits a low resistance. In order to produce a high resistance, a high resistivity material must be chosen which possesses a low atomic surface mobility enabling continuous structures to be attained in thinner films. It has been shown[26] that atoms of high melting

point metals lose their energy and come to equilibrium with the substrate faster than atoms of lower melting point materials. This leads to the formation of continuous films sooner in the deposition process. This implies that resistor materials should possess high melting points. Other desirable features are good adhesion to the substrate and ease of evaporation.

1.7.2 Chromium films

Chromium is often used because it readily forms a protecting oxide layer which renders it structurally stable after annealing and provides strong adhesion to the substrate.

Various workers[27,28,29] have demonstrated the dependence of the electrical properties of chromium films on the preparation conditions. Recent work by Gould[30] attempted to correlate the observed film structure with measurements of film density, impurities and residual gas present during deposition. It was concluded that the films consist of grains of relatively pure chromium with impurities at their boundaries and that the resistive properties of these films depend on the grain size and impurity content of the films. Chapman[29] states that it is possible to produce resistors having sheet resistivities in the range 300 to 600$\Omega/\square$ and temperature coefficients between -5 and -300 p.p.m./^{o}C. Though chromium possesses many attractive features as a resistor material its sensitivity to the deposition conditions detracts from its widespread use.

1.7.3 Tantalum films

A great deal of effort has been devoted to the study of tantalum as a suitable material. It is possible to deposit tantalum films by sputtering and then anodise the surface to form a tantalum oxide dielectric layer. By depositing another layer of tantalum on top it is possible to form capacitors. Since the thickness of the dielectric can be controlled accurately by the anodising voltage, this is a very attractive way of making thin film circuits[31]. Another advantage is the ability to adjust the thickness of the tantalum resistor elements by anodisation. The oxide layer produced also serves as a protective layer for the resistor.

When tantalum is sputtered in pure argon[32] the films have a resistivity only three or four times that of bulk tantalum and a temperature coefficient of about 1000 p.p.m./^{o}C. Gerstenberg and Calbick[33] have shown that resistivities can be increased by an order of magnitude by introducing small amounts of nitrogen, oxygen or methane during the sputtering process. These films then include the nitrides, oxides and carbides of tantalum as impurities. Reactive sputtering is now used to produce tantalum nitride resistors having temperature coefficients of resistance in the range + 300 to - 300 p.p.m./^{o}C and sheet resistivities in the region of 200$\Omega/\square$. Tantalum is probably the most popular material employed in the production of thin film resistors in circuits.

1.7.4 Cermets

It is apparent from the two previous examples that the most useful electrical characteristics are achieved by the addition of impurities to an initially pure metal. An extension of this process has been to evaporate mixtures of metals and dielectric or semi-conducting materials thus producing films known as cermets.

A popular combination is a mixture of chromium and silicon monoxide. The proportions of the mixture and the deposition conditions are often impirically derived and not widely known. Himes, Stout and Thun[34] have produced resistors with sheet resistivities in the region of 600$\Omega/\square$ and temperature coefficients around - 100 p.p.m./^{o}C. The composition they used was 65% Cr and 35% SiO. The conduction mechanisms in cermets are poorly understood and are currently being investigated.

1.7.5 Alloys

The high resistivities and low temperature coefficients of resistivity of alloys are well known and have led to their use as resistance wires and heating elements. Alloys were one of the first kinds of material used to make thin film resistors. Some alloys which have been investigated are:-

(i) nickel-chromium - various compositions;

(ii) stainless steels containing 8% Ni and 18% Cr;

(iii) chromium 24% - silicon 76%;

(iv) chromium - titanium, nitrided in ammonia.

Much of the work on alloy films suffers from the disproportionation of the components during deposition owing to their different vapour pressures. As a consequence of this, work has tended to be empirical. The presence of chromium in each of these examples seems significant, although this is never explained. It is probable that chromium increases the adhesion of the film to the substrate and stabilises the film by the formation of chromium oxide which diffuses to grain boundaries and inhibits further oxidation.

One of the aims of this work is to provide a better understanding of conduction processes in nichrome thin films. The next section will review work on nichrome thin films and explain the nature of the work described in this thesis.

1.8 Review of work on nichrome thin films

The earliest studies of nichrome thin films arose from their use as waveguide attenuator vanes. Following earlier work by Siddall[35] and Holland[36] the first publication concerning nichrome thin film resistors was by Alderson and Ashworth[37] in 1957. Films were condensed onto boresilicate glass substrates at 350°C in a vacuum better than 10^{-4} torr. The composition of the alloy which was evaporated from a tungsten boat was 80% Ni and 20% Cr. This composition is commonly used for resistance wire and is known as Nichrome V.

The most significant result to emerge from this work was that

the film composition depended on the source temperature. Their curve illustrating this is shown in Fig. 1.2. This behaviour is obviously due to the higher vapour pressure of chromium. The ratio of evaporation rates of the constituents of a binary alloy is given by

$$\frac{E_1}{E_2} = \frac{W_1 P_1 M_2^{\frac{1}{2}}}{W_2 P_2 M_1^{\frac{1}{2}}} \qquad (1.5)$$

where P is the vapour pressure of the pure substance, M its molecular weight and W its concentration by weight. This means that at 1200°C the evaporation rate of chromium is seventy five times that of nickel using an 80/20 nichrome alloy. In practice chromium evaporates from the surface first, leaving a nickel rich region causing the evaporation rate of nickel to increase. Eventually, owing to diffusion, a dynamic equilibrium occurs at a particular temperature producing a vapour composition which depends on the source temperature and the geometry of the alloy specimen. The analysis of this problem is complicated and has been computed by Huijer et al.[38]. Alderson and Ashworth produced films with a composition approaching the starting composition by using a source temperature greater than 1600°C. These films exhibited temperature coefficients of resistance between 100 and 200 p.p.m./°C which depended on the composition and the film thickness.

In an attempt to eliminate source contamination, Lakshmanan[39]

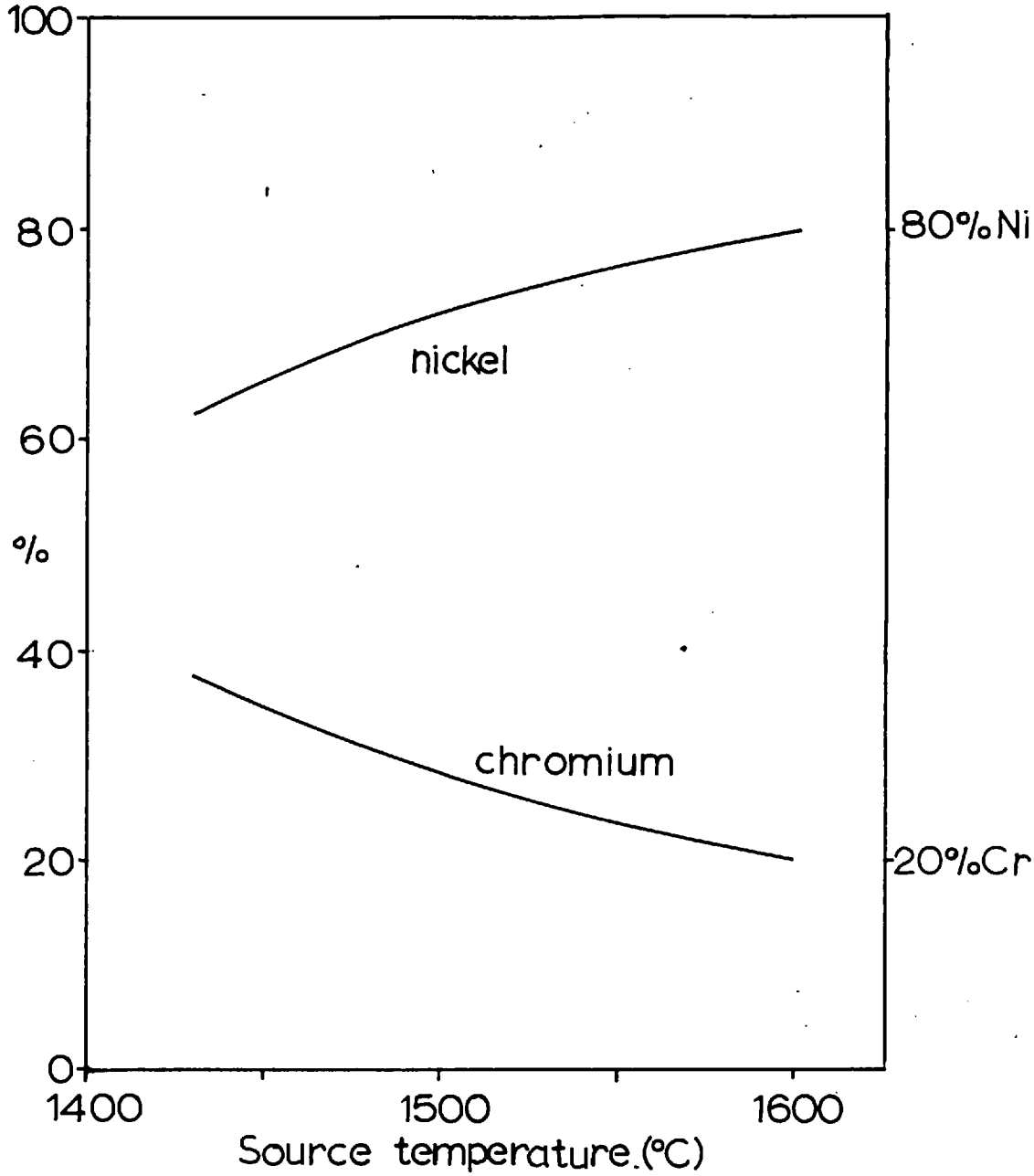

Fig (1.2) Alloy composition versus source temperature

sublimed nichrome from wires of different compositions. By using an X-ray fluorescence technique, he was able to determine the composition of films produced by successive sublimations from the same wire. The initial sublimations produced chromium rich films which became increasingly nickel rich as the chromium was consumed. Though a graph of temperature coefficient plotted against sheet resistivity is given, it is not meaningful because of the varying compositions of the films he considered.

Siddall and Probyn[40] used an electron bombardment technique to prepare nichrome films. This involved the evaporation of an 80/20 nichrome wire which was continuously fed onto the hearth of an electron bombardment furnace. These depositions were performed using a vacuum of 5×10^{-4} torr. These workers found that the lowest values of T.C.R. were achieved under conditions favouring the oxidation of the films. It is known that the oxides of nickel and chromium are both defect semiconductors[41]. The films which were deposited at higher rates possessed increasingly positive temperature coefficients reaching a maximum at a particular rate. This was explained by assuming that by increasing the rate of deposition less oxidation occurred and the deposit became more metallic. In order to increase the deposition rate it was necessary to increase the furnace temperature inevitably leading to a change in vapour composition. It was suggested this might have accounted for the maximum observed.

Disproportionation effects have tended to confuse the results of the work on alloy films of various kinds. By using the flash evaporation technique, Campbell and Hendry[42] have been able to prepare films of constant composition accurate to within $\pm$ 1% of the starting composition. This technique will be described in more detail later. These evaporations were carried out in a vacuum of 5×10^{-5} torr. The interesting features of their work are illustrated by the graph in Fig. 1.3.

Both high nickel and high chromium content films exhibited increasing temperature coefficients as the film thickness increased. This behaviour was reversed for films having the composition 80% Ni and 20% Cr. When the chromium content was increased to 55% the T.C.R. was almost independent of thickness. A further increase in chromium content to 57% led to an abrupt return to the behaviour exhibited by high chromium content films.

In an earlier study of nichrome films Blackburn, Bicknell, Campbell and Stirland[43] showed that in the thickness range under consideration the films possessed an island structure connected by an amorphous chromium-oxygen phase[44]. It has been suggested that the unusual behaviour of 80/20 nichrome films is due to this skin. In thin films the greater temperature coefficient is thought to be caused by a variation of the height of the intergranular potential barrier with temperature. When the thickness is greater the crystallites touch and the effect diminishes leading to a decrease

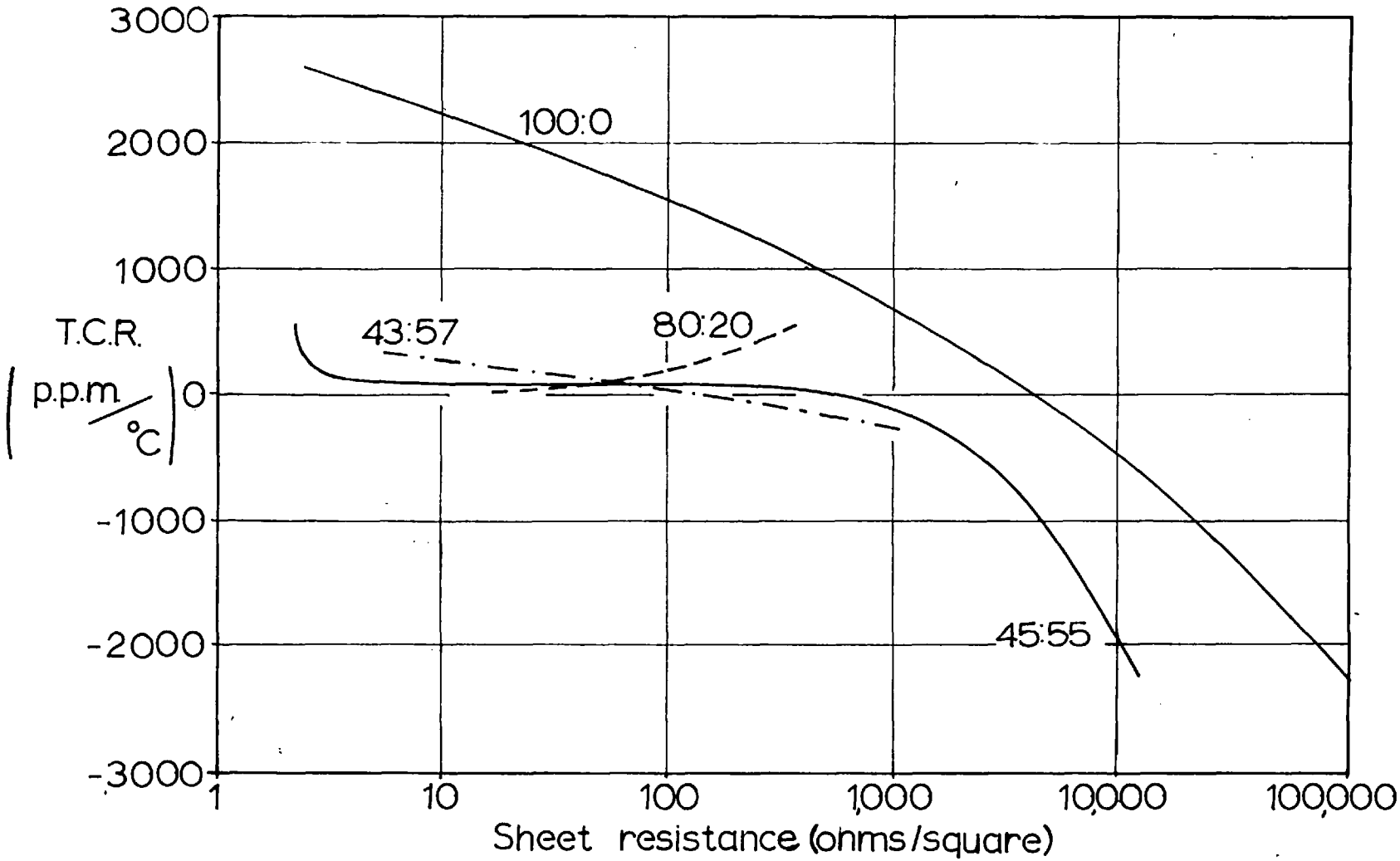

Fig (1.3) T.C.R. v Sheet resistance for various NiCr compositions

of the temperature coefficient of resistance.

When the chromium content is increased to 55% it seems likely that sufficient chromium is oxidised for the film to consist of a uniform matrix of metal and oxide, rather like a cermet film. This would mean that the same conduction processes operate in thin films as for thicker ones. If this were the case, the T.C.R. could be independent of thickness.

The behaviour of films with higher chromium contents is complicated by the existence of a phase change. The chromium content at which this occurs is not necessarily that of the bulk material but is probably modified by the consumption of chromium as an oxide.

1.9 Objects of this work

1.9.1 Continuous films

Very little work has been done on the influence of surface scattering in continuous films on their temperature coefficient of resistance. This work will develop formulae relating the temperature coefficient of a thin film with that of the bulk material. Experiments on gold films will enable a comparison to be made of electron mean free paths deduced from resistance and temperature coefficient measurements.

1.9.2 Discontinuous films

Though the results of Campbell et al. on nichrome films are

complicated by the formation of oxides they are valuable because the alloy compositions were preserved. It has therefore been considered useful to use this deposition technique to repeat this work at 10^{-5} torr. and then to extend it to superior vacuum conditions which minimise the effects of oxidation.

CHAPTER II

CONDUCTION MECHANISMS IN THIN METAL FILMS

2.1 Introduction

In Chapter I the stages in the growth of a thin film were described and it was shown that as far as the electrical properties of films are concerned they can be classified as either continuous or discontinuous. The conduction processes described briefly then will now be treated more fully and related to conduction in bulk metals. This chapter will first consider electrical conductivity in bulk metals and then take into account processes which occur as a film becomes thinner and eventually discontinuous.

2.2 Electrical conduction in bulk metals

2.2.1 The perfect lattice and the effects of non-periodicity

A crystal is a three dimensional lattice of atoms having a regular geometrical structure. This lattice has associated with it an electrostatic field which possesses the periodicity of the lattice. According to the wave mechanical theory of electrons an electron can be regarded as a wave which satisfies the Schrodinger wave equation in a given potential field. Bloch[45] has shown that when an electron passes through a periodic potential it does so without loss of energy

i.e. without being scattered. Only when the periodicity of the potential field is disturbed does the electron experience any resistance to its motion. This phenomenon is quite general for waves of other types propagating through periodic structures (46).

In an insulator the highest band of allowed energy states is full and it follows from the Pauli Exclusion Principle that when electrons are scattered they can only interchange energy states. This means that there cannot be a net increase of energy or momentum when an electric field is applied. On the other hand, in a metal the highest band of energy states is only partially full. In this case scattered electrons can move into the un-occupied states and produce an overall component of momentum in the field direction. This is illustrated by the equivalent energy level and Brillouin zone diagrams for metals and insulators, see Figs. 2.1 and 2.2. The Brillouin zone diagram shows how the electron distribution is shifted in momentum space under the action of a field; this is clearly not possible when the band of states is full as in an insulator.

When an electric field is applied to a metal crystal with a periodic lattice the energy of a conduction electron will increase steadily by taking energy from the electric field until its wavelength is such that it interferes with the lattice and it suffers an elastic reflection. At this stage its energy is limited to that of the upper edge of the energy band which contains it. In most metals these energy

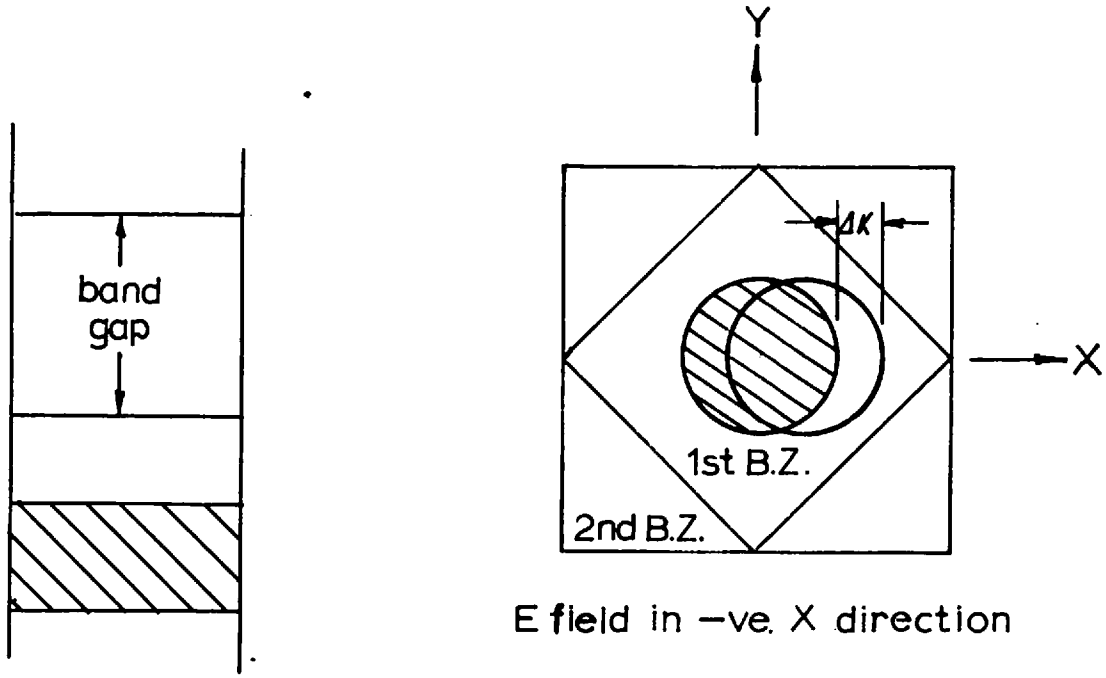

Fig (2.1) Equivalent energy band and B.Z. diagrams for a metal

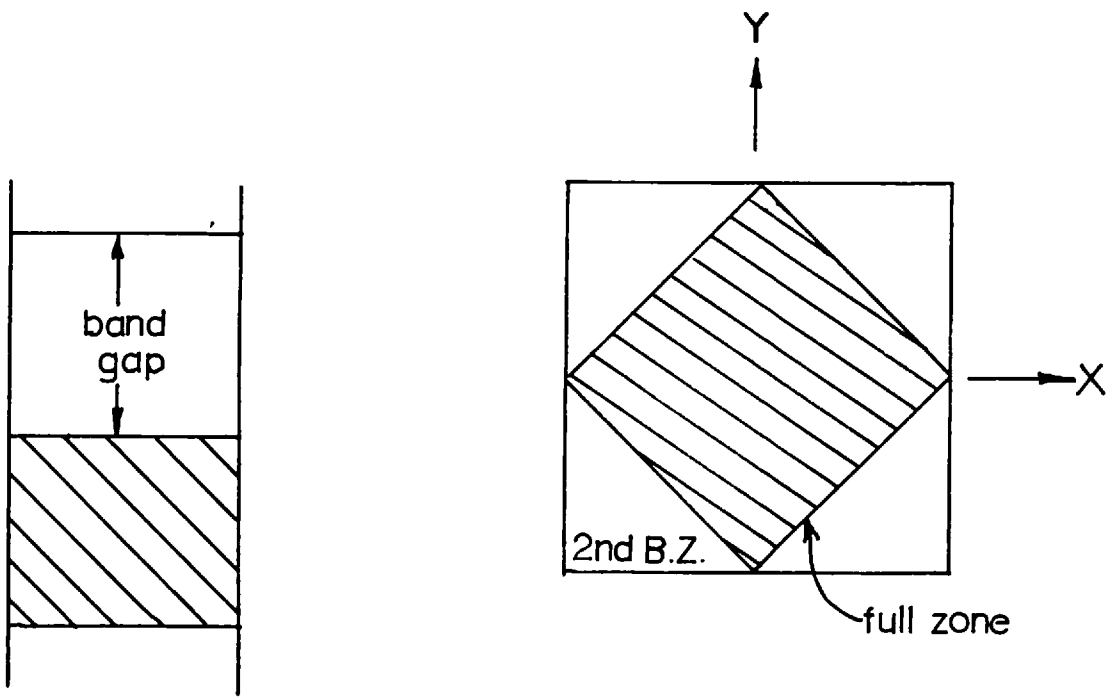

Fig (2.2) Equivalent energy band and B.Z. diagrams for an insulator

bands overlap and this limit is not imposed, however in practice electrons are scattered by deviations from the periodicity of the potential and lose their energy to the lattice before elastic reflections become possible.

2.2.2. The relaxation time and Matthiesens Rule

It is convenient to define a time τ which is the average time during which an electron can gain energy from the electric field before losing this energy to the lattice by means of a scattering process. After each scattering event the electron loses its momentum in the field direction. In classical terms τ is the time between scattering events or in statistical terms, it is the time taken for the electron-lattice system to reach equilibrium when the field is removed, i.e. the relaxation time.

In a single carrier system the electrical conductivity is given by

$$\sigma = Ne\mu$$

N is the effective number of conduction electrons per unit volume. Since only electrons near to the Fermi surface can be scattered into vacant states the number of electrons which contribute to conduction is limited and is usually equivalent to one electron per atom. These electrons move with the Fermi velocity V_F which is much greater than the drift velocity V_D superimposed on this motion by the electric field. The electron mobility μ is defined as the increase in drift velocity per

unit electric field.

The force on an electron due to an electric field E is Ee

$$\therefore \quad Ee = m\frac{dV}{dt}$$

An electron acquires an average velocity V_D between collisions

$$\therefore \quad Ee = m\left(\frac{V_d}{\bar{\tau}}\right)$$

but

$$\frac{V_d}{E} = \mu$$

hence $$\mu = \frac{e\bar{\tau}}{m}$$

and

$$\therefore \quad \sigma = Ne.\frac{e\bar{\tau}}{m} = \frac{Ne^2\bar{\tau}}{m}$$

$$\text{or } \rho = \frac{m}{Ne^2}\cdot\frac{1}{\bar{\tau}}$$

In practice, the lattice potential is disturbed by various mechanisms which will be described later in this section. It is possible to assign a relaxation time to each process and one can think of $\frac{1}{\tau_i}$ as being the frequency of scattering events due to process i. Applying the Principle of Superposition

$$\frac{1}{\bar{\tau}} = \sum_{i=1}^{n}\frac{1}{\tau_i} = \text{the net probability of scattering.}$$

Clearly

$$\rho = \frac{m}{Ne^2}\sum_{i=1}^{n}\frac{1}{\tau_i}$$

$$= \sum_{i=1}^{n}\rho_i$$

This is known as Matthiesens[47] Rule and simply states that the resistivity contributions due to different mechanisms are additive. This applies in practice so long as the effective number of free electrons is not changed by these scattering mechanisms and that the vibrational spectrum of the lattice is undisturbed.

2.2.3 Scattering mechanisms in real lattices.

In real crystal lattices deviations from the periodicity of the potential field occur which are due to the following phenomena.

(a) lattice vibrations

(b) structural imperfections

(c) impurity scattering

Since the mechanisms (b) and (c) are virtually independent of temperature and remain at low temperatures when lattice vibrations have disappeared their combined effect is often termed the residual resistance. Thus

$$\rho = \rho(T) + \rho_{residual}$$

This section will consider each mechanism in turn.

(a) Lattice vibrations

An atomic lattice can be regarded as an arrangement of masses coupled by springs which represent the interatomic forces. Thus when an atom is displaced from its equilibrium position it is acted on by restoring forces. So long as the displacements are small the vibrations

can be considered simple harmonic. It is these vibrations which contain the thermal energy of the lattice.

In the Einstein model the vibrations of each atom are assumed to be independent of the others and all of the same frequency, often called the Einstein frequency. The quantum mechanical solution of a harmonic oscillator reveals that the energy of the oscillator is quantised. At any given temperature the proportion of modes having a particular energy is given by Maxwell-Bol^{+}zmann statistics. This leads to the result that the average energy of an oscillator is given by

$$\epsilon = \frac{h\nu_E}{e^{\frac{h\nu_E}{KT}} - 1}$$

at temperatures greater than T_E where

$$h\nu_E = KT_E$$

ϵ approximates to KT and the system behaves classically. T_E is known as the Einstein temperature and is a characteristic of each metal. Typical values are given in Table (2.2). See Page 46.

A more exact model is the Debye model which postulates that the vibrations are coupled and form a frequency spectrum of the form

$$dN = a\nu^2 \, d\nu$$

where dN is the number of modes in the frequency range ν to $\nu + d\nu$. The spectrum has a maximum frequency ν_D, the Debye frequency, which defines a characteristic temperature, the Debye temperature θ. Like the Einstein model it yields the result that the average energy of an

oscillating mode is proportional to the absolute temperature, above the Debye temperature. For the present purpose the simpler Einstein model will be employed since the only serious discrepancy occurs at low temperatures. However, it is the Debye temperature which is most frequently quoted in the literature, and in general

$$T_E \sim {}^3/_4\theta \quad .$$

The temperature dependence of lattice scattering can now be deduced using a simple classical model.

If the restoring force on a displaced atom is - bX where b is a constant, its equation of motion is

$$M\ddot{X} + bX = 0.$$

$$\therefore \quad \frac{b}{M} = 4\pi^2 \nu_E^2$$

It has been shown that above the Einstein temperature the average energy per mode is KT, therefore the average potential energy of the vibration is $\frac{KT}{2}$.

hence $\quad \frac{1}{2} b\bar{X}^2 = \frac{KT}{2}$.

where $\bar{X}^2$ is the mean square atomic displacement.

The probability of an electron being scattered is proportional to the scattering cross section $\bar{X}^2$.

but $\quad \bar{X}^2 = \frac{KT}{b} = \frac{KT}{4\pi^2 \nu_E^2 M}$

$$\therefore \quad \bar{X}^2 = T \cdot \frac{h^2}{4\pi^2 K T_E^2}$$

Thus the lattice scattering of electrons is proportional to the absolute temperature above the Einstein temperature.

An empirical relationship between the lattice component of resistivity and absolute temperature has been derived by Gruneisen and is of the form

$$\rho = \frac{4AT^5}{\theta^4} \int_0^{\theta/T} \frac{\xi^5 d\xi}{(e^{\xi}-1)(1-e^{-\xi})}$$

which yields $\rho \propto T^5$ when $T < \theta$

and $\rho \propto T$ when $T > \theta$

In fact, Wilson[48] states that $\rho \propto T$ when $T \gg 0.2\ \theta_D$.

In pure metals the major component of resistivity at room temperature is due to lattice vibrations and is of the order of $5\mu\Omega$.cm. Temperature coefficients of resistance are usually several thousand parts per million per ^{o}C. Where α has the usual form $\frac{1}{\rho} \cdot \frac{d\rho}{dT}$.

(b) Structural imperfections

Thermodynamically one expects imperfections in an otherwise perfect lattice in equilibrium at some finite temperature. The number of a particular kind of defect will depend on its energy of formation, the absolute temperature and the mechanical history of the specimen. They can be of several types.

(i) point defects; caused by the misplacement of an atom producing a vacancy or an extra atom located at a lattice interstice.

(ii) dislocations; these are formed by a lattice plane which is terminated within the lattice and produces an extra half plane of atoms. This sometimes gives rise to 2 partial dislocations and a stacking fault in which lattice planes slide over one another to reduce the misfit.

(iii) grain boundaries; these occur at the surfaces of individual crystallites and result in a misorientation of the lattice.

Owing to the difficulties in counting defects and performing controlled experiments to produce them, there is considerable uncertainty about their contribution to electrical resistivity. Table 2.1 summarises the kinds of defects occurring in metals, their resistivities and likely concentrations in thin films.

TABLE 2.1

Resistivities of defects and their concentrations in thin films[49][50]

Type	Resistivity	Concentration
Vacancies	1-6$\mu\Omega$.cm/atomic %	0.01%
Interstitials	1-6$\mu\Omega$ cm/atomic %	Very small
Dislocations	1-20 x 10^{-14}N$\mu\Omega$.cm	N = 10^{13}/cm^2
Stacking faults	5 x $10^{-7}\beta$ $\mu\Omega$.cm	β = 10^5/cm.

The components of resistivity due to imperfections are virtually constant with temperature providing that

(i) the temperature excursion is not sufficient to alter the defect density;

(ii) the vibrational spectrum of the lattice is unchanged by the presence of defects.

In practice for changes of temperature less than 100°C these assumptions hold since the rates of formation of defects in a metal near to thermal equilibrium are small.

(c) Impurity scattering

When foreign atoms are included in a metal lattice, the potential field is disturbed by both the deformation of the lattice due to the different size of the impurity atom and by the field arising from the different valence of the impurity. In general, the latter effect is greater.

Linde[51] has derived a numerical relationship

$$\rho \propto Z^2$$

between the increase in resistance associated with an impurity atom and its valence, for noble metal solvents. Z is the difference in the number of electrons outside the closed d shells of solvent and impurity atoms. In practice, one has to correct for the screening effect of the electrons. This phenomenon has been demonstrated by Linde. See Fig. (2.3).

The composition dependence of the resistivity of binary alloys is described by Nordheim's[52] Rule. It states that the residual

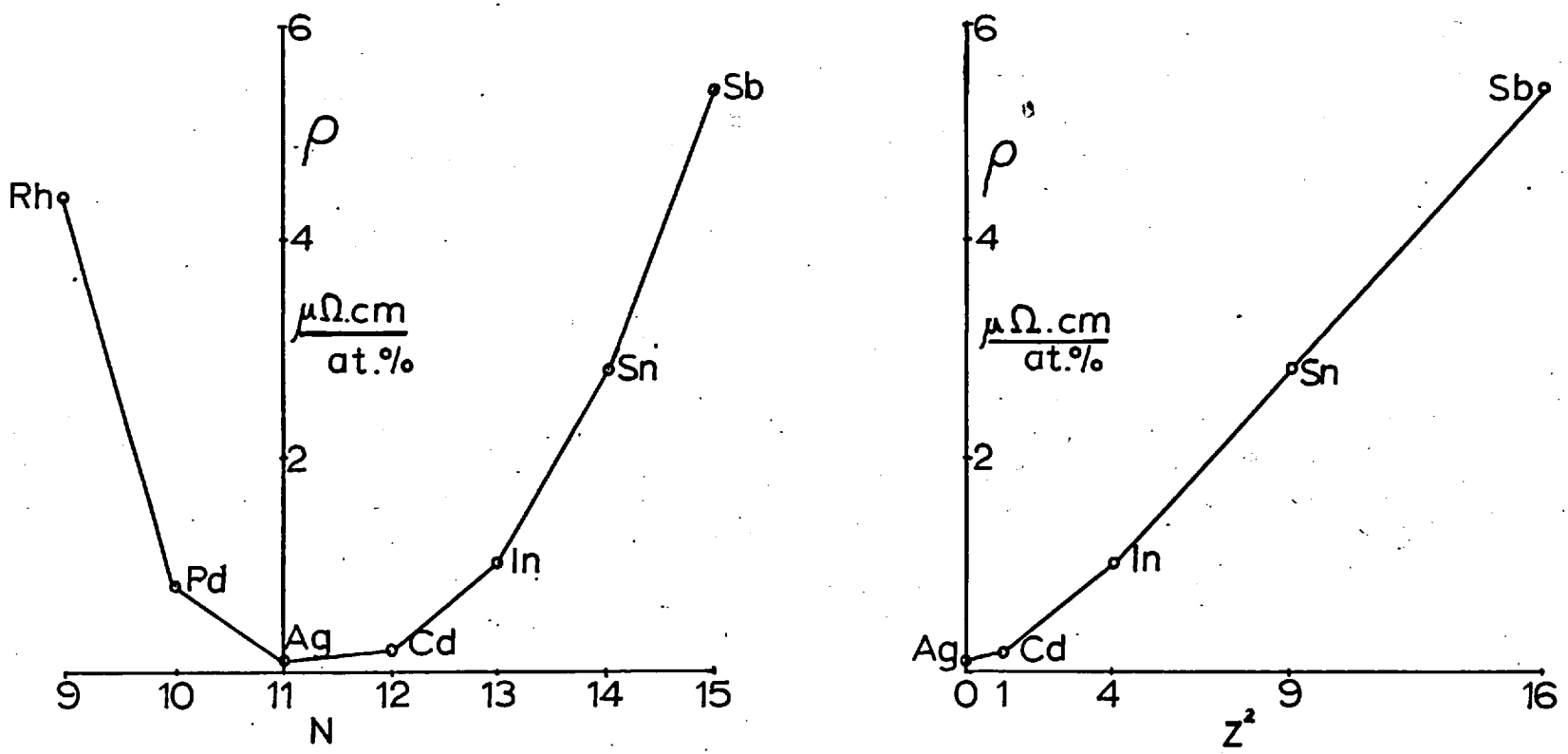

Fig. (2.3) Increase in the resistance of Cu due to 1 at.% of various metals in solid solution. N denotes the number of electrons outside an inert gas shell; $Z = N - 11$[51].

resistivity of a binary alloy containing a mole fraction x of metal A and (1-x) of B is of the form

$$\rho_r \propto x(1-x)$$

This assumes that the metals are always in solid solution. Clearly this is parabolic and approximates to Matthiesen's Rule near the extremes of the composition range. In practice, the resistivity can be considered to vary linearly up to 15%- 20% of solute. A classic example of this is shown in Fig. (2.4). The break-down of Matthiesen's Rule arises from the alteration of the vibrational spectrum of the lattice which can no longer be regarded as a perturbed version of the solvent lattice.

In practice, deviations from this simple behaviour occur because of the formation of ordered phases and superlattices. The increase in order associated with these structures causes sharp reductions in resistivity at particular alloy compositions. Fig. (2.5) shows an example of this for an ordered copper-gold alloy system. Providing that an alloy is in thermal equilibrium there will be negligible changes in structure for small temperature excursions.

2.2.4. The temperature coefficient of resistivity of metals and alloys

When estimating the T.C.R. of metals one has to consider the temperature variations of the individual components of resistivity. It has been shown that the probability $(\frac{1}{\tau})$ of scattering by lattice

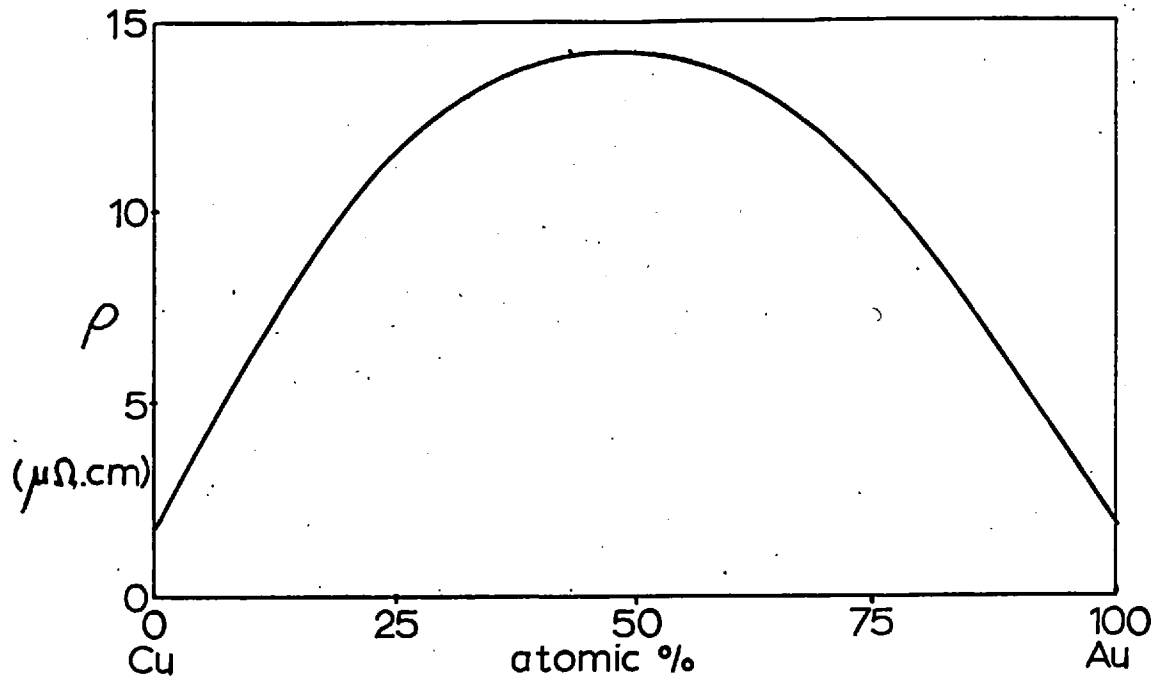

Fig. (2.4) Resistivity of a disordered binary alloy illustrating Nordheim's Rule[53].

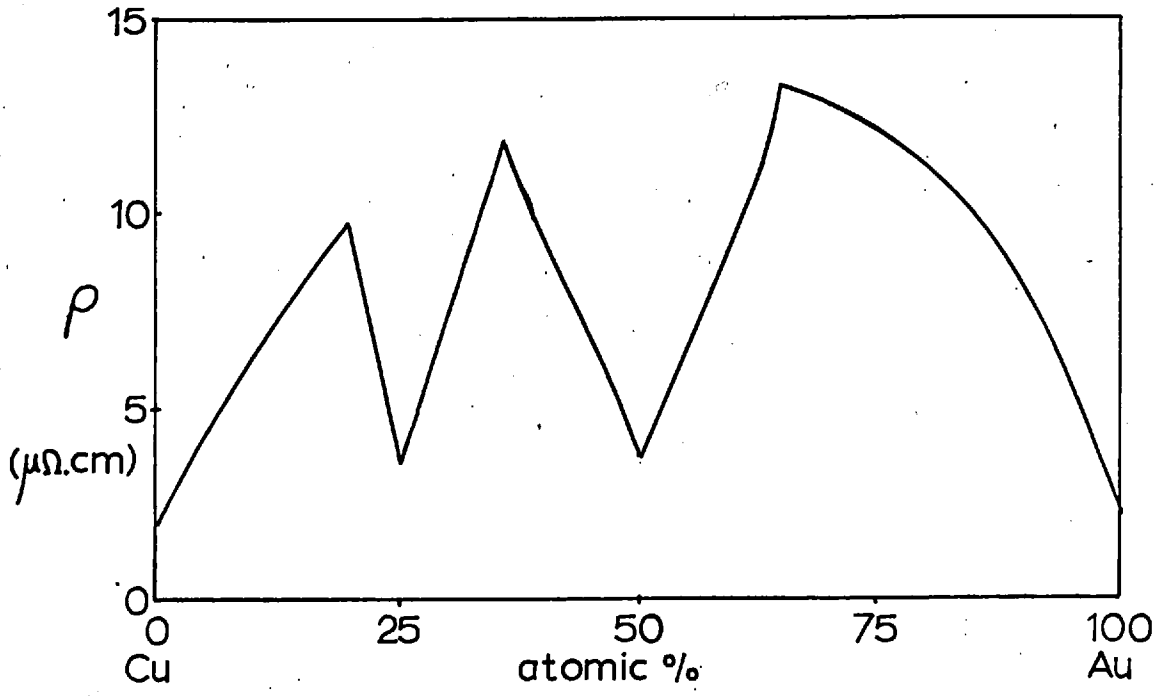

Fig. (2.5) Effect of ordered phases on the resistivity of a binary alloy[53].

vibrations is proportional to the absolute temperature at normal temperatures. It therefore follows that this resistivity component will be linearly dependent on temperature. Also, providing the metal is close to thermal equilibrium the components comprising the residual resistance will be independent of temperature.

Hence $\rho = \rho(T) + \rho_{resid}$

The T.C.R. α is defined as

$$\alpha = \frac{1}{\rho} \cdot \frac{d\rho}{dT}$$

$$\therefore \alpha = \frac{1}{(\rho(T)+\rho_{resid})} \cdot \frac{d\rho(T)}{dT} .$$

If the vibrational modes of the lattice are not changed by the presence of defects and impurities, $\rho(T)$ will be independent of the residual component. This applies except for alloys having large concentrations, when the scattering probabilities are not additive and Matthiesen's Rule no longer holds. It is clear that the value of α falls as the residual resistance increases; this is why alloys have much smaller T.C.R.'s than pure metals. Table (2.2) shows values of ρ and α for some common metals and alloys.

TABLE 2.2

The electrical properties of common metals and alloys

Material	$\rho(\mu\Omega.cm)$	α p.p.m./^oC	θ_D ^oK +	Source
Cu	1.55	4330	335	Kaye and Laby
Au	2.04	3980	165	Kaye and Laby
Ni	6.58	6750	413	Kaye and Laby
Cr	12.57	3000	403	Kaye and Laby
Ag	1.51	4100	210	Kaye and Laby
90%Pt 10%Ir	24.8	1300		Kaye and Laby
90%Pt 10%Rh	18.7	1660		Kaye and Laby
87%Pt 13%Rh	18.0	1560		Kaye and Laby
80%Ni 20%Cr	10.3	100		Kaye and Laby
80%Ni 20%Cr	10.8	210		Amer. Inst. of Phys. Handbook
80%Ni 20%Cr	10.0	400		Handbook of Chem. & Physics
80%Ni 20%Cr	11.2	85		A.S.M. Handbook

+ Values of the Debye temperatures were taken from the Handbuch der Physik Vol XIX.

80%Ni 20%Cr	9.8 10.3	180		Smithells
80%Ni 20%Cr	10.1	100		Hans Thomas, Zeit für Phys. 128, 1951

2.3 Size effects

2.3.1 The electron mean free path

In the previous section it was shown how electrical conduction in metals can be described in terms of relaxation times peculiar to individual scattering processes. If the net relaxation time τ is considered as the average time between scattering events it is possible to define an electron mean free path

$$l = \tau V_F$$

where V_F is the velocity of a conduction electron at the Fermi surface. At normal temperatures the electron mean free path in metals is several hundred angstroms. Clearly when the dimensions of a conductor become comparable with the electron mean free path an increasing proportion of the electrons will interact with the surface before completing the normal mean free path. This section will consider the kind of interaction and its effect on the conductivity and temperature coefficient of conductivity of a thin film. It will be assumed that the films are laminar sheets and not aggregated structures.

2.3.2 Surface scattering of electrons

There is no detailed theory of the interaction of conduction electrons with boundaries and it is necessary to resort to a phenomenological description. In this case, it is useful to think of an electron as a wave with wavelength λ given by the de Broglie relation

$$p = \frac{h}{\lambda}$$

If the bounding surface is smooth, i.e. the electron wavelength is large compared with the surface detail, the electron will be reflected specularly. In this case, there is no change in momentum parallel to the surface and the normal component is reversed in direction only. On the other hand, when the surface features have dimensions of the same order as the wavelength the wave will be diffusely reflected losing all memory of its initial components of momentum. The two cases are illustrated in Fig. (2.6).

Since it is impossible to describe film surfaces analytically a statistical parameter p is defined where p is the proportion of specular collisions with the surface. A very perfect surface will have a value $p = 1$ and a very rough one $p = 0$. Since an electron which collides with a specular surface does not experience a change in momentum parallel to the boundary, i.e. in the field direction, it does not contribute to the resistance to current flow. Therefore a film having specular surfaces will have the same resistivity as the bulk material.

The wavelength of conduction electrons is usually only several angstroms and since most films have irregular surfaces comprising crystallites comparable in size with the electron wavelength p is generally zero. The effect of surface scattering must therefore be considered. However, under certain circumstances it is possible to produce films comprising large crystallites with perfect sides and p tends to unity

Fig (2.6)

The same surface appears rough (p=0) for short waves but smooth (p=1) for long waves

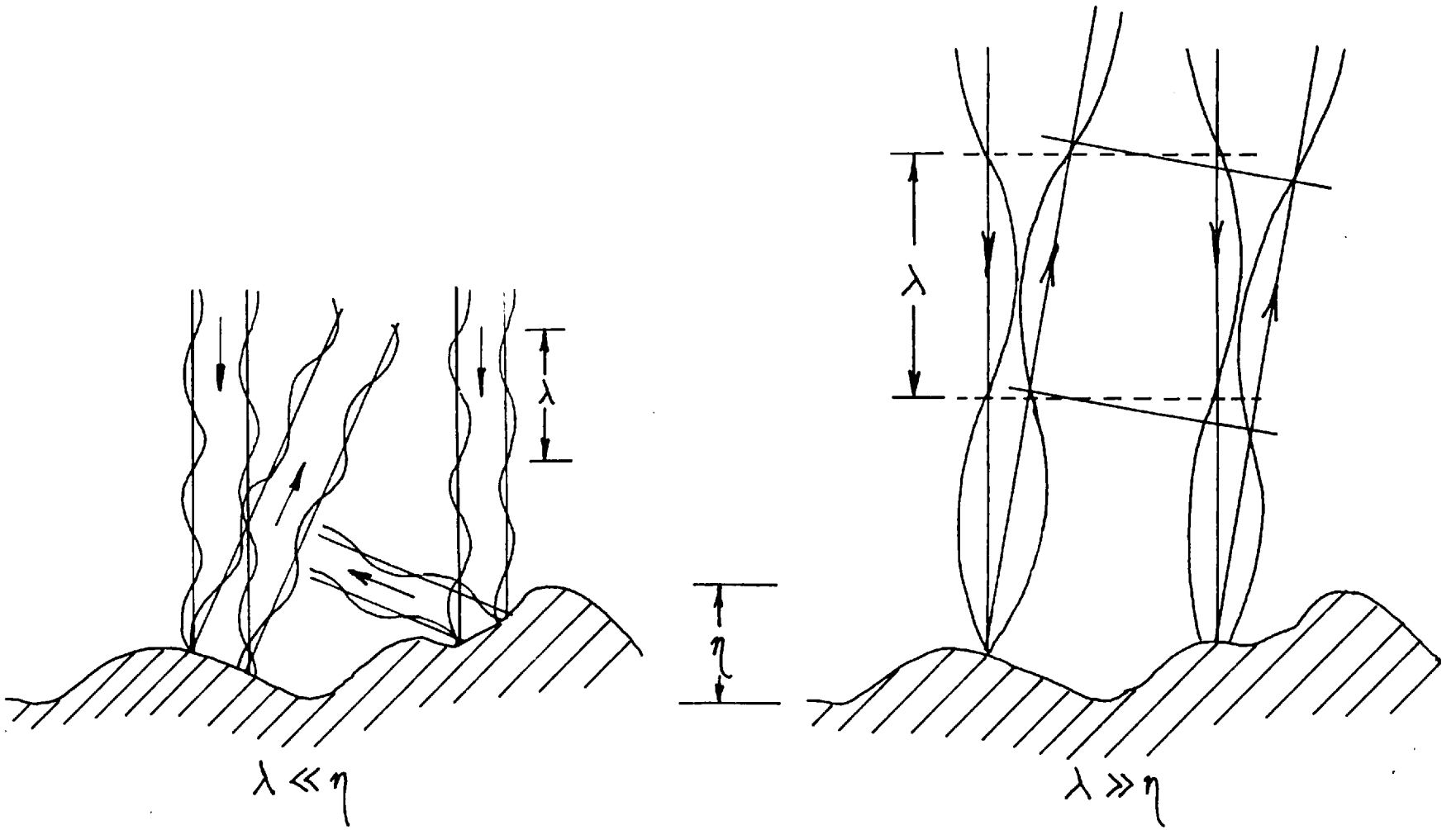

2.3.3 Thomson's model

The first attempt to account for surface scattering was by Thomson[3] who calculated the average mean free path of electrons in terms of the film thickness and the bulk electron mean free path. It is useful first to describe his simple approach and go on to the more rigorous statistical treatment of Fuchs and Sondheimer.

Let l_o be the mean free path of an electron in the bulk metal and d the film thickness

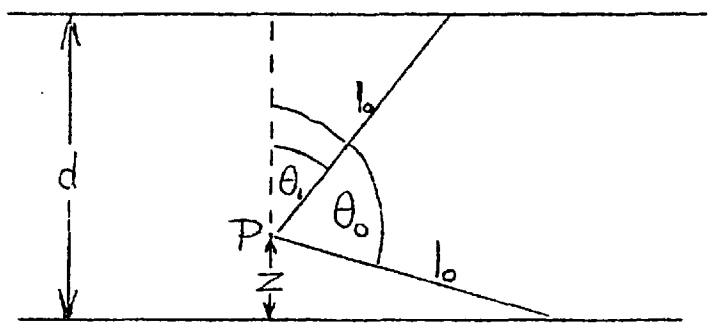

Fig. (2.7) Thomson's model of surface scattering

All collisions with the surface are assumed to be diffuse. Consider an electron at P moving at an angle θ with the Z axis, its free path l is given by

$$l = \begin{cases} (d-Z)/\cos\theta & (0 \leqslant \theta \leqslant \theta_1) \\ \lambda_o & (\theta_1 \leqslant \theta \leqslant \theta_o) \\ -Z/\cos\theta & (\theta_o \leqslant \theta \leqslant \pi) \end{cases}$$

where $\cos\theta_1 = (d-Z)/l_o$ and $\cos\theta_o = -Z/l_o$.

The mean free path is determined by taking the mean free path over all angles and $0<Z<d$

hence

$$\bar{l} = \frac{1}{2d} \int_0^Z dZ. \int_0^\pi l \sin\theta \, d\theta.$$

$$= \frac{d}{2}\left[\log \frac{l_o}{d} + 3/2\right]$$

Since the resistivity is inversely proportional to the mean free path,

$$\therefore \frac{\rho}{\rho_o} = \frac{2l_o}{d} \cdot \frac{1}{\left[\log \frac{l_o}{d} + 3/2\right]}$$

A similar approach by Lovell (1936)[13] but making the assumption that all electron trajectories begin on the film surface gave the relationship

$$\frac{\rho}{\rho_o} = \frac{l_o}{d} \cdot \frac{1}{\left[\log \frac{l_o}{d} + 1\right]}$$

Lovell's assumption is strictly true only for very thin films.

However, both approaches suffer from the following short comings

(i) In assessing the mean free path, all electrons in a metal should be considered at a given moment and their free paths averaged.

(ii) The statistical distribution of the free paths about l_o in the bulk material is neglected.

These deficiencies were pointed out by Fuchs[15], and he overcame them by using a statistical treatment employing the Boltzmann transport equation. The approach was later expanded by Sondheimer.

2.3.4 The Fuchs-Sondheimer model

An electron distribution can be described by a distribution function f which expresses the numbers of electrons having particular velocities and positions. A relationship between the change in the distribution function under applied forces and internal relaxation mechanisms can be derived. This is known as the Boltzmann transport equation. Thus,

$$\underset{\text{applied forces}}{\frac{\partial f}{\partial t}} - \underset{\text{relaxation mechanisms}}{\frac{\partial f}{\partial t}} = \frac{\partial f}{\partial t}$$

In equilibrium

$$\underset{\text{applied forces}}{\frac{\partial f}{\partial t}} = \underset{\text{relaxation mechanisms}}{\frac{\partial f}{\partial t}}$$

$$\therefore X\frac{\partial f}{\partial u} + Y\frac{\partial f}{\partial v} + Z\frac{\partial f}{\partial w} + u\frac{\partial f}{\partial x} + v\frac{\partial f}{\partial y} + w\frac{\partial f}{\partial z} = \underset{\text{relaxation mechanisms}}{\frac{\partial f}{\partial t}} \qquad (2.1)$$

where X, Y and Z are external applied forces and u, v and w orthogonal velocity components.

In the case of a film with an applied electric field in the x direction

$$X = \frac{-eE}{m} \quad , \quad Y = Z = 0$$

Also, since there are no constraints in the x and y direction, i.e. infinite in extent

$$\frac{\partial f}{\partial x} = \frac{\partial f}{\partial y} = 0.$$

The equation (2.1) therefore simplifies to

$$\frac{-eE}{m} \frac{\partial f}{\partial u} + w \frac{\partial f}{\partial z} = \left(\frac{\partial f}{\partial t}\right)_{\substack{\text{relaxation} \\ \text{mechanisms}}}$$

The relaxation mechanisms which operate are those of the bulk material and for simplicity can be represented by a single relaxation time τ.

If the equilibrium distribution f_o has been disturbed to f and allowed to relax

$$(f - f_o)_{t=t} = (f - f_o)_{t=0} \; e^{-t/\tau}$$

Differentiating, we have

$$\frac{\partial f}{\partial t} = \frac{-(f - f_o)}{\tau} \; t=t$$

since

$$\frac{\partial f_o}{\partial t} = 0 \text{ in equilibrium.}$$

Hence,

$$\frac{-eE}{m} \frac{\partial f}{\partial u} + w \cdot \frac{\partial f}{\partial z} = \frac{-(f - f_o)}{\tau}$$

It is useful to write

$$f = f_o + f_1 (\underline{V} , z) \quad ,$$

since the perturbation is independent of x and y.

$$w \frac{\partial f_1}{\partial z} + \frac{f_1}{\tau} = \frac{eE}{m} \frac{\partial f_o}{\partial u}$$

The general solution of this equation is

$$f_1 = \frac{eE\tau}{m} \cdot \frac{\partial f_o}{\partial u} \left[1 + F(\underline{V})\, e^{-z/\tau w} \right]$$

where $F(\underline{V})$ is an arbitrary function depending on the boundary conditions.

From the symmetry of the problem

$$f_1(u,v,w,z) = f_1(u,v,-w,(d-z))$$

This results in two solutions, one describing the electrons approaching a surface and the other describing those leaving. Thus,

$$f_1(\underline{V},z) = \begin{cases} \frac{eE\tau}{m} \cdot \frac{\partial f_o}{\partial u} \left[1 + F(\underline{V})\, e^{-z/\tau w} \right] = f_1^{+} & (w > 0) \\ \frac{eE\tau}{m} \cdot \frac{\partial f_o}{\partial u} \left[1 + F(-\underline{V})\, e^{(d-z)/\tau w} \right] = f_1^{-} & (w < 0) \end{cases}$$

It is at this stage that the description of the surfaces is introduced. The distribution function of the electrons arriving at the surface $z = 0$ is

$$f_o + f_1^{-}(\underline{V},\ z = 0)$$

a proportion p of these is scattered elastically giving a contribution

$p(f_o + f_1^{-}(-\underline{V},\ z = 0)$ to the distribution leaving the surface. Hence,

$$f_o + f_1^+(\underline{V},\ z = 0) = p\left[f_o + f_1^-(-\underline{V},\ z = 0)\right] + g$$

where g is the inelastically scattered component and does not depend on the angle of scattering in this model.

$$g = f_o + f_1^+(\underline{V},\ z = 0) - p\left[f_o + f_1^-(-\underline{V},\ z = 0)\right]$$

substituting expressions for f_1^+ and f_1^-

$$g = f_o - pf_o + f_1^+(\underline{V},\ z = 0) - pf_1^-(-\underline{V},\ z = 0)$$

$$= (1-p)f_o + \frac{eE\tau}{m}\frac{\partial f_o}{\partial u}\left[1 + F(\underline{V}) - p - pF(\underline{V})\ e^{-d/\tau w}\right]$$

$$= (1-p)f_o + \frac{eE\tau}{m}\frac{\partial f_o}{\partial u}\left[(1-p) + F(\underline{V})\left(1 - pe^{-d/\tau w}\right)\right]$$

Since g is independent of the direction of $\underline{V}$ the square bracket must be zero. Hence,

$$F(\underline{V}) = \frac{-(1-p)}{1-pe^{-d/\tau w}}$$

$$\therefore\ f_1(\underline{V},z) = \begin{cases} \dfrac{eE\tau}{m}\dfrac{\partial f_o}{\partial u}\left[1 - \dfrac{1-p}{1-pe^{-d/\tau w}}\cdot \exp\ \dfrac{-z}{\tau w}\right] & (w > 0) \\ \dfrac{eE\tau}{m}\dfrac{\partial f_o}{\partial u}\left[1 - \dfrac{1-p}{1-pe^{-d/\tau w}}\cdot \exp\ \dfrac{d-z}{\tau w}\right] & (w < 0) \end{cases}$$

The current density at z is given by

$$J = -2e\left(\frac{m}{h}\right)^3 \int \underline{V}.f.d\underline{V}$$

Introducing polar coordinates V, θ and ϕ in $\underline{V}$ space such that $w = V\cos\theta$ then integrating over V, ϕ and θ

$$J(z) = \frac{2e^2\pi m^2 \tau V^3 E}{h^3} \int_0^{\pi/2} \sin^3\theta \left\{ 2 - \left(\frac{1-p}{1-pe^{-d/l\cos\theta}} \right) \left[\exp\left(\frac{-z}{l\cos\theta}\right) + \exp\left(\frac{z-d}{l\cos\theta}\right) \right] \right\} d\theta$$

The net current flowing in the film can then be obtained by integrating over the film thickness $z = 0$ to d.

σ_o, the bulk conductivity, is given by putting the upper limit of z equal to infinity

Hence,

$$\sigma = \sigma_o \left[1 - \frac{3}{2}\frac{l}{d} \int_0^{\pi/2} \sin^3\theta\cos\theta \left(\frac{1-p}{1-pe^{-d/l\cos\theta}} \right) \left(1 - \exp\frac{-d}{l\cos\theta} \right) d\theta \right]$$

substituting $t = \frac{1}{\cos\theta}$ and $K = \frac{d}{l}$

$$\frac{\sigma}{\sigma_o} = \left[1 - \frac{3(1-p)}{2K} \int_1^{\infty} \left(\frac{1}{t^3} - \frac{1}{t^5} \right) \left(\frac{1-e^{-Kt}}{1-pe^{-Kt}} \right) dt \right]$$

When perfectly inelastic scattering occurs $p = 0$ and

$$\frac{\rho}{\rho_o} = \frac{1}{1 + \frac{3}{4}Z(K - \frac{K^3}{12}) - \frac{3}{8K}(1-e^{-K}) - (\frac{5}{8} - \frac{K}{16} - \frac{K^2}{16})e^{-K}}$$

where $Z = \int_K^{\infty} \frac{e^{-t}}{t}\, dt$, an exponential integral which has been tabulated.

Fig.(2.8) shows curves of ρ/ρ_o plotted against K for values of p between zero and unity.

Fig (2.8)

Variations of ρ/ρ_0 with K for various values of p

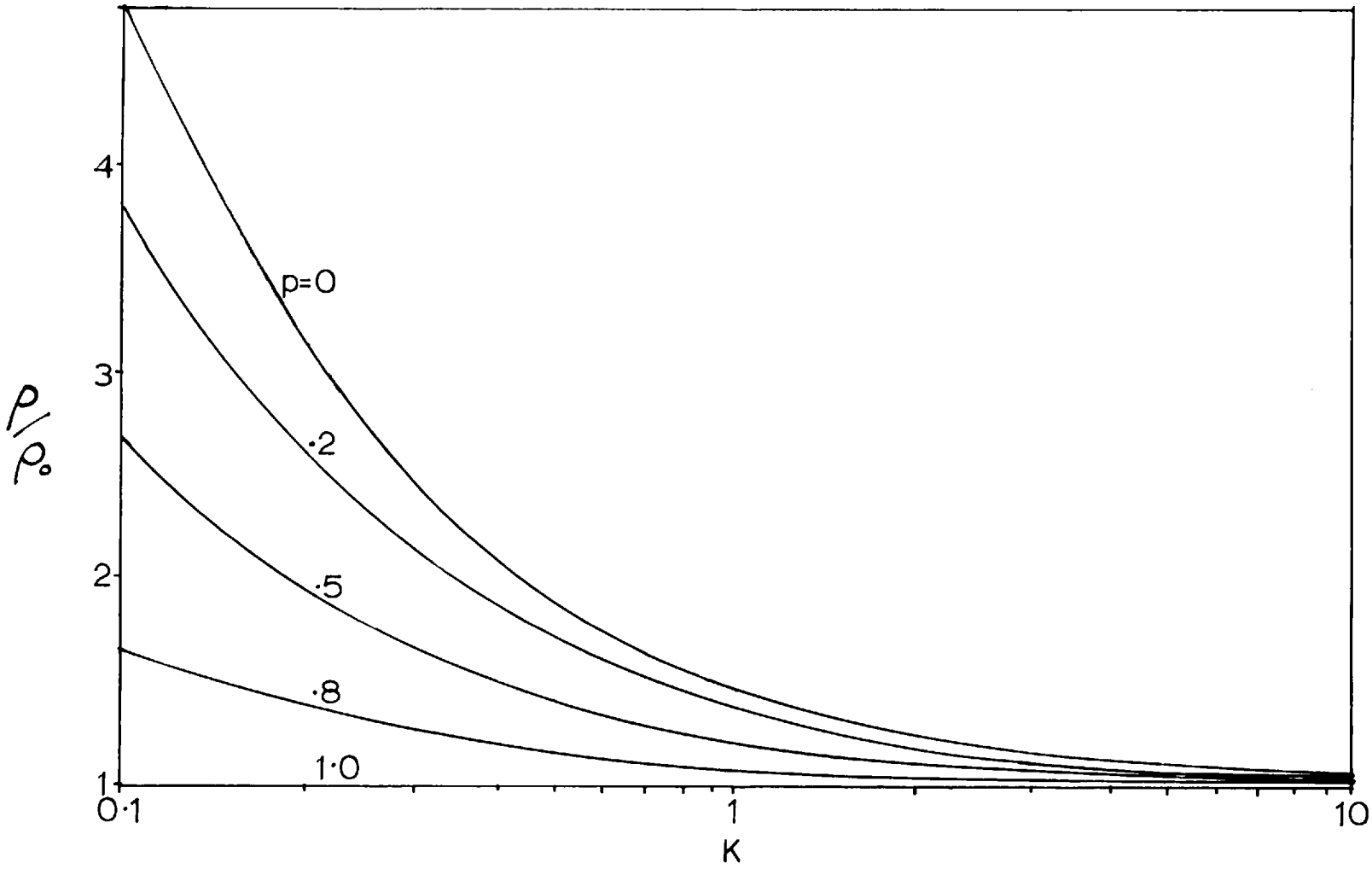

2.3.5 The effect of size on the temperature coefficient of resistance of a film

The increase in resistivity owing to surface scattering has been calculated in terms of the bulk resistivity and K the thickness - mean free path ratio. In calculating the modified temperature coefficient one must consider the effect of temperature on K since this parameter describes the extent to which the electron distribution interacts with the bounding surfaces.

If $\frac{\rho}{\rho_o}$ is expressed as $\frac{\phi(K)}{K}$

then

$$\frac{d\rho}{dT} = \frac{d\rho}{dK} \cdot \frac{dK}{dT}$$

$$\therefore \quad \alpha = \alpha_o + \frac{K}{\phi(K)} \cdot \frac{d(\frac{\phi(K)}{K})}{dK} \cdot \frac{dK}{dT}$$

it is most convenient to work in terms of $\frac{K}{\phi(K)}$

$$\therefore \quad \alpha = \alpha_o - \frac{\phi(K)}{K} \cdot \frac{dK}{dT} \cdot \frac{d(\frac{K}{\phi(K)})}{dK}$$

but $\alpha_o = \frac{1}{K} \cdot \frac{dK}{dT}$

Hence $$\alpha = \alpha_o \left[1 - \phi(K) \cdot \frac{d(\frac{K}{\phi(K)})}{dK} \right]$$

It remains now to substitute the expression already derived for ρ, ρ_o.

This yields,

$$\frac{\alpha}{\alpha_o} = \frac{1 - \frac{3}{4}(1-p)\int_1^\infty (\frac{1}{t^3} - \frac{1}{t^5})\frac{1-e^{-Kt}}{1-pe^{-Kt}}\,dt + \frac{3}{2}(1-p)^2\int_1^\infty (\frac{1}{t^2} - \frac{1}{t^4})\frac{e^{-Kt}}{(1-pe^{-Kt})^2}\,dt}{1 - \frac{3}{2K}(1-p)\int_1^\infty (\frac{1}{t^3} - \frac{1}{t^5})\frac{1-e^{-Kt}}{1-pe^{-Kt}}\,dt} \qquad (2.2)$$

When p = 0 and perfectly inelastic scattering occurs

$$\frac{\alpha}{\alpha_o} = \left[1 - \frac{Z(1-K^2/4)\cdot\frac{1}{2K^2} - \frac{e^{-K}}{4}(1 + \frac{2}{K^2} + \frac{2}{K} - K)}{Z(1-\frac{K^2}{12}) - \frac{1}{2K^2} + \frac{4}{3K} + \frac{e^{-K}}{4}(\frac{2}{K^2} - \frac{10}{3K} - \frac{1}{3} + \frac{K}{3})}\right] \qquad (2.3)$$

Though equation (2.2) was derived independently here equation (2.3) has recently been quoted by Young and Lewis[54] and is attributed to Savornin[55].

Curves of $\frac{\alpha}{\alpha_o}$ plotted against K for various p values are shown in Fig. (2.9). These values of ρ/ρ_o and $\frac{\alpha}{\alpha_o}$ were computed by Campbell[56] in a parallel study.

2.3.6 Discussion of mean free path effects

Figs. (2.8) and (2.9) show clearly that surface scattering is expected to lead to an increase in resistivity and a decrease in the temperature coefficient of resistance as films become increasingly thin. The expression for $\frac{\alpha}{\alpha_o}$ takes into account the varying interaction of the electron distribution with the film surfaces as the temperature changes the bulk mean free path and hence K. Lucas[17] has calculated an expression for ρ/ρ_o for films having different scattering parameters

Fig(2.9)

Variations of $\frac{\alpha}{\alpha_0}$ with K for various values of p

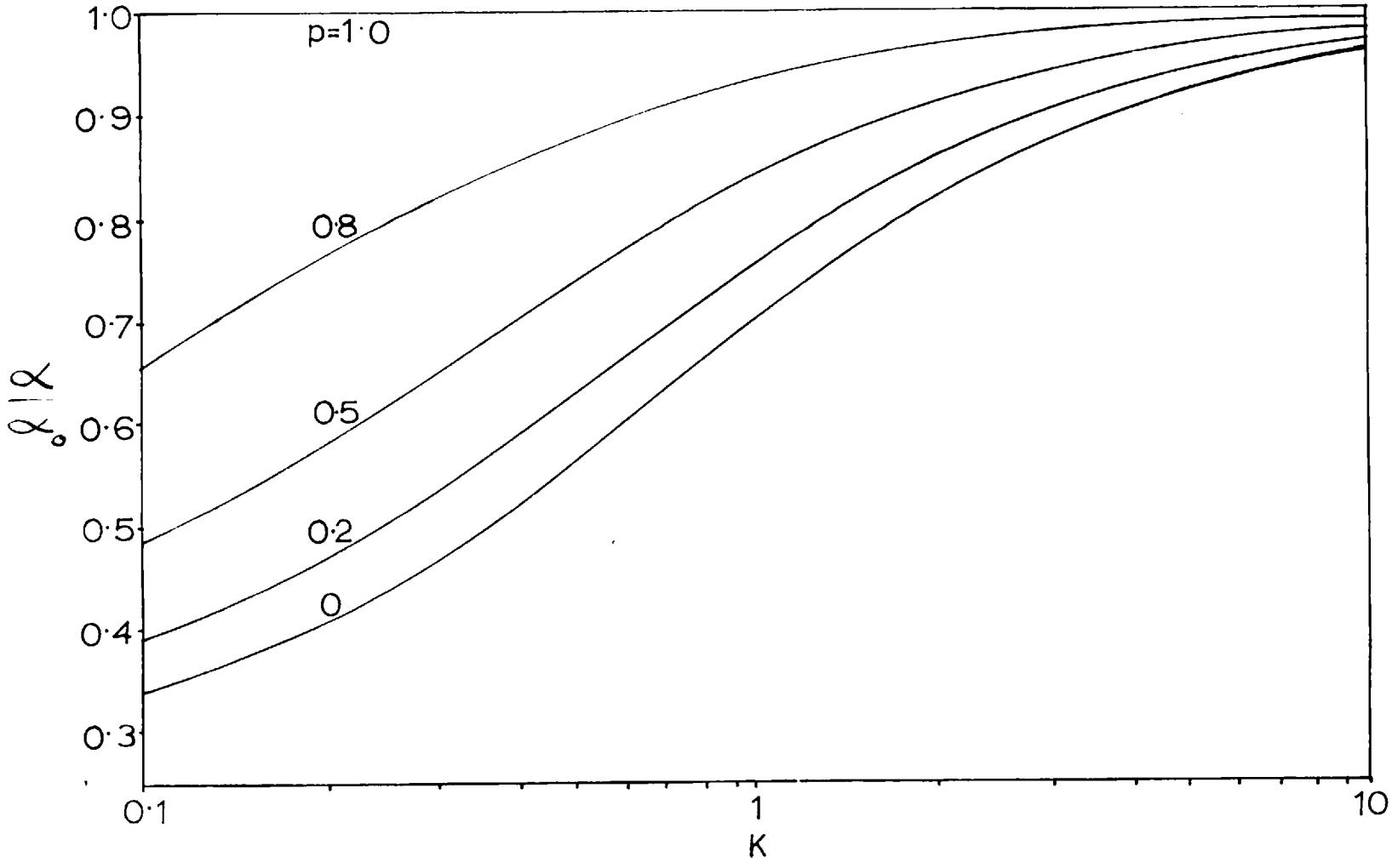

p and q for each surface. His results are shown for comparison in Fig. (2.10). The expressions which have been derived for $\frac{\rho}{\rho_o}$ and $\frac{\alpha}{\alpha_o}$ are cumbersome to use and approximations are given in Table 2.3. To illustrate their ranges of validity they are shown plotted in Figs. (2.11) and (2.12).[56] In examining a mean free path effect in a thin film it is necessary to know the bulk value of mean free path to calculate values of K. The situation is often complicated by the fact that the "bulk" resistivity of film material is greater than that of the starting material. This is due to the mode of growth of a thin film which incorporates a greater number of imperfections and dislocations into the structure. The effect is an increase in the residual resistivity which will be termed $\rho_{preparation}$ and depends on the method of preparation. Clearly bulk values of l_o cannot be used.

It would be possible to determine the values by preparing thick films. According to Figs. (2.8) and (2.9), their thickness would have to be ten times the mean free path in order to eliminate surface scattering. To prepare such films is often awkward and inconvenient. However, a plot of $\frac{\alpha\rho}{\alpha_o\rho_o}$ against K, Fig. (2.13), indicates that this function is independent of K above $K \sim 1$. Thus, it is only necessary to reach thicknesses equal to the mean free path before K can be deduced. Values of α_o and ρ_o for the bulk material can still be used since

$$\alpha_o\rho_o = \frac{d\rho_{phonon}}{dT} = (\alpha\rho)_{thick\ film}$$

Fig(2.10)

Variations of ρ/ρ_o with K showing the effect of different surface reflection coefficients p and q

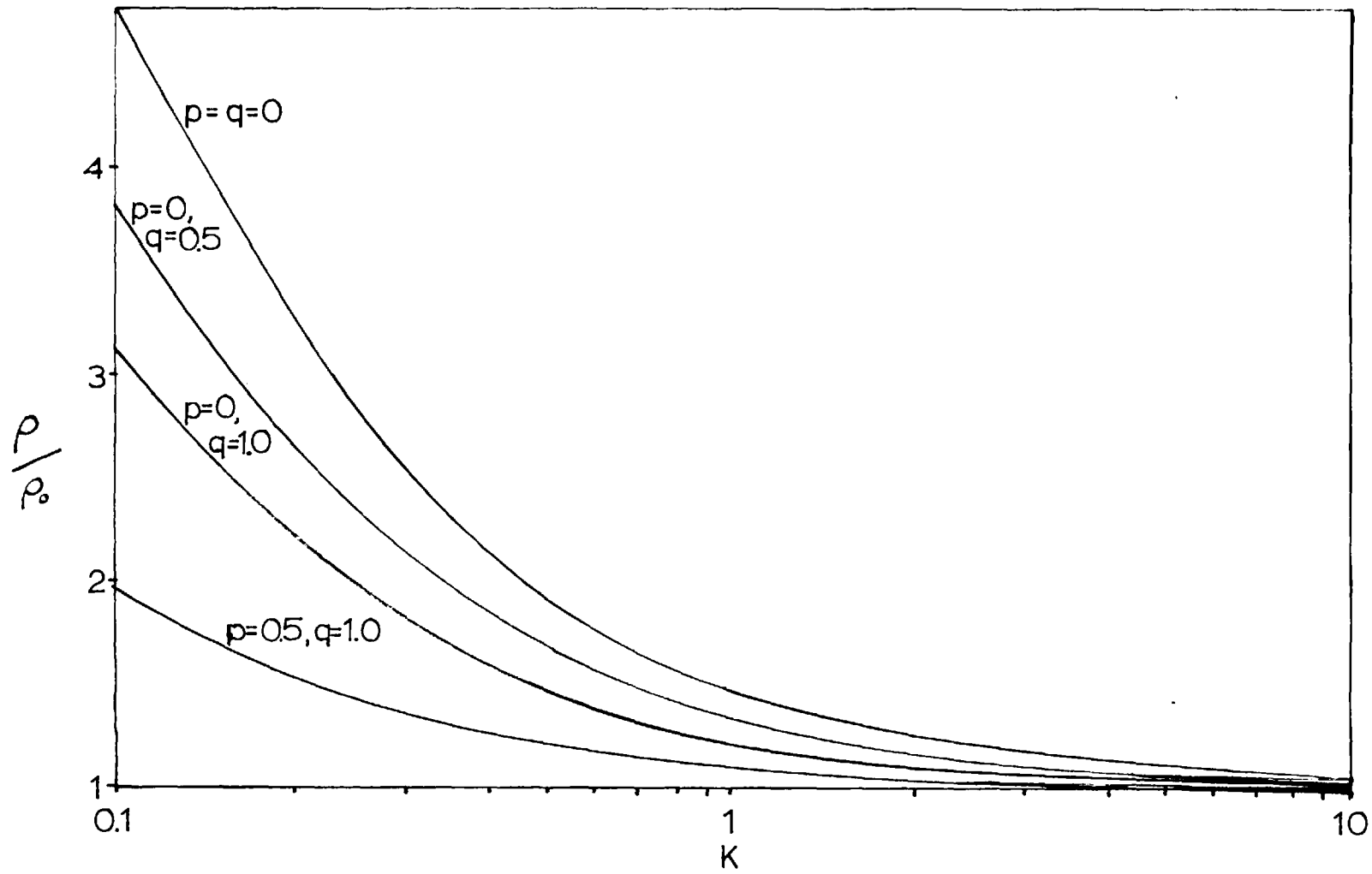

TABLE 2.3

Approximations to ρ/ρ_o and α/α_o

Thick films $K \gg 1$	Thin films $K \ll 1$
Sondheimer[16] $\frac{\rho}{\rho_o} = 1 + \frac{3(1-p)}{8K - 3(1-p)}$ (2.4)	Mayer[93] $\frac{\rho}{\rho_o} = \frac{4}{3K(1+2p)\log\frac{1}{K} + 0.4228}$ (2.5) Sondheimer $\frac{\rho}{\rho_o} = \frac{4(1-p)}{3(1+p)K\log\frac{1}{K}}$ (2.6) (valid only for small p).
$\frac{\alpha}{\alpha_o} = 1 - \frac{3(1-p)}{8K}$ (2.7)	(p = 0) $\frac{\alpha}{\alpha_o} = \frac{1}{\log\frac{1}{K} + 0.4288}$ (2.8)

Fig(2.11)
Approximate forms of ρ/ρ_0 plotted against K (see Table 2.3)

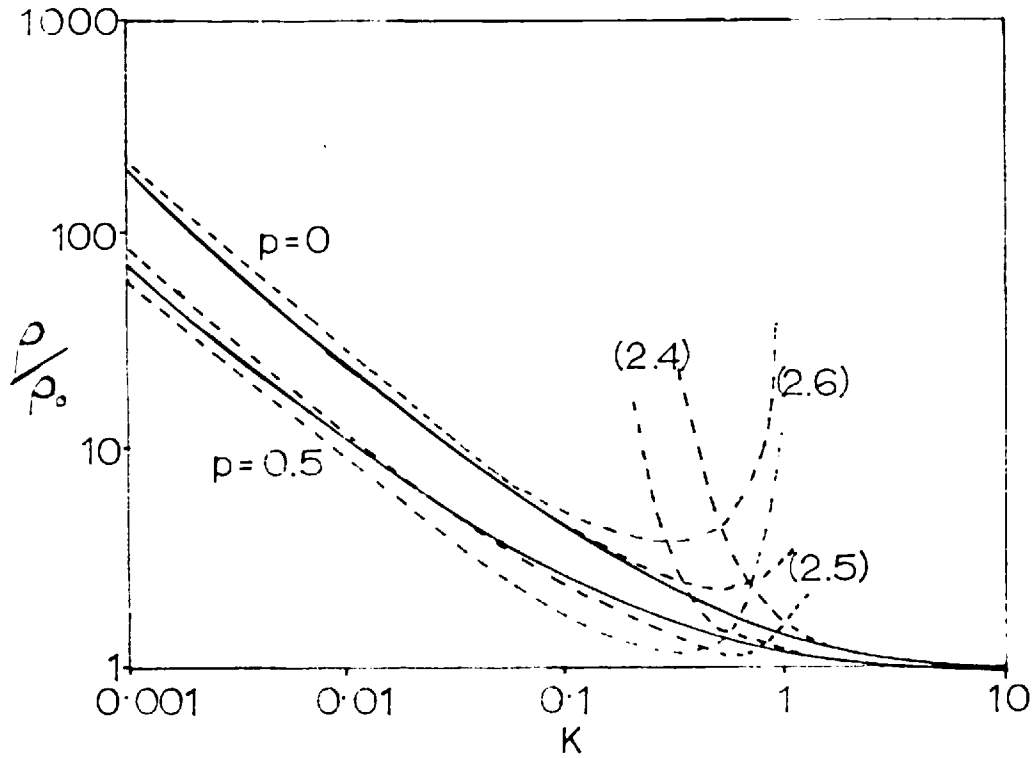

Fig(2.12)
Approximate forms of α/α_0 plotted against K (see Table 2.3)

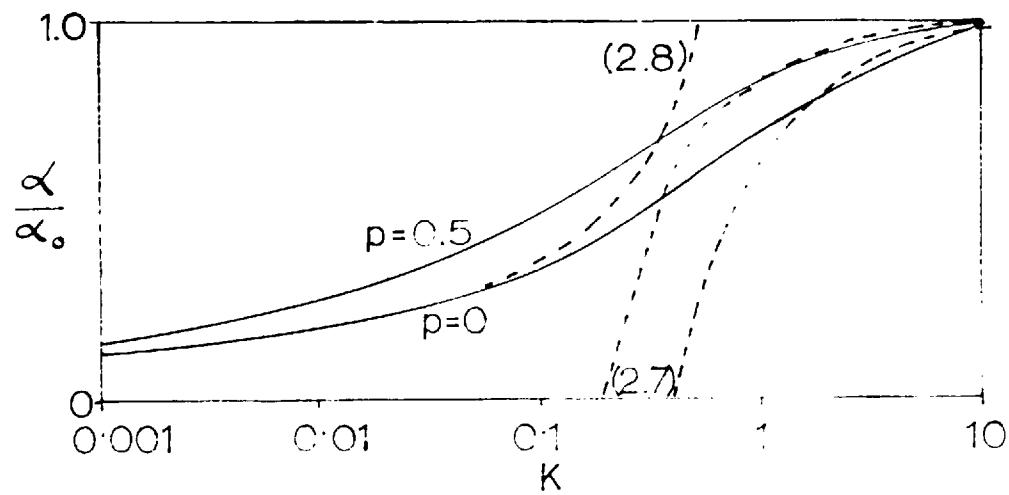

Fig(2.13)

$\frac{d\rho}{d\tau} / \frac{d\rho_0}{d\tau}$ plotted against K for various values of p

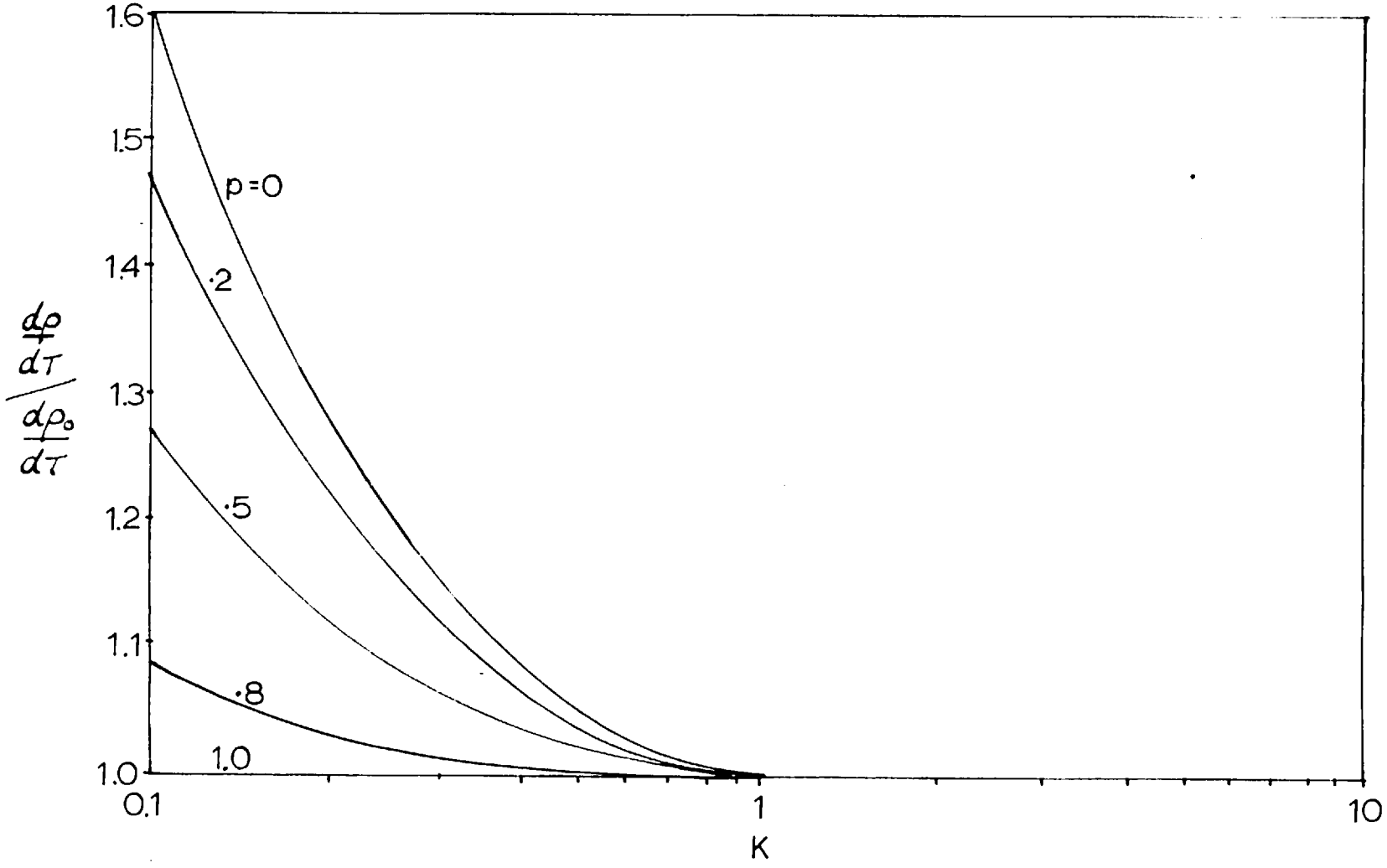

An advantage is that the purity of the material used to determine α_o and ρ_o is not critical since $\frac{df_o}{dT}$ is independent of defect and impurity concentration provided that Matthiesen's Rule remains valid. This technique will be assessed using measurements on gold films.

2.4 Conduction in discontinuous films

It is well known that electrical conduction occurs in aggregated films. Their conductivities are several orders smaller than continuous films of comparable thicknesses and also exhibit negative temperature coefficients of resistance. Rather than consider the various theories which have been suggested, an account of these phenomena will be presented which draws to some extent on each of them and attempts to provide a unified treatment.

2.4.1 The conduction mechanism

Essentially the resistance of an aggregated film is associated with the transport of electrons between the metal aggregates, the resistance within each being negligibly small. For simplicity a discontinuous film may be considered as a uniform array of square metal prisms lying on a plane dielectric substrate as shown by Fig. (2.14). Plate (1.1) shows that they are in fact round and far from uniform in size.

In considering the conduction of electrons between the metal islands one must consider the potential barrier through or over which

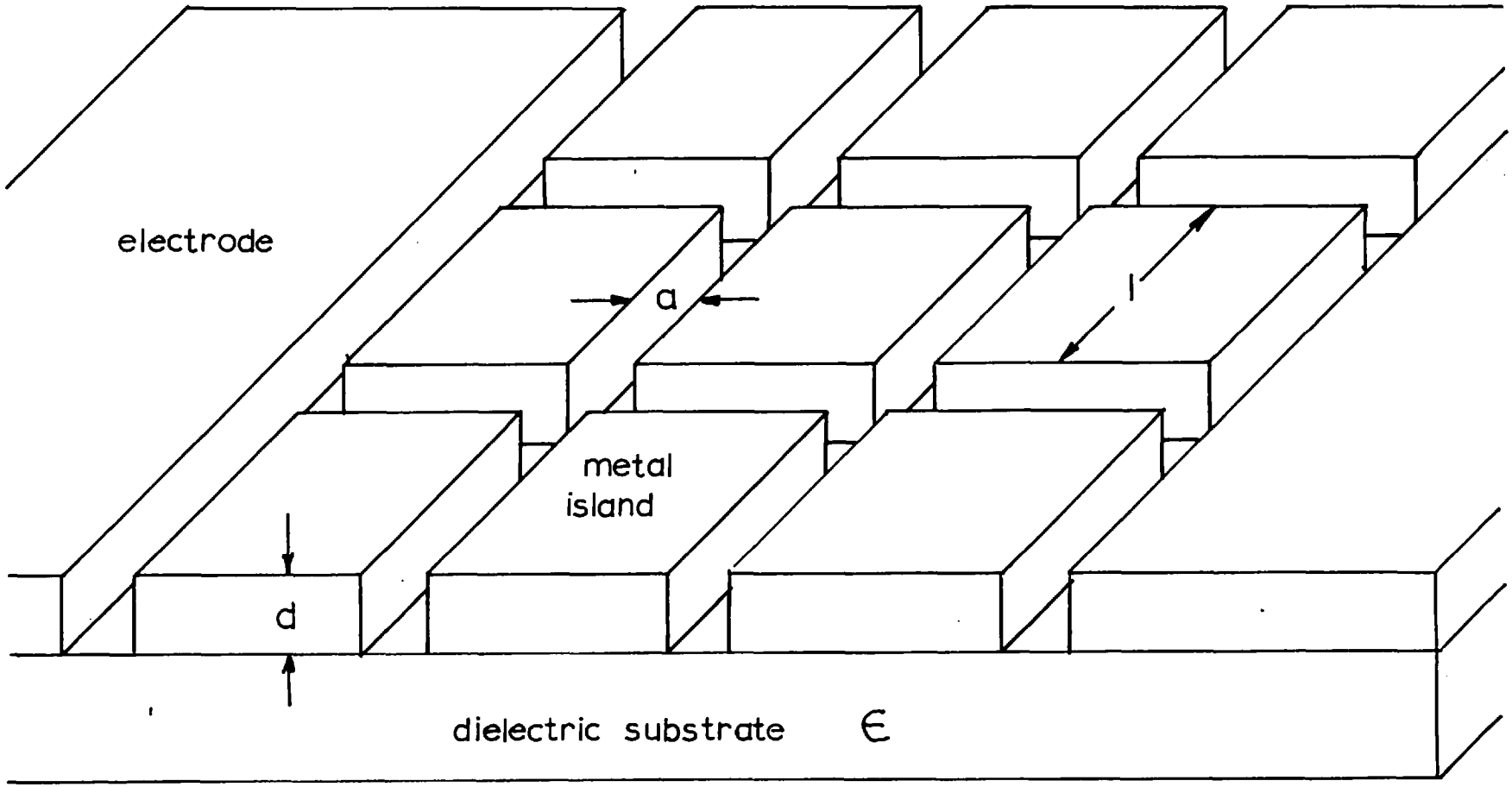

Fig (2.14) An idealised representation of a discontinuous metal film

the electrons must move. Fig. (2.15) (a) shows the potential barrier between two metal islands separated by free space. In this case the barrier height is equal to the metal work function ϕ and is typically $\sim$ 4 - 6eV. Though the application of an electric field between the islands would cause a lowering of the barrier $\Delta\phi$, i.e. the Schottky effect, it would be very small.

$$E = 1000 \text{ V/cm.} \qquad \phi \sim 0.01 \text{ eV}$$

In practice the islands are separated by a dielectric substrate and the barrier is modified, as shown in Fig. (2.15) (b). Its height is the difference in energy betwe n the Fermi level of the metal the bottom of the conduction band of the dielectric or the difference of the metal work function and the electron affinity of the dielectric. Typically the height of such a barrier is $\sim$1 - 3eV.

At ordinary temperatures the thermionic current over a barrier this high is much smaller than 1 amp/cm^2 which is a typical current density in a discontinuous film with an applied field of 10 volts/cm. However, a value of this order can be achieved by quantum mechanical tunnelling when the electrodes are several tens of angstroms apart. This would appear to be the only way of realising a large enough current density. Unfortunately the temperature dependence of tunnelling is too small to be compatible with values obtained experimentally $\sim$ - 2000 p.p.m. /^{o}C.

In an effort to invoke a tunnelling process Neugebauer and Webb[19] suggested that the temperature dependence of conductivity is associated

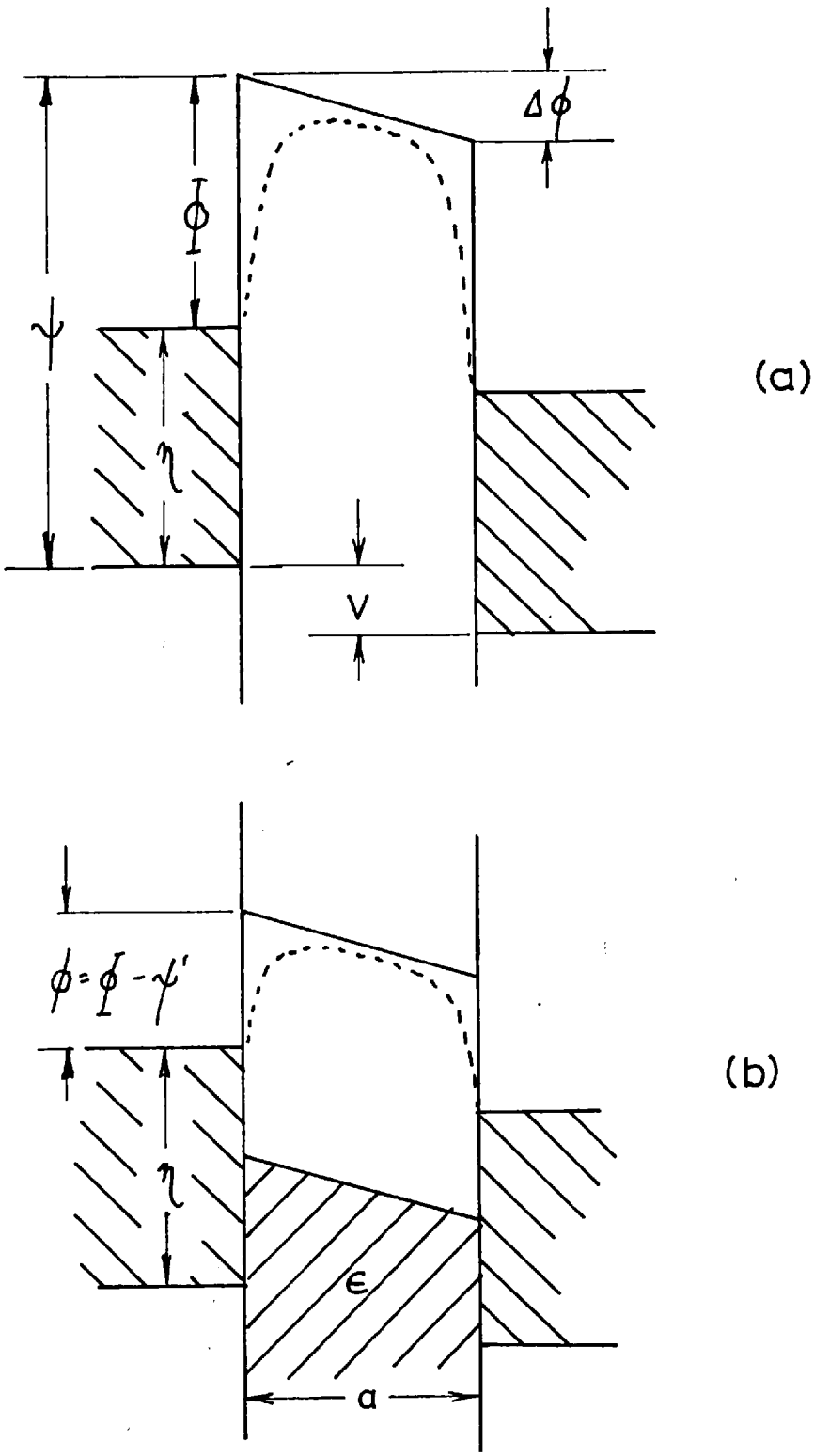

Fig(2.15) Energy level diagrams of adjacent islands separated by (a) free space
(b) dielectric, permittivity ϵ

with a charge carrier creation process which is temperature dependent. It has been shown qualitatively by several workers[19][21] that the activation energy of this process is equal to the energy required to charge an island positively by one electronic charge. This account embodies these ideas and suggests why this occurs.

2.4.2 A general expression for conduction through a potential barrier

At a particular energy E the number of electrons participating in conduction is proportional to the number of occupied states in island 1, $N_1(E)f_1(E)dE$ and to the probability of there being an empty corresponding state in island 2, $f_2(E)$. Referring to Fig. (2.17), the current flux at that energy is proportional to the integral

$$J_{1\rightarrow 2} \alpha \int_0^{\pi/2} n(\theta).v(\theta).D(\theta)d\theta$$

where $v(\theta)$ is the component of velocity in the x direction, $n(\theta)$ is the number of electrons having total energy E which possess a component of velocity $v(\theta)$ in the x direction and $D(\theta)$ is the quantum mechanical transmission probability of an electron having velocity $v(\theta)$ normal to the barrier. This is summarised by Fig. (2.16)

Hence, the component of current from island 1 to 2 is given by

$$J_{1\rightarrow 2} = e \int_0^{\infty} \left[N_1(E)f_1(E)(1-f_2(E)) \int_0^{\pi/2} n(\theta)v(\theta)D(\theta)d\theta \right] dE$$

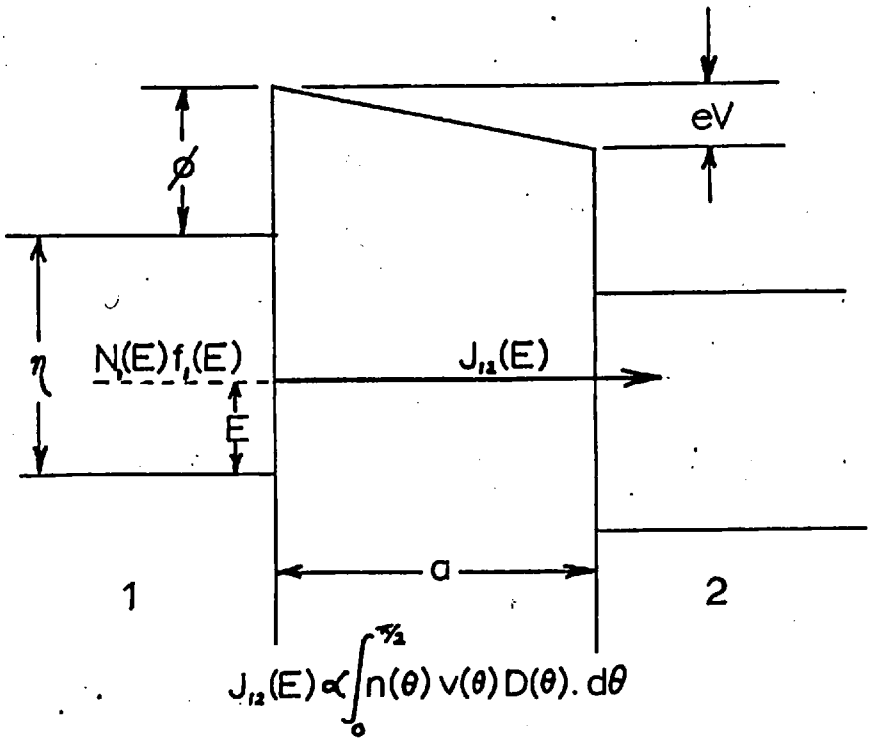

$$J_{12}(E) \propto \int_0^{\pi/2} n(\theta)\, v(\theta)\, D(\theta).\, d\theta$$

Fig (2.16) An inter-island potential barrier

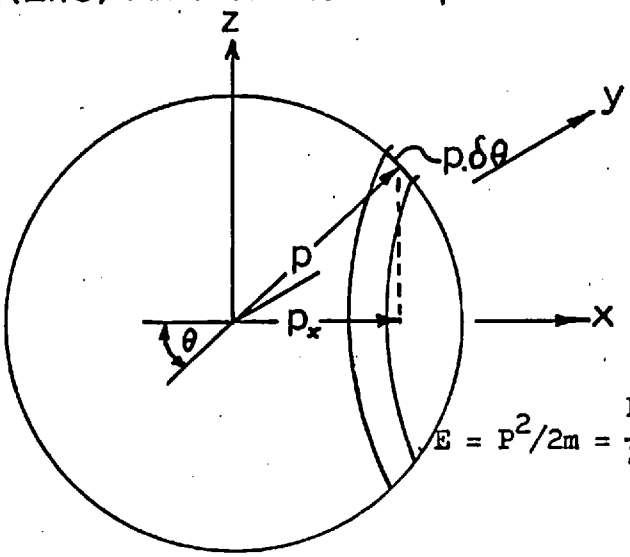

$$E = P^2/2m = \frac{P_x^2}{2m} + \frac{P_y^2}{2m} + \frac{P_z^2}{2m} = E_x + E_y + E_z = \eta$$

$$v(\theta) = \frac{P}{m}\cos\theta \qquad n(\theta) = \frac{\sin\theta}{2}\,\delta\theta \qquad D(\theta) = \exp\frac{-4\pi}{h}\int_0^a \left[2m(\eta+\phi_x-E\cos^2\theta)\right]^{\frac{1}{2}} dx$$

Fig (2.17) The surface of the electron distribution in momentum space

As the potential difference between adjacent islands is $\sim 10^{-5}$ volts the product of $f_1(E)$ and $(1-f_2(E))$ is only finite near to the Fermi energy η, say in the range $\eta \pm 0.2$ KT. Also since $N_1(E)$ is proportional to $E^{\frac{1}{2}}$ it is possible to simplify $J_{1\to 2}$.

$$J_{12} = eN_1(\eta)\left[\int_0^{\pi/2} n(\theta)v(\theta)D(\theta)d\theta\right]_{E=\eta} \times \int_0^{\infty} f_1(E)(1-f_2(E))\, dE.$$

This form is much easier to evaluate. It remains now to determine the form of its particular components.

2.4.3 Thermodynamic equilibrium

When an electron transfers from one island to another by what ever means the charge on the receiving island increases by -e and the transmitting island assumes a positive charge +e. The energy required to charge the islands can be calculated by the method of images. For convenience the islands will be assumed spherical, radius r and separation d.

Fig. 2.18 Spherical model

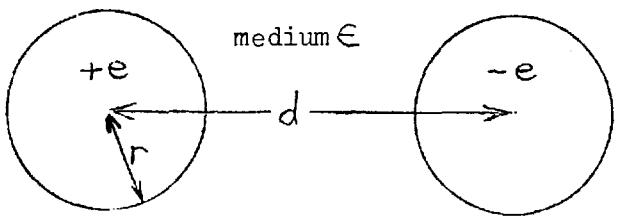

The capacity of the pair of spheres is C where

$$C = \frac{4\pi\epsilon\epsilon_o r}{2}\left[1 + f(m)\right]$$

and $f(m) = m + m^2 + m^3 + 2m^4 + 3m^5 \ldots \qquad m = {}^{r}/_{d}.$

as $m \to 0 \quad f(m) \to 0.$

The energy required to charge the arrangement by a single electron transfer

$$= {}^{1}/_{2}\, e^2/c = {}^{1}/_{2}.e^2.\frac{2}{4\pi\epsilon\epsilon_o r\left[1 + f(m)\right]}$$

$$= \frac{e^2}{4\pi\epsilon\epsilon_o r\left[1 + f(m)\right]} = W$$

Since $Q = VC$

$$V = \frac{2e}{4\pi\epsilon\epsilon_o r\left[1 + f(m)\right]}$$

Therefore the potential of each island will change by

$$\frac{e}{4\pi\epsilon\epsilon_o r\left[1 + f(m)\right]} = \frac{W}{e}$$

This is illustrated by Fig. (2.19).

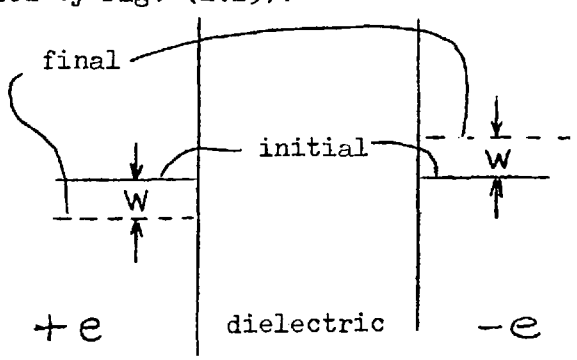

Fig. (2.19) The displaced energy level system of a charged island pair

Thus unless an electron has an energy greater than W above the undisplaced Fermi level of the transmitting island it will be unlikely to encounter a vacant state at that energy in the displaced energy level system of the receiving island.

If there are N islands in the array described by Fig. (2.14) then 2n will be charged where n is given by

$$\frac{2n}{N-2n} = e^{-W/KT}$$

where, for simplicity, Boltzmann statistics are assumed.

hence $$2n = \frac{Ne^{-W/KT}}{(1+e^{-W/KT})}$$

Of these, half will be positive and half negative. Therefore at temperature T

$\frac{Ne^{-W/KT}}{2(1+e^{-W/KT})}$ islands will be positive and negative,

and $\frac{N}{1+e^{-W/KT}}$ islands will remain neutral.

Fig. (2.20) shows their relative proportions plotted against W/KT.

2.4.4. The four types of electron transition

Having established an equilibrium distribution of charged islands one must now go on to consider the transitions of electrons from one kind of island to another. There are four possibilities,

(i) neutral and neutral

(ii) negative and neutral

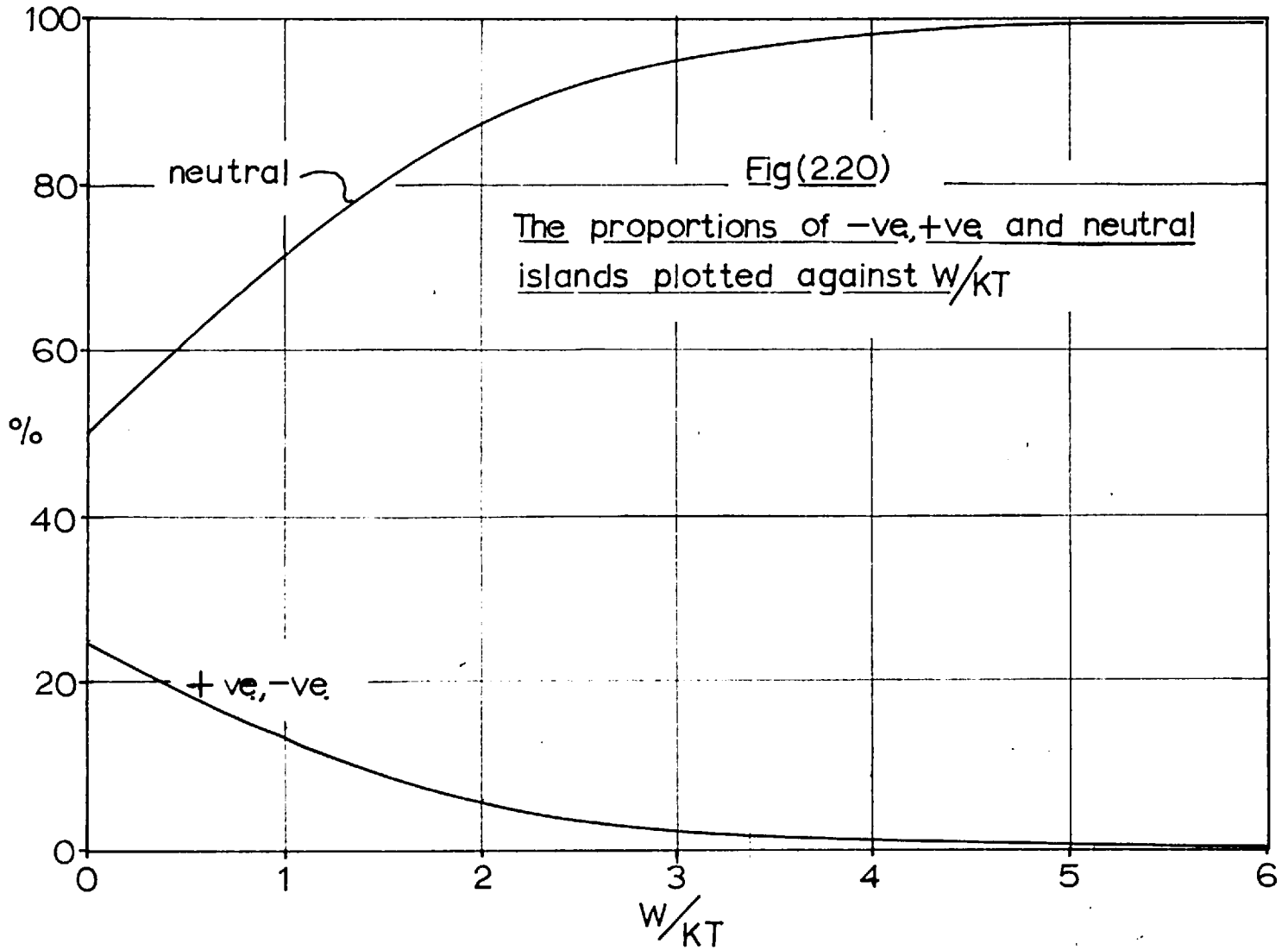

Fig(2.20)

The proportions of −ve, +ve and neutral islands plotted against W/KT

(iii) positive and neutral

(iv) positive and negative

Clearly when very few of the islands are ionised transitions of the fourth kind will be very unlikely. A general expression involving all of the processes will be derived and approximations provided for high and low values of W/KT. Fig. (2.21) describes the energy level systems of three adjacent islands for each of the four cases to be considered. The diagrams show the positions of the Fermi levels before and after the electron has transferred between adjacent islands.

First consider <u>case (i), neutral and neutral</u>

When no field is applied the components of current to the right and left are equal and there is no net current flow. The component to the right is given by

$$J \alpha N \frac{1}{(1+e^{-W/KT})^2} \int_{-\infty}^{+\infty} f(E)\,(1 - f(E - W))\,dE.$$

Applying a field so that $V_1 - V_2 = V_2 - V_3 = V$, then the total current is given by

$$J \alpha N \left(\frac{1}{1+e^{-W/KT}}\right)^2 \int_{-\infty}^{+\infty} f(E)\left[f(E - W - eV) - f(E - W + eV)\right] dE.$$

Let us denote these integrals by I_1 and I_2 respectively.

<u>Case (ii), negative and neutral pairs</u>

Without an applied field the component of current to the right is given by

Fig (2.21) Energy level diagrams showing the four electron transfer cases

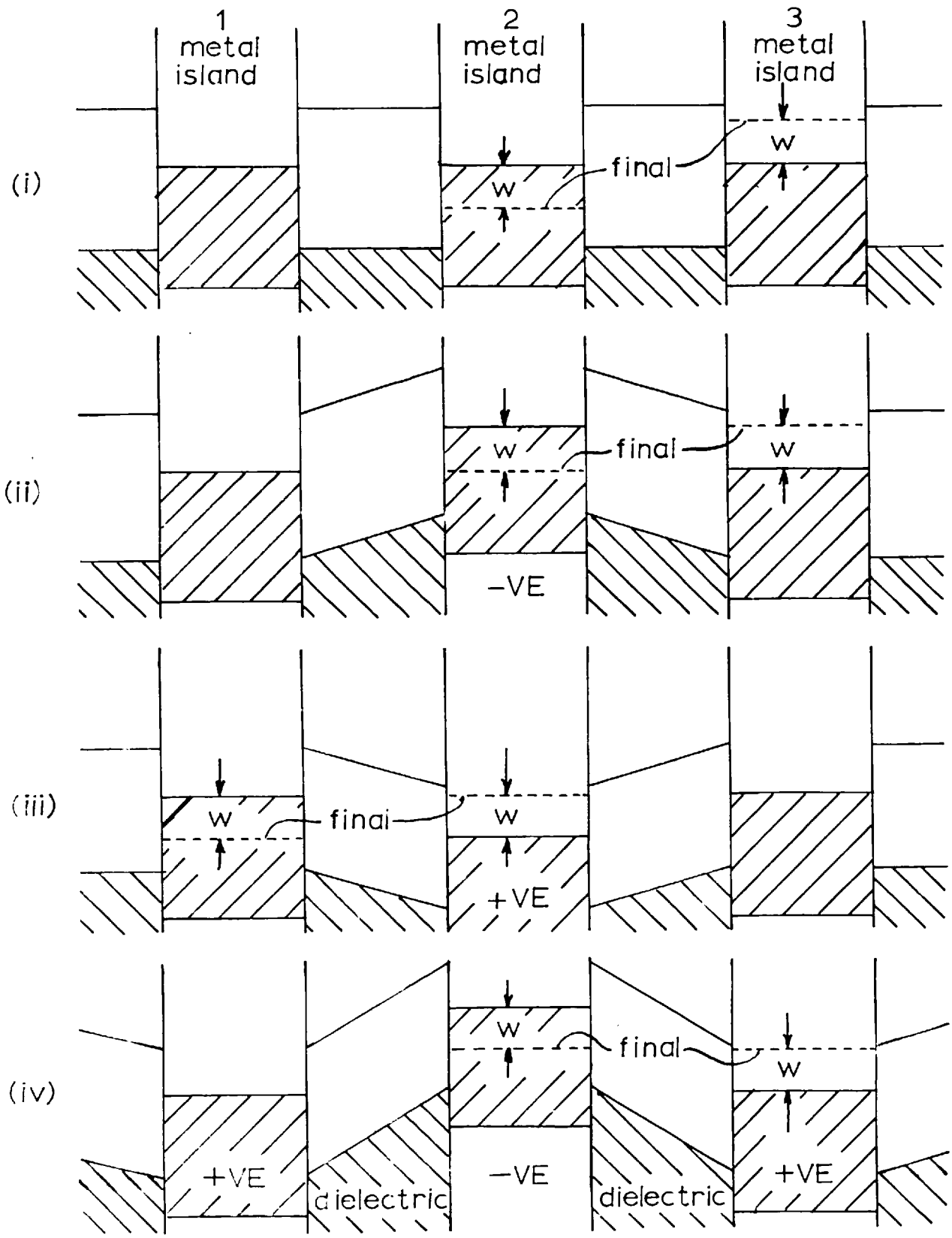

$$J \alpha N \frac{e^{-W/KT}}{2(1+e^{-W/KT})^2} \int_{-\infty}^{+\infty} f(E)\,(1 - f(E))\,dE$$

and applying a field as before it becomes

$$J \alpha N \frac{e^{-W/KT}}{2(1+e^{-W/KT})^2} \int_{-\infty}^{+\infty} f(E) \left[f(E-eV) - f(E+eV) \right] dE,$$

let us denote these integrals by I_3 and I_4 respectively.

Case (iii), positive and neutral pairs

Without an applied field the component of current to the right is given by

$$J \alpha N \frac{e^{-W/KT}}{2(1+e^{-W/KT})^2} \int_{-\infty}^{+\infty} f(E)\,(1 - f(E)\quad dE.$$

Applying a field,

$$J \alpha N \frac{e^{-W/KT}}{2(1+e^{-W/KT})^2} \int_{-\infty}^{+\infty} f(E) \left[f(E - eV) - f(E + eV) \right] dE$$

These are integrals I_3 and I_4.

Case (iv), positive and negative pairs

Without an applied field the component of current to the right is given by

$$J \alpha \frac{N}{4} \frac{e^{-2W/KT}}{(1+e^{-W/KT})^2} \int_{-\infty}^{+\infty} f(E)\,(1 - f(E + W))\quad dE.$$

On applying the field the current is given by

$$J \alpha \frac{N}{4} \frac{e^{-2W/KT}}{(1+e^{-W/KT})^2} \int_{-\infty}^{+\infty} f(E) \left[f(E+W-eV) - f(E+W+eV) \right] dE$$

Denote these integrals by I_5 and I_6 respectively.

It is useful at this point to refer to Fig. (2.14) describing the idealised model of a thin film. The total current flowing in the film flows through a row of islands perpendicular to the field direction. Let N now be the number of islands per unit length of such a row. The total current can now be obtained by adding the four contributions. The integrals involved are all of the form

$$\int_{-\infty}^{+\infty} f(E) \left[f(E - W - eV) - f(E - W + eV) \right] dE$$

and have been evaluated in Appendix A.

Thus the total current is given by

$$J_{total} \alpha N \left[\frac{1}{(1+e^{-W/KT})^2} (I_1 - I_2) + \frac{e^{-W/KT}}{(1+e^{-W/KT})^2} (I_3 - I_4) + \frac{e^{-2W/KT}}{4(1+e^{-W/KT})^2} (I_5 - I_6) \right]$$

On substitution of the integrals this reduces to

$$J_{total} = NeV. \frac{3}{2} . \frac{(2+e^{-W/KT})}{(1+e^{-W/KT})^2 (1+e^{W/KT})}$$

Let this be denoted NeV. P(T). The function P(T) has been plotted against $^{W}/_{KT}$ in Fig. (2.22). The form of this will be discussed later with reference to the temperature dependence of conductivity. The relative values of the three processes are shown in Fig. 2.23.

2.4.5 The electron flux

The previous section was concerned with the occupancy of transmitting and receiving states. It has been pointed out that the function

$$f(E)\ (1 - f(E))$$

is only finite near to the Fermi level. This means that the only contribution is that of electrons at or close to that energy η. As the density of states function is $g \propto E^{\frac{1}{2}}$ it will vary little between $(\eta - 0.2eV)$ and $(\eta + 0.2eV)$ when η is typically 6eV. Hence g will be assumed constant at $g(\eta)$ over that range.

The electron flux is of the form

$$F = \int_0^{\pi/2} g(\eta)\ n(\theta)\ v(\theta)\ D(\theta)\ d\theta$$

Referring back to Fig. (2.17), which is a diagram of the Fermi surface in momentum space, $n(\theta)$ is the proportion of states having an x directed velocity $\frac{P}{m}\cos\theta$

$$n(\theta) = \frac{2\pi p \sin\theta\ p\ \delta\theta}{4\pi p^2} = \frac{\sin\theta}{2} \cdot \delta\theta.$$

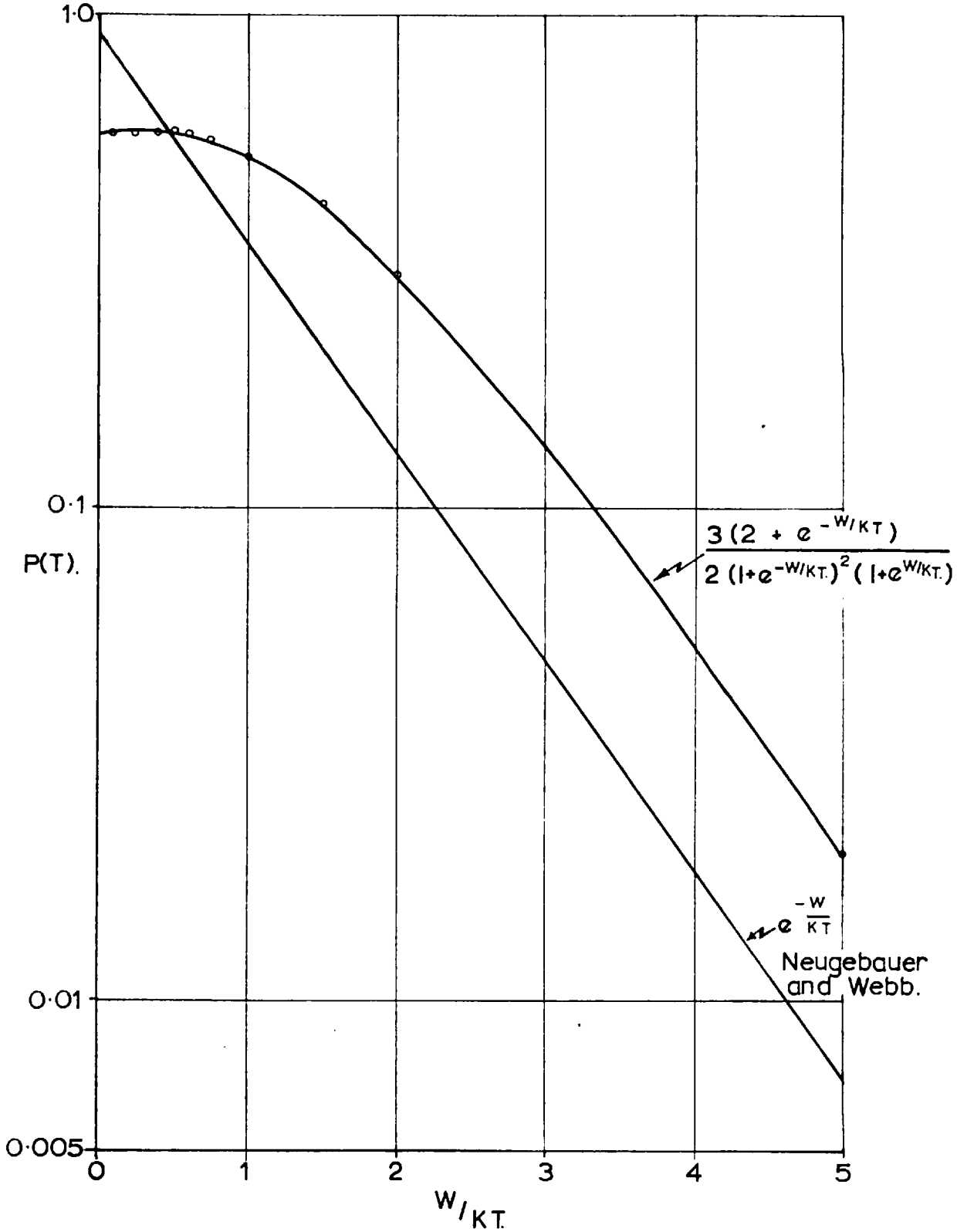

FIG. 2·22. P(T) plotted against W/KT.

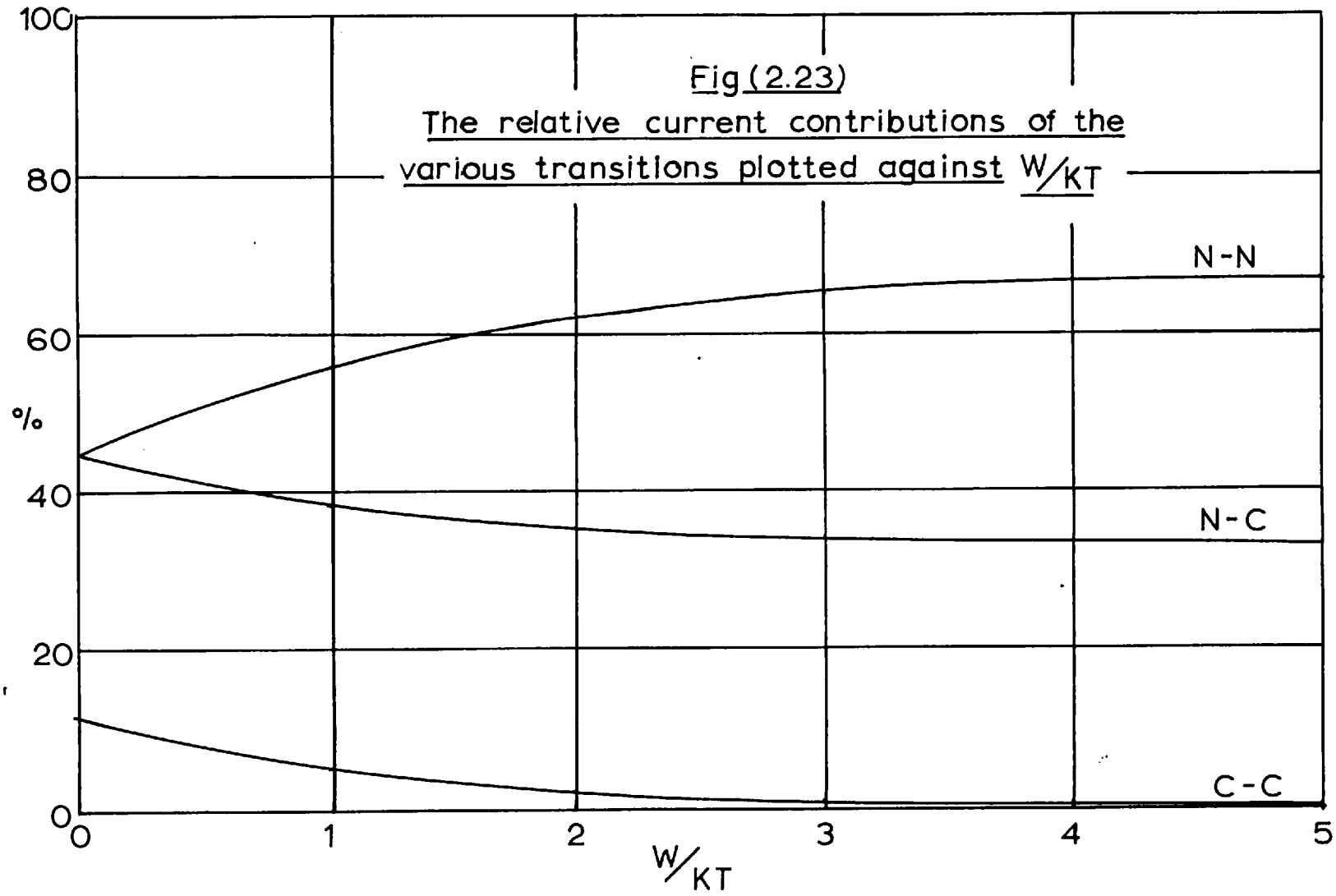

Fig (2.23)

The relative current contributions of the various transitions plotted against W/KT

$$\therefore F(\eta) = g(\eta) \int_0^{\pi/2} \frac{p \sin\theta \cos\theta}{2m} \cdot D(\theta)\, d\theta.$$

$D(\theta)$ is the W.K.B.[57] approximation of the quantum mechanical tunnelling probability of an electron having an x velocity $\frac{p\cos\theta}{2m}$.

$$D(\theta) = \exp\left[-\frac{4\pi}{h}\int_0^a (\eta+\phi_x - \eta\cos^2\theta)^{\frac{1}{2}}\,(2m)^{\frac{1}{2}}\,dx\right]$$

This can be applied to a rectangular barrier, width a and ϕ high. It will be shown later that more complicated barrier shapes can be approximated to a rectangular form with appropriate parameters.

$$\therefore D(\theta) = \exp\left[-\frac{8\pi a m^{\frac{1}{2}}}{h\sqrt{2}}\,(\eta+\phi-\eta\cos^2\theta)^{\frac{1}{2}}\right]$$

denoting $\frac{8\pi a m^{\frac{1}{2}}}{h\sqrt{2}}$ as Ha

then

$$F(\eta) = g(\eta)\,\frac{(2m\eta)^{\frac{1}{2}}}{4m}\int_0^{\pi/2} \sin 2\theta \exp - Ha(\eta+\phi-\eta\cos^2\theta)^{\frac{1}{2}}.\, d\theta.$$

Let $F(\eta) = g(\eta)\,\frac{(2m\eta)^{\frac{1}{2}}}{4m} \cdot M$

changing variables to $\cos 2\theta = x$

$$M = -\tfrac{1}{2}\int_{+1}^{-1} d(\cos 2\theta)\exp\left[-Ha\left[\eta+\phi-\tfrac{\eta}{2}(\cos 2\theta+1)\right]^{\frac{1}{2}}\right]$$

$$= \tfrac{1}{2}\int_{-1}^{+1} \exp\left[-Ha\left(\eta+\phi-\tfrac{\eta}{2}(x+1)\right)^{\frac{1}{2}}\right].dx$$

$$= -\frac{2}{(} \left[\left(\eta+\phi - \frac{\eta}{2}(x+1)\right)^{\frac{1}{2}} \exp - Ha \left(\eta+\phi - \frac{\eta}{2}(x+1)\right)^{\frac{1}{2}} \right]_{-1}^{+1}$$

$$= \frac{2}{Ha} \left[\phi^{\frac{1}{2}} \exp(- Ha\phi^{\frac{1}{2}}) - (\eta+\phi)^{\frac{1}{2}} \exp(- Ha(\eta+\phi)^{\frac{1}{2}}) \right]$$

when typical values are substituted say,

$$a = 10A^{\circ} \ , \quad \eta = 6eV \quad \text{and } \phi = 1eV$$

$$\exp (- Ha\phi^{\frac{1}{2}}) = e^{-10.3}$$

clearly the other exponential term is negligible in comparison and the expression reduces to

$$F(\eta) = g(\eta) \cdot \frac{h}{8\pi am} \quad (\frac{\phi}{\eta})^{\frac{1}{2}} \exp(- Ha\phi^{\frac{1}{2}})$$

Substituting

$$g(\eta) = 4\pi \ (\frac{2m}{h^2})^{3/2} \cdot \eta^{\frac{1}{2}}$$

$$F(\eta) = \frac{(2m\phi)^{\frac{1}{2}}}{h^2 a} \cdot \exp(- Ha\phi^{\frac{1}{2}})$$

This function is very strongly dependent on the separation of the islands a. It is shown plotted in Fig. (2.24) against a for two typical values of ϕ.

2.4.6 Calculation of the sheet resistivity and T.C.R. of a discontinuous film

The function $F(\eta)$ expresses the maximum possible electron flux

Fig(2.24)

$\log_{10}F(\eta)$ v island separation

(η =6eV.)

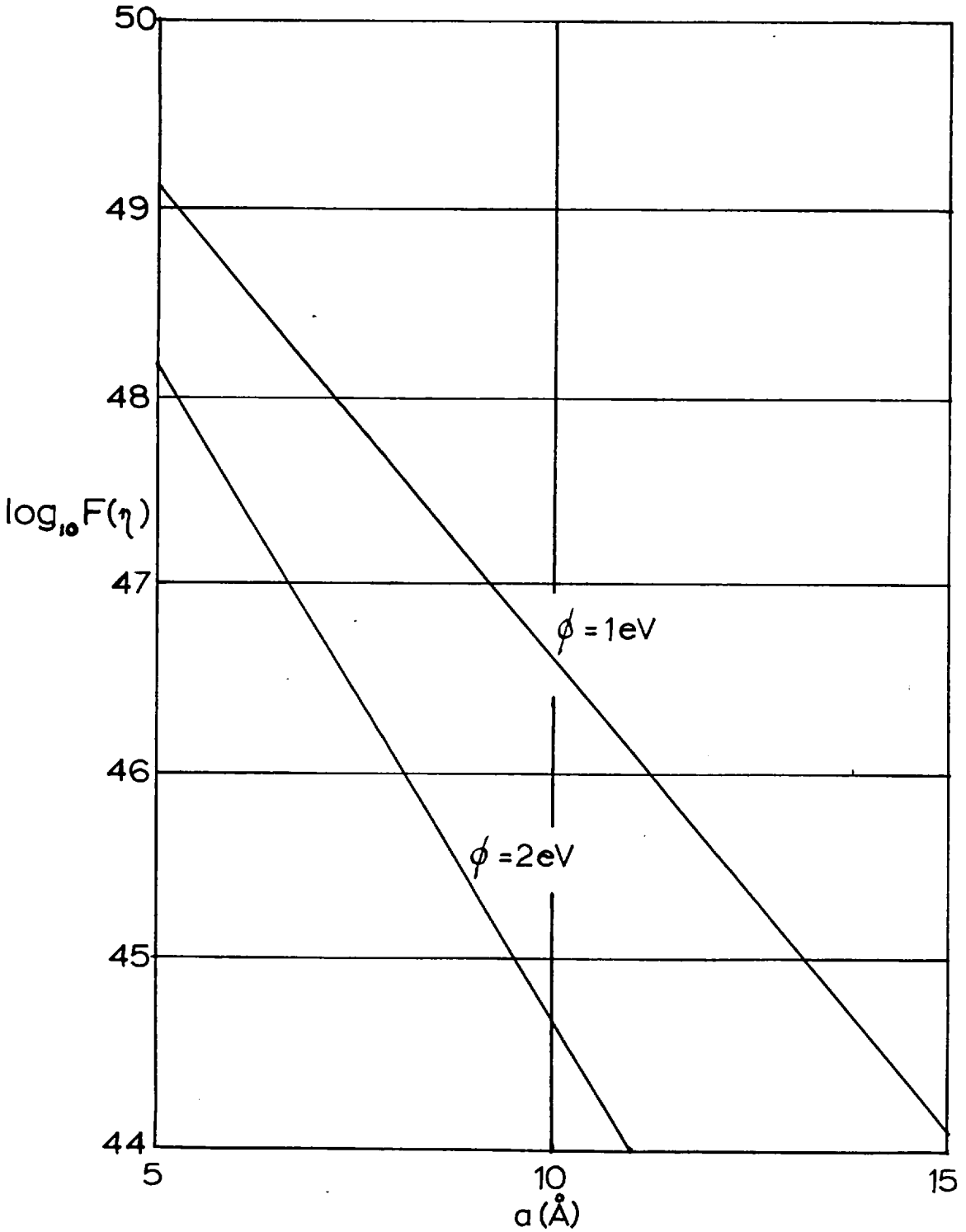

through a rectangular potential barrier. To determine the actual current it must be modified by the expression involving the function P(T) which describes the occupation of electron states on both sides of the gap.

The total current is given by,

$$I = eVN\,P(T) \cdot F(\eta) \cdot e \cdot \text{x island cross-sectional area.}$$

where N is the number of islands per unit width of film, and is given by:-

$$N = \frac{1}{(1+a)} \text{ per unit width}$$

V is the interisland potential difference, if $V_{applied}$ is the voltage per unit length of film

i.e. $V = V_{applied} \times (1+a)$

assuming that there is negligible voltage drop in the islands. Thus,

$$I = eV_{applied}\,P(T) \cdot F(\eta) \cdot e \cdot ld$$

giving an expression for the sheet resistivity

$$\rho_{sheet} = \frac{1}{e^2 \cdot ld \cdot P(T) \cdot F(\eta)}$$

$$= \frac{2h^2 a \exp(Ha\phi^{\frac{1}{2}})}{3e^2 ld(2m\phi)^{\frac{1}{2}}} \cdot \frac{(1+e^{-W/KT})^2(1+e^{W/KT})}{(2+e^{-W/KT})} \qquad (2.9)$$

This is rather complicated but it can be approximated when $W/KT > 2.5$.

$$\rho_{sheet} = \frac{h^2 a \exp(Ha\phi^{\frac{1}{2}})}{3e^2 ld(2m\phi)^{\frac{1}{2}}} \cdot e^{W/KT}.$$

and when $\frac{W}{KT} \rightarrow 0$.

$$\rho_{sheet} \quad \frac{16h^2 a \exp(Ha\phi^{\frac{1}{2}})}{9e^2 ld(2m\phi)^{\frac{1}{2}}}$$

The dependence on island size and separation is shown in Figs. (2.25) and (2.26).

Neugebauer and Webb considered only the charged and neutral island transitions. Since the expression for sheet resistivity is dominated by the term $e^{aH\phi^{\frac{1}{2}}}$ the two theories correspond to within a factor of two or three. Figs. (2.25) and (2.26) show comparison curves.

The expression for sheet resistivity can be differentiated to derive the temperature coefficient of resistance. This yields

$$\alpha = + \frac{W}{KT^2} \quad \frac{3e^{-W/KT} + e^{-2W/KT} - 2e^{+W/KT}}{(1+e^{W/KT})(1+e^{-W/KT})(2+e^{-W/KT})}$$

This predicts a zero T.C.R. when $\frac{W}{KT} = 0.35$ and it passes through a maximum of ~ 40 p.p.m./^{o}C at $W/KT = 0.2$. On decreasing W/KT still further $\alpha \rightarrow 0$ as W/KT tends to zero. This contrasts with the simple exponential dependence which emerges from considering only the charged and neutral island pairs. The two dependencies are shown plotted for typical values of W/KT in Fig. (2.27).

The agreement between the two theories improves as W/KT becomes large. This is expected because the transitions are mainly charged-neutral and neutral-neutral. Though Neugebauer and Webb only considered charged-neutral pairs the temperature dependence would be the same

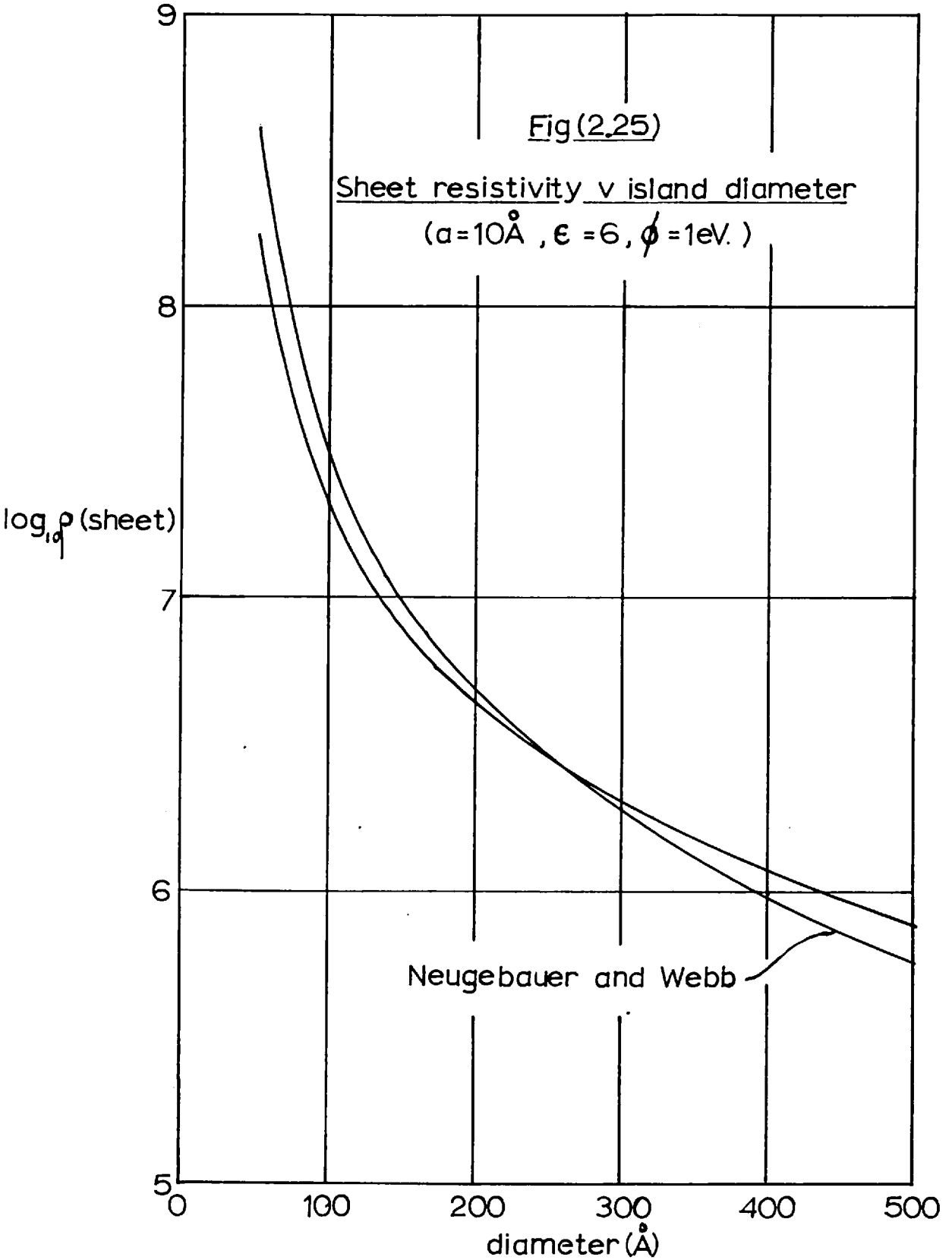
Fig (2.25)
Sheet resistivity v island diameter
(a = 10Å , ε = 6, ϕ = 1eV.)
log10 ρ (sheet)
9
8
7
6
5
0
100
200
300
400
500
diameter (Å)
Neugebauer and Webb

Fig(2.26)

Sheet resistivity v island separation

(island diameter = 100Å, $\epsilon = 6$, $\phi = 1$eV.)

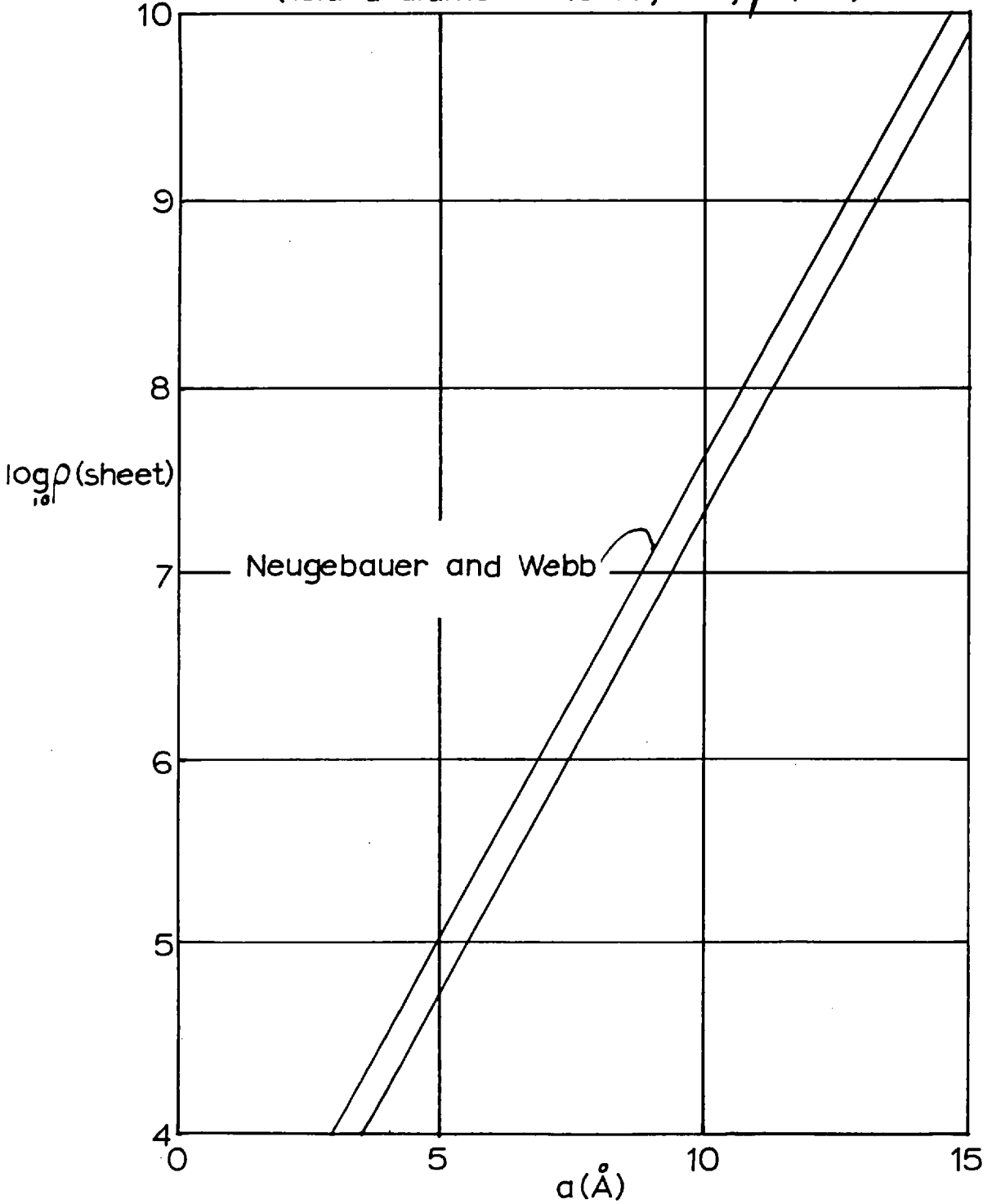

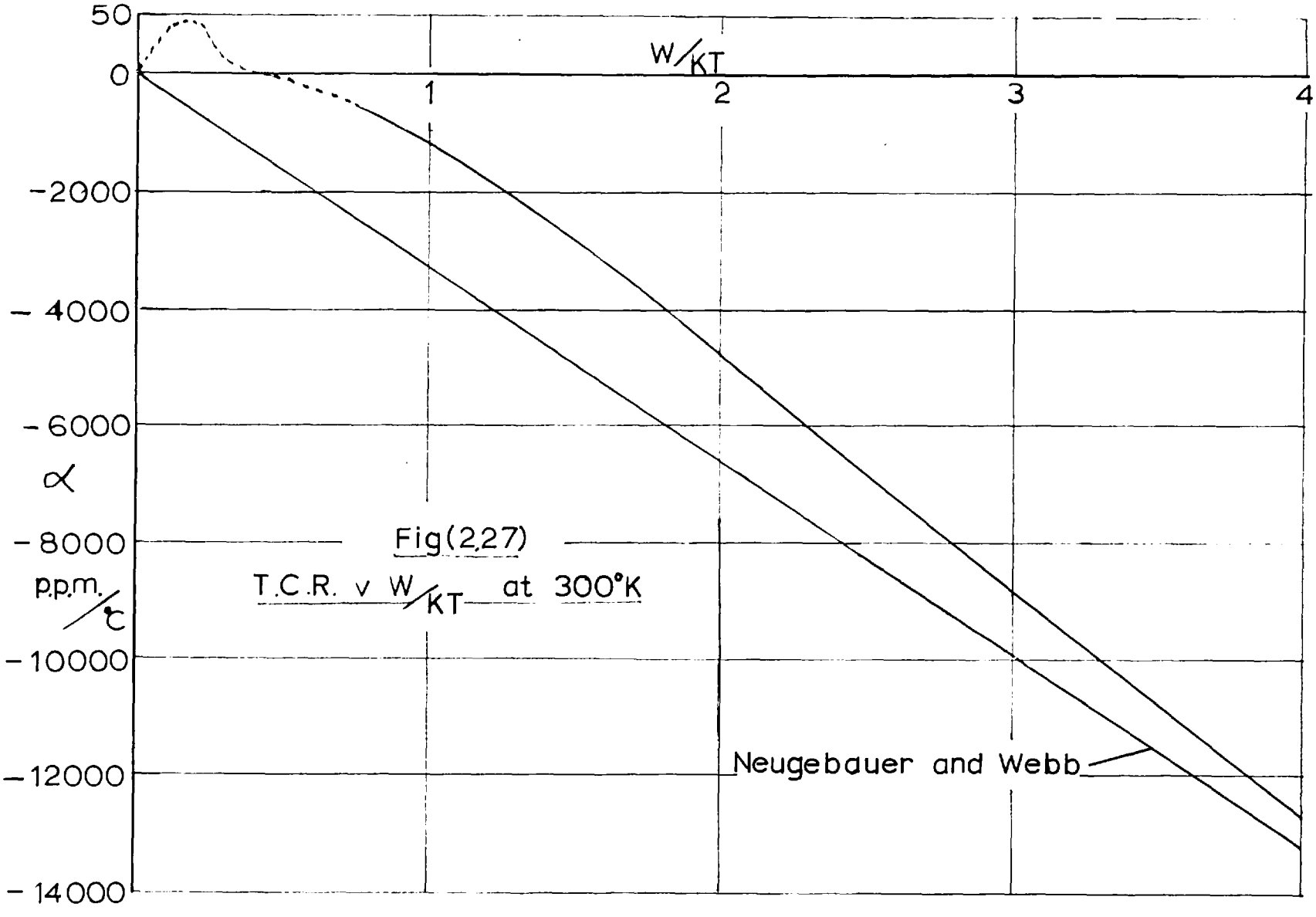
50
0
W/KT
1
2
3
4
-2000
- 4000
- 6000
α
- 8000
p.p.m./°C
- 10000
- 12000
- 14000
Fig(2.27)
T.C.R. v W/KT at 300°K
Neugebauer and Webb

because one generates the other. However, as $^{W}/KT$ decreases, the number of charged islands increases so increasing the importance of transitions involving them. At the same time the number of neutral islands is reduced so that the contributions from the neutral-neutral transitions decreases. This eventually leads to the net rate of increase of current being negative. When $^{W}/KT$ is very small the system saturates so that 50% of the islands are charged and the other half are neutral. There is then no further change of current when $^{W}/KT$ is reduced, giving a zero temperature coefficient of resistance. For convenience the dependence of T.C.R. on island size is shown in Fig. (2.28) and this can be directly related to Fig. (2.27).

In practice it would be difficult to separate the positive effect of the metallic component of resistance which would become apparent as the films grow thicker. Also, it has been assumed that islands gain and lose only one electron. They would of course become multiply ionised if $^{W}/KT$ were small enough. Under these circumstances the problem becomes exceedingly complicated because of the multitude of transitions which are possible. Since it requires four times the energy to doubly ionise an island than to singly ionise one the model might be expected to breakdown when $^{W}/KT \sim 0.75$ when the number of doubly ionised islands would be 0.05 of the number of singly ionised ones.

2.4.7. Real potential barriers (i) Image forces

The model of conduction described above is based on tunnelling

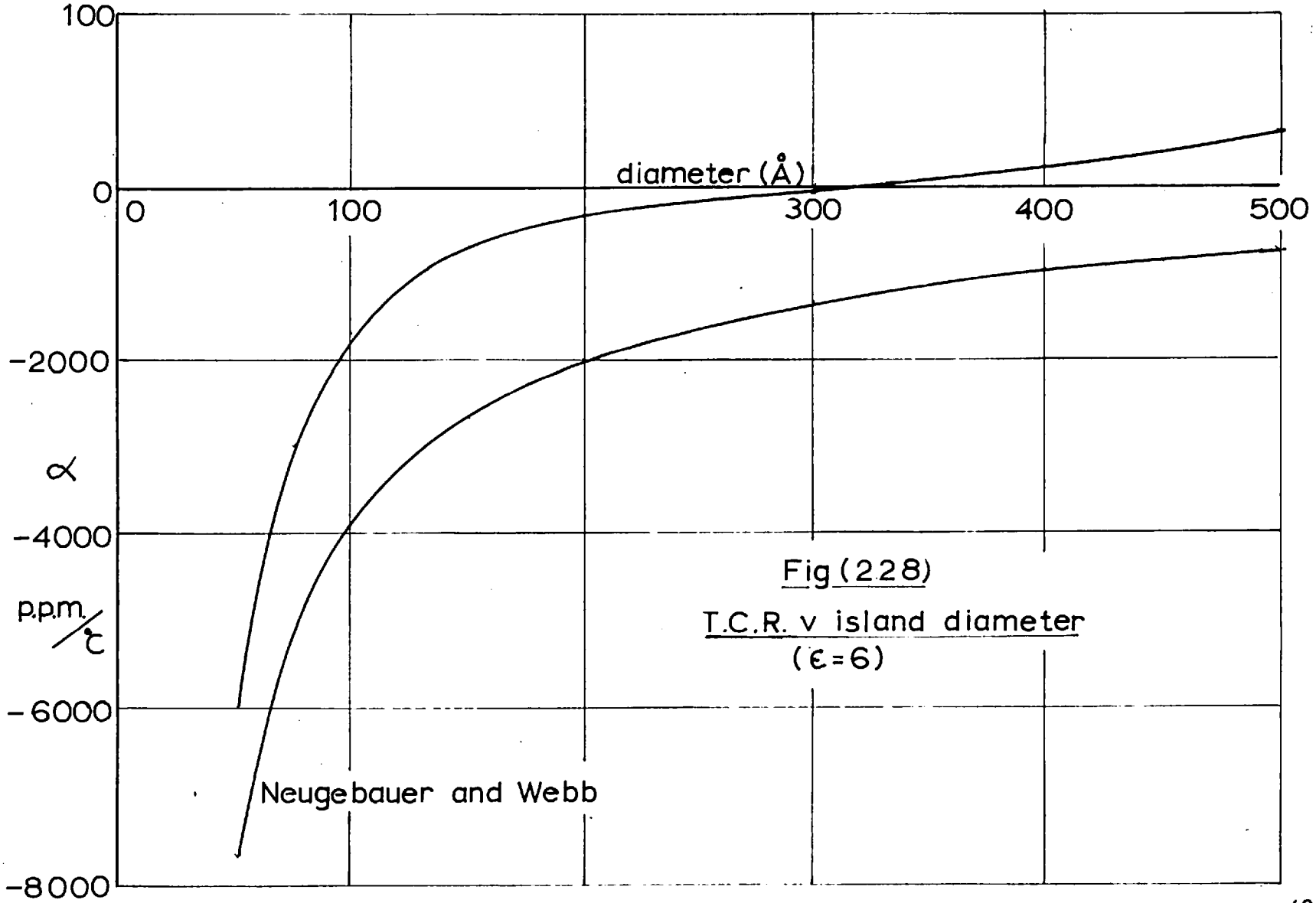

Fig (228)

T.C.R. v island diameter

($\epsilon = 6$)

through a rectangular potential barrier as this was easy to handle analytically. In practice barrier shapes deviate from the rectangular form owing to the potential due to image forces. When particles are separated by very small distances, as are islands in a thin film, the effect of multiple images must be considered. With spherical particles this is difficult to analyse, however, Hill[58] has shown that the shape of the image potential is very similar to that between plane parallel electrodes.

This case has been considered by Simmons[59] and the potential was found to approximate to

$$\phi(x) = \phi_o - \frac{1.15\ \ln_e 2\ ea}{8\pi\epsilon\epsilon_o\ x(a-x)} \qquad (eV)$$

ϕ_o is the undisturbed potential barrier ht. w.r.t. the F rmi level, a is the gap width, x the position in the gap and ϵ the relative permittivity of the dielectric.

The new quantum mechanical transmission probability can be obtained by substitution in the W.K.B. formula,

$$D(E_x) = \exp\left[-\frac{4\pi}{h}\int_o^a (\eta + \phi(x) - E_x)\ (2m)^{\frac{1}{2}} dx\right]$$

Simmons has simplified this form to give

$$D(E_x) \simeq \exp\left[-\frac{4\pi\Delta x(2m)^{\frac{1}{2}}}{h}\ (\eta + \overline{\phi} - E_x)^{\frac{1}{2}}\right]$$

where $\overline{\phi}$ is the average value of $\phi(x)$

$$\overline{\phi} = \frac{1}{\Delta x} \int_{x_1}^{x_2} \phi(x)\, dx$$

x_1 and x_2 are the values of x at the Fermi level; the width of the barrier at all energies is assumed to be that at the Fermi level

i.e., $-x_1 + x_2 = x$.

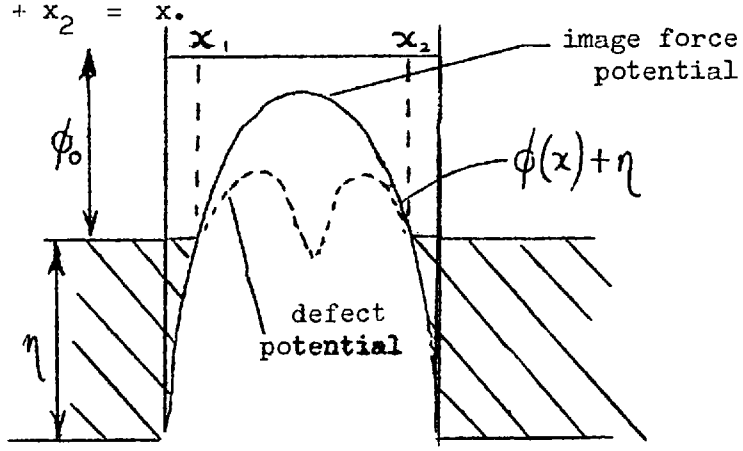

Fig. (2.29) The effect of image forces and charged defects

(ii) Defect states

The shape of the barrier can also be modified by the presence of charged defects in the dielectric. In an oxide substrate this may be due to metallic impurity ions or oxygen vacancies. Fig. (2.29) shows the effect of a positive ion on an otherwise normal potential barrier when the ion is situated near the centre of the barrier.

Penley[60] and Schmidlin[61] have deduced the effect on the transmission coefficient assuming a coulombic potential field near the ion. If the potential well formed is shallow it may only depress the barrier but a deeper well may trap electrons and act as a source of electrons,

or virtual cathode, near to the receiving island. Fig. (2.30) shows the influence of singly and doubly ionised defects on the tunnel current. To arrive at this Schmidlin assumed one defect per unit square thickness of film.

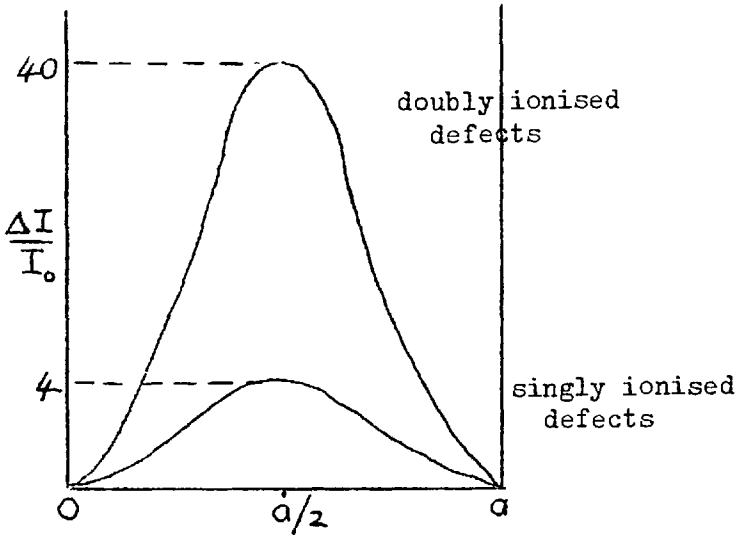

Fig. (2.30) Schmidlins curve of increased tunnel current in a thin film sandwich.

(iii) Amorphous substrates

In most practical cases thin films are deposited on amorphous substrates, e.g. SiO, glass, Al_2O_3. Since they lack a regular periodic structure their band structure is not well defined as in a crystal. Frohlich[62] has suggested that the edges of the energy bands are not abrupt but decay exponentially. This would lead to a potential barrier containing a spectrum of allowed states within the energy gap. This is shown schematically in Fig. (2.31).

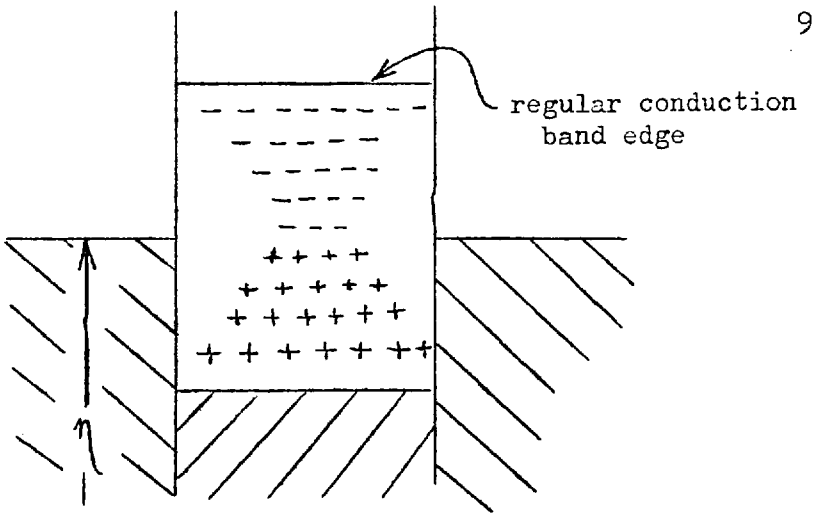

Fig. (2.31) Schematic diagram showing the extra states in an amorphous dielectric

It was Hill[22] who first pointed out that the presence of such states could increase the transmission probability by permitting tunnelling to an intermediate state and then to the next island. If the density of states were large enough, tunnelling could proceed from one state to another, rather like impurity band conduction in semiconductors. This may well be the only way by which electrons can transfer from one island to another when the gap size is $\sim$100 A^{o}, such that the transmission probability would otherwise be zero[21]. It is extremely difficult to predict this effect quantitatively since the spectrum of defect states is not easily determined.

2.5 Summary

It has been shown that the effect of surface scattering of electrons in thin films is not apparent in measurements of ρ and α until the film thickness has been reduced to approximately ten times the electron mean

free path in the material. Its effect is to increase the resistivity and decrease the T.C.R. In gold this would be first apparent when the film thickness was approximately 4000A°, assuming a bulk value of mean free path. It is expected that the size effect should disappear at a thickness approximately equal to the mean free path when the function $\frac{d\rho}{dT}/\frac{d\rho_o}{dT}$ is plotted against thickness and would therefore provide a means of determining the mean free path using thinner films.

Unless steps are taken to maintain continuity down to small thicknesses films become discontinuous at about 200A° depending on the material, the substrate and the growth conditions. At that stage the resistance rises rapidly and the temperature coefficient becomes negative. A theory has been constructed to account for this using inter-island tunnelling and an activation process. Although the model bears a close resemblance to that of Neugebauer and Webb[19] it is felt that it provides a more realistic picture of the conduction process. The two models provide values of resistivity which are in close agreement because this is mainly determined by the island separations. Disagreement arises when the island activation energies are small compared with thermal energies. Under these conditions the new model predicts that temperature coefficient becomes positive, passes through a maximum and assymptotically approaches zero. The decrease to zero is so gradual that it is only noticeable at extremely small values of W/KT. On the other hand the theory of Neugebauer and Webb fails to

produce a maximum and predicts that the T.C.R. remains negative and approaches zero at small values of $^{W}/_{KT}$. Experimentally it would be difficult to confirm either dependence owing to the onset of metallic conduction in thicker films and multiple ionisation.

For an island separation of $10A^{\circ}$ the sheet resistivity predicted is $\sim 10^{7}\Omega/\square$. This indicates that serious distortion of the inter-island potential barriers must result when conduction is observed in films with islands $\sim 50A^{\circ}$ apart. It is likely that charged impurities and electron states within the band-gap of the separating media could explain this. However, there is at present little quantitative information concerning their population and their effect on potential barrier shapes. Whilst the conductivity is extremely dependent on the island separation, its effect on the T.C.R. is negligible since this is mainly controlled by the island charging process.

CHAPTER III

Experimental apparatus and techniques

3.1 Introduction

The experimental work falls naturally into two parts

(i) the preparation and examination of nichrome and nickel films to relate their electrical properties to their structure.

(ii) the preparation and examination of continuous gold films to study surface scattering.

The origins and aims of this programme have been described in the previous chapters. Many of the techniques used which are common to both parts will only be described in Section 3.2.

3.2 Nichrome and nickel films

3.2.1 Introduction

The essential feature of this work was to prepare 80/20 nichrome films by flash evaporation at 10^{-5} torr and at pressures sufficiently low to eliminate oxidation of the films during deposition. It was decided to prepare a similar series of nickel films under the same conditions to study any effect of the added chromium. Preliminary experiments had shown that the resistance of discontinuous films increased on exposure to air, Fig. (3.1). It was therefore decided to perform the electrical measurements within the vacuum system at the

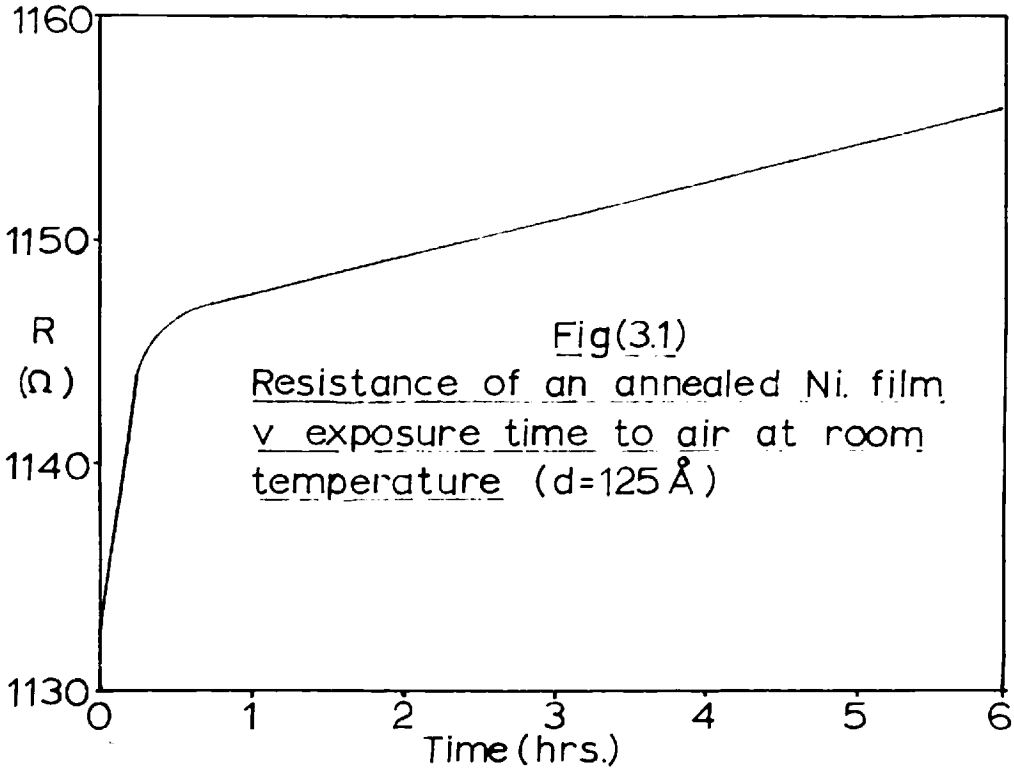

Fig (3.1)
Resistance of an annealed Ni. film v exposure time to air at room temperature (d=125 Å)

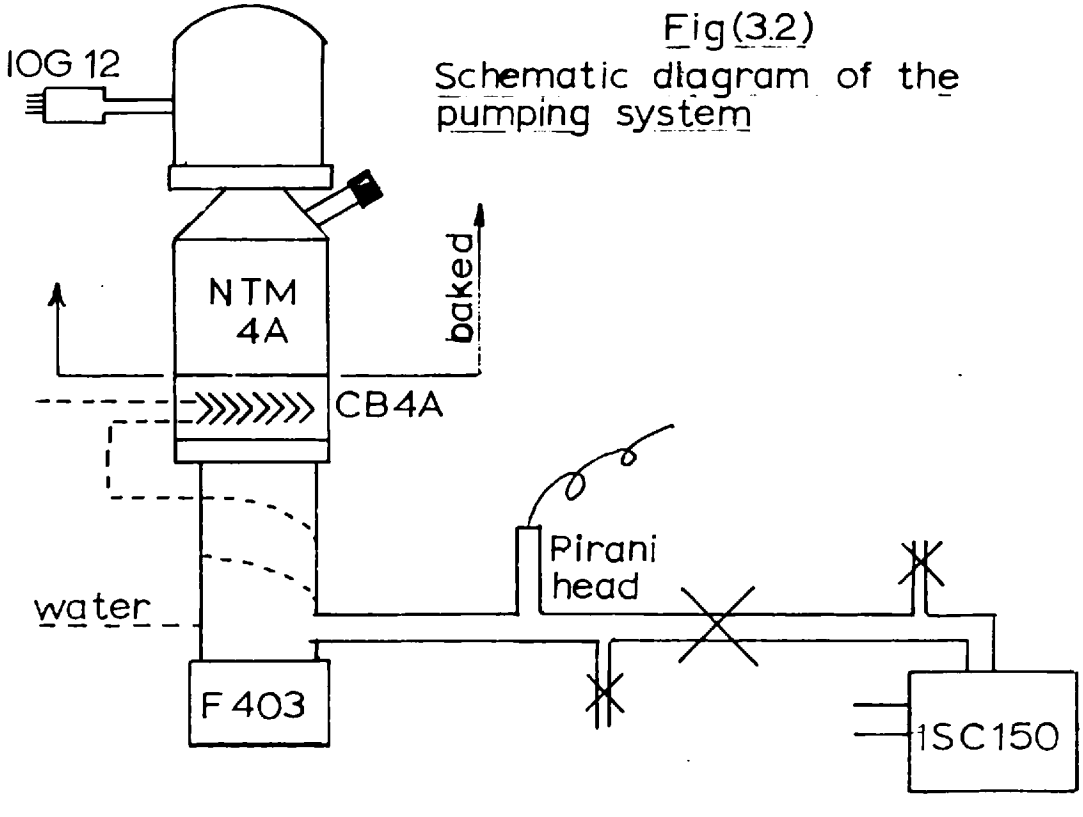

Fig (3.2)
Schematic diagram of the pumping system

preparation pressure.

3.2.2 The vacuum system

3.2.2.1 The pumping system

To these ends an ultra-high vacuum system was designed having an ultimate pressure in the 10^{-10} torr. pressure range. Fig. (3.2) is a schematic diagram of the pumping system comprising components manufactured by Edwards High Vacuum Ltd., Crawley. A 4"D. fractionating diffusion pump, type F403, and a low vapour pressure silicone oil MS705 were chosen to minimise oil contamination. The other high components were made of EN58 B stainless steel and were sealed together using metal ring gaskets.

The gaskets were either of 0.015"D annealed fine gold wire or $^1/_{32}$" D aluminium wire. No difference in their sealing capability was noticed. Gold seals were simply made by cold welding the overlapping ends of the ring of annealed wire during compression. The aluminium rings had to be butt welded in a gas flame using Alotectic flux and were often difficult to remove from the sealing surfaces. Schnorr high temperature conical spring washers were used to take up the thermal expansion of the sealing bolts on baking to 400°C.

3.2.2.2 The electrode inlet system and the experimental chamber

The electrode inlet system was mounted directly above the liquid nitrogen trap. It comprised a stainless steel annulus, 6"I.D., having 8 radial holes, $^3/_4$" D. Seven of these were used as electrode inlets

and the eighth was used as a connecting port to an ionisation gauge, type IOG12. The electrodes were originally designed for high power transmitting valves and are rated at 100 amps. These were manufactured by A.E.I. Ltd., type no. S70. Two of these electrodes were modified to carry four low current leads each, for the measuring leads and fuse wires. The electrodes were sealed to the ground surfaces of the annulus using metal gaskets.

The experimental chamber is shown in Plate 3.1. It was fabricated from a 15" length of stainless steel tube 6" I.D. and two 9" D flanges which were argon arc welded onto the tube. This was done by the British Oxygen Co. Ltd., Cricklewood. The sealing surfaces were then ground. The top plate of the chamber was a stainless steel disc containing three $^{3}/_{4}$" D electrode inlet holes and a 2" D hole used as a viewing port. One of the electrode inlet holes was used as a port for a low resolution mass spectrometer, another for a variable leak valve (Vacuum Generators type no. M6), and the third one was spare. An overall view of the system is shown in Plate 3.2.

3.2.2.3 The performance of the vacuum system

Using a 4KW oven which was rolled over the vacuum system it could be baked to $\sim 400^{\circ}C$. After baking for several hours the ultimate pressure of the system was $\sim 3 \times 10^{-10}$ torr., though this deteriorated over two years to 9×10^{-10} torr. This was presumably due to contamination and small leaks due to thermal cycling. By baking at $250^{\circ}C$ for

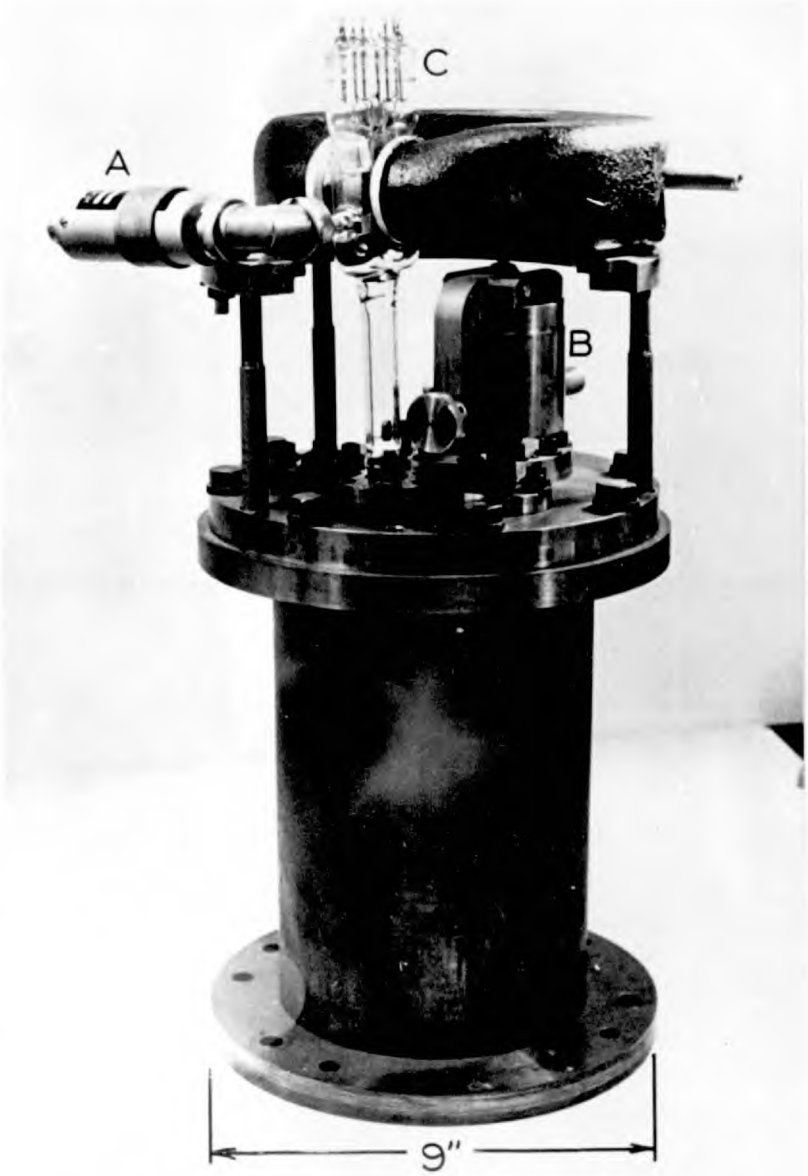

Plate (3.1)

The experimental chamber and mass spectrometer assembly

A electrometer amplifier

B bakable leak valve

C mass spectrometer tube

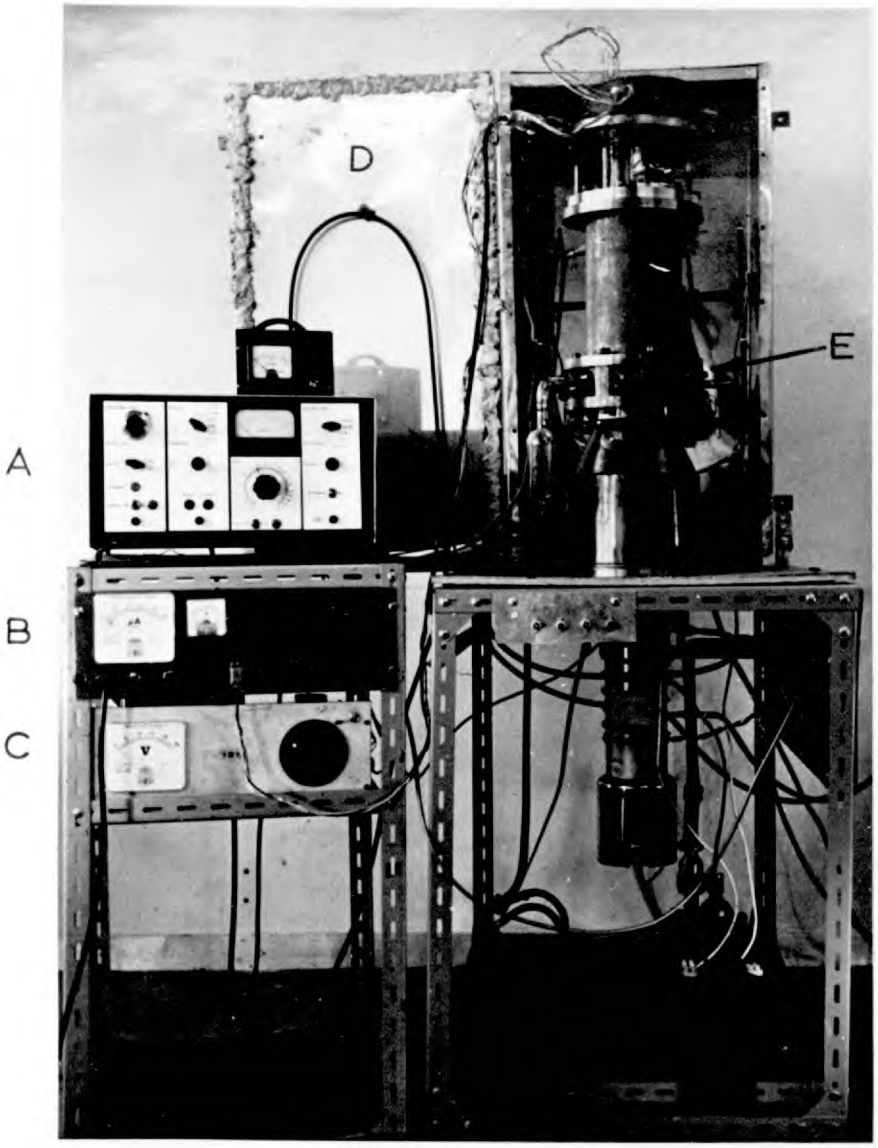

Plate(3.2)
An overall view of the system

A ion current amplifier (M.S.10 control unit)

B emission stabiliser

C voltage scanning unit

D baking oven

E electrode inlet ring

3 hours an ultimate pressure of 3×10^{-9} torr. could easily be achieved.

Using a 6" I.D. glass bell-jar sealed with a Viton-A L-gasket the ultimate pressure was 8×10^{-9} torr. after baking at 150°C for 2 hours. After preliminary baking this arrangement could achieve 3×10^{-8} torr. after several hours pumping without further baking. A bakable U.H.V. valve was not employed owing to its high cost. Unfortunately, this meant that the diffusion pump had to cool before letting the chamber upto air. The extra time involved, however, was only a small proportion of a typical experimental cycle time of one day. Another disadvantage was that oil which had back-streamed through the chevron baffle was trapped on the surface of the cold trap which was later baked. This must inevitably have been a source of contamination but did not seriously affect the ultimate pressure of the system.

3.2.3 The mass spectrometer

The mass spectrometer was of the 180° deflection type, it being an improved version of the tube, type 29D18, marketed by A.E.I. Ltd.. A full description of this design has been published by Goldstone[63]. The main improvements are:-

(i) it has narrower resolving slits resulting in a theoretical resolution of fifty compared with twenty for the 29D18.

(ii) it is made entirely of molybdenum enabling the tube to be heated by an r.f. induction heater to ~600°C for thorough degassing

The tube used, late 3.3, was partly constructed by Goldstone and had a resolution of ~30 and a sensitivity of ~2/torr.

The filament current was supplied from a 12 volt accumulator via an emission stabiliser. The scanning voltage applied between the ion source and the analyser was derived from a helical potentiometer driven by a variable speed motor through suitable reduction gearing. The amplifier in an MS10 control unit was employed as an ion current amplifier and drove a chart recorder. A mass scan from mass 12 to 40 could be made in two minutes without loss of resolution. The amplifier gave a full scale deflection of 10^{-13} amps. on its most sensitive range. A typical trace is shown in Fig. (3.3).

Plate 3.1 shows the MS10 electrometer head mounted close to the collector electrode of the tube to improve the electrostatic screening of the tube. For the same reason the tube had an aquadag coating; this is not shown in the photographs. The 4 KG. magnet was supported on a tripod with extendable legs to facilitate the alignment of the magnet which was found to be critical and could be adjusted by maximising the electron collector current and minimising the current collected by the ion source.

3.2.4 Evaporation sources

3.2.4.1 Flash evaporation

The difficulties involved in evaporating alloys owing to dispro-

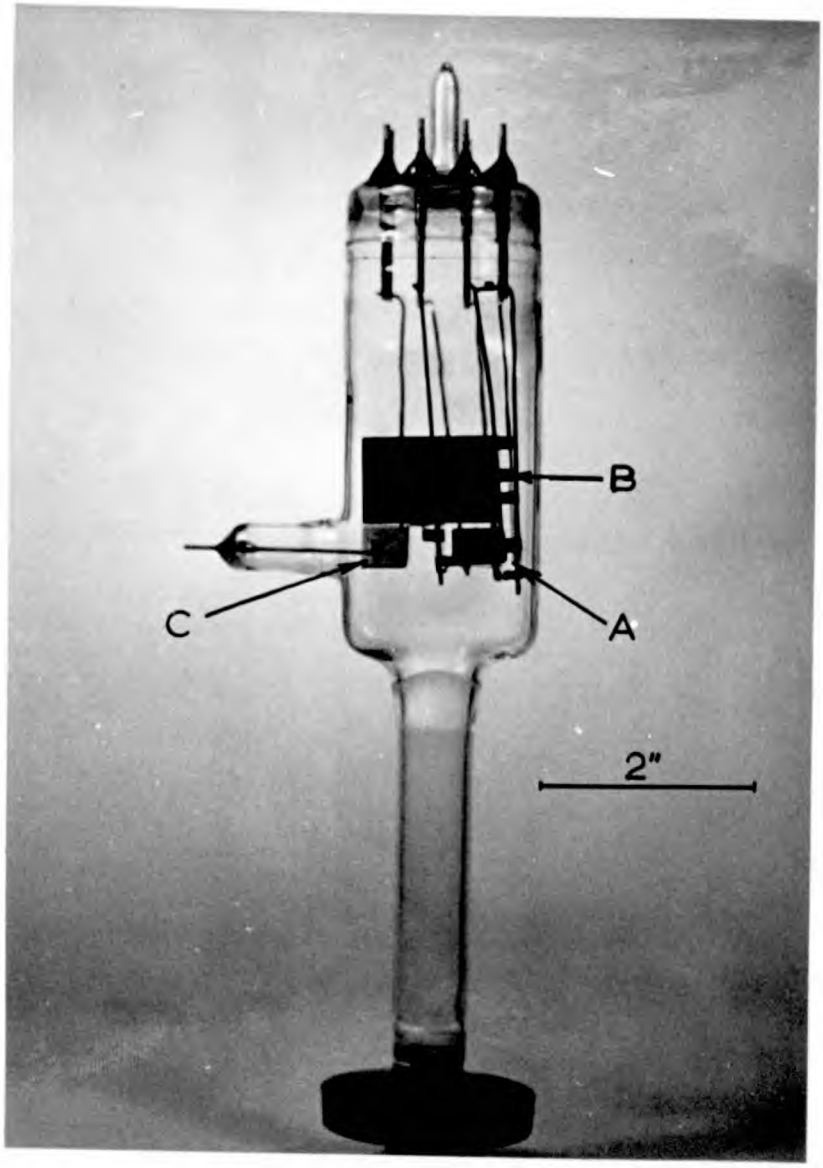

Plate(3.3)

The mass spectrometer tube

A ion source

B analyser

C ion collector

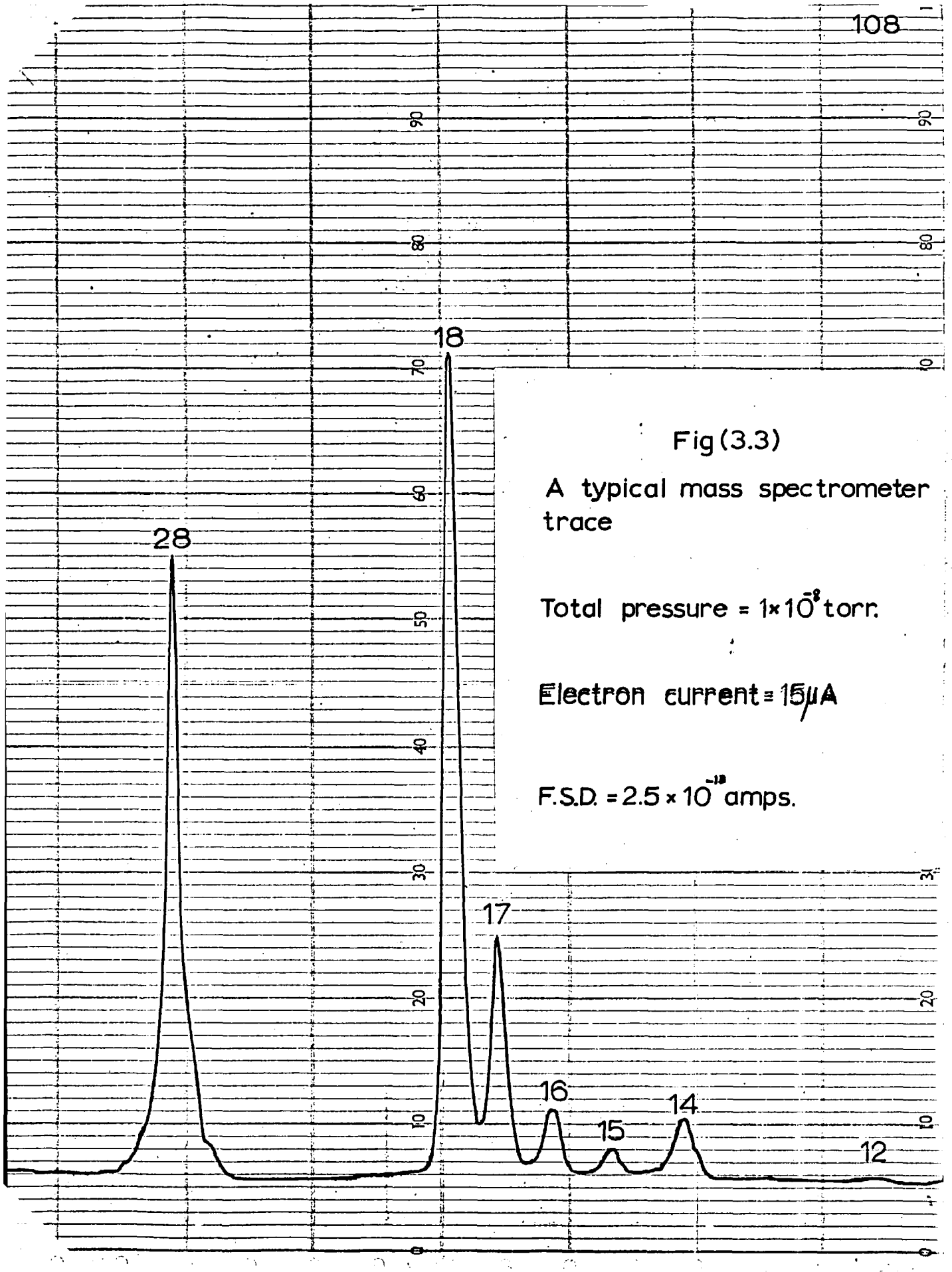

Fig (3.3)

A typical mass spectrometer trace

Total pressure = 1×10^{-8} torr.

Electron current = 15 μA

F.S.D. = 2.5×10^{-13} amps.

portionation have been discussed in Chapter I. Using flash evaporation Campbell[42] has been able to deposit nichrome films having compositions deviating from the starting value by only ± 1%.

The flash evaporation process involves the evaporation of a powder from a source which is very much hotter than the highest boiling point of the alloy components. By sprinkling the powder grain by grain onto such a source the particles can achieve the source temperature much faster than a conventional charge, enabling the alloy components to evaporate simultaneously so preserving the composition. If the source temperature is not high enough the composition of the vapour will tend to be rich in the more volatile component. This technique was first employed by Harris and Siegel[64] and has been used to evaporate compound semiconductors[65] and other multicomponent alloys.

3.2.4.2 The powder dispenser and evaporation sources

The flash evaporation process requires a means of metering powder onto the flash source. Since the experiments were to be performed inside a vacuum system which was able to be baked to $\sim 400^{\circ}C$, it was not possible to use rotary seals and mechanical drives to excite a dispenser.

A simple arrangement involving an electromagnetic vibrator was eventually used. This is shown in Plage (3.4). The glass powder hopper was clipped to a vibrating strip which formed one limb of a magnetic circuit. The exciting coil comprised eight turns of 18 S.W.G.

Plate(3.4)

The powder dispenser and source arrangement

A powder dispenser

B tungsten strip flash source

C subsidiary sources

D electrode terminations

copper wire wound onto a tubular glass former which fitted over a cylindrical limb of the magnetic circuit. One of the remaining limbs was slotted so that the airgap could be adjusted for optimum operati n. A current of about 10 amps. A.C. was necessary to drive the vibrator. Since radiation from the flash source increased the coil resistance the current had to be maintained constant using a Variac.

Judging visually, the rate remained constant once the device had been set up, though it was difficult to predetermine the exact rate of deposition. Using values of rate determined from the deposition time and final thickness the rate could be predetermined to $\pm$ 25%. Fig. (3.4) shows the rise in substrate temperature due to radiation from the flash source. This large temperature change and the high system bake-out temperature precluded the use of a quartz crystal rate monitor. It is felt that considerably more effort should be devoted to the production of a reliable well engineered powder dispenser.

The flash source was a resistively heated tungsten strip 0.01" thick. It was 4 cms. long and 0.8 cms wide and required a current of 120 amps. to heat it to its operating temperature of 2200^{o}C. Each source could be used five or six times before erosion caused it to burn out. A spectrographic analysis of the evaporated nichrome films failed to show any tungsten. It is thought that erosion occurred by tungsten alloying with nickel and simply resulting in localised thinning, the material being displaced to produce thickening around the thinned area.

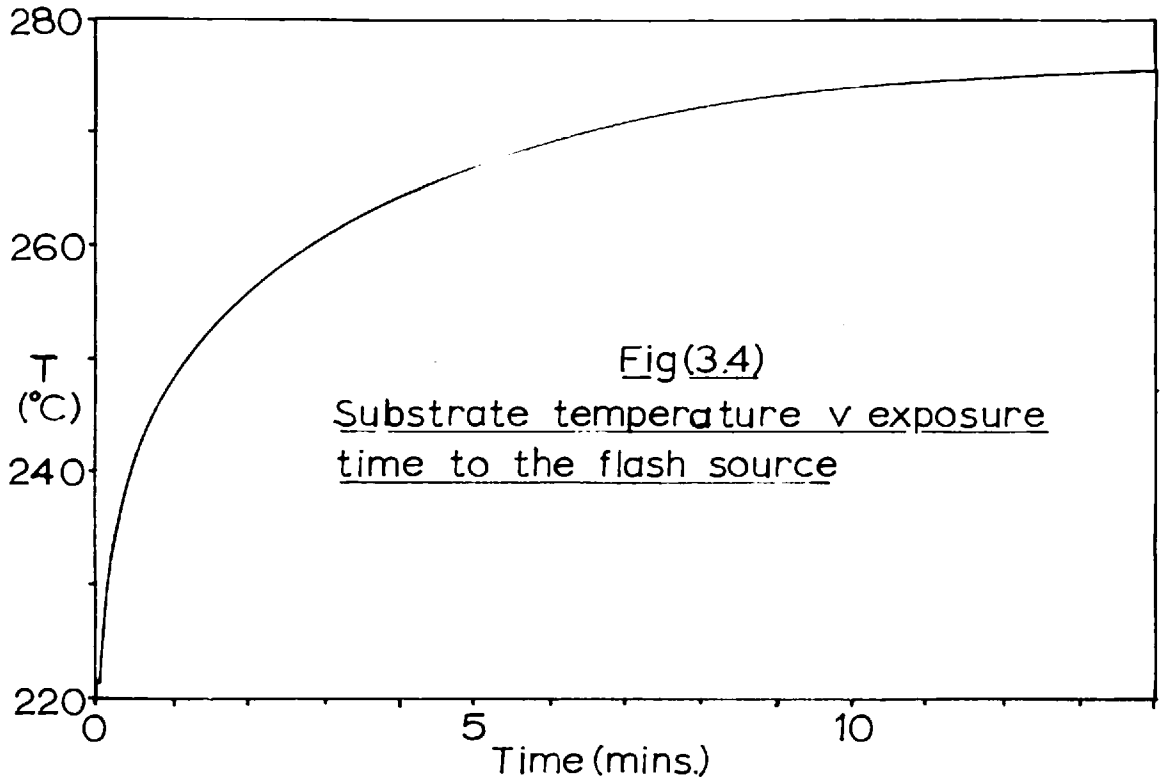

Fig (3.4)

Substrate temperature v exposure time to the flash source

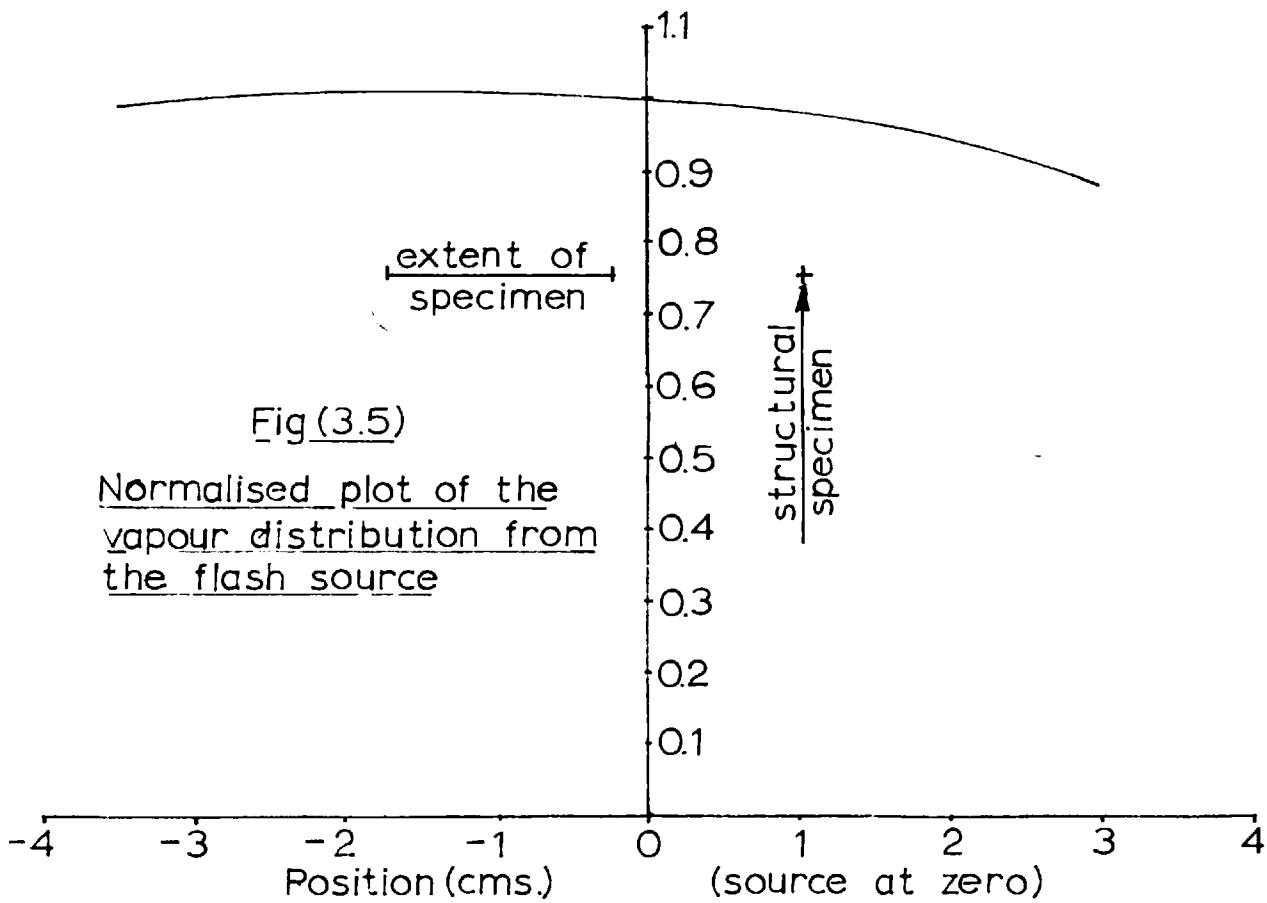

Fig (3.5)

Normalised plot of the vapour distribution from the flash source

Measurements of the source weight before and after evaporation showed that about 1% by weight of the powder impinging on the source remained there.

Fig. (3.5) shows a normalised plot of the vapour distribution from the flash source which was situated centrally within the experimental chamber. This was obtained by measuring the thickness at points along a film edge which lay along a line through the centre of the distribution. It is clear that the flux was constant to within $\pm$ 1.5% over the extent of the specimens.

Two other sources are shown in Plate 3.4. These were used for subsidiary evaporations of SiO and CuMn to be described later.

3.2.5 The substrate jig

3.2.5.1 The substrate heater

The substrate heater and mask changer are shown in Plate 3.5. The substrate heater comprised a stainless steel block measuring $3" \times 1\ ^1/_8" \times\ ^3/_{16}"$ to which substrates could be clipped or pressed into contact. It was heated by a tantalum wire heating element sheathed in alumina thermocouple tubing. A power input of approximately 60 watts was necessary to raise the substrate to 270°C. Owing to mains voltage variations it was found necessary to use a Voltstat constant voltage transformer to ensure thermal stability when making measurements. Owing to its massive nature it required about an hour to reach thermal

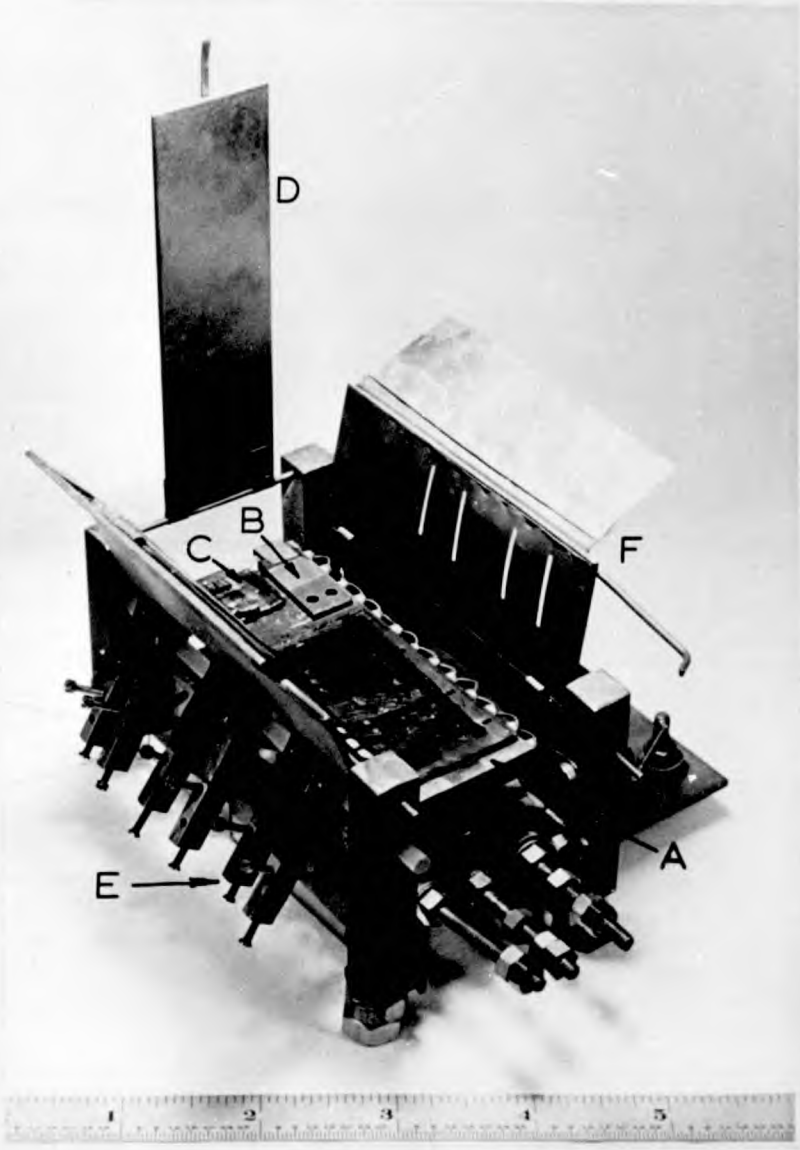

Plate(3.5)

The substrate holder

A substrate heater
B microscope grid holder
C thin film thermocouple
D shutter
E tensioned electrical contacts
F connections mask

equilibrium which made for long thermal cycling times. Its main advantage was uniform heating over its surface.

3.2.5.2 Pressure contacts

In order to eliminate contact resistances a four terminal method of resistance measurement was used. This necessitated forming a film pattern as shown at A in Plate 3.6. The long stripe was the film under examination and the four thin stripes were films connecting the specimen to the pressure pads. Owing to its good adhesion to the substrate the pressure pads and connecting films were made of copper-manganese. Connections to the pressure pads were made by means of spring contacts made from nickel-silver relay leaves. They had the advantages of remaining springy after heating to 400°C and of having spherical contact tips which minimised abrasion of the contact pad. These leaves were spot welded onto arms which were pivoted on a quartz rod axle and could be tensioned by means of screws bearing onto a quartz pressure plate. This mechanism is shown schematically in Fig. (3.7). Six contacts were used, the other two being used to connect to a thin film thermocouple.

3.2.5.3 The mask changer

A subsequent structural study[66] of overlapping film contacts showed that discontinuities can arise by the formation of an agglomerated region caused by seeding of the overlapping film at the edges of the lower film. This problem can be very serious when the lower film is

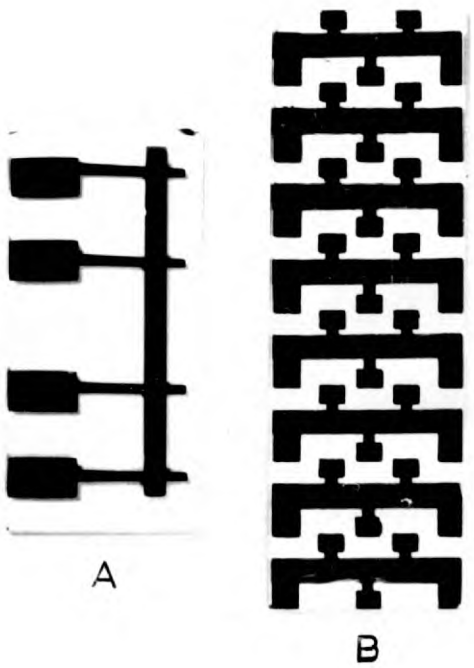

Plate (3.6)

The two types of substrate lay-out used (actual size)

A as used for the nichrome investigation

B as used for the gold films

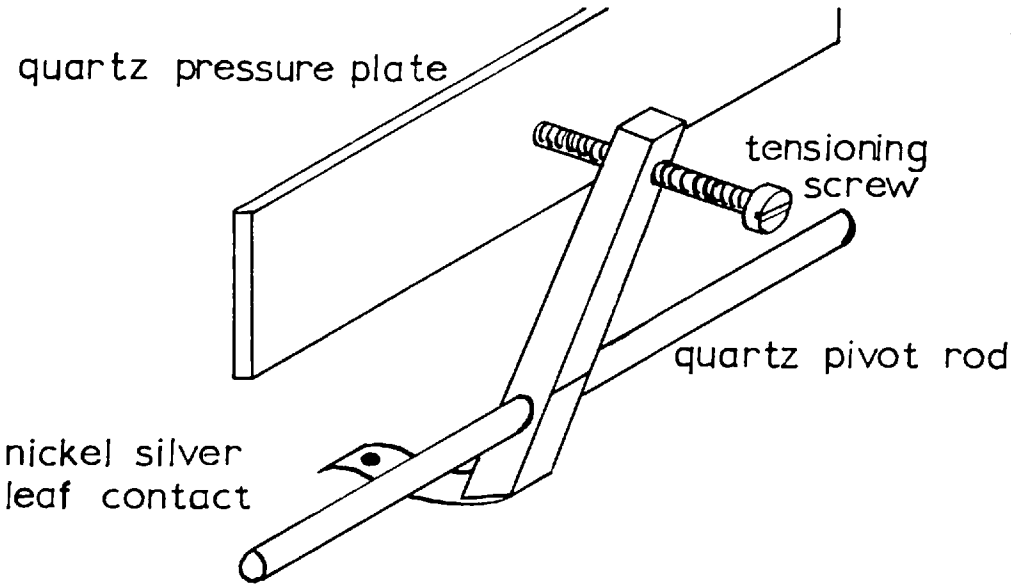

Fig(3.7) Schematic diagram of a pressure contact

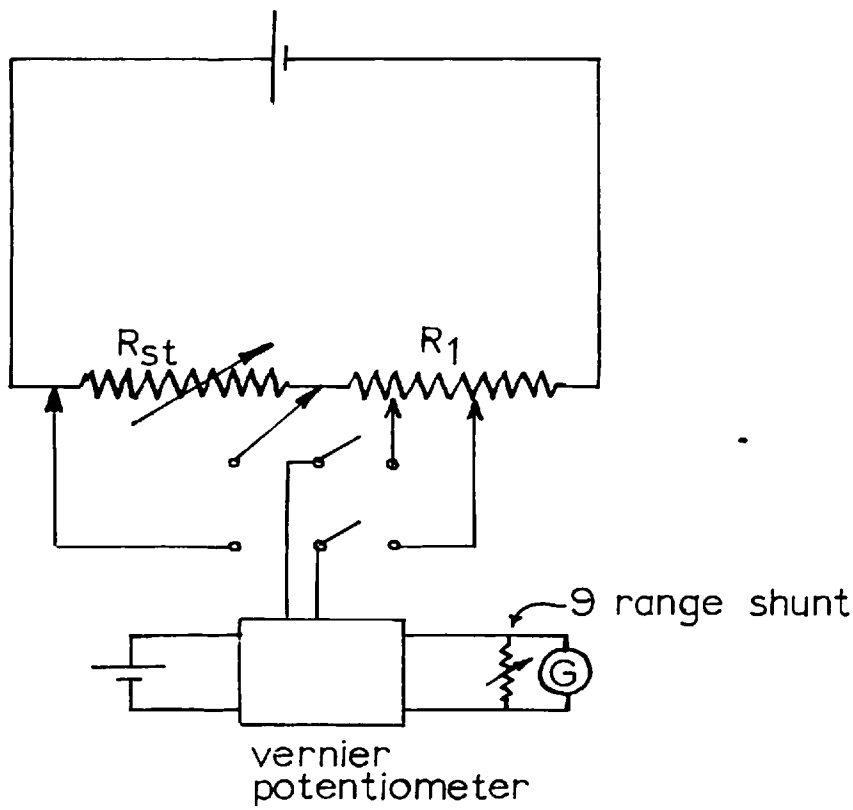

Fig(3.8) The circuit for measuring film resistances

much thicker than the top one. Fortunately, this had been anticipated and was obviated by forming the thinner specimen film first and then depositing the thicker copper manganese stripes which connected it to the pressure pads.

The masks are shown in position in Plates (3.5) and (3.7). They were made of 0.005" molybdenum foil and were formed by the spark erosion process. Though this is not as accurate as the photo resist technique, masks could be made accurate to $\pm$ 0.1 mm. It is ideal for cutting simple geometrical shapes. The masks were spot welded onto stainless steel frames which swung in and out of position. They were released by fuse wires and were actuated by gravity. The photographs, Plates 3.5 and 3.7 show them out of contact with the substrate.

The sequence of events was as follows,

(i) the specimen mask was in contact with the substrate and covered by the shutter;

(ii) the shutter was released to initiate the specimen deposition

(iii) on terminating the specimen deposition the specimen mask was released under gravity;

(iv) the connections mask was brought into position under the action of a counter weight;

(v) the copper manganese connecting stripes were deposited;

(vi) the connections mask was removed under the action of a second falling counter weight.

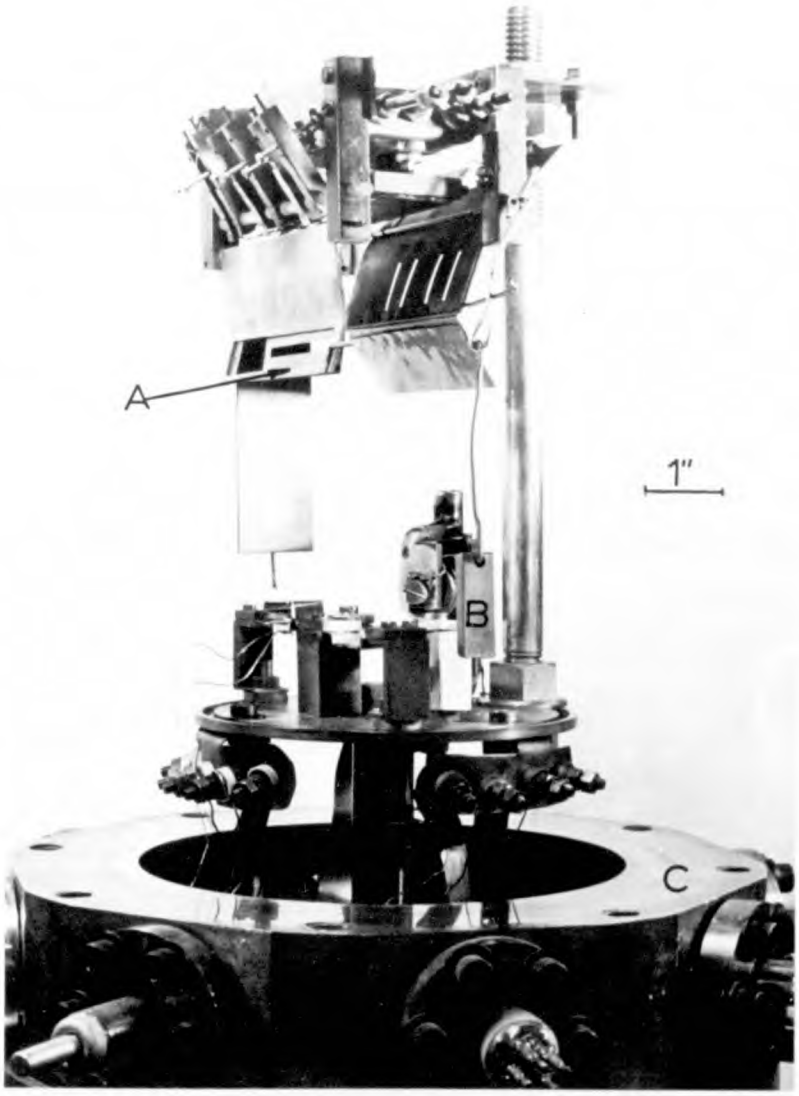

Plate(3.7)

The complete deposition arrangement

A specimen mask

B second counter-weight

C electrode inlet ring

The disadvantages associated with this arrangement were that the mask changing operations were not reversible and that it was impossible to monitor the film resistance during its deposition. Plate (3.7) shows the substrate jig in position over the evaporation sources. The pressure contacts and fuse wires were connected to two arrays of four electrode terminations on the evaporation source assembly. Only two of the connecting wires are shown in the photograph.

3.2.6 Substrates

3.2.6.1 The choice of substrate

3.2.6.1.1 The electrical specimen

Preliminary measurements on high resistance discontinuous gold films deposited onto soda glass microscope slides had revealed instabilities in their resistance. Further measurements showed that their resistance increased rapidly on applying a measuring voltage. This phenomenon became more pronounced as the temperature of the film was increased. The effect was attributed to thermally activated ionic motion in the glass which produced polarisation leading to a decay in its conductivity. This occurred even when the substrate was coated with silicon monoxide. For this reason soda glass was abandoned and replaced by a barium alumino silicate glass type 7059, manufactured by Corning and supplied by Gooch and Housego, Ilminster.

7059 was developed for use as a substrate for the fabrication of micro-electronic circuits. Its low ionic conductivity arises from the incorporation of barium ions as a network modifier. Since these are larger than the openings in the network of silicon-oxygen tetrahedra they inhibit the motion of other ions through the glass network and reduce the ionic conductivity. This low conductivity was maintained when it was coated with silicon monoxide. It suggests that ionic motion can occur in silicon monoxide but when 7059 glass was used the source of ions was elminated.

7059 is one of the range of glasses known as "Microsheet" and has a very smooth surface finish. The makers claim that asperities do not exceed 20A°. Fig. (3.6) shows the surface profiles of 7059 and soda glass microscope slides taken using a Talysurf (see Section 3.2.7.3.). The electrical properties of various substrate materials are summarised in Table 3.1[67].

3.2.6.1.2 Electron microscopy specimens

One of the methods of preparing a specimen for transmission electron microscopy is to detach the film from its substrate and mount it on a metal grid. Owing to the strong adhesion between nichrome and glass it was impossible to detach the films without causing serious structural damage to them. It was therefore decided to prepare electron transparent support films having a similar structure to glass and to condense films onto these during the deposition of the electrical specimen.

Silicon monoxide was chosen since it has an amorphous network

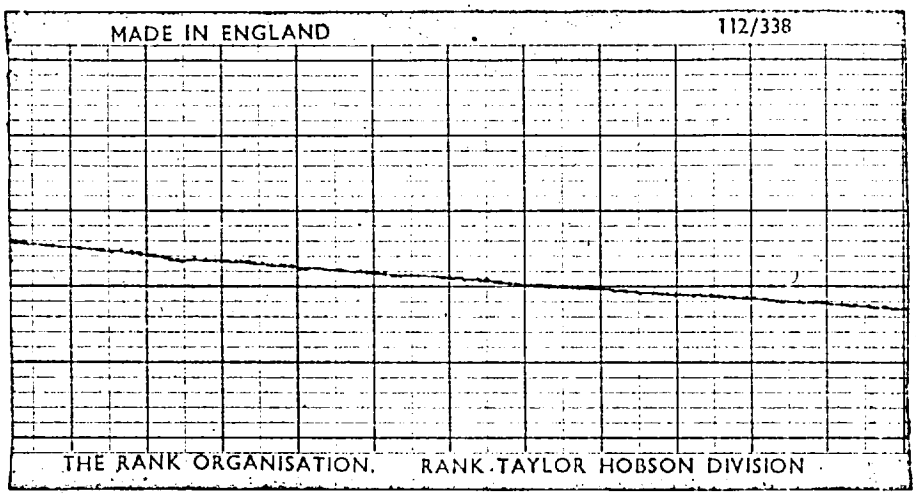

Corning 7059

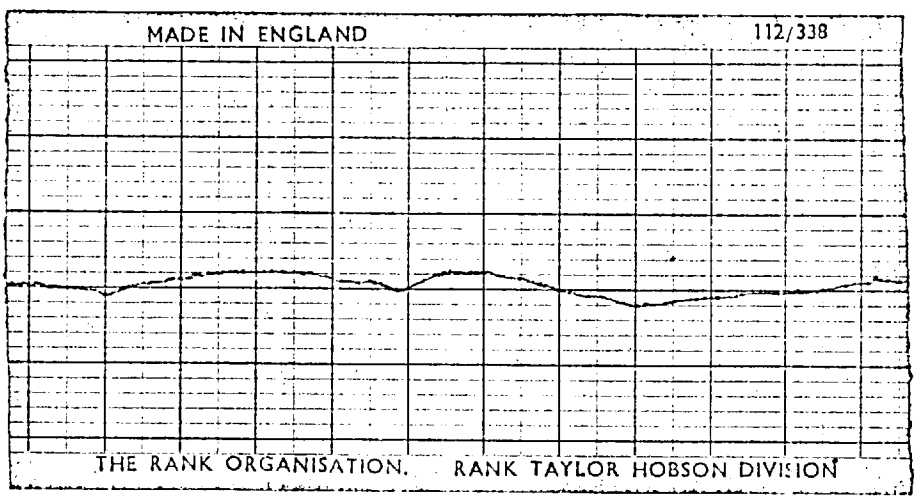

Soda glass

Fig(3.6) The surface profiles of 7059 and soda glass

Vertical magnification = 100,000
Horizontal magnification = 100
Stylus size = 2.5μ

TABLE 3.1

Properties of glass substrate materials[67]

Corning Glass Code Number	0080	0211	1715	7059	7740	7900	7940
Glass Type	Soda lime	Alkali Zinc Boro-silicate	Lime Alumino-silicate Alkali-free	Barium Alumino-Silicate Alkali-free	Alkali Boro-silicate (Pyrex)	96% Silica	Fused Silica
Volume Resistivity $\log_{10}\rho(\Omega\text{-cm})$ (250°C)	6.4	8.3	13.6	13.5	8.1	9.7	11.8
(350°C)	5.1	6.7	11.3	11.3	6.6	8.1	10.2
Dielectric constant (25°C)							
10^2 c/s	8.3	6.8	6.0	5.9	4.9	3.9	3.9
10^6 c/s	6.9	6.6	5.9	5.8	4.6	3.9	3.9
Loss tangent (25°C)							
10^2 c/s	0.078	0.01	0.0018	0.0011	0.027	0.0006	0.00066
10^6 c/s	0.01	0.0047	0.0024	0.0011	0.0062	0.0006	0.00002
Dielectric Strength(250°C) Kv. (r.m.s.)	0.35	2.0	> 10	>10	2.0	7.0	> 10
Linear coeff.of thermal expansion (0°-300°C)x10^{-7}/°C	92	72	35	45	32.5	8	5.6
Density (gms./cm^3)	2.47	2.57	2.48	2.76	2.23	2.18	2.20
Softening point (°C)	696	720	1060	872	820	1500	1580

structure like that of glass[68]; the 7059 glass slides could easily be coated too in order to provide similar electrical and structural specimen substrates. Amorphous carbon films were not used since there was some doubt[69] as to the effect of a conducting substrate on the initial growth behaviour of a thin film. Work by Fuschillo[70] has shown that SiO is structurally stable upto 350°C when small (150A°) nuclei appear eventually recrystallisation occurs at 800°C. In the same work it was shown that small (200A°) nuclei occurred at 200°C in carbon films; these increased in size to 1800A° at 600°C.

3.2.6.2 Substrate preparation

Films of silicon monoxide about 400A° thick were found to be mechanically strong and electron transparent using 60 KV. electrons. They were prepared from Viacote-Q silicon monoxide evaporated at a pressure of 5×10^{-5} torr. and at a rate of about 10A°/sec. The films were detached from the glass substrates by floating them off in warm water. Fragments of the film were then floated onto specimen grids and allowed to dry naturally. The ease of separation from the glass surface was extremely variable. It is thought that this depended largely on the state of the glass surface prior to deposition, since films deposited after a long pump-down could be detached more readily. This seems to correspond with work by Siddall[71] which suggests that oil contamination facilitates the removal of carbon films from glass.

A 7059 glass substrate measured 2" x 1" x 0.05". In order to remove gross impurities it was first washed in a hot Teepol solution

and then ultrasonically cleaned for thirty minutes in an organic decontaminant RBS 25. On removal from the ultrasonic bath it was rinsed in distilled water to remove the cleaning solution and was then assumed to be free from organic impurities. The final process involved rinsing it in redistilled iso-propyl alcohol for several hours in a re-circulator. The dry substrate was eventually removed and coated with a layer of silicon monoxide about 1000A° thick. This had the effect of smoothing any surface irregularities[72] besides making the final surface similar to that of the electron microscopy specimens. The four pressure contact pads of copper-manganese were deposited at 300°C and the substrate was placed in its jig ready for mounting in the evaporator. Ideally, it would have been better to have coated the substrate with a final layer of SiO in the experimental chamber prior to the specimen deposition. This would have produced an atomically clean surface; unfortunately, this would have necessitated the use of a complicated reversible mask changer.

3.2.6.3 Location of the substrates

The microscope specimens were retained in a tray which could be clipped onto the substrate heater, whilst the glass substrate was pressed into contact by the pressure contacts. Using the plot of the vapour distribution, Fig. (3.5), their positions were so arranged that the position of the two microscope grids corresponded geometrically to the centre of the specimen film. This ensured the same incident flux

at a similar angle of incidence. The source-substrate separation was 13 cms.

3.2.7 Measurements

3.2.7.1 Resistance measurements

It has already been mentioned that a four terminal method of resistance measurement was used to eliminate contact resistances. The copper-manganese contact pads and connecting films had resistances of about 20 ohms and could only have been neglected when measuring high resistance films.

The measuring circuit is shown in Fig. (3.8). R_{st} was a standard decade resistance box having a maximum value of 10KΩ. The potentiometer and specimen circuit supplies were provided by 2 volt accumulators. The vernier potentiometer was made by the Cambridge Instrument Co. Ltd., and had three ranges having maximum values of 1.9, 0.19 and 0.019 volts. On the 1.9 volt range the descrimination was 10μV. The system could be standardised using a Weston Standard Cell. Owing to drift in the e.m.f. of the accumulator this was done prior to each resistance measurement.

The detector was a short period galvanometer having magnetic damping. It produced a deflection of 32 cms. for a current of 1μA on a scale situated at one metre. The galvanometer resistance was 22.02 ohms. Using a specimen with a resistance between the voltage probes of 3000Ω a 10μV voltage change caused a deflection of 1 mm. A nine range universal

shunt was used in parallel with the galvanometer to limit its sensitivity.

The value of resistance is simply given by

$$R_1 = R_{st} \times \frac{V_1}{V_2} .$$

In practice, the voltages could be measured to $\pm$ .001% and R_{st} was accurate to $\sim$0.01%. Thus absolute measurements or resistance were accurate to $\pm$ 0.01%.

3.2.7.2 Temperature measurements

Since heat loss occurs from a substrate by radiation from its surface there is a temperature gradient through its thickness. For this reason it was considered undesirable to take the substrate heater temperature as that of the substrate surface. It was therefore decided to construct a thin film thermocouple to measure film temperatures.

As most of the films to be examined were made of nichrome this was chosen as one of the couple materials for two reasons:

(i) using similar substrates the temperature of a thin film thermocouple can only assume that of the specimen film if their thermal absorption and emissivity are similar;

(ii) nichrome adheres well to glass and is robust.

Gold was chosen as the other element because this combination produced a high output voltage at a given temperature; 23μV/$^{\circ}$C. Unfortunately, gold does not adhere well to glass but a protecting overcoat of silicon

monoxide did not appear to disturb the thermocouple calibration.

Its construction is illustrated in Fig. (3.9). Two pieces of platinum foil were fused into the glass surface to form contact pads for the pressure contacts. The two couple films were deposited to overlap these and therefore introduced two other junctions. Since these were at the substrate temperature they required compensation by similar negative e.m.f.'s. Nichrome and gold wire leads wrapped round the pressure contacts provided this and connected the couple to the electrode terminations. Fig. (3.10) is a diagram of the junctions involved.

The thermocouple was calibrated from liquid nitrogen temperatures to 270°C using a platinum resistance thermometer. The calibration curve is shown in Fig. (3.11) and was found to be reproducible for four couples which were made. Temperatures were ascertained with respect to ambient temperature, which was itself determined after each measurement. These were accurate to $\pm$ 0.5°C. The thin film thermocouple was held in contact with the substrate heater by the pressure contacts. A comparison of the substrate temperature and that of the substrate heater showed differences of upto 90°C. This is shown in Fig. (3.12) and is convincing evidence for the use of thin film thermocouples in film temperature measurement. The position of the couple with respect to the substrate is shown in Plate (3.5).

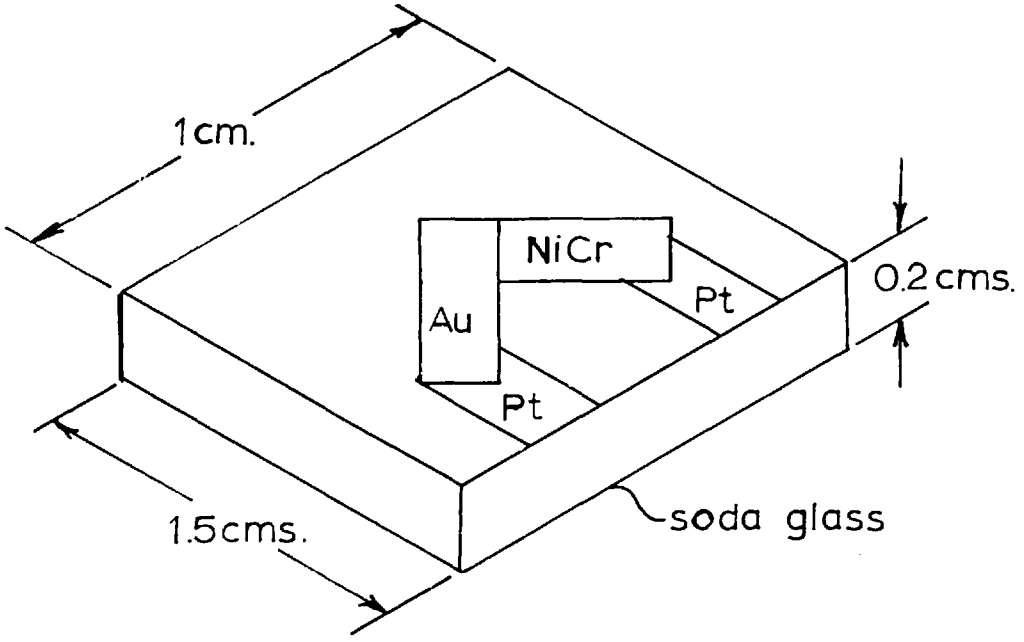

Fig (3.9) Construction of the thin film thermocouple

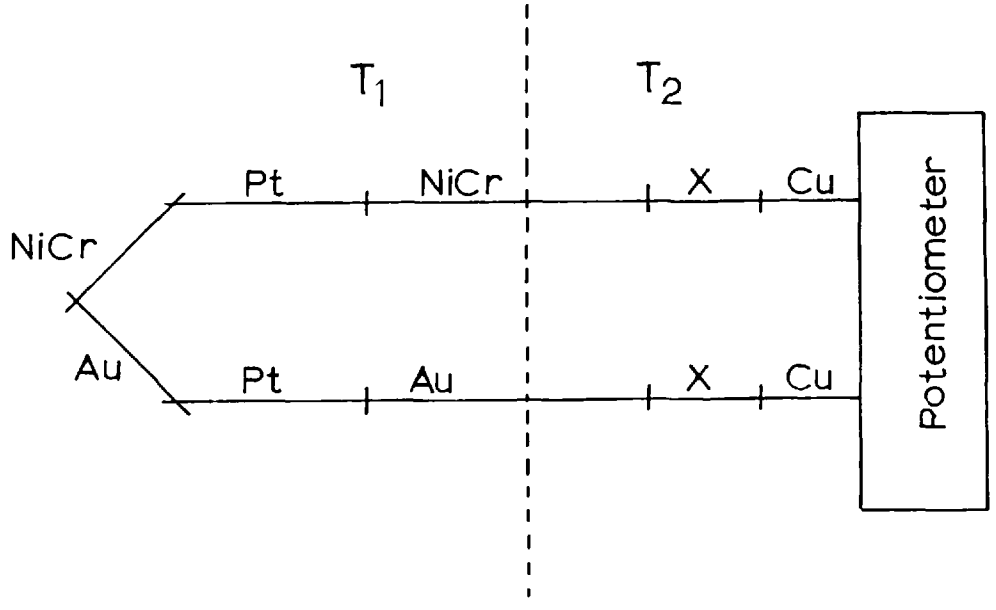

X denotes the vacuum lead-in material

Fig (3.10) Junction diagram of the measuring circuit

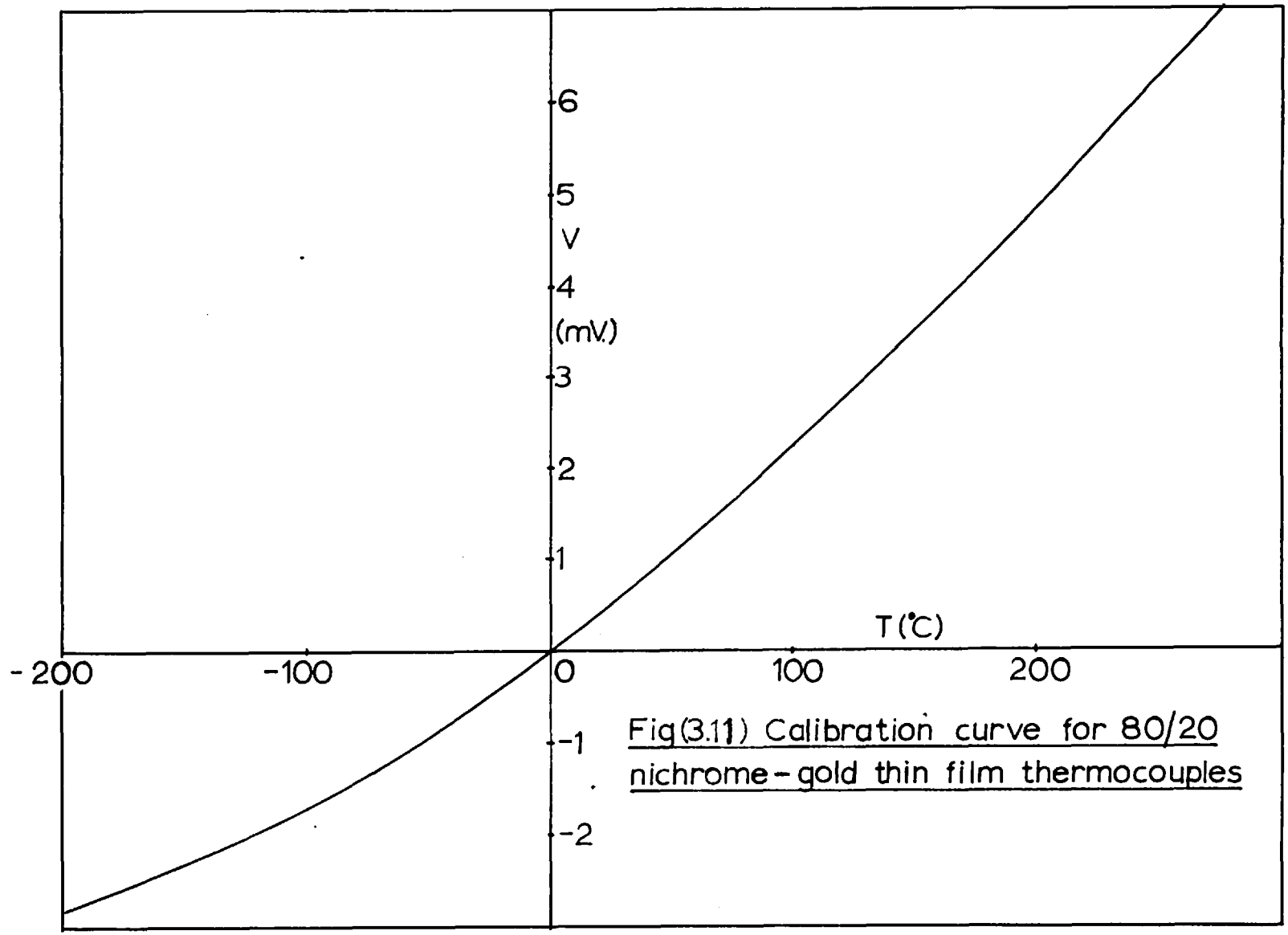

Fig(3.11) Calibration curve for 80/20 nichrome-gold thin film thermocouples

Fig(3.12) Temperature difference between the film and the substrate heater v the substrate heater temperature

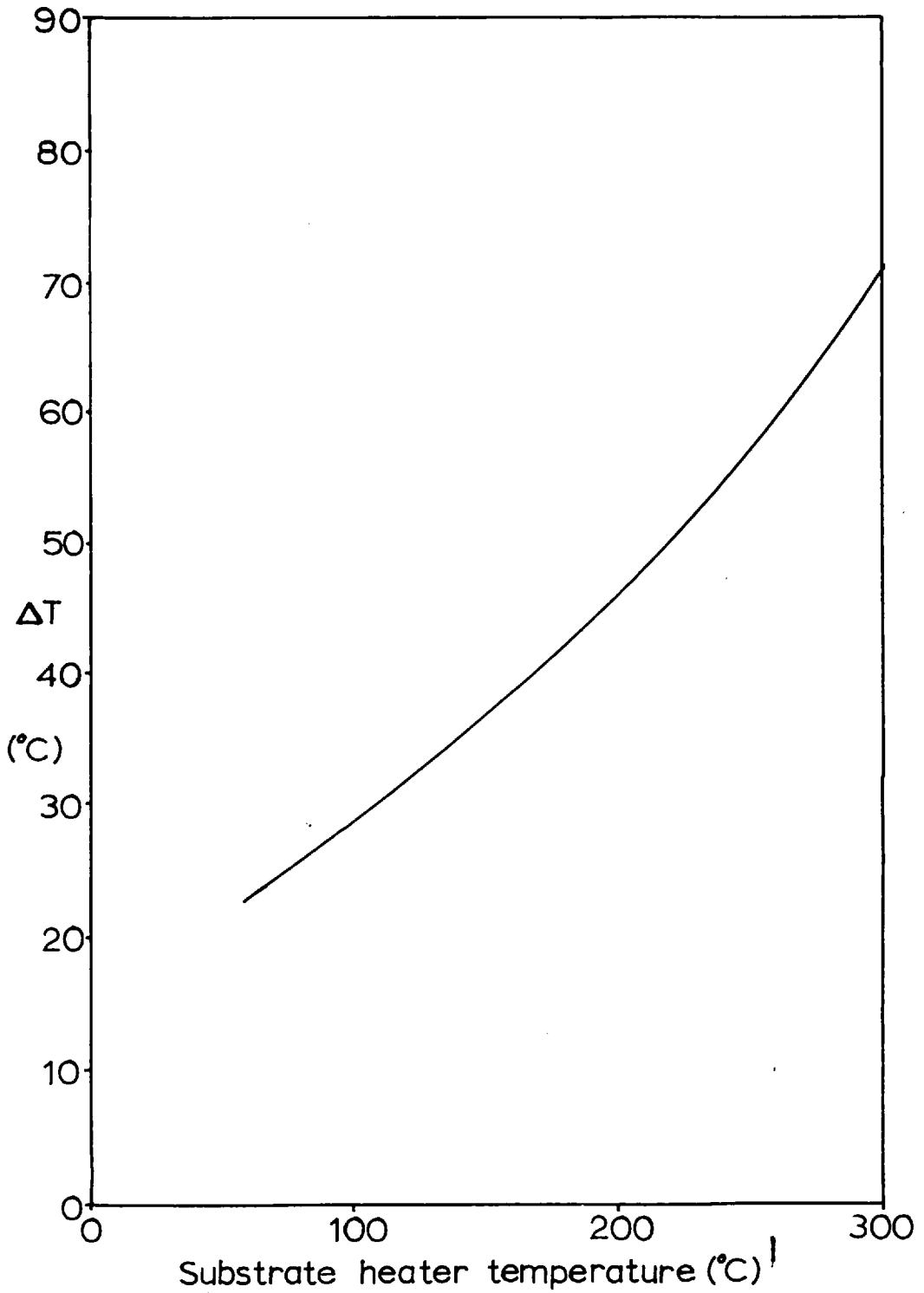

3.2.7.3 Thickness measurement

3.2.7.3.1 The principle

Film thicknesses were measured[73][74] using a surface profile instrument called the Talysurf made by Taylor-Hobson Ltd., Leicester. This comprised a skid which served as a reference and a stylus which was free to move up and down with respect to the skid. This arrangement is shown schematically in Fig. (3.13). It could be automatically traversed across a surface and the displacement of the stylus with respect to the skid sensed electrically, amplified and displayed on a moving chart. As the stylus encountered a film edge a step in the trace occurred which could be measured to obtain the film thickness. Similarly a scratch could be used but this has the disadvantage of being destructive.

3.2.7.3.2 Precautions

Several precautions were necessary for optimum use,

(i) an extremely smooth surface was required in order to differentiate small features, e.g. 25A°. 7059 glass was eminently suitable.

(ii) The surface between the underside of the substrate and the bed of the instrument had to be free of dust to avoid rocking of the substrate during the traverse.

(iii) Soft and poorly adherent films, e.g. Ni and Au, had to be coated with several hundred angstroms of a hard material,

Fig(3.13)

Schematic diagram of the surface profile monitor

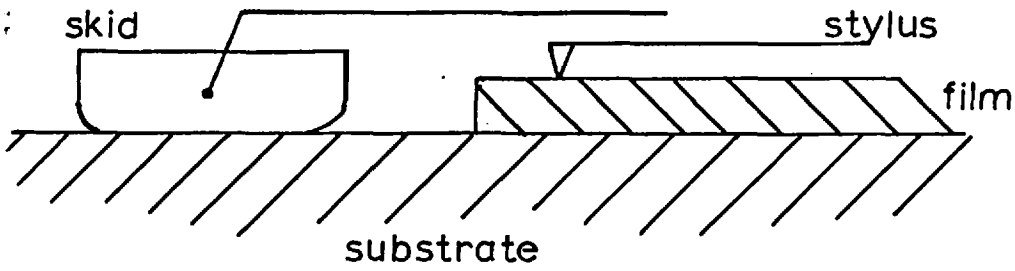

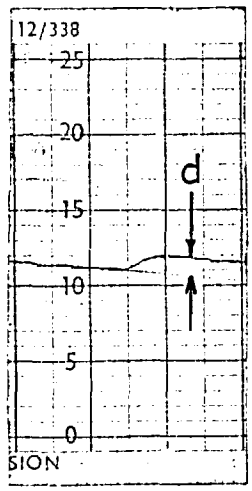

d ≡ 230Å ± 25Å

Fig(3.14) A typical Talysurf trace
(vertical magnification = 100,000)

e.g. SiO to avoid damaging the specimen film. This was necessary despite the reduced tip-force of 20 mgms.

In general six traverses were made for one thickness measurement. Each result fell within 25A° of the mean value providing that these precautions were observed. The maximum vertical magnification was 100,000 times, therefore the deviations corresponded to 0.25 mms. on the trace. The precision was governed by trace noise and inaccuracies in measuring the trace. An accuracy of ± 25A° was assumed.

3.2.7.3.3 Interpretation

Fig. (3.14) is a typical trace over a film edge. It is interesting to note that the background slopes. Referring to Fig. (3.15), it is clear that the instrument is continuously measuring the difference in height between points which are a fixed distance apart; it infact differentiates the surface profile. Thus a sloping surface yields a horizontal straight trace and a parabolic surface a sloping line. When the stylus encounters a step it simply moves vertically by d an amount equal to the film thickness. The corresponding distance on the trace is measured perpendicular to the motion of the paper.

Quite apart from the effect just described, the angle θ which the film makes with the direction of traverse introduces an error which is usually negligibly small. This is shown by Fig. (3.16), it is clear that the stylus actually moves vertically by a distance d' where

$$d' = \frac{d}{\cos\theta}$$

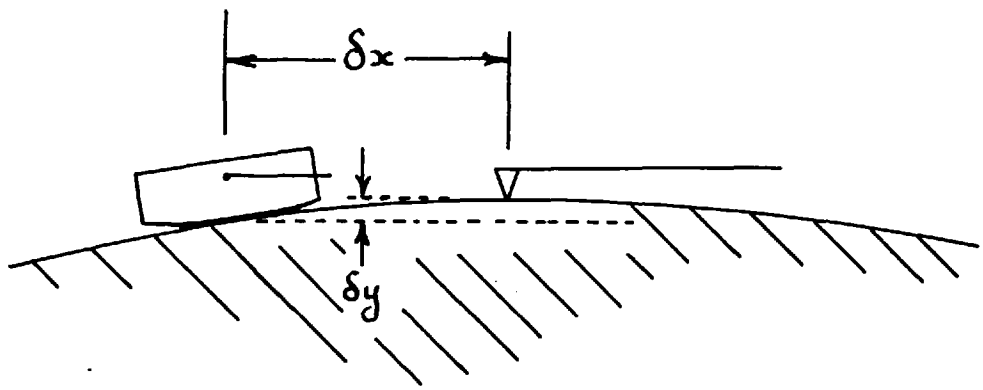

Fig (3.15) The differentiating action ($\delta x = 0.1''$)

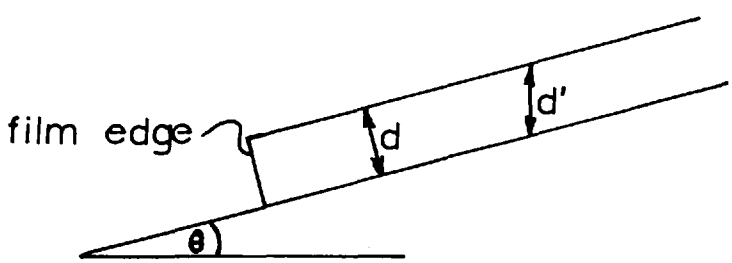

Fig (3.16) The actual vertical displacement of the stylus

In the diagram θ has been grossly exaggerated and is usually so small that $\cos\theta = 1$.

The dimensions of the stylus are necessarily much larger than the size of aggregates in discontinuous thin films and is approximately 1μ. Therefore, the stylus rides on the extremities of the aggregates and the indicated thickness cannot be directly related to the volume of condensed material. The thickness indicated is only an effective thickness unless a correction taking into account island shape is applied. Obviously, this does not apply to continuous films.

3.2.7.4 The accuracy of the electrical parameters

Absolute measurements of resistance were accurate to ± 0.01%. A calculation of the resistivity of a film involves the use of an expression of the form

$$\rho = \frac{Rwd}{l}$$

where w and l are the length and width of the film. The ratio of w and l was five and was constant for each film; it was known to within ± 3%. For a film thickness of 200A°, the accuracy of the thickness is ± 12%; this is the most inaccurate part of the thickness range. For a film of 1000A° thickness this improves to ± 2.5%. Therefore, the total accuracy of the resistivity values varies between ± 5.5% for a thickness of 1000A° to ± 15% at 200A° whilst that of sheet resistivity is constant at ± 3%.

Measurements of the temperature coefficient of resistance are based on an expression of the form

$$\alpha = \frac{1}{R} \cdot \frac{\Delta R}{\Delta T}$$

and were obtained from a curve of resistance plotted against temperature. Each resistance value has an accuracy of $\pm$ 0.5% whilst ΔT was known to $\pm$ 2% when $\Delta T = 100^{\circ}C$. Therefore, the total accuracy of the values of T.C.R. is $\pm$ 3.5%.

3.3 Continuous gold films

3.3.1 Introduction

This part of the work was concerned with the surface scattering of electrons in continuous thin films. Gold was chosen because its properties are well known in bulk and thin film forms. It has the advantage of being chemically inert. For the following reasons it was decided to perform the measurements in air:-

(i) gold does not oxidise and should be electrically stable;

(ii) the films to be studied were continuous and less sensitive to gaseous adsorption than discontinuous ones;

(iii) the films had to be prepared in a general vacuum system, an Edwards 12E6, so that time was limited.

3.3.1.1 Method of formation

In order to examine deviations from the bulk behaviour due to

surface scattering it was necessary to minimise effects due to aggregation which normally appear in gold films at a thickness of $\sim 500A^{\circ}$. A technique used to prepare continuous gold films thinner than this was described by Gillham, Preston and Williams[25]. This comprised depositing the gold films onto an underlayer of bismuth oxide. In their work they used oxide layers which were several hundred angstroms thick. The effect of the underlayer was to increase the binding energy between the deposit and the substrate. This resulted in a lowering of the mobility of the gold on the substrate and caused the films to become continuous at an early stage in their growth. They also demonstrated that an overlayer of bismuth oxide enabled the films to be annealed at temperatures as high as $350^{\circ}C$ before aggregation occurred. By employing this technique it was hoped to prepare continuous gold films at room temperature and anneal them at higher temperatures to increase their crystallite size, so increasing the electron mean free path in the material.

3.3.1.2 The preparation of the films

3.3.1.2.1 The substrate

It was decided to prepare sets of seven specimen films each having a different thickness. This meant that each of the seven would be prepared under similar conditions assuming that the rate of deposition was kept constant. The film configuration was as shown at B in Plate (3.6). The eighth film was just bismuth oxide and was

used to check the conductivity of the under-layer. The substrate used was a 3" x 1" x 0.03" soda glass microscope slide. After depositing the copper manganese electrical contacts and coating with a bismuth oxide over layer the slide was cut into eight pieces to facilitate the electrical measurements. Though the surface finish of 7059 glass is superior to that of soda glass the latter was used because the hard surface of 7059 glass made it difficult to cut without special apparatus. In these experiments the ionic conductivity of soda glass was unimportant because of the low resistance of the specimens. The slides were cleaned in the manner described above before coating with bismuth oxide.

3.3.1.2.2 The bismuth oxide underlayer

Initially some difficulty was experienced in preparing bismuth oxide films by evaporation from a molybdenum boat. The films had a metallic lustre and exhibited resistances of several hundred ohms. Examination using electron microscopy revealed that the films were not amorphous and readily recrystallised in the electron beam to form crystals several thousand angstroms across. It was eventually concluded that the films were in fact bismuth and that reduction of the oxide by the molybdenum boat had occurred. When a tantalum boat was used very rapid erosion of the boat occurred and similar films were formed. Eventually[75][76] a platinum boat source was used from which amorphous insulating bismuth oxide films could easily be

deposited. These had a yellowy-brown appearance. Plate (3.8) is a micrograph of a bismuth oxide film having a thickness of 150A°. Owing to its discontinuous nature thicker films, ~ 600A°, were used in an attempt to produce smoother films. This is consistent with the work of Gillham, Preston and Williams who used similar thicknesses. Unfortunately, the total thickness of the oxide-gold-oxide sandwiches was too great to permit examination using electron microscopy. Watt[77] has shown that serious disruption of the structure of the gold films occurs when the bismuth oxide layers are dissolved away.

3.3.1.2.3. Masks and substrate holder

Two masks made of 0.002" molybdenum sheet were used, one for the formation of the gold specimen films and the other for the copper-manganese contacts. Owing to their relatively complicated shape they were made by the Kodak photo-resist technique using 5:1 photographic reduction.

An exploded view of the substrate holder is shown in Fig. (3.17). This arrangement necessitated letting the system up to air between depositions for the insertion of the next mask. Seven different thickness films were produced by the movement of a sliding shutter. This was actuated manually using a rotary drive.

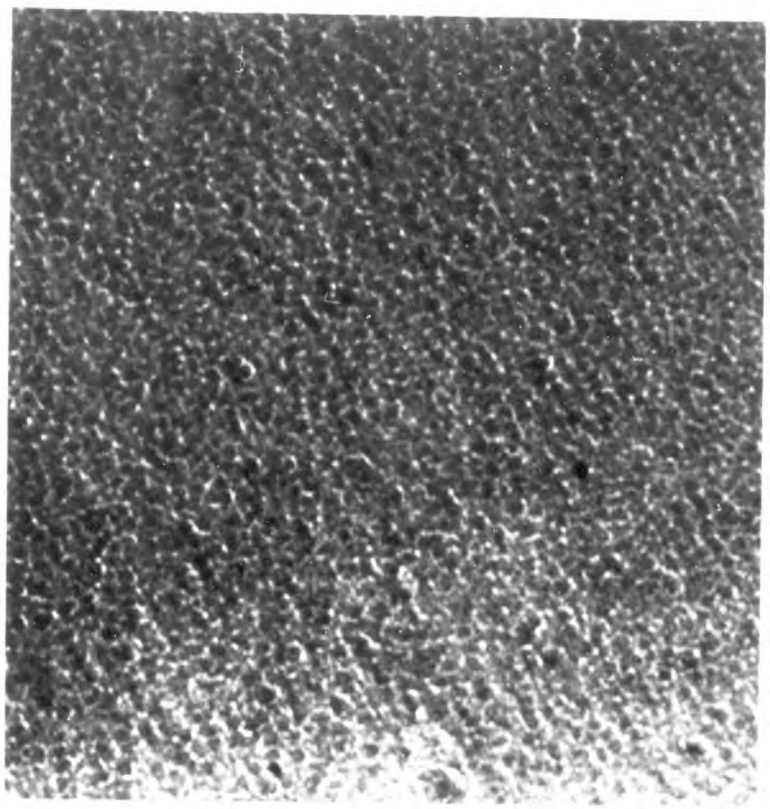

1000Å

Plate (3.8)

A 150Å film of bismuth oxide deposited onto a SiO support film

preparation pressure = 2×10^{-4} torr

Pt foil boat source

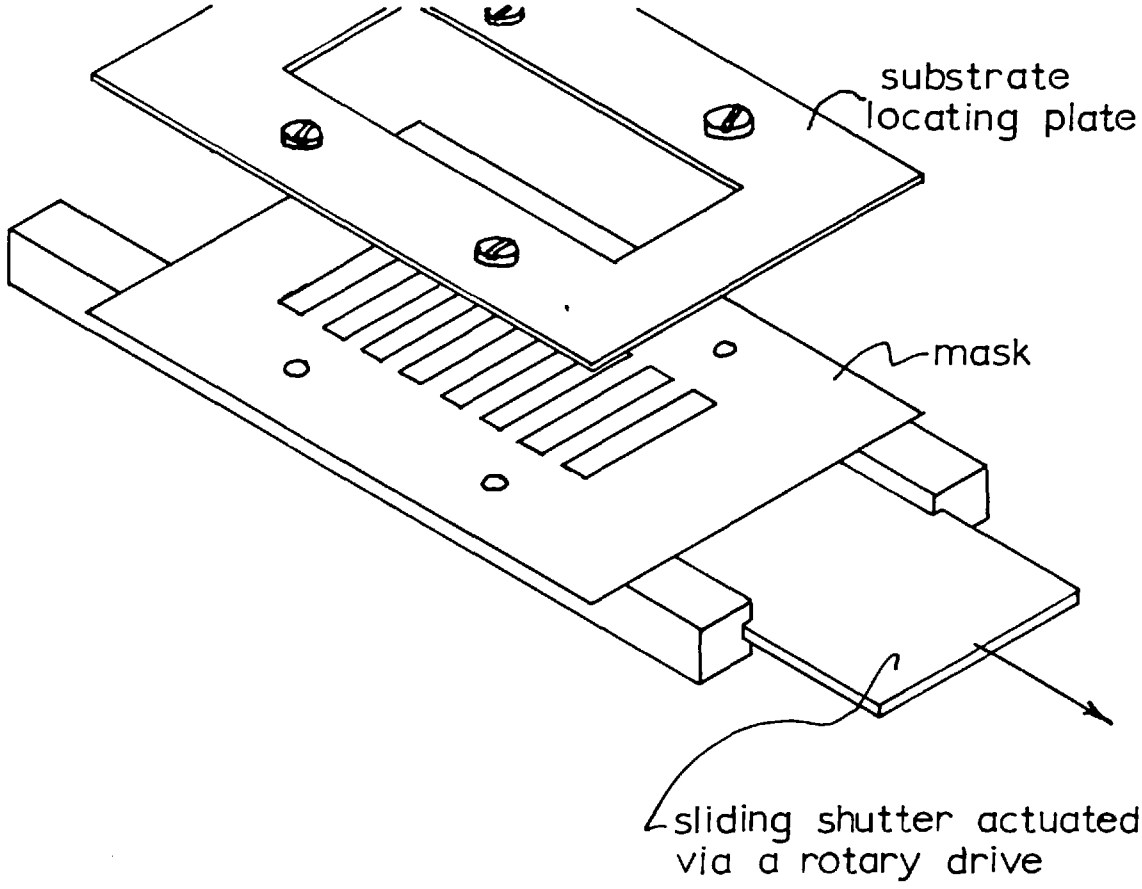

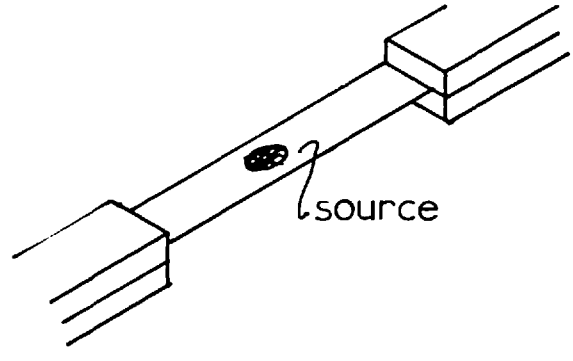

Fig(3.17) The substrate holder and sliding shutter

3.3.1.3 Measurements

3.3.1.3.1. Thickness determination and system calibration

A quartz crystal rate monitor was used to measure the evaporation rate and the film thicknesses. This was a standard apparatus manufactured by Edwards High Vacuum Ltd.. The position of the crystal was fixed with respect to the source and substrate, the source to substrate separation being 30 cms. A large separation was required to ensure uniformity of the vapour stream over the extent of the substrate. An experiment in which the eight specimens were exposed simultaneously showed that their resistances were not the same. Further experiments showed that the ratios of their resistances were constant. This meant that the vapour distribution from the source was being distorted. The reason for this is not clear as the system was arranged symmetrically. Fig. (3.18) shows a plot of the normalised resistance over the array of eight films. This shows a spread of $\pm$ 7% from the central value, i.e. the mean of the values of the central pair. Since this was reproducible it was used to provide a correction factor for each film. The corrections relied on the assumption that the resistivity of continuous films of gold is constant between $\pm$ 7% of 1000A$^{\circ}$.

Predictions from the Fuchs-Sondheimer analysis using a likely value of mean free path, $\sim$ 200A$^{\circ}$, show that the resistivity would be constant over that range to $\pm$ 0.5%. Thus Fig. (3.18) provides

Fig (3.18)

Normalised resistance or thickness correction factor for the array of gold films

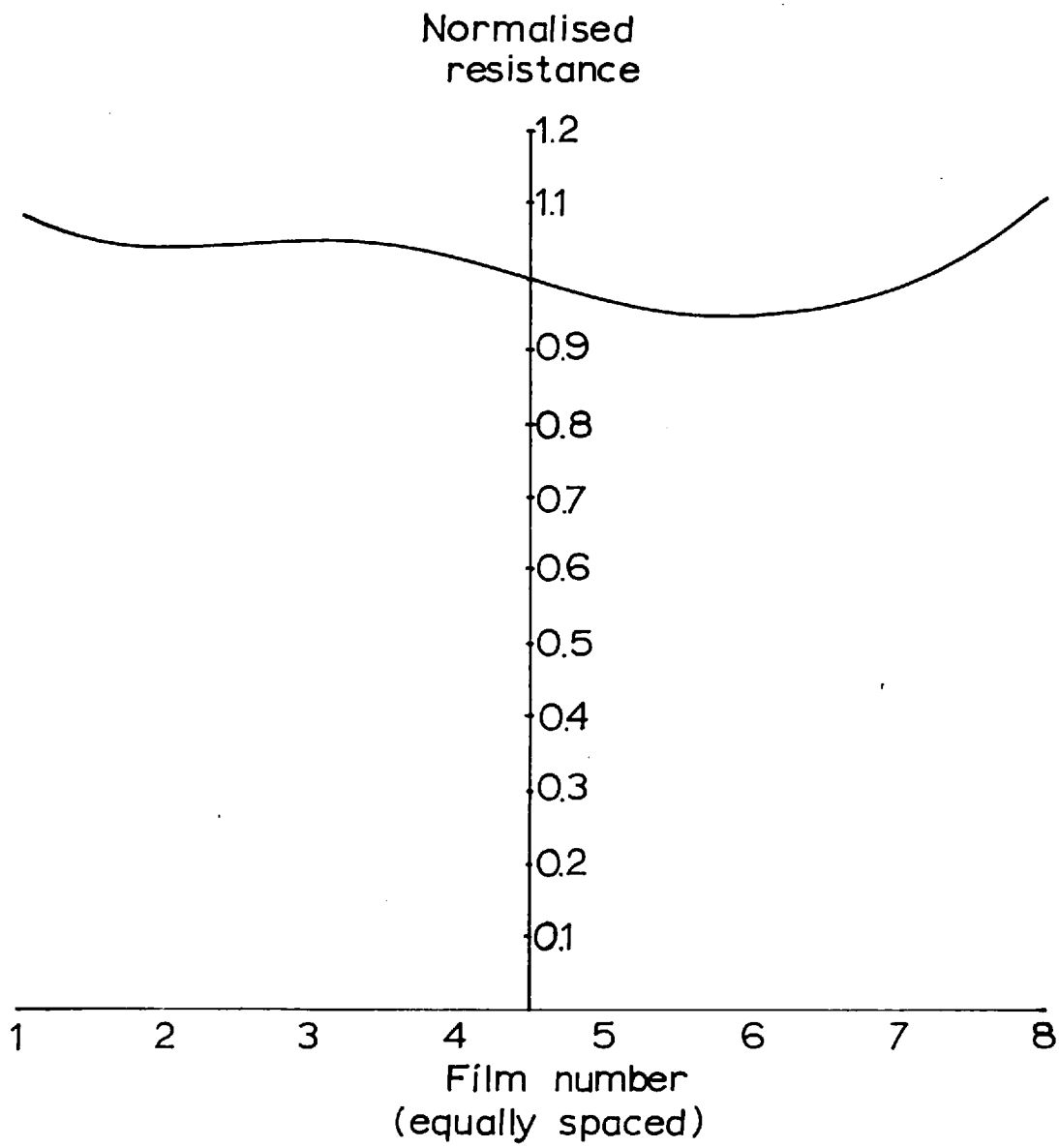

the correction factors directly since the film resistance is inversely proportional to its thickness. The system was finally calibrated by depositing about 1000A° of gold, measuring the crystal frequency shift and measuring the thicknesses of the two central films using the Talysurf. In order to avoid damaging the films they were over-coated with silicon monoxide.

The calibration experiment was subject to the following errors

(i) ± 2% - Talysurf measurement on 1000A° films;

(ii) ± 1% - frequency measurement;

(iii) ± 0.5%- resistivity approximation.

giving a total error of ± 3.5%. This was a constant error which occurred with all of the films. There was also a random error of ± 4% associated with each thickness measurement which had the following components

(i) ± 1% - frequency measurement;

(ii) ± 2% - rate control;

(iii) ± 1% - exposure time.

Thus the total error was ± 7.5%. In retrospect this could have been improved to ± 5.5% by using a frequency counter to measure the frequency shifts.

3.3.1.3.2 Electrical and temperature measurements

The electrical measurements were performed in air using the measuring equipment described above. The films were thermally cycled

by placing them in a warm air stream provided by a hair dryer. The film temperature was measured using a chromel-alumel thermocouple cemented to the back of the glass substrate using Durofix. Since the substrate was completely immersed in the air stream, the temperature of the film was taken as that of the thermocouple. Allowing 15 minutes to achieve thermal equilibrium at each temperature the measurements were accurate to $\pm$ 0.25°C. Since the resistance measurements were accurate to $\pm$ 0.01% and the width to length ratio $W/_{l}$ was known to $\pm$ 1% the resistivity measurements were accurate to $\pm$ 8.5% of which $\pm$ 3.5% was a constant error. The values of temperature coefficient were accurate to $\pm$ 2%.

C H A P T E R IV

Experiments and Results

4.1 Introduction

Chapter III described the apparatus and techniques required to carry out the preparation and examination of the films involved in this study. This chapter will now describe the experiments performed and present their results. These will be analysed and discussed in the following chapter. Like Chapter III this one will be divided into two parts; one describing the work on nichrome and nickel films and the other that on continuous gold films.

4.2 Nichrome and nickel films

4.2.1 Vacuum conditions

Since this study of nichrome films principally involves the comparison of sets of films prepared under two types of vacuum environment it was first necessary to characterise the conditions.

4.2.1.1 Baked equipment

It has been described how an ultimate vacuum pressure of 3×10^{-9} torr. could be readily achieved by baking the system for three hours at 250°C. On turning up the flash source to its operating temperature the pressure rose, after an initial transient, to an

equilibrium pressure of 2 - 3 x 10^{-7} torr. This was due to outgassing of the immediate surroundings of the source. Thorough outgassing was achieved by running the source for an hour and then allowing the system to cool. This permitted the source to be turned on again for periods of upto ten minutes without the pressure rising above 6 - 7 x 10^{-8} torr. This background which existed before the evaporation of the powder is described by the mass spectrum in Fig. (4.2). Fig. (4.1) shows a spectrum recorded just before turning on the source again after outgassing it. Though the ionisation efficiencies of the gauge for the various gases are not known the spectra provide a qualitative picture of the conditions within the system. Comparison of these two spectra shows an increase in the components associated with mass peak 28, i.e. carbon monoxide and nitrogen, when the source is turned on. Thus the background contained mainly water, nitrogen and carbon monoxide.

When the powder dispenser was switched on the pressure rose to approximately 5 x 10^{-7} torr. owing to outgassing from the powder when it impinged on the hot source. The exact equilibrium pressure depended on the rate of evolution of gas and therefore on the evaporation rate. In order to preserve a pressure of 5 x 10^{-7} torr. the rate was not allowed to exceed 5 - 7 A^{o}/sec. Initial experiments showed that prolonged baking of the vacuum system at 400^{o}C did not noticably outgas the powder. Proper outgassing would have necessitated

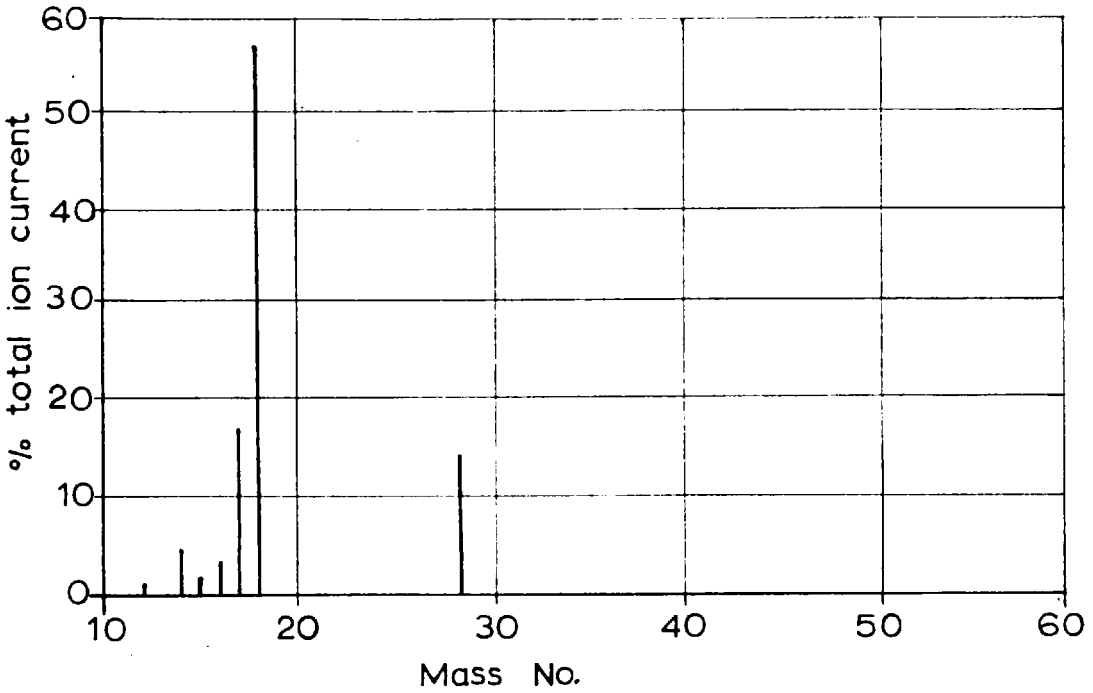

FIG. 4·1. Spectrum before turning on source.
(Total pressure = $1{\cdot}5 \times 10^{-8}$ torr.)

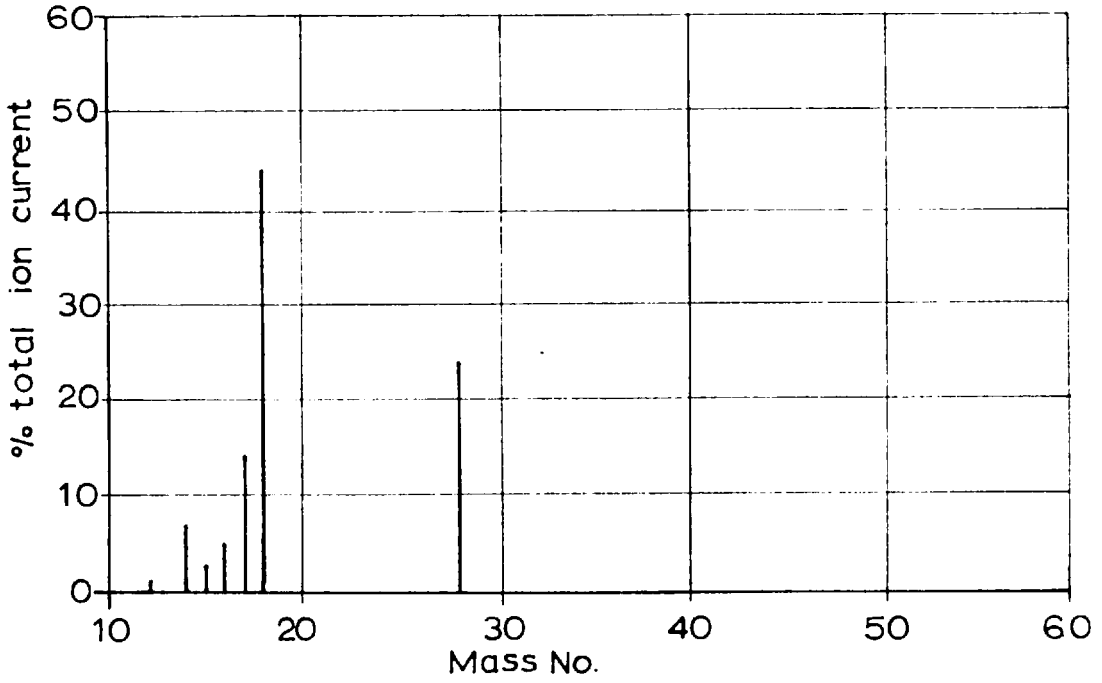

FIG. 4·2. Spectrum ~1 min. after turning on source.
(Total pressure = 6×10^{-8} torr.)

heating the powder to near to its melting temperature since the quantity of gas evolved depends exponentially on the outgassing temperature. To do this would have been extremely difficult for two main reasons:

(i) sintering would have occurred;

(ii) the powder would have had to be outgassed in a separate crucible within the system and then transferred to the dispenser.

Thus there was an upper limit to the vacuum pressure attainable during the deposition. Fig. (4.3) shows a mass spectrum recorded while the powder was being evaporated. This shows that the most significant component was nitrogen which had been increased by a factor of twenty four compared to a factor of two for water.

As these conditions could be readily achieved using the glass bell jar sealed by a Viton-A gasket this arrangement was used for most of the higher vacuum depositions. It had the advantage of providing better visibility and a quicker cycle time since the jar was outgassed at $\sim 150^{\circ}C$ by radiation from the source during the source outgassing process. Using this arrangement the background pressure was about 5×10^{-8} torr. after the source had been outgassed. Thus a reproducible set of conditions was established in which to perform the higher vacuum depositions.

FIG. 4.3 Spectrum during deposition
(Total pressure = 5×10^{-7} torr.)

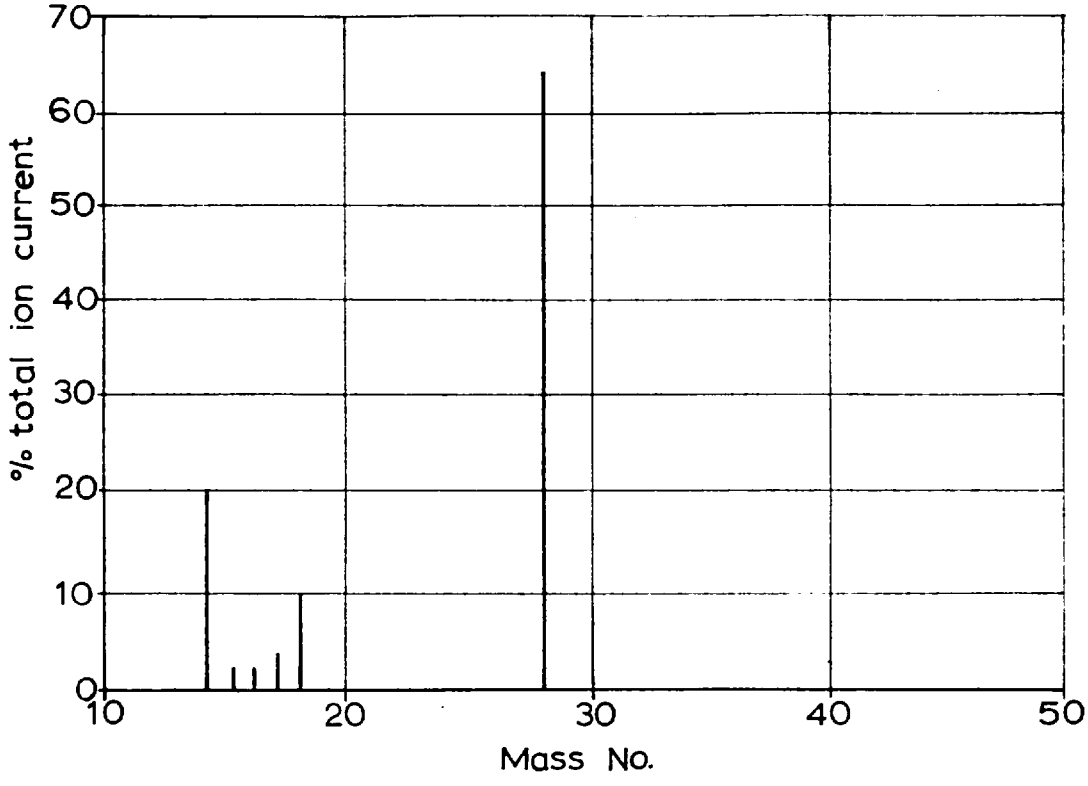

FIG. 4.4 Spectrum after running an empty source in an unbaked system.
(Total pressure = 2×10^{-5} torr.)

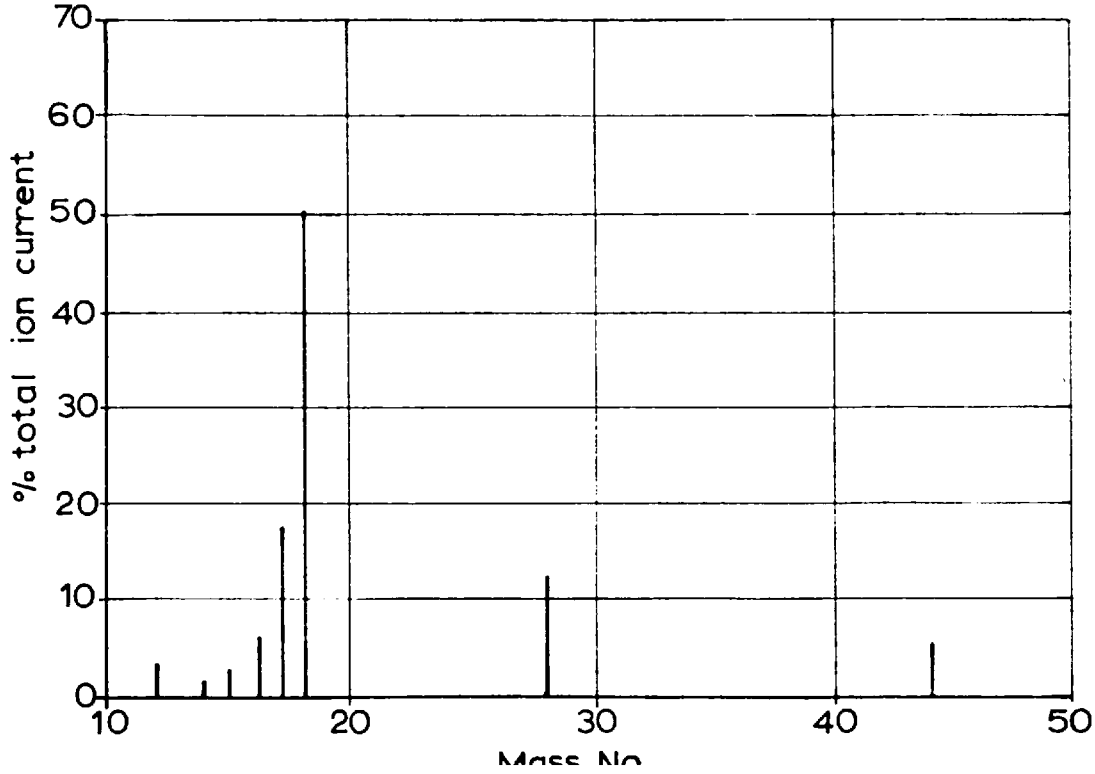

4.2.1.2 Unbaked equipment

After 2 - 3 hours pumping without baking or using the liquid nitrogen trap the vacuum pressure was 2 - 3 x 10^{-6} torr. On turning up the source to its operating temperature the pressure rose to 2 - 3 x 10^{-5} torr. Again, this was due to the outgassing of the immediate surroundings of the source. A mass spectrum of this background is shown in Fig. (4.4). The main component was water which was to be expected in an unbaked system.

When the source had been left on for about fifteen minutes, the pressure fell slowly as outgassing progressed. This period provided a well defined vacuum condition in which the pressure was steady at $\sim$2 x 10^{-5} torr. The high pressure depositions were performed in this environment. The only effect of evaporating the powder was a slight fall in pressure owing to gettering. This was more pronounced when depositing nichrome compared with nickel. The pressure rise to be expected from the outgassing of the powder was 5 x 10^{-7} torr., a small fraction of the total pressure.

None of the mass spectra include a peak at mass number 32. On bleeding air into the system the increase of the oxygen component was very small by comparison with the increase in nitrogen. This suggests that either the ionisation efficiency of the spectrometer for oxygen was very low or that oxygen was being gettered within the spectrometer by its tungsten filament. An improvement to minimise

the latter would be to run the filament at a lower temperature by using a low work function cathode, e.g. lanthanum hexaboride on rhenium. The presence of a peak at mass number 16 was probably due to methane, CH_4.

4.2.2 Deposition conditions

The films were prepared from a powder manufactured by B.S.A., Birmingham, and kindly donated by the Plessey Company Ltd.. The rates of deposition were in the range one to six angstroms per second except when the effect of much higher rates was being assessed. Immediately after the deposition of the specimen the copper-manganese contacts were deposited and the masks were removed from the substrate.

To ensure that the electrical measurements should be stable and reproducible on thermal cycling the films were annealed for several hours at the preparation temperature 270°C. This was chosen because it was considerably above 120°C, the highest temperature used in the measurement of the temperature coefficients of resistance. A twelve hour anneal was suitable since they could be left over night but in fact three hours was found to be the minimum required to achieve electrical stability.

After annealing, the specimen was cooled to room temperature in steps of 30 - 40°C. At each temperature the specimen was allowed to reach thermal equilibrium for a minimum of one hour before its

resistance and temperature were measured. For low resistance films it was necessary to introduce an external resistance to limit the current to $\sim$ 2mA. This was necessary to avoid ohmic heating of the film.

At room temperature the specimen was removed from the system and its thickness was measured using the Talysurf. The structural specimens were stored in air to await examination in the electron microscope. There was often a delay of several days but a comparison of films examined immediately and one week after deposition showed no difference in structure or in their electron diffraction patterns. All of the specimens were photographed at 100KV at a magnification of 50,000 times.

4.2.3 Summary of films prepared

Two series of 80/20 nichrome films were prepared ranging in thickness between 50A$^{\circ}$ and $\sim$1000A$^{\circ}$. The first was prepared at a pressure of 2 x 10^{-5} torr. and comprised specimens 1 to 23. Their parameters are tabulated in Table 4.1 and graphs of T.C.R., resistivity and sheet resistivity are shown plotted against thickness in Figs. (4.7), (4.5) and (4.6) respectively. In order that their electrical parameters can be related to the structure of the films the series is described by five micrographs and an electron diffraction pattern, see Plates 4.1 to 4.6.

The second series was prepared at a pressure of $\sim 7 \times 10^{-7}$ torr. and contained twenty films numbered 24 to 43. Their parameters are contained in Table 4.2 and graphs of T.C.R., resistivity and sheet resistivity plotted against thickness are shown in Figs. (4.10), (4.8) and (4.9) respectively. This series is described photographically by Plates 4.7 to 4.12.

In order to examine the effect of the chromium component on the structure and properties of nichrome two similar series of pure nickel films were prepared. The first comprised specimens 44 to 58 and their parameters are shown in Table 4.3. The variations of T.C.R., resistivity and sheet resistivity with thickness are shown in Figs.(4.13),(4.11) and (4.12) respectively. The structure of this series is illustrated by Plates 4.13 to 4.18, Plate 4.18 being a typical electron diffraction pattern.

The second series of nickel films is made up of specimens 59 to 72. Table 4.4 contains their parameters and graphs of T.C.R., resistivity and sheet resistivity versus thickness are shown in Figs.(4.16),(4.14) and (4.15) respectively. The corresponding photographic series is Plates 4.20 to 4.26.

TABLE 4.1

80/20 Ni/Cr films prepared at ~ 2 x 10^{-5} torr.

Spec.No.	d (Å)	R (Ω/□)	α p.p.m./°C	ρ μΩ-cm	rate Å/sec	p μ torr	Plate Nos.
1	300	32.7	83	98	2.5	9	4.5
2	950	10.2	68	97	5.3	10	
3	630	16.0	80	101	10.5	20	
4	100	152	260	152	2.5	20	
5	185	51.3	178	95	1.5	70	4.4
6	140	75.9	136	106	1.5	30	
7	125	74.7	218	93	2.1	20	
8	70	1060	120	742	1.5	25	4.2
9	230	31.6	182	73	4.0	15	
10	70	991	98	830	1.0	30	
11	145	45.6	159	66	3.2	15	
12	65	1223	122	795	1.0	20	
13	105	224	480	224	0.5	30	4.3,4.6
14	240	53.2	176	128	15	10	

TABLE 4.1 (Continued)

Spec.No.	d (A^o)	R ($\Omega/\square$)	α p.p.m./°C	ρ $\mu\Omega$-cm	rate A^o/sec	p μ torr	Plate Nos.
15	80	506	237	405	16	10	
16	250	46.8	213	117	17	3	
17	80	484	272	387	11	10	
18	80	1116	285	900	13	10	
19	130	153	376	198	26	10	
20	170	75	291	127	4.0	20	
21	50	6.1×10^6	-3000	3×10^6	1.0	10	4.1
22	120	470	341	565	4.0	15	
23	85	186	344	158	4.0	12	

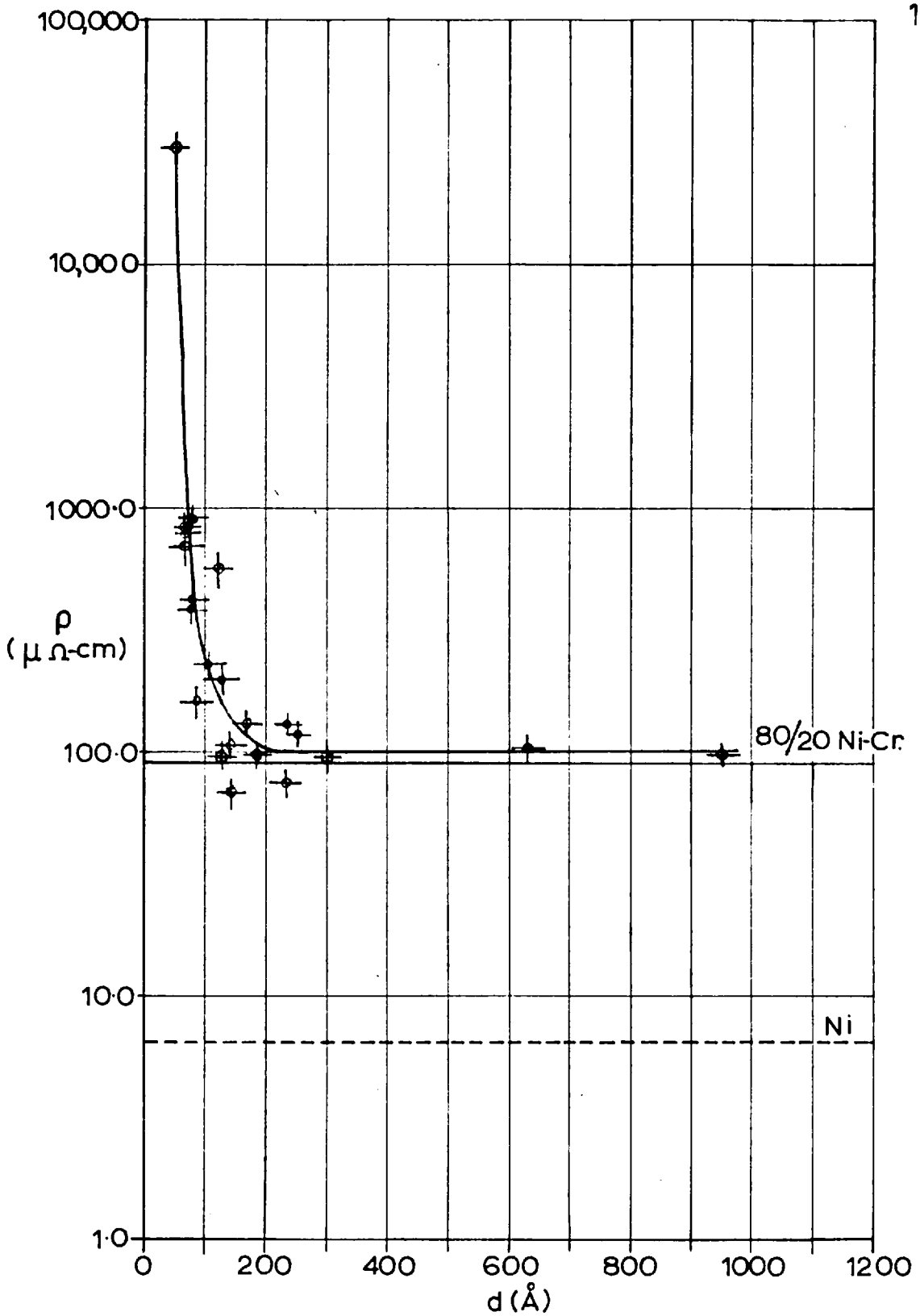

FIG. 4·5. Resistivity v thickness for 80/20 Ni-Cr films deposited at 2×10^{-5} torr

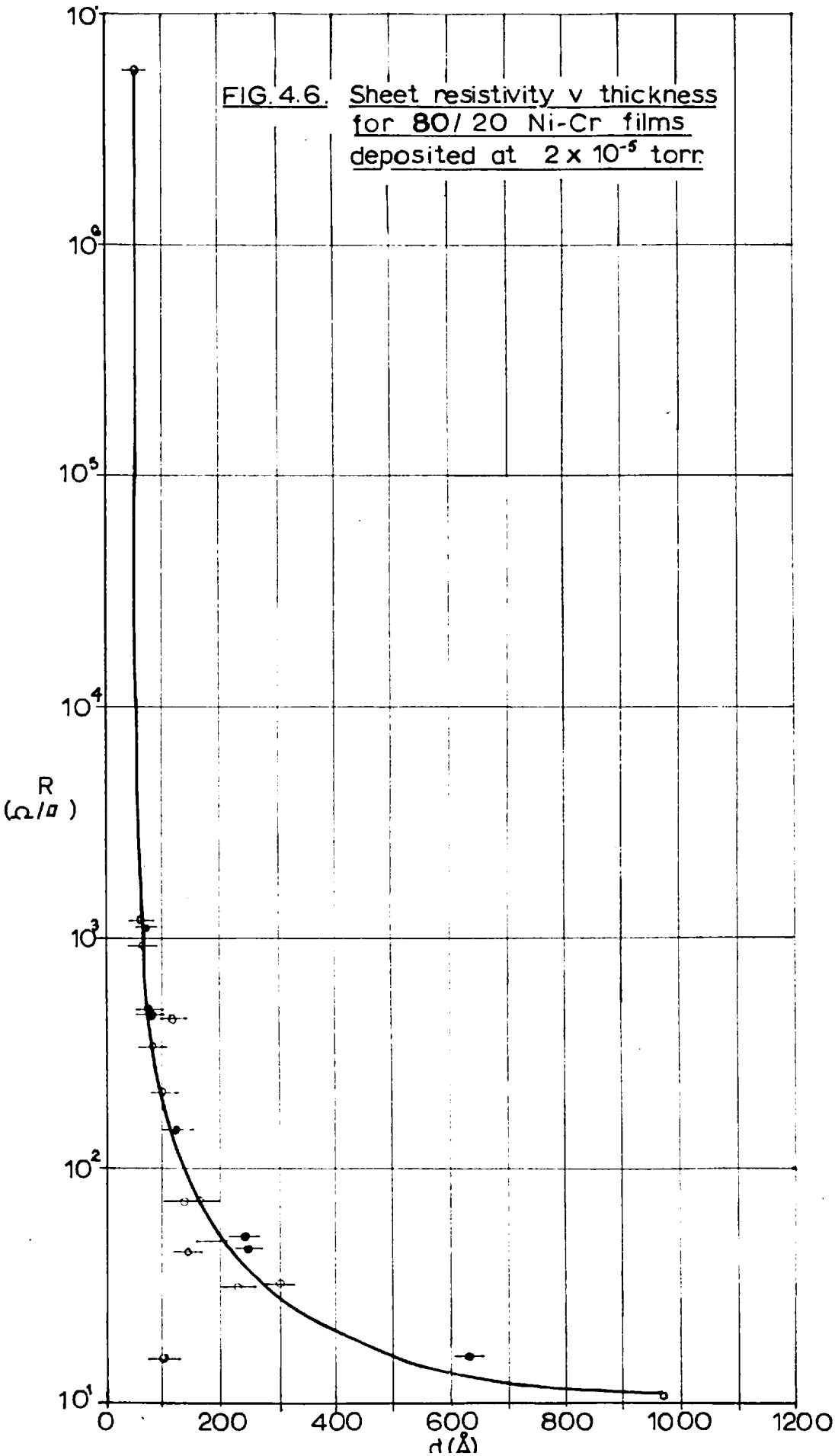

FIG. 4.6. Sheet resistivity v thickness for 80/20 Ni-Cr films deposited at 2×10^{-5} torr

FIG. 4.7 T.C.R. v thickness for 80/20 Ni-Cr films deposited at 2×10^{-6} torr.

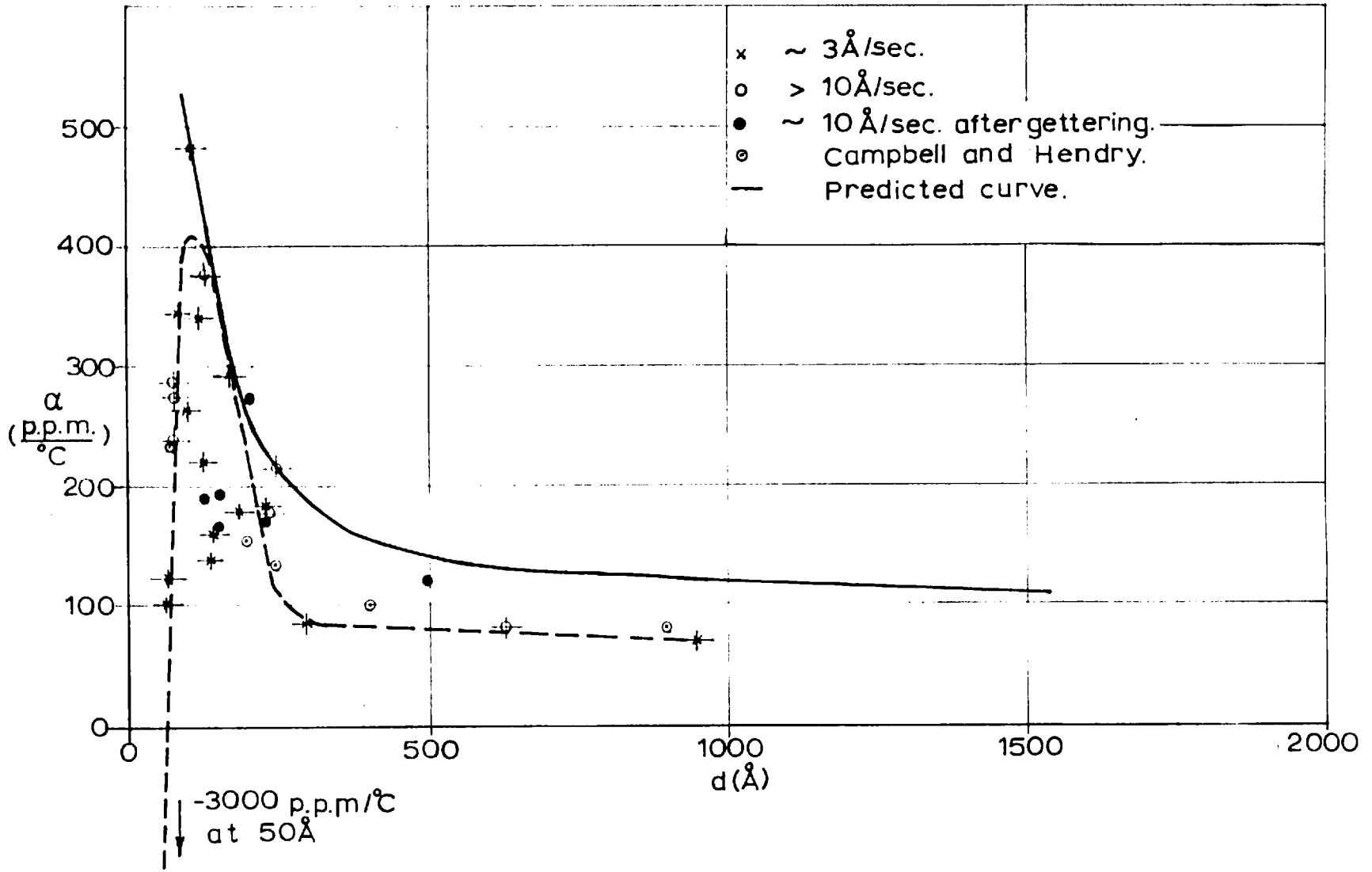

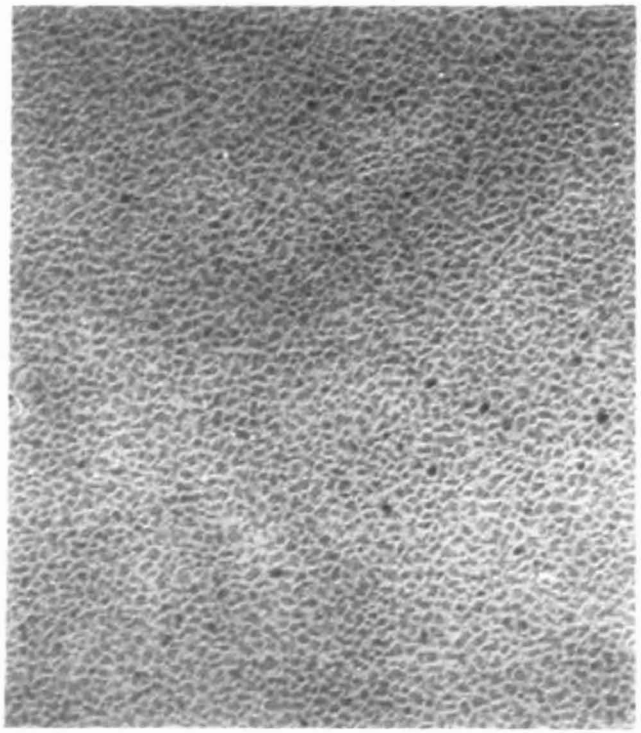

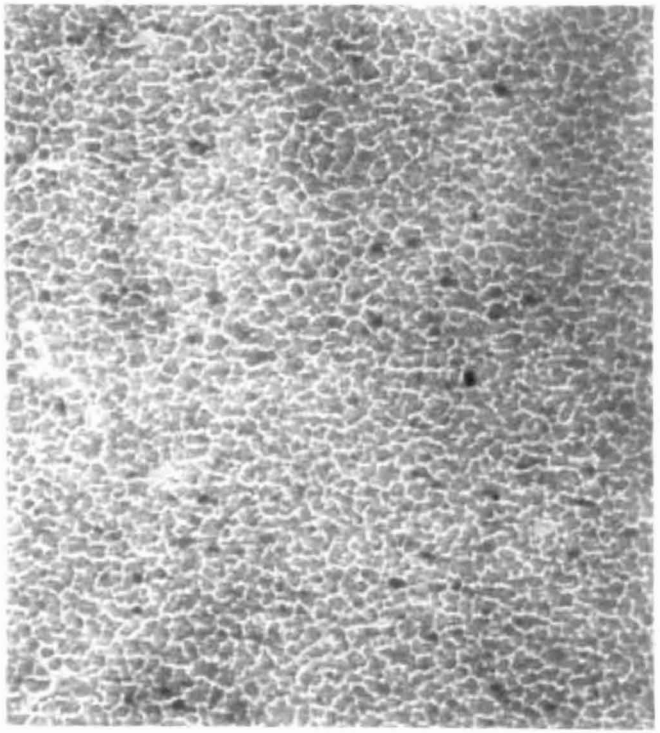

1000 Å

Plate (4.1)

Specimen 21

$R = 6.1 M\Omega/\square$ $\alpha = -3000$ p.p.m./°C

$d \sim 50$ Å $\rho = 3 \Omega.cm.$

Plate (4.2)

Specimen 8

$R = 1270 \Omega/\square$ $\alpha = 120$ p.p.m./°C

$d = 70$ Å $\rho = 8.9 \times 10^{-4} \Omega.cm.$

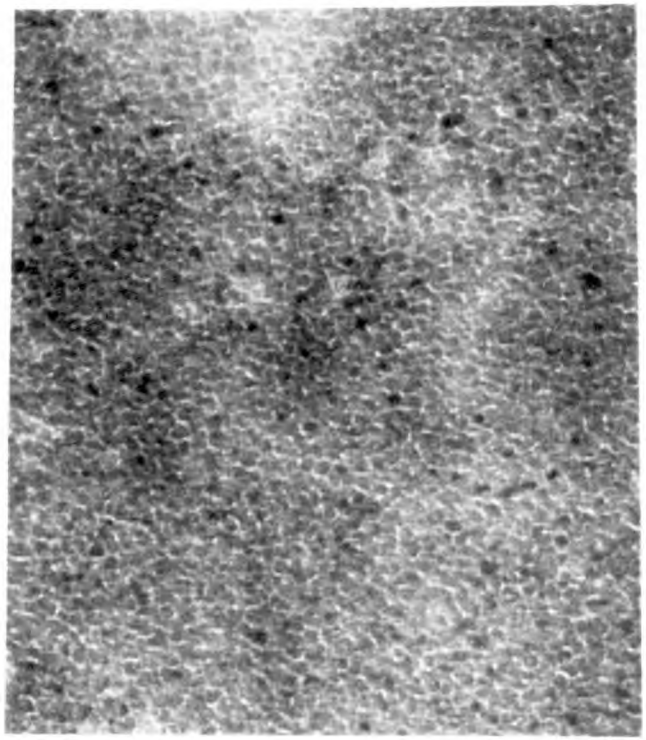

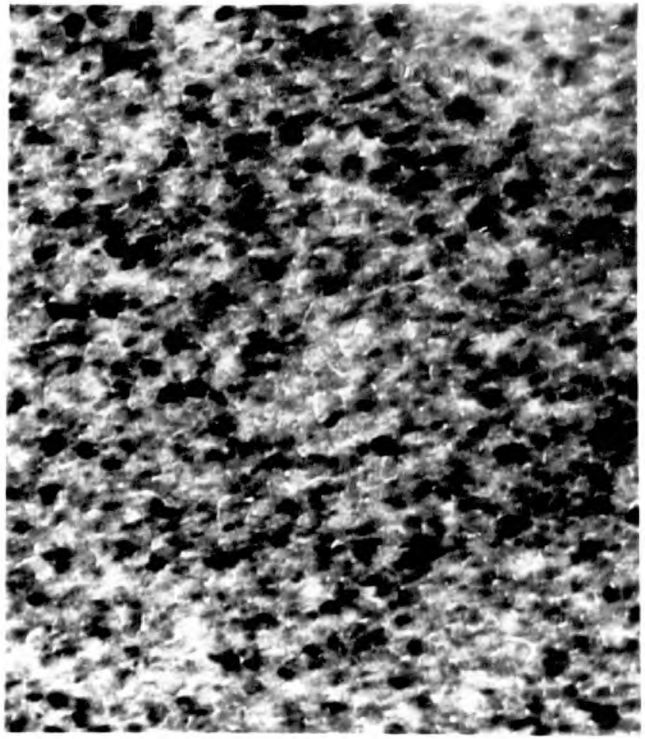

Plate (4.3)

Specimen 13

1000Å

Plate (4.4)

Specimen 5

R = 269Ω/□ α = 480 p.p.m./°C

d = 105Å $\rho = 2.8 \times 10^{-4}$ Ω.cm.

R = 61.7Ω/□ α = 178 p.p.m./°C

d = 185Å $\rho = 1.1 \times 10^{-4}$ Ω.cm.

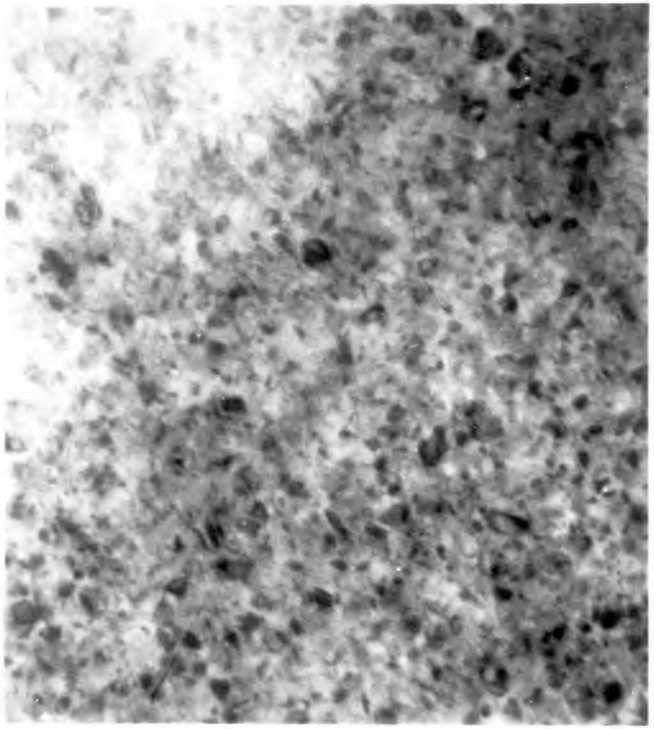

Plate (4.5)

Specimen 1

1000Å

Plate (4.6)

Specimen 13

$R = 39.2\,\Omega/\square$ $\alpha = 83$ p.p.m./°C

$d = 300$Å $\rho = 1.2 \times 10^{-4}\,\Omega.cm.$

A typical electron diffraction pattern (100 Kv.)

TABLE 4.2

80/20 Ni/Cr films prepared at $\sim 7 \times 10^{-7}$ torr.

Spec.No.	d(A^o)	R($\Omega/\square$)	α p.p.m./^oC	ρ ($\mu\Omega$-cm)	rate (A^o/sec)	p μ torr	Plate Nos.
24	540	17.8	78	96	4.5	2	4.11
25	460	21.2	68	98	5.0	1	
26	225	49.2	69	111	3.5	1	
27	250	49.3	71	123	4.0	0.7	
28	110	187	45	206	3.6	0.5	
29	150	86.5	58	129	2.5	0.5	
30	500	22.8	49	114	3.0	0.5	
31	550	17.5	63	96	4.5	0.7	
32	175	75.0	89	131	3.0	0.7	
33	1600	7.5	66	118	5.0	0.5	
34	1200	9.4	68	112	5.0	0.7	
35	50	O.C.				1.0	
36	130	O.C.			2.0	0.7	
37	180	73.9	109	133	2.0	0.5	

TABLE 4.2 (Continued)

Spec.No.	d(A°)	R(Ω/□)	α p.p.m./°C	ρ (μΩ-cm)	rate (A°/sec)	p μ torr	Plate Nos.
38	170	80.1	84	136	3.0	0.5	
39	170	115	234	196	2.5	0.5	
40	100	10^8			2.0	0.6	4.7
41	120	172	100	206	2.0	0.5	4.8
42	125	100	177	125	2.0	0.5	4.9
43	190	72.0	212	136	4.0	0.5	4.10,4.12

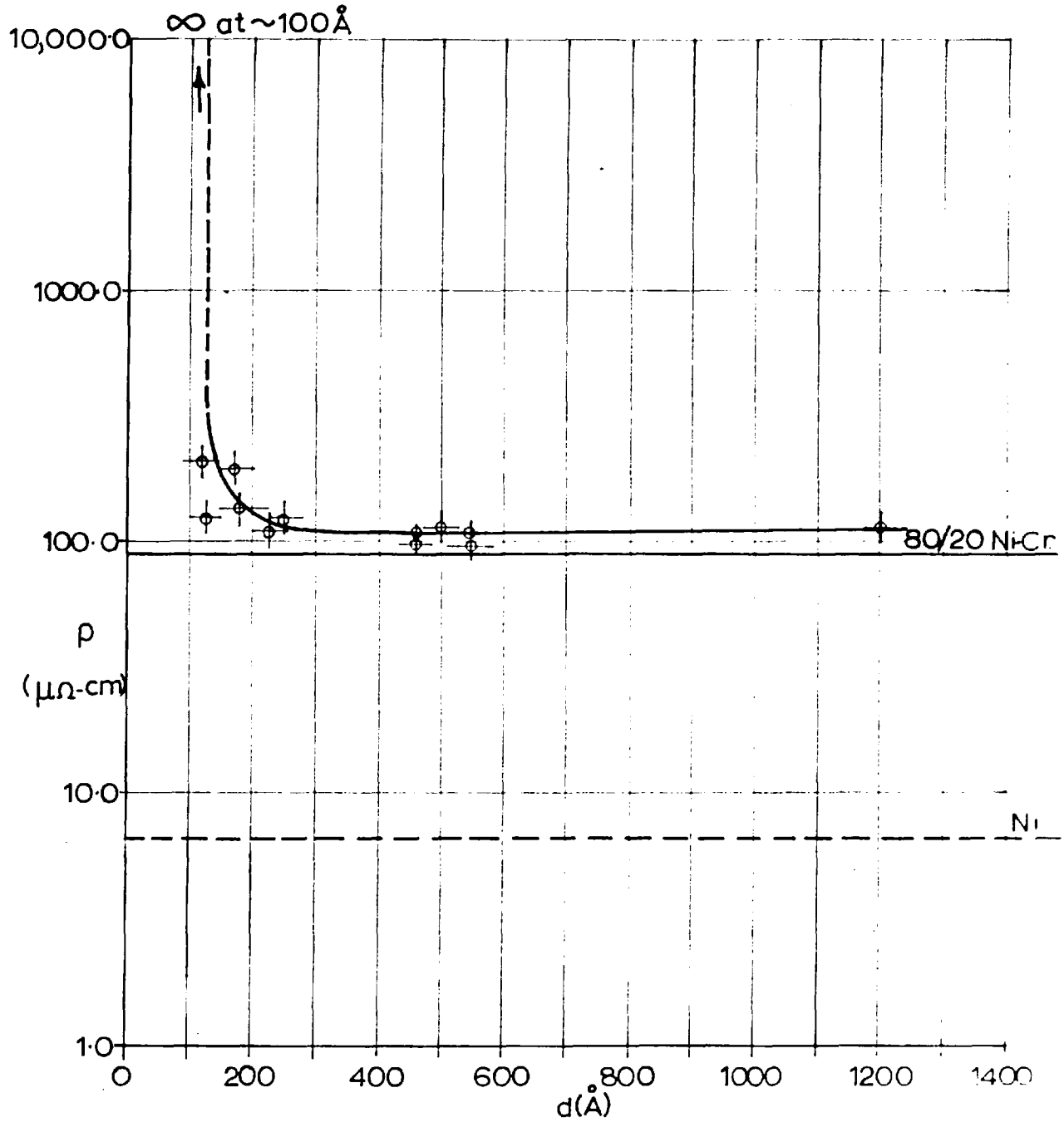

FIG. 4·8 Resistivity v thickness for 80/20 Ni-Cr films deposited at 7×10^{-7} torr

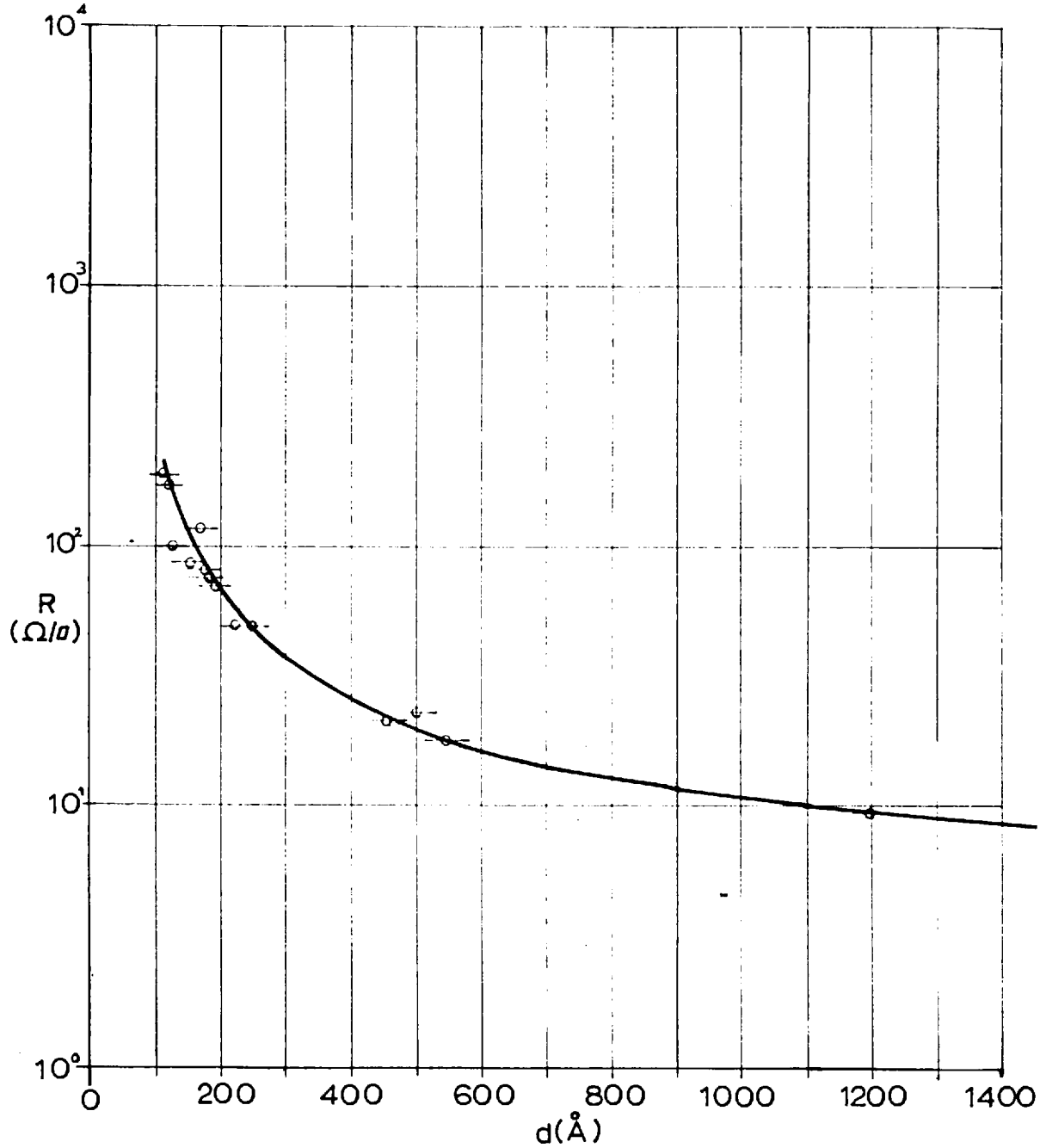

FIG. 4.9. Sheet resistivity v thickness for 80/20 Ni-Cr films deposited at 7×10^{-7} torr.

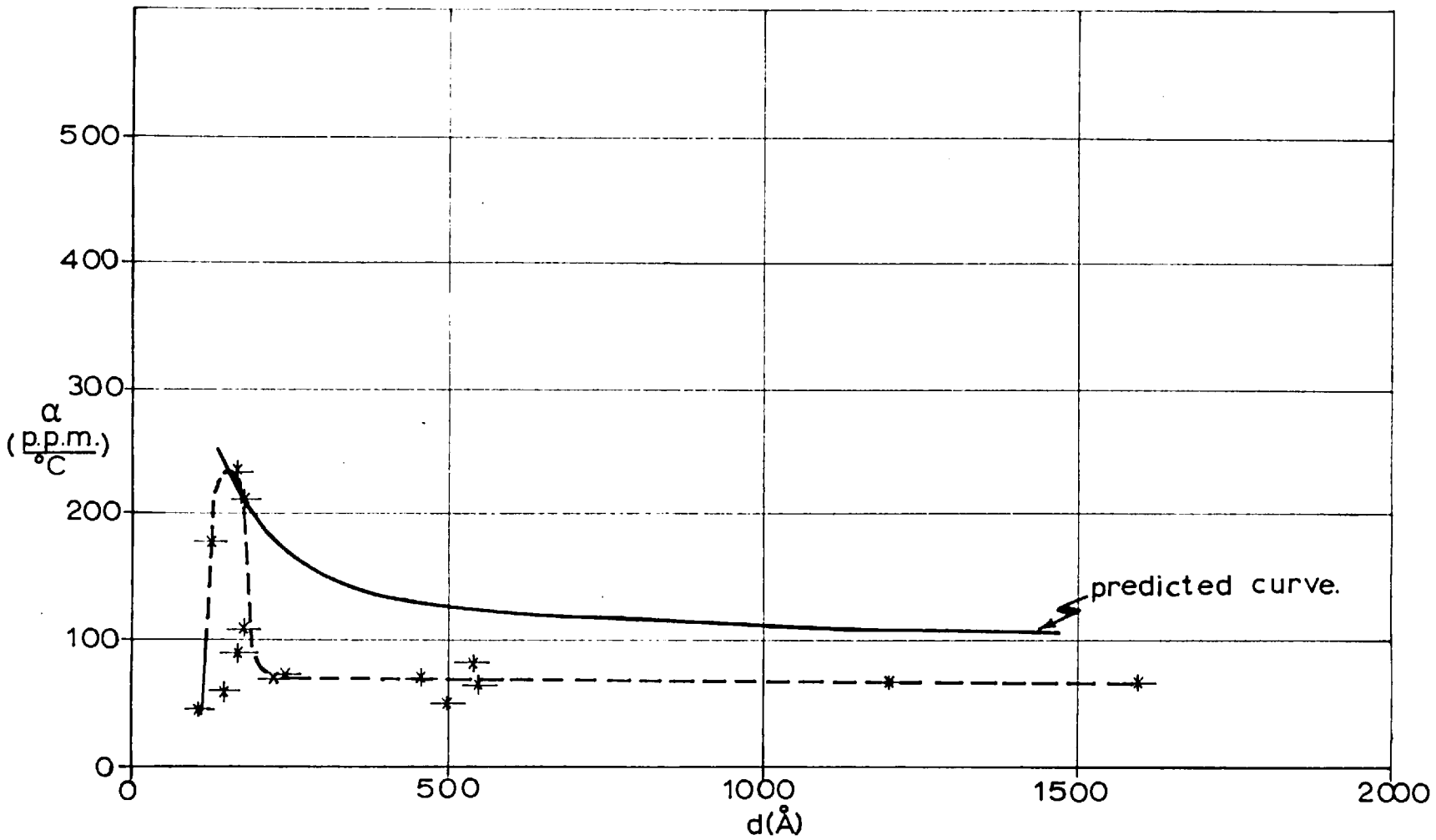

FIG. 4.10 T.C.R. v thickness for 80/20 Ni-Cr films deposited at 7×10^{-7} torr.

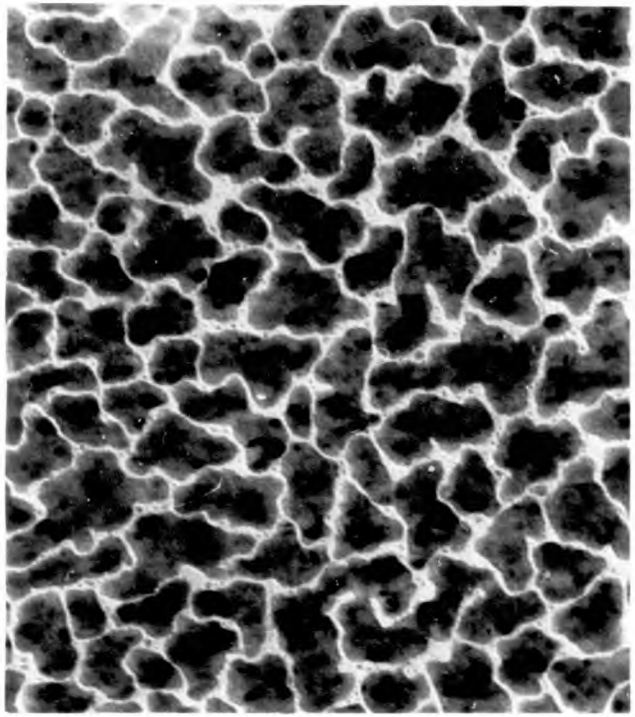

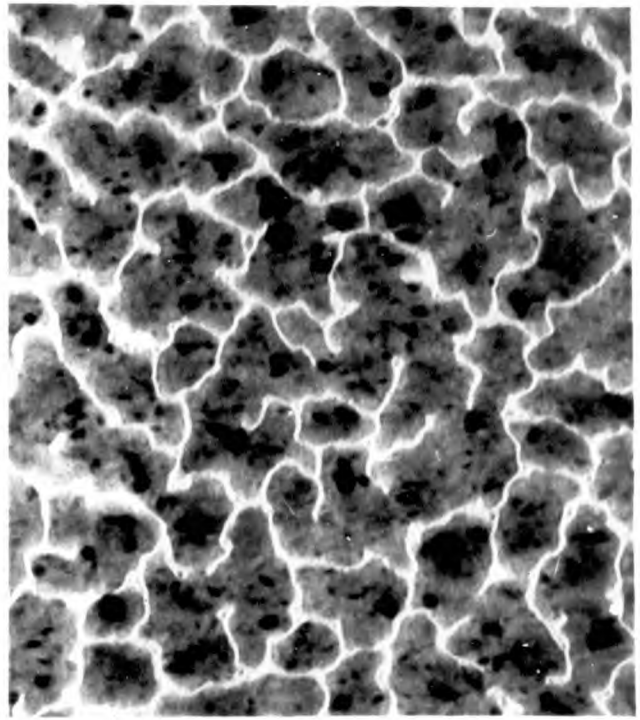

Plate (4.7)
Specimen 40

1000Å

Plate (4.8)
Specimen 41

Resistance ~ 100MΩ

d = 100Å

R = 172Ω/□

d = 120Å

α = 100 p.p.m./°C

$\rho = 2.1 \times 10^{-4}\ \Omega.cm$

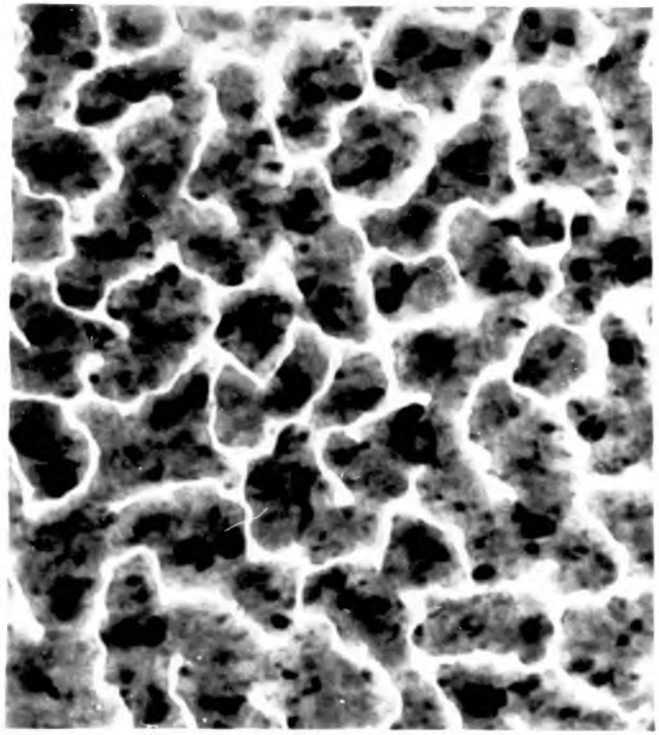

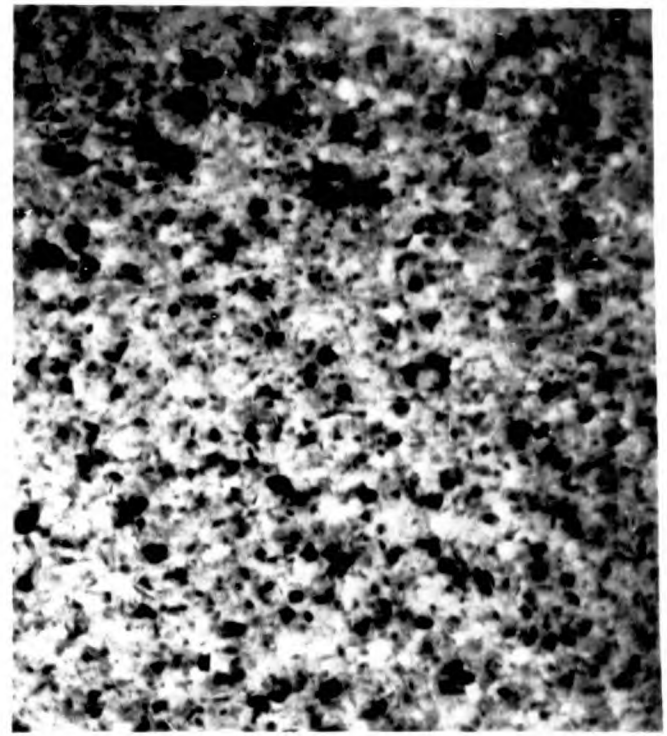

Plate (4.9)

Specimen 42

1000 Å

Plate (4.10)

Specimen 43

R = 100 Ω/ □ α = 177 p.p.m./ °C

d = 125 Å $\rho = 1.25 \times 10^{-4}$ Ω.cm.

R = 72 Ω/ □ α = 212 p.p.m./ °C

d = 190 Å $\rho = 1.36 \times 10^{-4}$ Ω.cm.

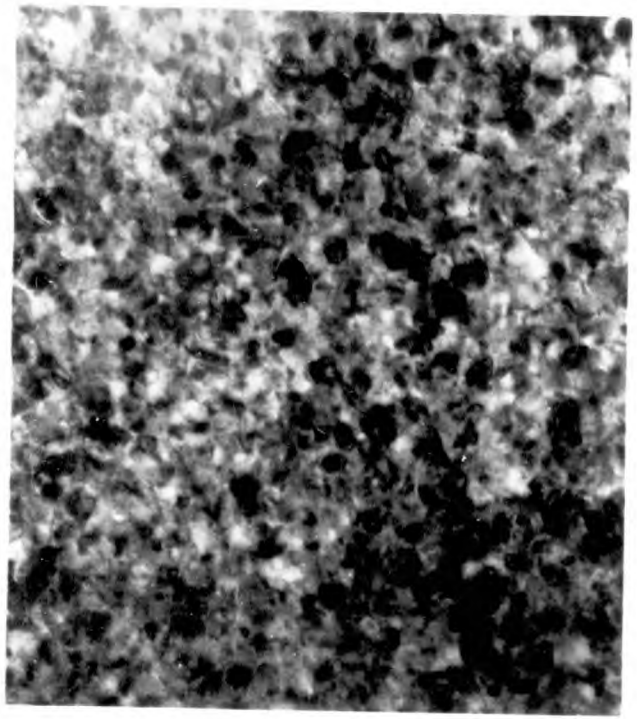

Plate (4.11)
Specimen 24

1000 Å

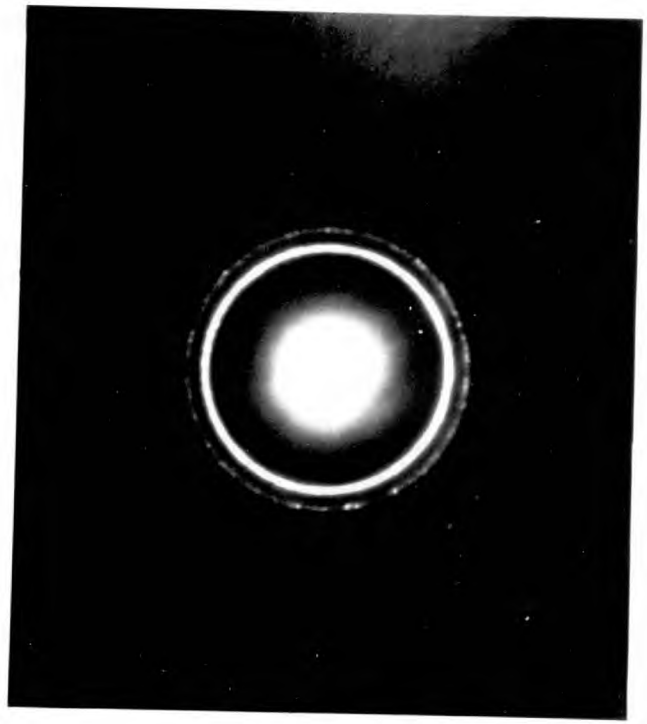

Plate (4.12)
Specimen 43

$R = 17.8\,\Omega/\square$

$\alpha = 79$ p.p.m./°C

A typical electron diffraction pattern (100 Kv.)

$d = 540$ Å

$\rho = 9.6 \times 10^{-5}\ \Omega.cm.$

TABLE 4.3

Nickel films prepared at $\sim 2 \times 10^{-5}$ torr.

Spec.No.	d(A^{o})	R($\Omega/\square$)	α (p.p.m./^{o}C)	ρ ($\mu\Omega$-cm)	rate (A^{o}/sec)	p μ torr	Plate Nos.
44	1150	1.11	5210	12.8	19	10	4.18
45	185	396	-192	732	3	16	4.15
46	300	55.0	2580	165	5	13	
47	250	15.7	3340	39.3	8	13	
48	180	O.C.			6	10	
49	190	109	62.2	200	6	40	
50	175	129	-1.5	225	4	15	4.16
51	180	68.0	3000	122	6	18	
52	200	265	566	530	2	25	
53	350	9.06	3800	31.7	5	20	4.17,4.19
54	325	6.00	3760	10.5	11	20	
55	130	646	-397	840	2	20	4.14
56	75	5180	-814	3890	1	20	
57	70	2980	-736	2100	1	20	4.13
58	2300	0.64	5000	14.6	11	20	

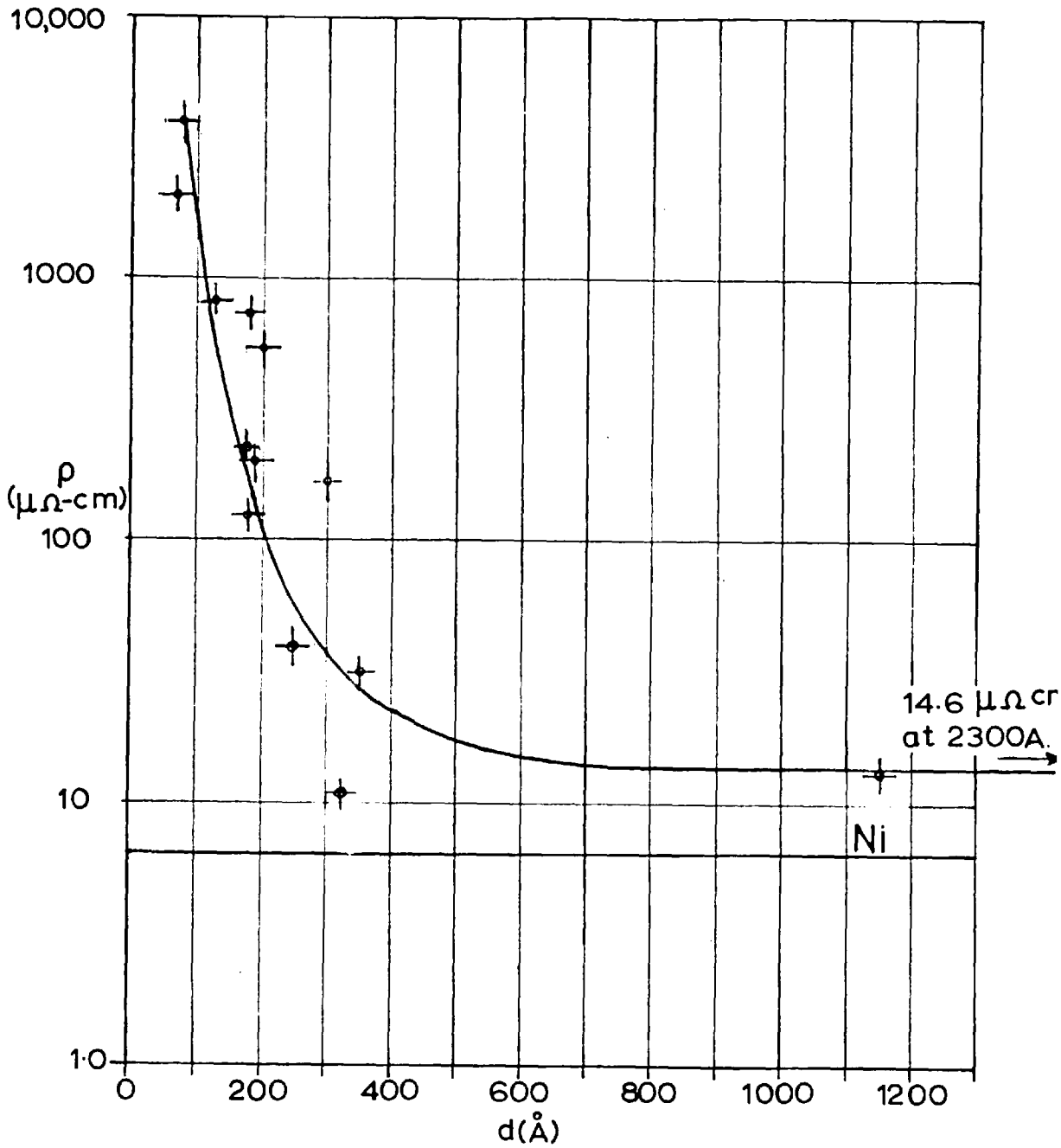

FIG. 4.11. Resistivity v thickness for Ni films deposited at 2×10^{-6} torr.

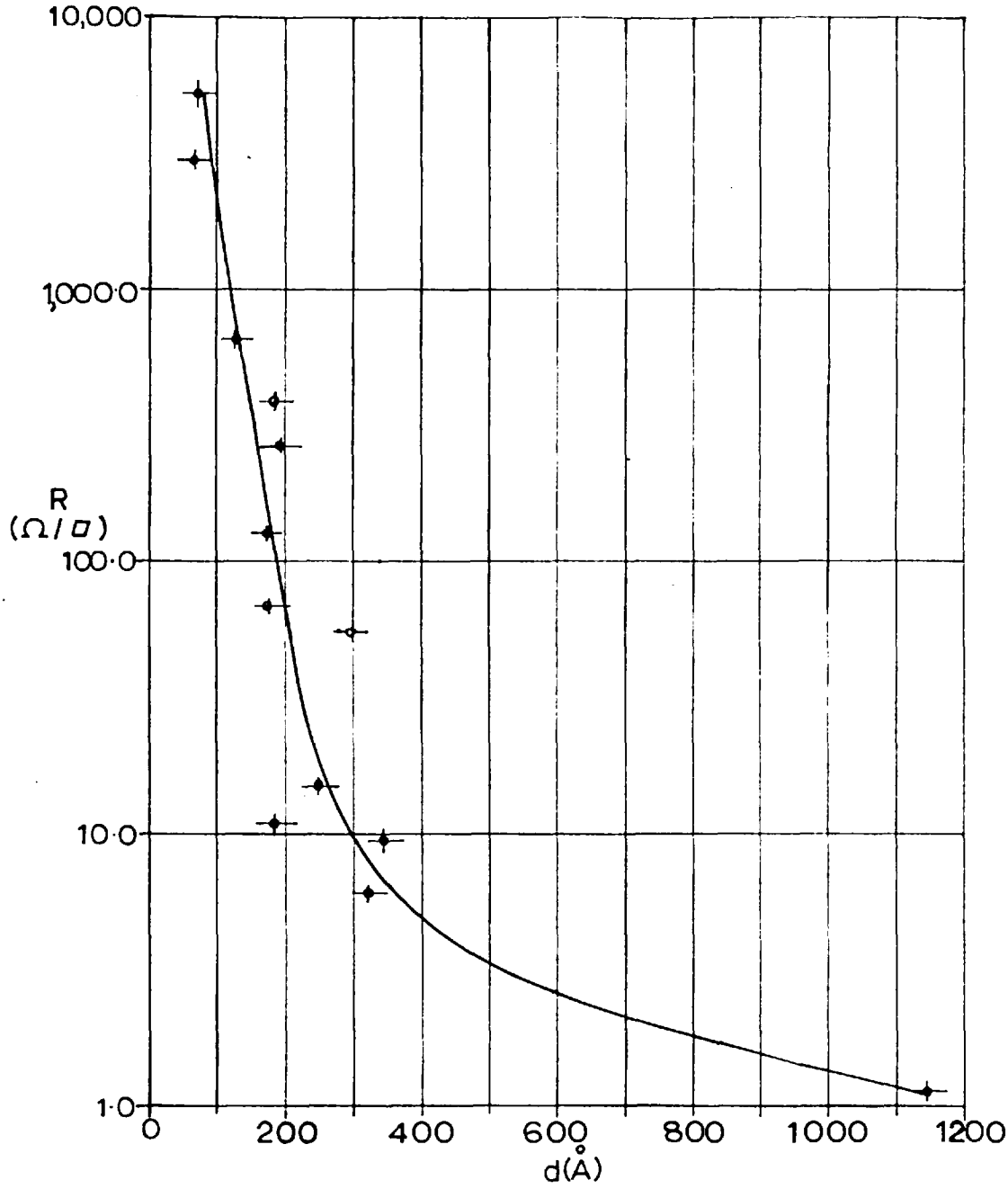

FIG. 4·12. Sheet resistivity v thickness for Ni films deposited at 2×10^{-5} torr.

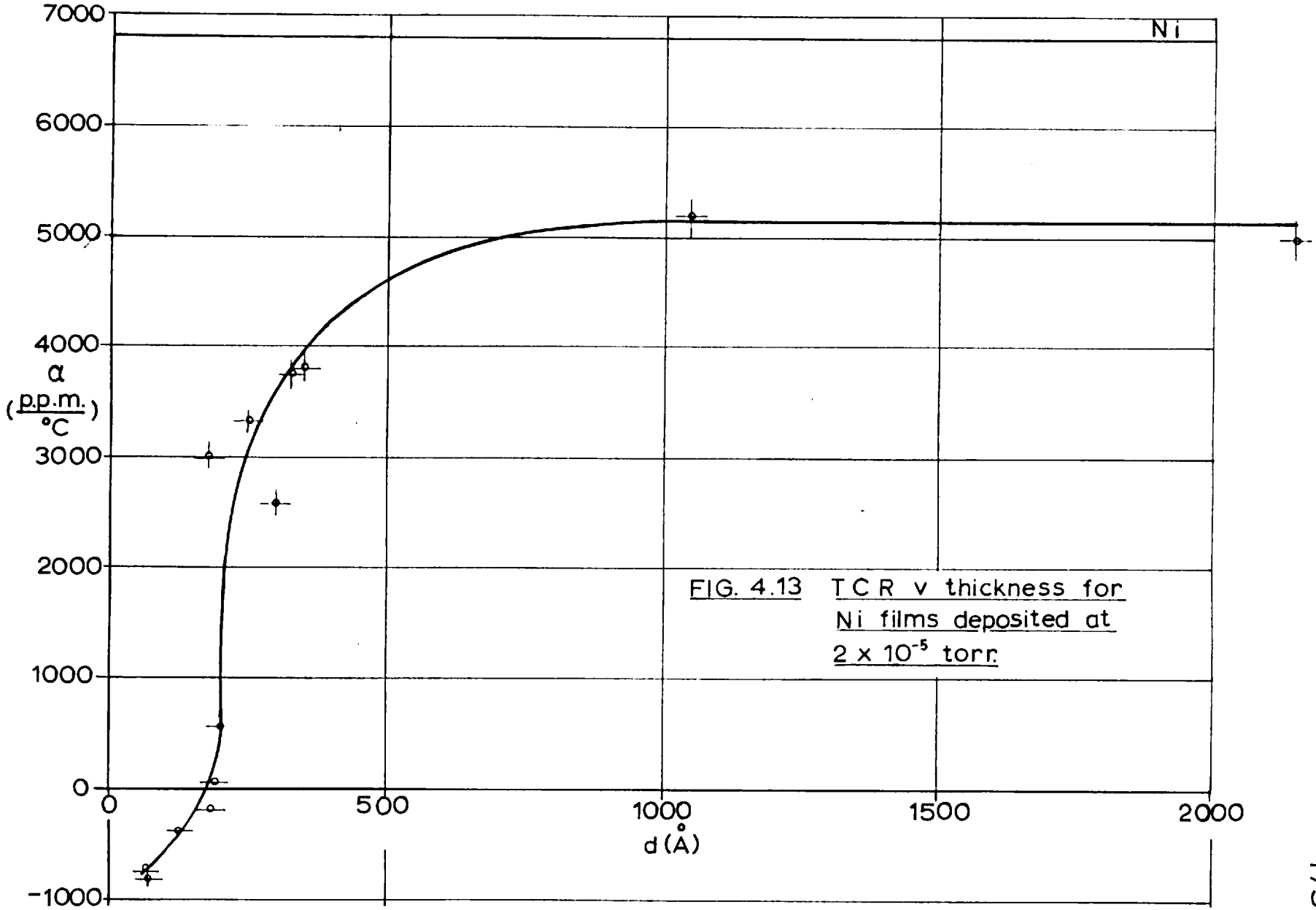

FIG. 4.13 TCR v thickness for Ni films deposited at 2×10^{-5} torr

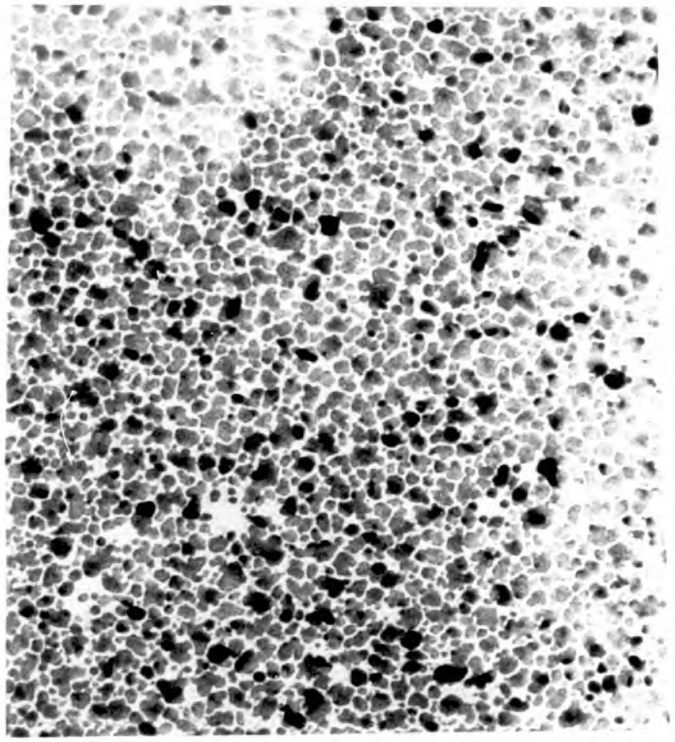

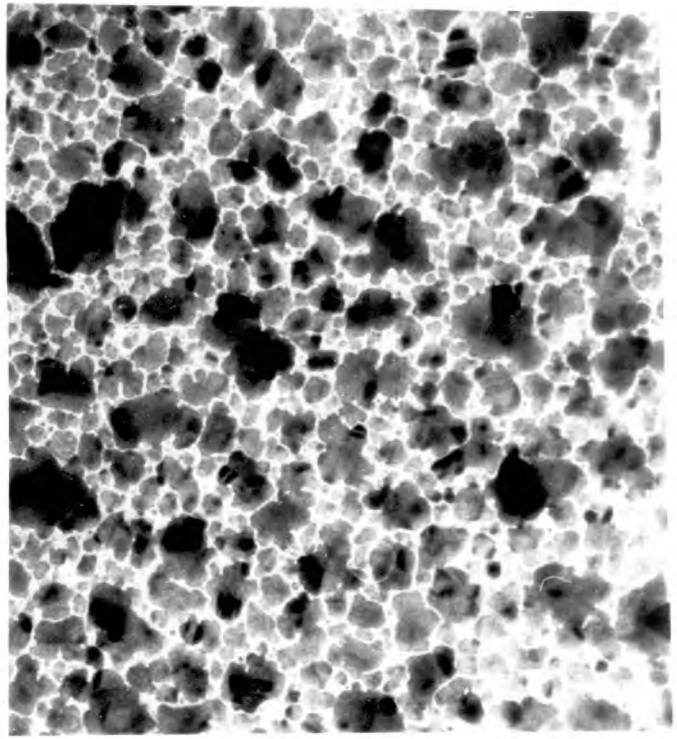

Plate (4.13)
Specimen 57

1000Å

Plate (4.14)
Specimen 55

R = 2976Ω/□ α = -736 p.p.m./°C

d = 70Å $\rho = 2.1 \times 10^{-3}$ Ω.cm.

R = 647Ω/□ α = -398 p.p.m./°C

d = 130Å $\rho = 8.4 \times 10^{-4}$ Ω.cm.

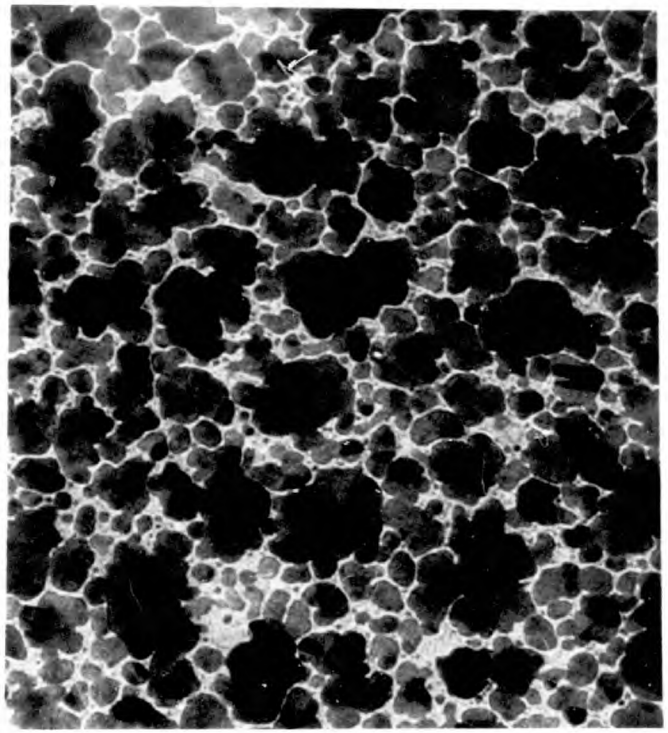

Plate (4.15)
Specimen 45

1000Å

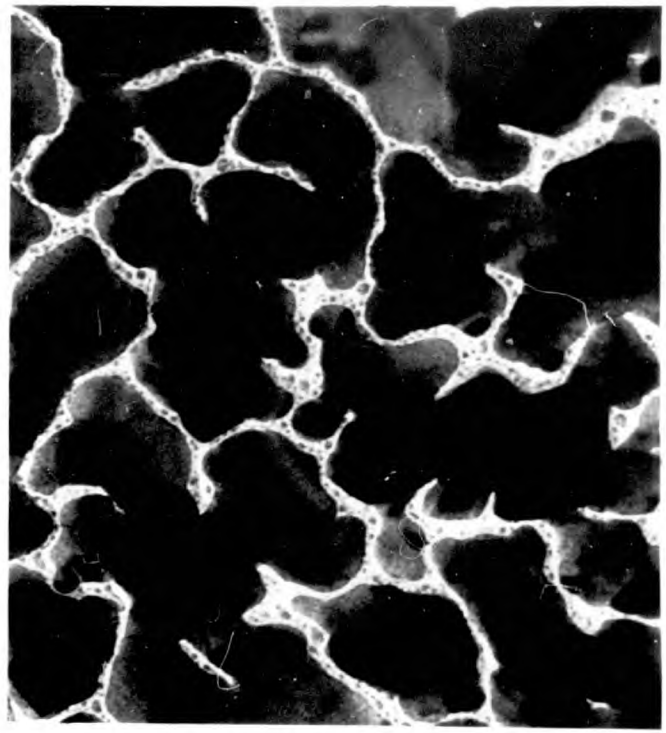

Plate (4.16)
Specimen 50

$R = 396\,\Omega/\square$ $\quad \alpha = -192$ p.p.m./ °C $\quad d = 185$ Å $\quad \rho = 7.3 \times 10^{-4}\,\Omega$.cm.

$R = 129\,\Omega/\square$ $\quad \alpha = -1.5$ p.p.m./°C $\quad d = 175$ Å $\quad \rho = 2.2 \times 10^{-4}\,\Omega$.cm.

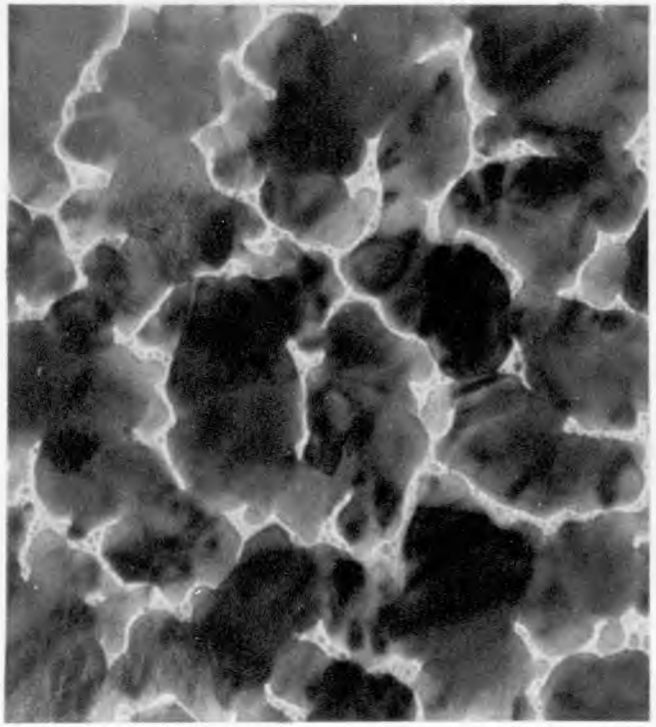

Plate (4.17)

Specimen 53

1000Å

Plate (4.18)

Specimen 44

$R = 9.1\Omega/\square$ $\alpha = 3800$ p.p.m./°C

$d = 350$Å $\rho = 3.2 \times 10^{-5}\ \Omega.cm.$

$R = 1.1\Omega/\square$ $\alpha = 5206$ p.p.m/°C

$d = 1150$Å $\rho = 1.3 \times 10^{-5}\ \Omega.cm.$

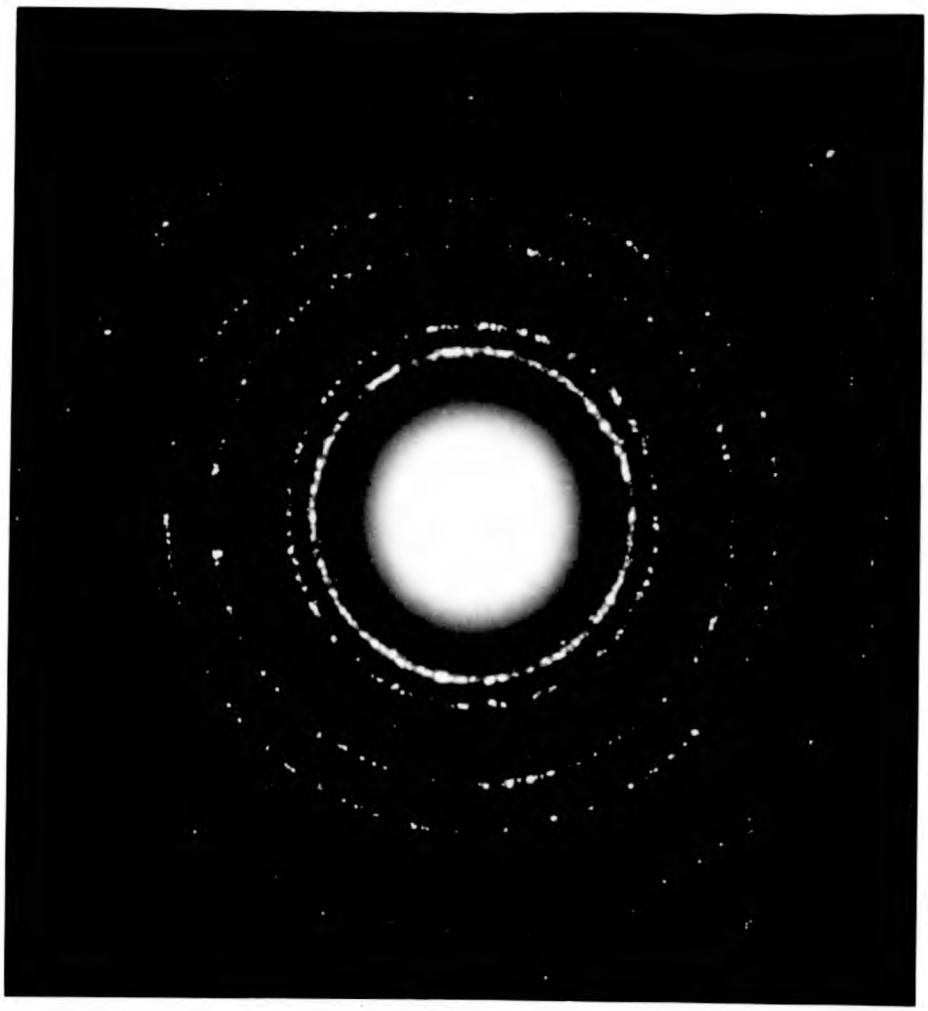

Plate(4.19)

Specimen 53

A typical electron diffraction pattern(100Kv.)

TABLE 4.4

Nickel films prepared at 7×10^{-7} torr.

Spec.No.	d(A°)	R($\Omega/\square$)	α (p.p.m./$^{\circ}$C)	ρ ($\mu\Omega$- cm)	rate (A°/sec)	p (μ torr)	Plate Nos.
59	1100	1.02	5740	11.2	18	0.2	4.25
60	550	3.10	4680	17.0	2.3	0.6	
61	490	3.12	3980	15.2	4.0	0.7	
62	395	6.05	3730	23.9	5.0	0.7	4.24,4.26
63	400	8.80	4200	35.2	3.3	0.7	
64	380	18.4	4120	69.8	4.0	0.7	
65	345	20.1	4960	69.2	3.6	0.6	4.23
66	225	40.2	3180	90	2.5	0.8	
67	240	68.2	3750	164	2.5	0.6	4.22
68	360	19.0	4000	68.3	11	0.6	
69	240	O.C.			3.0	0.6	
70	200	O.C.			2.0	0.7	4.21
71	80	O.C.			0.3	0.7	4.20
72	250	O.C.			2.6	0.8	

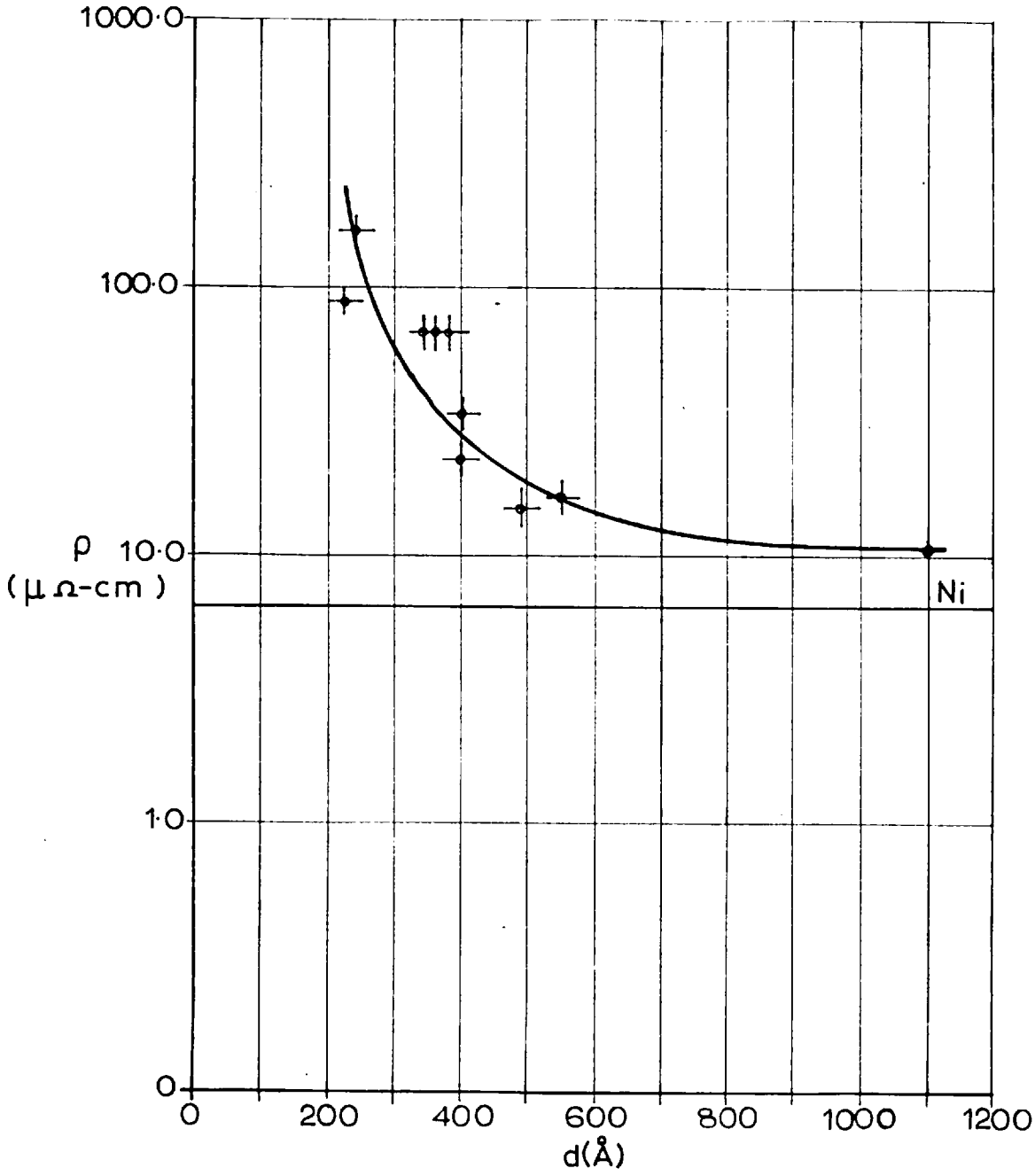

FIG. 4·14. Resistivity v thickness for Ni films deposited at 7×10^{-7} torr.

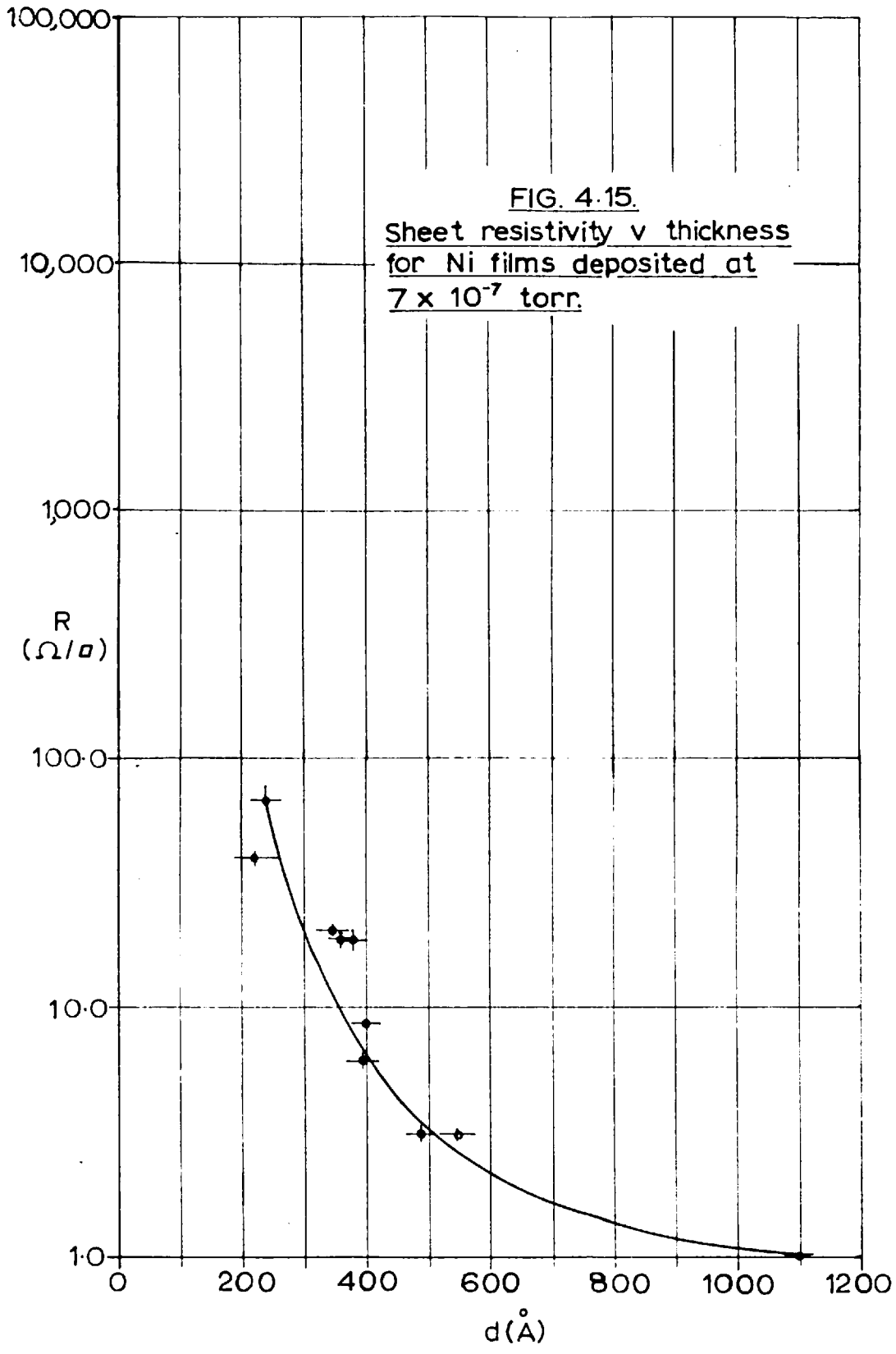

FIG. 4·15.
Sheet resistivity v thickness for Ni films deposited at 7×10^{-7} torr.

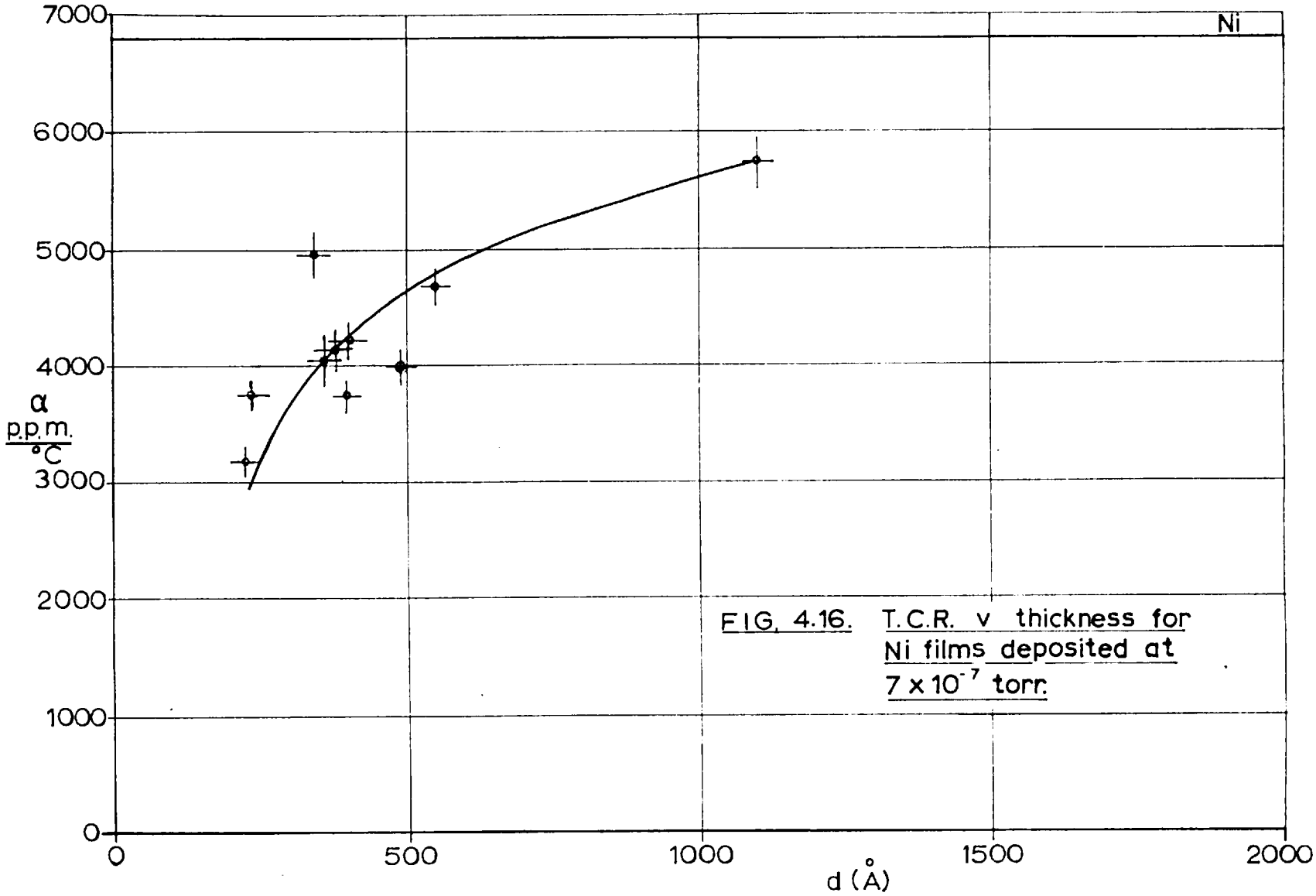

FIG. 4.16. T.C.R. v thickness for Ni films deposited at 7×10^{-7} torr.

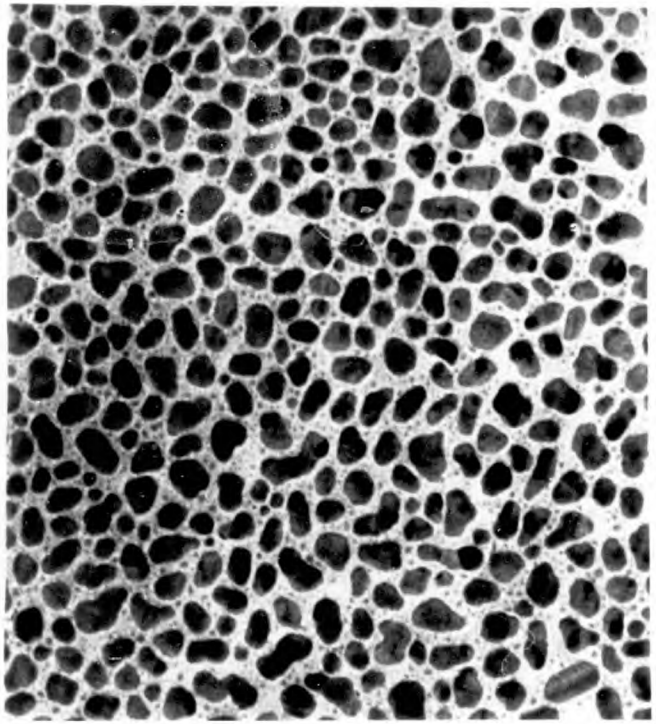

Plate (4.20)

Specimen 71

Resistance > 100MΩ

d = 80Å

1000Å

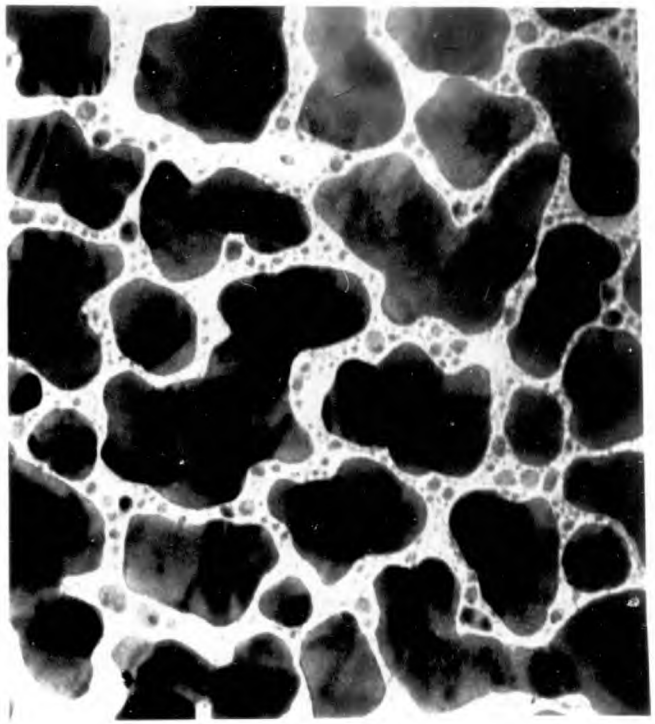

Plate (4.21)

Specimen 70

Resistance > 100MΩ

d = 200Å

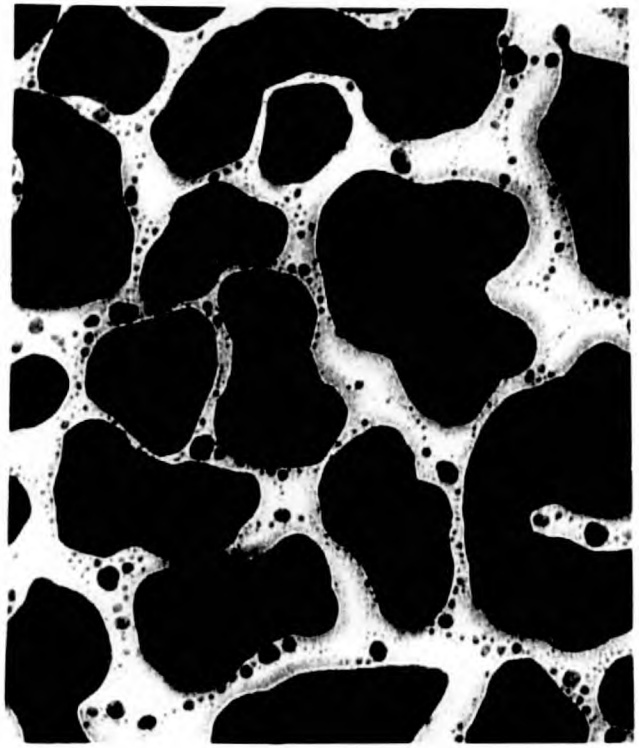

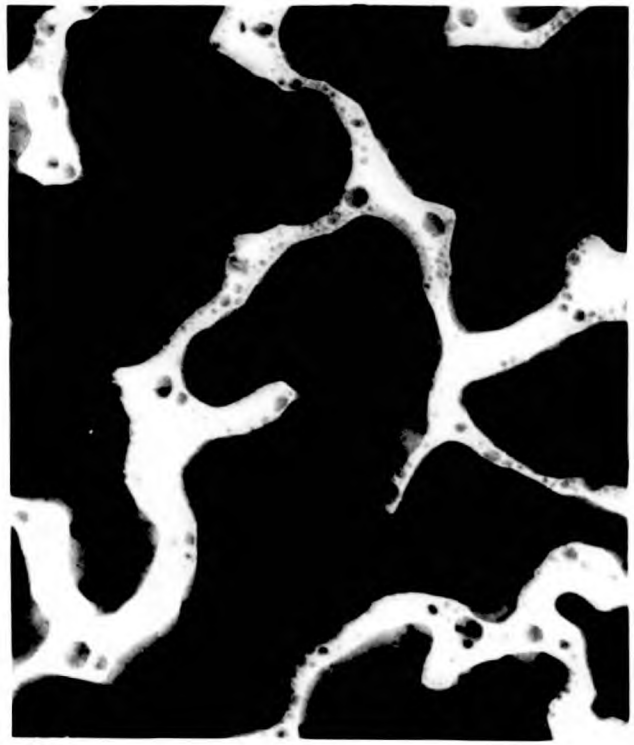

Plate (4.22)
Specimen 67

1000Å

Plate (4.23)
Specimen 65

R = 68.2Ω/□ α = 3750 p.p.m./°C

d = 240Å ρ = 1.6 x 10 Ω.cm.

R = 20.1Ω/□ α = 4960 p.p.m./°C

d = 345Å ρ = 6.9 x 10 Ω.cm.

1000Å

Plate (4.24)
Specimen 62

$R = 6.0\,\Omega/\square$ $\quad \alpha = 3730\,ppm/^{\circ}C$

$d = 395\,Å$ $\quad \rho = 2.4 \times 10^{-5}\,\Omega.cm.$

Plate(4 25)
Specimen 59

$R = 1.0\,\Omega/\square$ $\quad \alpha = 5740\,ppm/^{\circ}C$

$d = 1100\,Å$ $\quad \rho = 1.1 \times 10^{-5}\,\Omega.cm.$

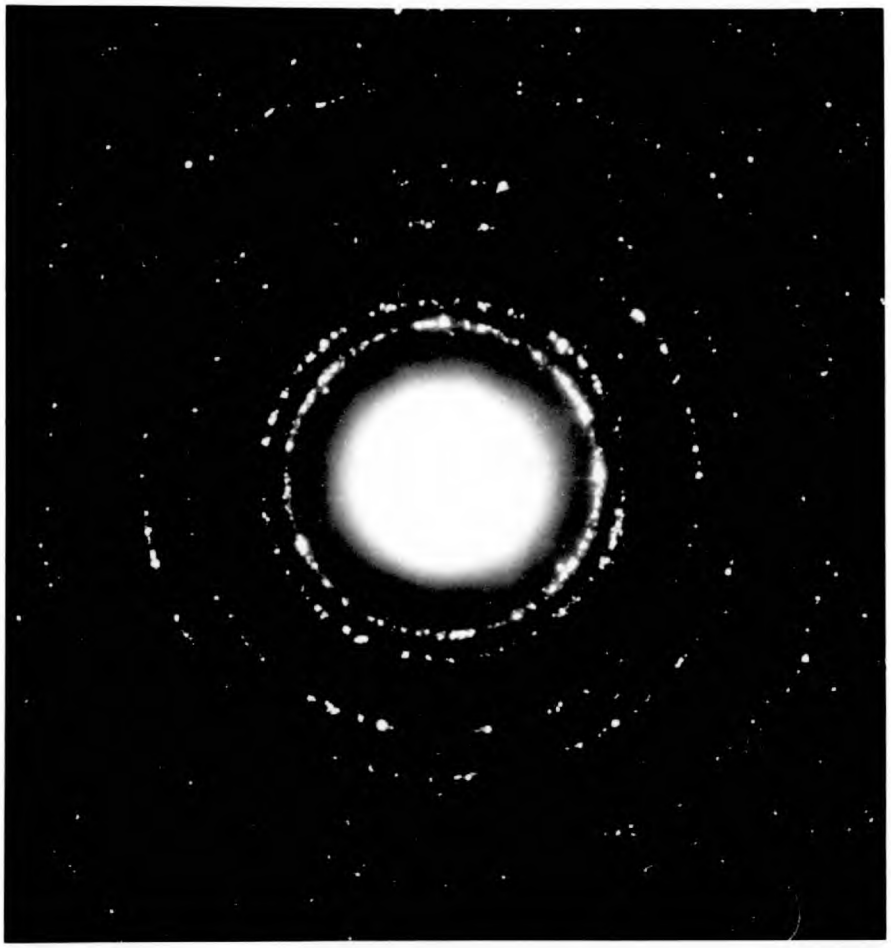

Plate (4.26)

Specimen 62

A typical electron diffraction pattern (100 Kv.)

4.3 Gold films

4.3.1 Preparation conditions

The films were prepared from "fine" gold wire supplied by Johnson Matthey Ltd.. The vacuum pressure during the depositions was approximately 2×10^{-5} torr.. After carefully melting the charge and allowing it to wet the molybdenum boat the rate could be held constant to about $\pm$ 2%. The rate during each of the experiments was 5A°/sec. and the substrate was at ambient temperature. When the contacts had been deposited and the films overlayed with bismuth oxide the substrate was removed for annealing.

4.3.2 Annealing and measurement

Four similar sets of seven films were prepared which were annealed at 100 C, 150°C, 200°C and 300°C. With the exception of the 100°C set this was done in vacuum to prevent oxidation of the copper contacts occurring. In each case the annealing time was one hour.

Each set of films was cut up to separate the individual elements, which were mounted in a specimen holder, connection being made using soft soldered wire connections. Every specimen was thermally cycled to check that it was electrically and therefore structurally stable. The temperature coefficients of resistance were measured between ambient and 45°- 50°C. The results are presented in Figs. 4.17 to

4.20. Each figure shows the variations of T.C.R. and resistivity with thickness for a particular set of films. As already explained, examination of their structure was not possible, owing to their instability and the excessive thickness of the sandwiches.

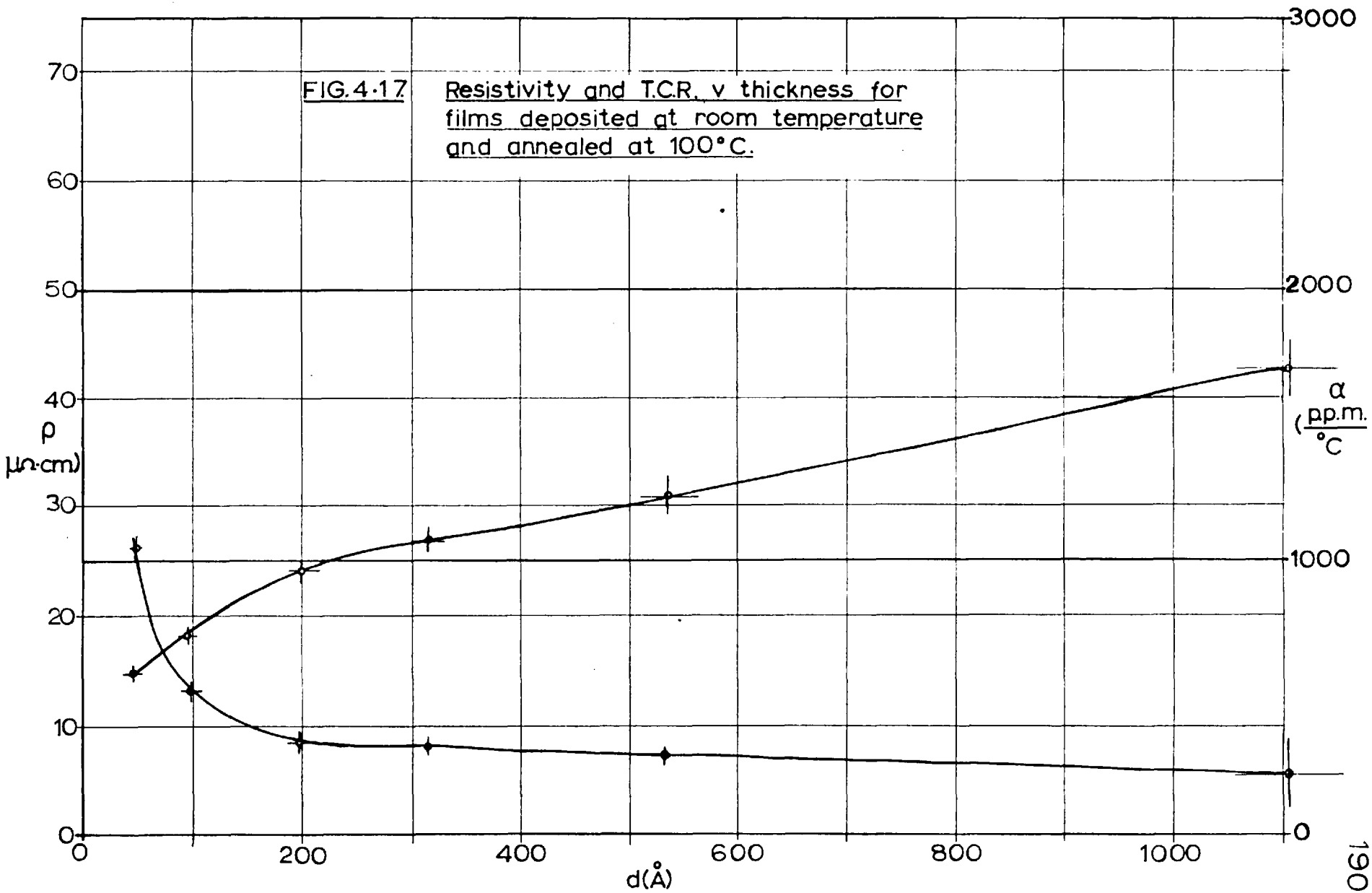

FIG. 4·17 Resistivity and T.C.R. v thickness for films deposited at room temperature and annealed at 100°C.

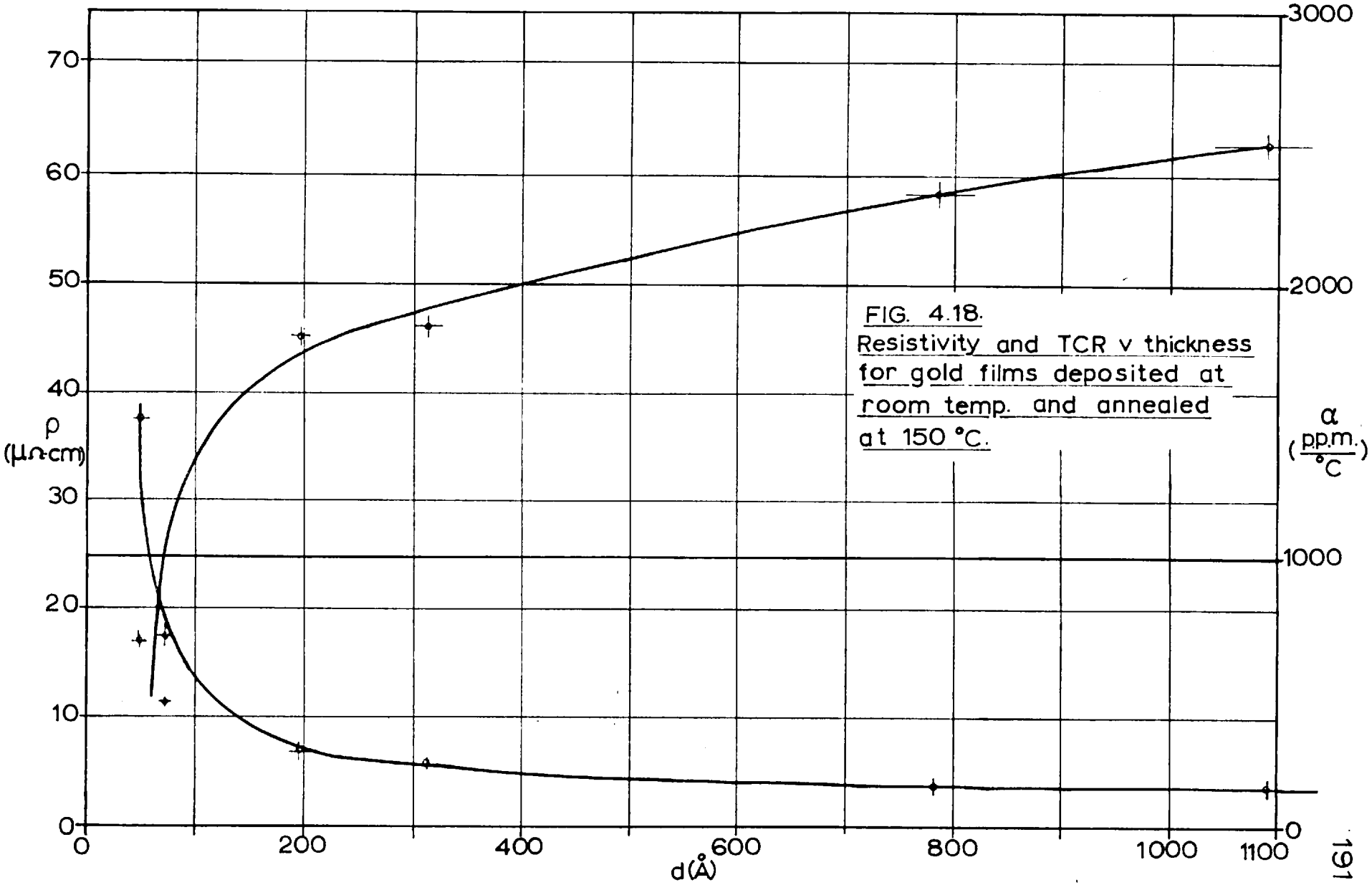

FIG. 4.18.
Resistivity and TCR v thickness for gold films deposited at room temp. and annealed at 150 °C.

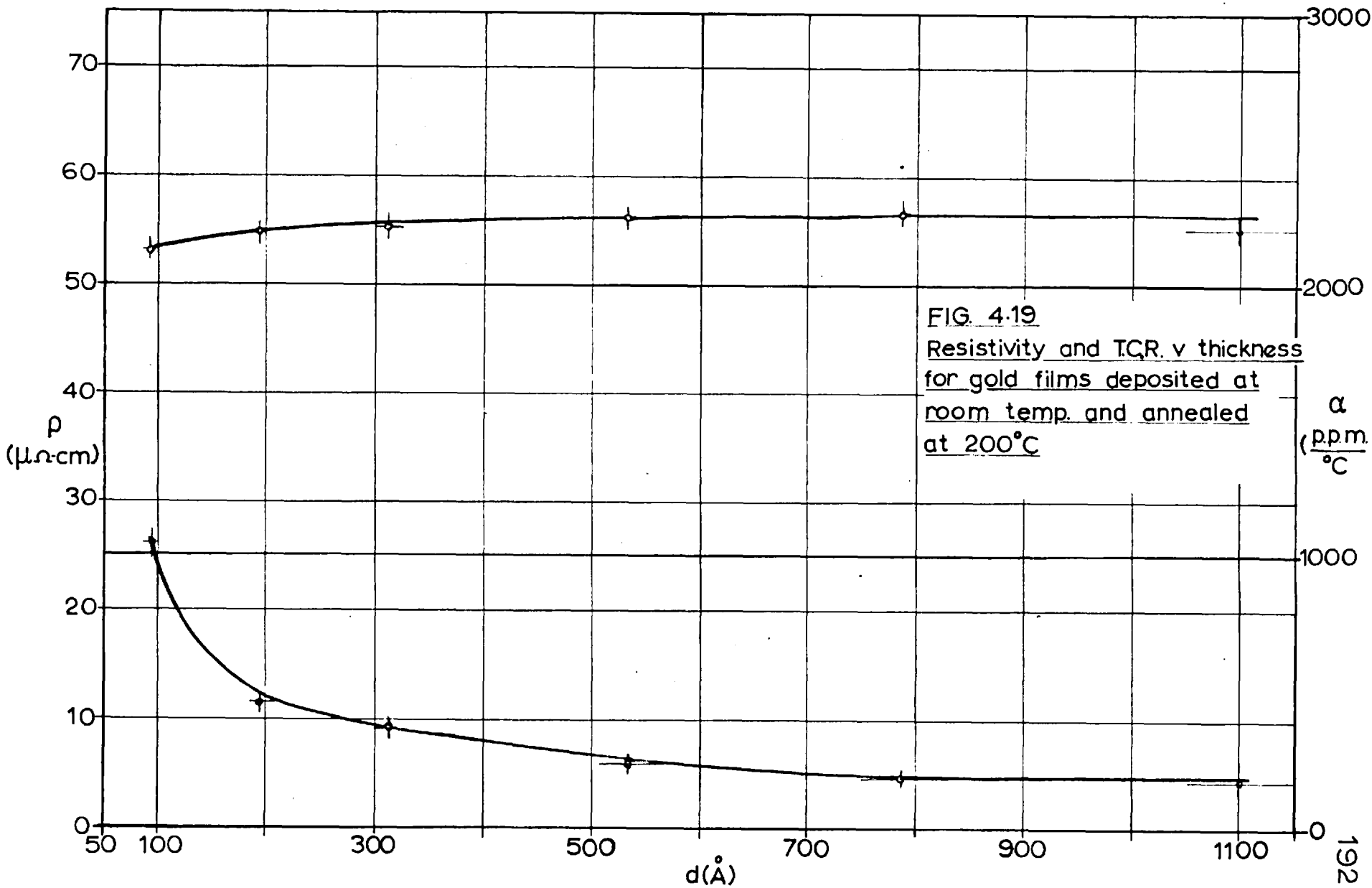

FIG. 4·19
Resistivity and T.C.R. v thickness for gold films deposited at room temp. and annealed at 200°C

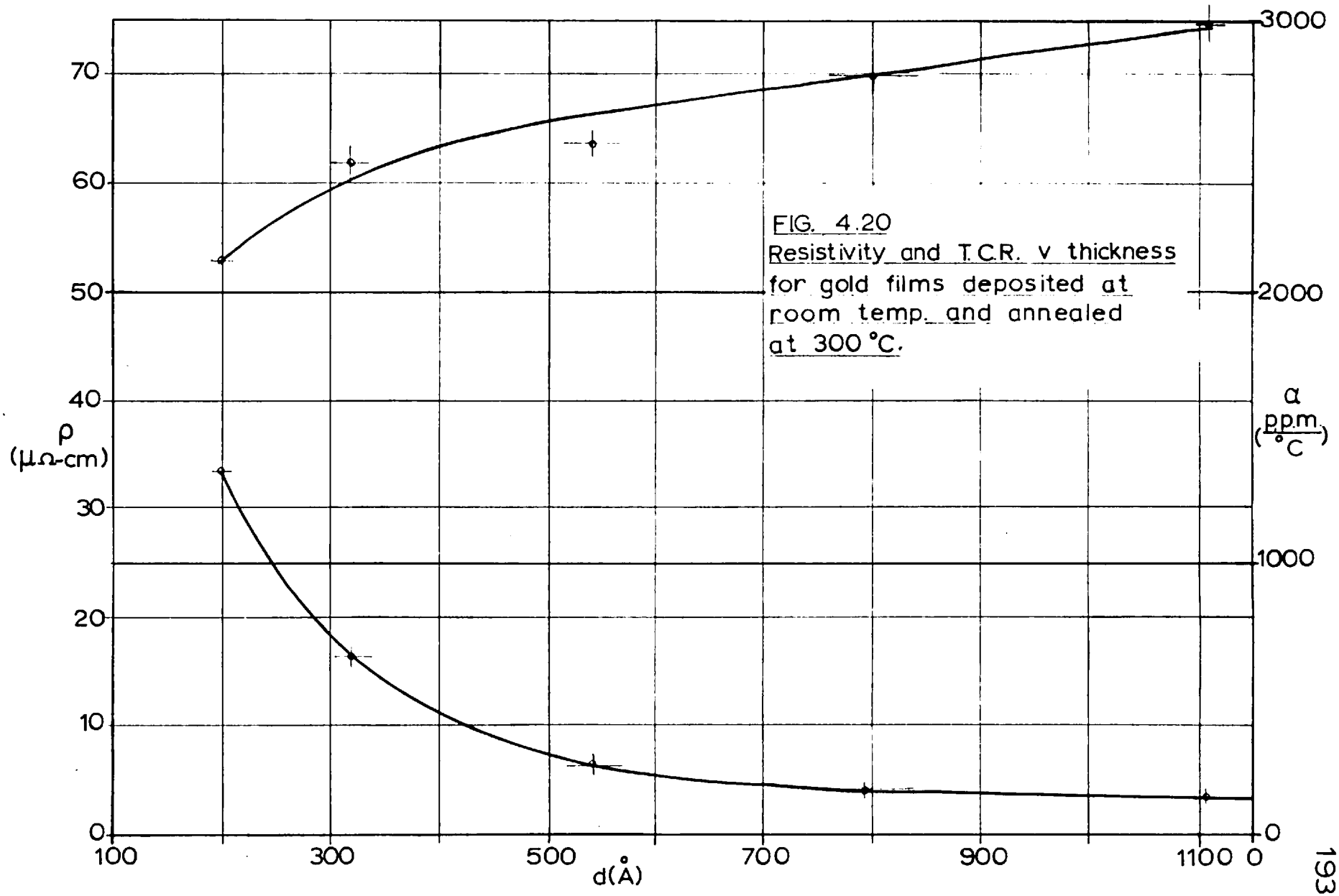

FIG. 4.20
Resistivity and T.C.R. v thickness for gold films deposited at room temp. and annealed at 300 °C.

CHAPTER V

Discussions and Conclusions

5.1 Introduction

It is perhaps most logical to consider the results which have been obtained on nickel films first and to examine the differences between the films prepared under the two kinds of vacuum conditions. This will serve as a basis for the examination of the effects of the addition of chromium in the nichrome films. The results on gold films will again be considered separately.

5.2 Structural considerations

Before attempting to correlate the electrical results with the photographs of film structure it is well to consider the factors which could have caused discrepancies between them. The most obvious weakness is the difference in the method of preparation of the substrates. The electrical and structural specimen substrates were prepared under similar conditions in the same vacuum plant but during different evaporations. Also the supporting layers of silicon monoxide for electron microscopy had been floated off the glass substrate in distilled water and allowed to dry in air.

Two structural specimens were prepared corresponding to each electrical specimen. There was no noticeable difference in structure between them even when they were from different batches of silicon monoxide prepared on separate occasions. Examination of several uncoated support layers failed to reveal any evidence of gross contamination due to the stripping process though the possibility of atomic contamination cannot be discounted. The structural specimen substrates were so featureless that it was barely possible to reveal any detail down to a resolution of $\sim 7A^{\circ}$.

Before evaporation the substrates were held for several hours at $270^{\circ}C$ in vacuum. This means that the surfaces of the structural and electrical specimen substrates would have been in equilibrium with the same vacuum environment and should have been covered with similar layers of adsorbed gases. This and the lack of visible contamination suggests that it is fair to assume that the substrates were similar.

One possibility is that heating of the films by the electron beam in the electron microscope could have caused structural change. This was never observed but heating did sometimes cause large crystallites to bend giving rise to the movement of extinction contours. This effect occurred in nickel films and often took upto ten seconds to disappear. It is worth noting that heating could cause agglomeration in films which were weakly bound to the substrate

and might be so rapid that the process would be complete before the specimen had come to rest in the desired position for examination.

5.3 Nickel films

5.3.1 Films prepared at 10^{-5} torr.

Figs. (4.11), (4.12) and (4.13) show graphs of resistivity, sheet resistivity and temperature coefficient plotted against film thickness. The structure of this series of films is summarised by Plates (4.13) to (4.19).

The thinnest film in the series was $\sim 70A^{\circ}$ thick and had a temperature coefficient of - 730 p.p.m./$^{\circ}$C. Its structure is shown in Plate (4.13). Most of the islands are between $150A^{\circ}$ and $200A^{\circ}$ across, these appear to have formed from the coalescence of smaller islands. Some of these still remain and are about $50A^{\circ}$ in diameter. It is possible to trace paths through the film which do not involve these smaller islands. If this were not the case, the activation of electrons from the smaller islands would be the limiting process. The islands were condensed onto silicon monoxide which has a dielectric constant of six[78]. The model for conduction in discontinuous films developed in Chapter II predicts a value of T.C.R. between - 300 and - 700 p.p.m./$^{\circ}$C for the range of island sizes 150 to $200A^{\circ}$. This is in reasonable agreement when one considers that the island shapes are very irregular and their sizes form a

spectrum of values. It is interesting to note that the theory of Neugebauer and Webb predicts values between - 2500 and - 2000 p.p.m./^{o}C.

An accurate estimation of the island separations, see Plate 4.13, is difficult because of the inadequate resolution of the photograph. However, it is of the order of 10A^{o}. The sheet resistivity of the film was 3000$\Omega/\square$ and if one assumes a barrier height of 1eV the theory predicts a value of 6 x $10^{6}\Omega/\square$. If the two are to be reconciled a barrier height of between 0.5 and 0.6 eV must be assumed. In recent work on conduction in silicon monoxide by Hartman, Blair and Bauer[79] it has been suggested that conduction is limited by a potential barrier at the metal-dielectric interface. This could be caused by the formation of a space charge owing to traps at or near to the silicon monoxide surface. The potential barrier heights observed by these workers were between 0.4 and 0.7 eV and were independent of the electrode material. Thus, it appears that the value of 0.5 - 0.6 eV required for the measured value of sheet resistivity is consistent with this. Because of the exponential dependence of current on island separation it is difficult to claim any better correspondence between theory and experiment.

As films grow thicker coalescence of the islands occurs and it becomes difficult to isolate particular conduction mechanisms. The main difficulties are due to

(i) the spectrum of island sizes;

(ii) uncertainty as to the limiting species;

(iii) multiple ionisation;

(iv) the onset of metallic conduction.

The graph of T.C.R. versus film thickness Fig. (4.13) shows an abrupt increase from $\sim$ 500 p.p.m./^{o}C to 3000 p.p.m./^{o}C at a thickness of about 200A^{o}. The film structures above and below the increase are shown in Plate (4.17) and (4.16). The difference is that long chains of linked islands have formed in Plate (4.17) causing reversion to metallic conduction which is characterised by the large positive T.C.R.. In this region curves of T.C.R. and resistivity exhibit a large scatter which arises from the instability associated with an almost linked structure. The degree of linkage can cause large variations in the electrical parameters of films having the same film thickness. It is interesting to note that when a film is at the stage where it comprises linked chains and very few discontinuities, its resistivity is greater than a laminar film of the same thickness because the current path is meandered. However, since the temperature coefficient is defined as

$$\alpha = \frac{1}{\rho} \cdot \frac{d\rho}{dT}$$

α only depends on proportionate changes of resistance. The scattering mechanism is the same but the path length is greater. Hence the temperature coefficient is not affected by the changed geometry so long as the width of the chains is sufficient to preclude surface

scattering from the sides of the chains.

Above this region the films exhibit a size effect. Before relating these results to the Fuchs-Sondheimer theory it is necessary to decide on the values to be used for the "bulk" resistivity and temperature coefficient. The values for the bulk metal are ρ = 6.6μΩ-cm and α = 6800 p.p.m./°C. If 0.6 electrons per atom are assumed the mean free path is 440A°. The plot of T.C.R. versus thickness shows no sign of any further increase above 5200 p.p.m./°C and the resistivity for very thick films is 13.5μΩ-cm. This value of resistivity is equivalent to a mean free path of 215A°. The $\rho\alpha$ products, i.e. $\frac{d\rho}{dT}$, differ by a factor of ~2; from this it is clear that the vibrational spectrum of the lattice in the thickest films does not correspond with that of nickel and Matthiesen's Rule ceases to apply. This is hardly to be expected because the resistivity has been doubled by defects and impurities.

Using values of ρ, α and l_o which correspond to the thickest films, curves of ρ/ρ_o, $\frac{\alpha}{\alpha_o}$ and $\frac{\alpha\rho}{\alpha_o\rho_o}$ versus K have been plotted. These are shown in Figs. (5.1), (5.2) and (5.3). The $\frac{\alpha}{\alpha_o}$ plot shows that for films thicker than 800A° the scattering parameter is greater than = 0.8. This indicates that the surface scattering is almost entirely elastic. The 1100A° thick film, Plate (4.18), comprises crystallites which are at least 1000A° across and some are as large as 2500A°. They are featureless indicating that they are very perfect

Fig (5.1)

Variation of ρ/ρ_0 with K for Ni films prepared at 2×10^{-5} torr.

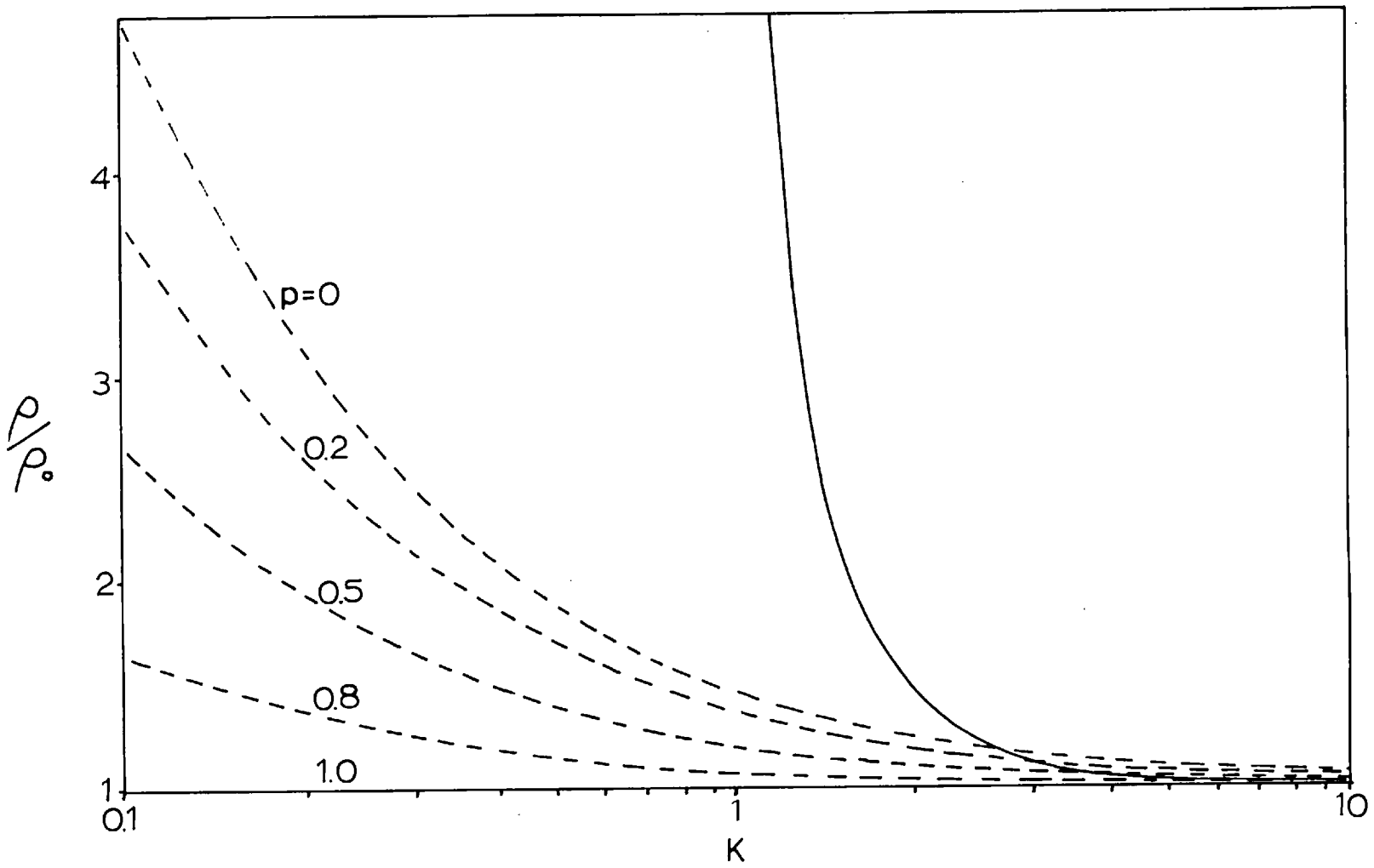

Fig (5.2)

Variation of $\frac{\alpha}{\alpha_o}$ with K for Ni films prepared at 2×10^{-5} torr.

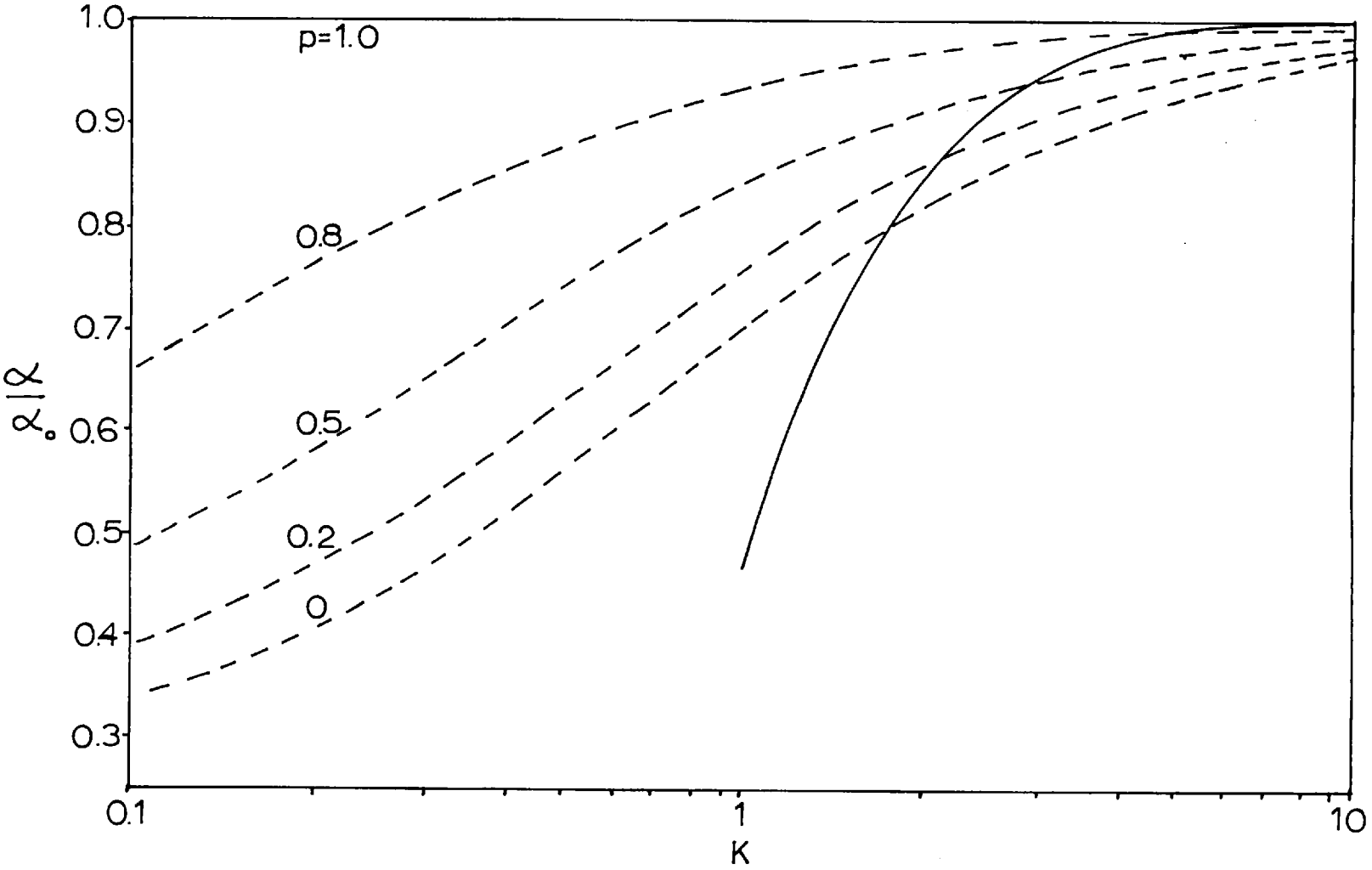

Fig (5.3)

Variation of $\frac{d\rho}{d\tau}/\frac{d\rho_o}{d\tau}$ with K for Ni films prepared at 2×10^{-5} torr.

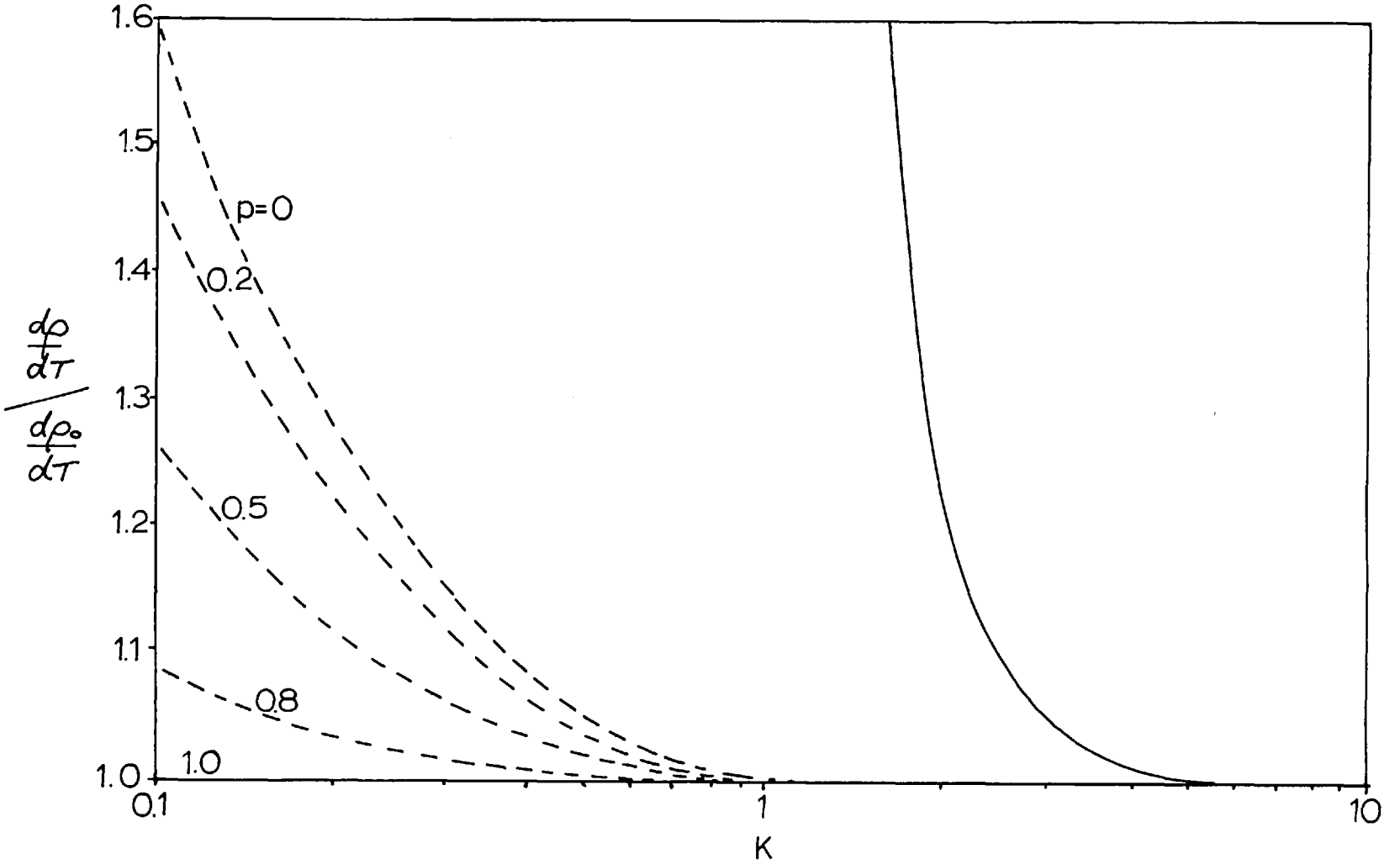

and flat; this would correspond with a high value of p. Below 800A^{o} the curve deviates and cannot be fitted to a particular scattering parameter. This may mean that surface collisions become more and more inelastic as the film gets thinner or that the T.C.R. begins to be affected by discontinuities causing it to decrease. Certainly, the latter must be the case when p is apparently negative. It is likely that both effects occur since the crystallite size gets smaller with decreasing film thickness; the effect would be to "roughen" the film surfaces. Comparison with the curves of ρ/ρ_o and $\frac{\alpha\rho}{\alpha_o\rho_o}$ shows that the deviations occur at greater thicknesses possibly in the meandering chain region in which only the resistivity would be affected.

In summary, the island structure films had negative values of temperature coefficient and high resistances. As their thickness increased there was a monotonic transition to metallic behaviour involving a size effect which disappeared in the thickest films. The parameters of these were determined by the impurity content and imperfections. This kind of electrical behaviour will be termed normal.

5.3.2 Films prepared at 7 x 10^{-7} torr.

Figs. (4.14), (4.15) and (4.16) show graphs of resistivity, sheet resistivity and temperature coefficient of resistance plotted against film thickness. The structure of this series of films is

summarised by Plates (4.20) to (4.26). These films show a marked difference in structure compared with the series prepared at 10^{-5}torr. This is easily seen by comparing Plates (4.13) and (4.20). They show films of about the same thickness prepared under conditions which were similar except for the vacuum pressures. Clearly, coalescence seems to have occurred more readily in the higher vacuum case.

In the island stage in the growth of a thin film there are channels between the islands. When the vapour atoms land in them they migrate over the substrate surface before finally being trapped in a substrate potential minimum or colliding with another atom or condensed nucleus. The migration distance depends on the magnitude of the binding forces to the substrate. If the channel is so wide that the incident atom does not have sufficient energy to migrate to the wall of the channel then nucleation in the channel will occur. There will be a band around each island in which nucleation is unlikely, it is effectively a "clean" area.

The concept of clean regions surrounding the condensed material has been used[80] in the measurement of saturation island density. This mechanism governs the channel width; when the channels are wide it indicates that the atoms are not so strongly bound to the substrate. Eventually, as the islands grow the separation becomes less than the equilibrium channel width and they touch one another. If the free energy of the two islands is greater than the free energy of the

island formed by their coalescence then they will merge. It has been suggested by Adamsky[81] that ccalescence may even occur before they actually touch. In this case he postulated that there is an exchange of atoms between the islands and the gas of atoms in the channel and that the material flows from one island to the other without a bridge actually nucleating.

The very much larger channel widths appear to be partly due to this and partly due to the "clean up" of small islands which occurs under high mobility conditions leaving clean areas on which fresh nucleation occurs. In the 10^{-5} torr. case islands could grow very much closer before coalescence occurred. An explanation of this higher surface mobility must be sought by considering the component gases of the two vacua. The mass spectra which describe the vacua during growth are shown in Figs. (4.3) and (4.4). They show that the main difference between the conditions is the predominance of water at 10^{-5} torr. The gases present at 5×10^{-7} torr. were mainly nitrogen and carbon monoxide which were evolved from the powder. It is possible that the greater binding energy at 10^{-5} torr. could be due to a layer of chemisorbed water which formed OH bonds with the substrate surface and nickel oxygen bonds with the film. There would of course be such a layer at 5×10^{-7} torr. though the coverage would be very much less since the ratio of partial pressures of water was $\sim 200 : 1$.

The greater tendency to coalesce and the accompanying large channel width resulted in the onset of conduction being delayed until the inter-island gaps were small enough to permit tunnelling. It will be evident from the plot of resistivity versus thickness that it proved impossible to produce films with high resistances owing to the sharpness of the transition. Films tended to be either open circuit, i.e. $>100M\Omega$, or had a relatively low resistance corresponding to the linked chain structure. The transition occurred at $\sim 200A^{\circ}$. Above this point the electrical behaviour was normal. Unfortunately, insufficient films were prepared to fit the results to surface scattering curves.

The structures of two films $\sim 240A^{\circ}$ thick are shown in Plates (4.21) and (4.22). Their structures are similar but one corresponds to an open circuit film whilst the other had a resistivity only three times that of bulk nickel. The structure of the low resistivity one is anomalous since the smallest island gaps are about $50A^{\circ}$. This effect was noticed in other films in this series close to the transition. The reason may be that in this region the structure is very sensitive to thickness, evaporation rate and substrate temperature, so much so that a slight difference in either parameter could result in the film being either continuous or open circuit.

The vapour distribution Fig. (3.5) shows that the flux on the

microscope specimen was 3% less than on the electrical specimen. This would have resulted in a 3% reduction in both thickness and rate. It is possible that the microscope grid supporting the structural specimen reached a higher temperature than the glass surface of the electrical specimen since it was seated in a metal holder. The sum of these effects might be very pronounced in high surface mobility films in which the substrate binding forces were low compared with the 10^{-5} torr. series in which the anomaly was not apparent. Once continuity had been achieved, there was very little difference between the series prepared at 7×10^{-7} torr. and 2×10^{-5} torr.

5.4 Nichrome films

5.4.1 Films prepared at 2×10^{-5} torr.

The curves of resistivity, sheet resistivity and temperature coefficient plotted against thickness for the 2×10^{-5} torr. series are displayed in Figs. (4.5), (4.6) and (4.7) respectively. The most obvious feature of the graph of T.C.R. is the peak centred on a thickness of 100A°. It is extremely difficult to draw a curve through the scatter of points which form the peak. This scatter must form part of the evidence in seeking an explanation for the peak. This will be discussed separately later in this chapter.

The thinnest film examined was approximately 50A° thick. Since the Talysurf has an accuracy of $\pm$ 25A° it is clearly impossible to

make more than a crude estimate of its thickness. The structure of this film is shown in Plate (4.1). The island sizes are in the range 50A° to 100A°. According to the theory in Chapter II the corresponding T.C.R. for $\epsilon = 6$ lies between - 1700 and - 6000 p.p.m./°C. The actual value was - 3000 p.p.m./°C. Agreement can be claimed to within an order of magnitude. The theory of Neugebauer and Webb would predict values in the range - 4000 to - 7750 p.p.m./°C. With this relatively small island size the effects of multiple ionisation would be negligible. The real difficulty in making a comparison lies in the assessment of the island size. Again it is difficult to measure island separations but if a value of 10A° is used one would expect a sheet resistivity for this film of $6 \times 10^7 \Omega/\square$ using a barrier height of 1eV. Exact correspondence can be achieved if this is taken as 0.9eV which is slightly higher than the interfacial barrier heights encountered by Hartman, Blair and Bauer.

The most comprehensive account available of the electrical properties of nickel chromium alloys in bulk form is that of Thomas[82]. This gives values of resistivity and T.C.R. of 101.0 $\mu\Omega$-cm and 100 p.p.m./°C respectively for the 80/20 composition. Other values for this alloy are listed in Table 2.2. Whilst there is good agreement between the values of resistivity, the values of T.C.R. vary between 85 and 400 p.p.m./°C. There is no obvious correlation between these values of ρ and α. The consensus points to a value of

$\sim$100 p.p.m./^{o}C. It is this value which will be assumed here. Fig. (5.4) shows curves of ρ and α plotted against composition for the bulk alloys.

If one assumes that the number of conduction electrons per atom is 0.6 as one does for nickel, then the mean free path of the electrons in 80/20 nichrome is approximately 30A^{o}. Thus according to the Fuchs-Sondheimer theory one could not expect to notice a size effect in curves of ρ and α above a thickness of 300A^{o}. The experimental curves show that these parameters are constant down to $\sim$ 300A^{o}, below this thickness the behaviour is obscured by the scatter of points forming the peak in the T.C.R. curve. It is interesting to notice the downward scatter in the region of that peak in the resistivity curve, Fig. (4.5).

The value of resistivity for thicker films is in good agreement with the bulk value but the corresponding values of T.C.R. are in the range 70 to 80 p.p.m./^{o}C compared with 100 p.p.m./^{o}C. It is not easy to explain this reduction as the resistivity does not appear to have increased as one would expect if this were due to impurities or imperfections which had modified the residual resistivity.

5.4.2 Films prepared at 7 x 10^{-7} torr.

The results for the 7 x 10^{-7} torr. series are shown plotted in Figs. (4.8), (4.9) and (4.10). There is no real difference between

Fig (5.4)

T.C.R. and resistivity v composition of Ni-Cr alloys (82)

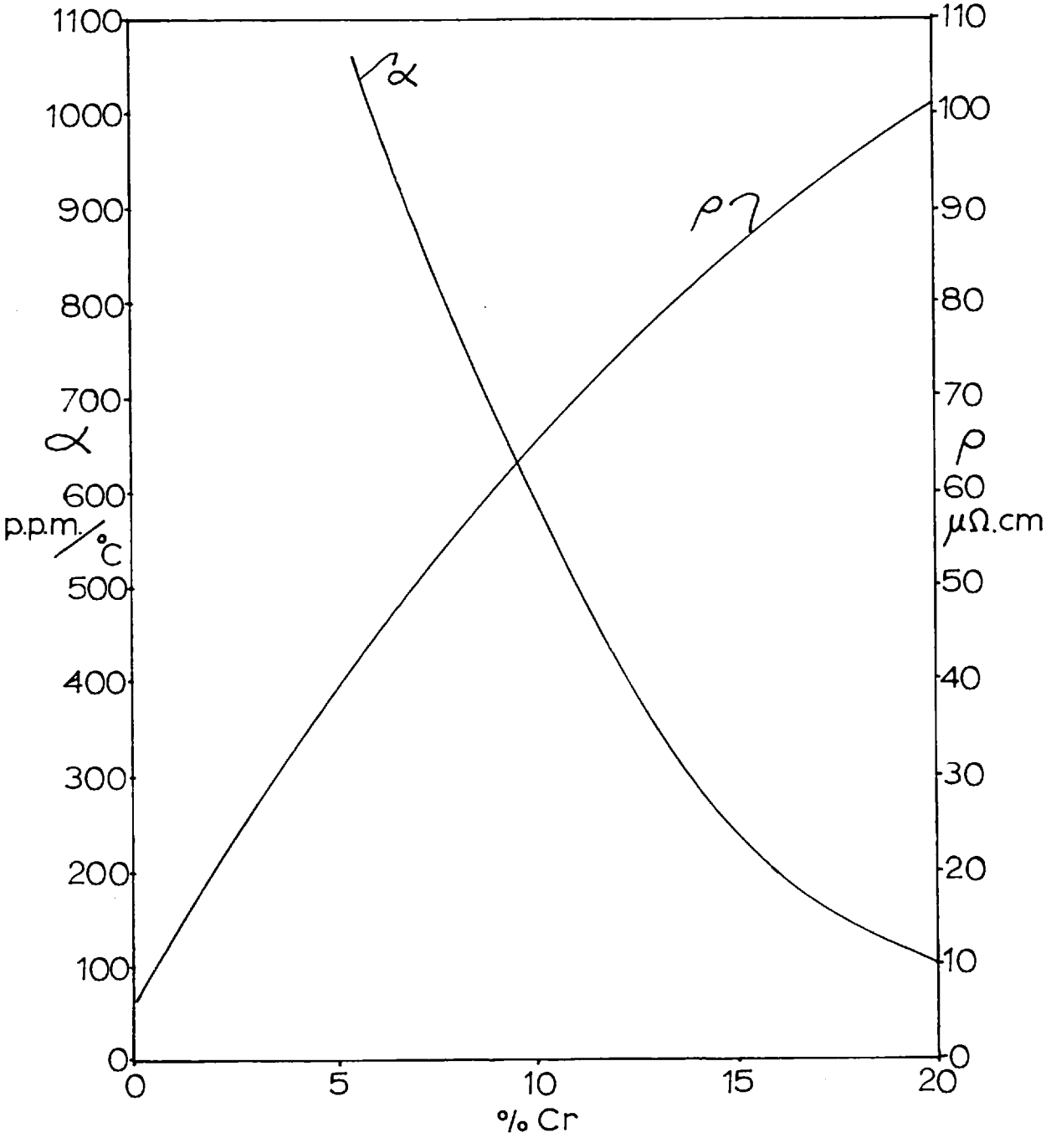

the properties of these films and the ones just discussed except that the peak in the T.C.R. curve is smaller and narrower. It is centred on a thickness of 150A°. The resistivity of the thicker films is ~ 110p.Ω -cm which is slightly higher than for the other series. The corresponding values of T.C.R. are 70 p.p.m./°C. This is lower, pointing to the fact that the effects are complimentary as they would be if this was due to different residual resistivities.

Structurally there are differences, see Plates (4.1) to (4.12), between the series which are typical of those encountered in the nickel films. The higher vacuum films possessing larger islands and channel widths suggesting higher atomic mobilities on the substrate surface during condensation. These effects made it impossible to prepare films with sheet resistivities greater than 200Ω/□ because thinner films had channels which were too wide to permit measurable conduction, (> 100MΩ).

5.4.3 Oxidation of nickel-chromium alloys

Various workers[83][84] have noted the appearance of a mixed oxide phase on the surfaces of 80/20 Ni-Cr alloys and on steels containing nickel and chromium. This protective film is thought to have the spinel structure $NiO.Cr_2O_3$. The exact composition of this oxide is uncertain but it has been suggested by Lustman[85] that it is predominantly chromium oxide Cr_2O_3. The exact structure

would depend on the free energies of formation of the component oxides, on their electrical conductivity and therefore on its defect structure and on the rates of diffusion of the metal and oxygen ions through the oxide layer. Hauffe[86] has suggested that the structure may be graded so that the oxide at the metal-oxide interface is $NiO.Cr_2O_3$ whilst it is Cr_2O_3 at the oxide-oxygen surface. Whichever description is correct it is clear that chromium forms the greater metal constituent. The reason for this is probably the lower free energy of formation of Cr_2O_3 compared with NiO, i.e. - 244.8 and - 46.1 K cals./mole. respectively. This evidence suggests that chromium is oxidised preferentially in 80/20 Ni-Cr alloys. These phenomena have been observed in bulk materials and would certainly be present in the thin film form.

5.4.4 A model of the structure of thin nichrome films

The preferential oxidation of chromium will be used to try and explain the unusual peak in the T.C.R. curves of nichrome films. It will be assumed that there is an oxidising agent present at the substrate surface. Its exact nature and origin is not clear but will be discussed later in the light of these results.

When the nichrome alloy vapour impinges on the surface of the substrate an oxide phase will form. By comparison with bulk behaviour its composition will lie between the two extremes Cr_2O_3 and $NiO.Cr_2O_3$. As the deposition proceeds oxidation will decrease

owing to the exhaustion of the oxidising agent and the increased thickness of the oxide layer through which ion transport and electronic conduction must occur if the oxidation process is to continue. At a particular stage in the process there will exist an oxide layer having a graded structure and a covering alloy depleted of its constituents to varying extents. Since little is known about the oxidation process two assumptions will be made.

(i) Only chromium is oxidised.

(ii) The overlaying alloy is homogeneous.

It is likely that there is a concentration gradient through the thickness of the alloy film but since it is only $\sim$ 100A$^{\circ}$ thick atomic rearrangement by diffusion is very likely. Having established this simple model of the structure of a thin nichrome alloy film one can now deduce its electrical properties.

In the very early stages of the growth of the film it would consist of an oxide layer on which the nucleation of the alloy film occurred. It is unlikely that nucleation would occur in the conventional sense but that nuclei would begin to grow from the oxide as the oxidation process decayed and the oxide became more and more metallic. The growth of the nuclei would eventually give rise to an island structure film. In practice it would be difficult to attribute the onset of electrical conduction to either a tunnelling process or to a hopping process from one defect to another in the oxide. This

situation is very similar to that conceived by Hill[22] involving an amorphous dielectric. As more and more material is deposited the film would become continuous as more and more of the discontinuities disappeared. The now metallic film would no longer have its true composition but, making the assumptions above, would be depleted in chromium. The effect would have been to dilute the alloy.

Reference to Fig. (5.4) shows that for 80/20 nichrome this effect would produce an increase in T.C.R. and an accompanying reduction in resistivity. As more and more material is deposited the film would gradually acquire the original alloy composition and the values of ρ and α would revert to normal. This description predicts a maximum in the T.C.R. versus thickness curve and a minimum in the resistivity versus thickness curve. It remains now to compare this model with the variations observed experimentally and suggest the origin of the oxidising agent.

5.4.5 Comparison of the model with experiment

In each case the sets of photographs describing the two series of films correspond to the curves drawn through the scatter of points in plots of T.C.R. versus thickness, see Figs. (4.7) and (4.10). If the model is valid the scatter of points can be attributed to several factors. Clearly the T.C.R. will depend on the degree of continuity

in the film, the less continuous ones having less positive values. Therefore at a particular thickness there will be scatter particularly in the island-linking stage of growth, since small variations in the extent of linkage can cause large changes in the electrical parameters of a film. Another source of scatter is the extent to which segregation has occurred. This depends on the abundance of the oxidising agent and the degree to which the assumptions hold true in a particular film. If the oxide is not confined to a surface layer but blends into the film, impurity scattering of electrons will increase causing reductions in the values of T.C.R. and corresponding increases in the resistivity. The situation is very complicated, each effect interacts with the other to render particular conditions ir-reproducible.

In discussing the peaks it will be assumed that the effects which operate to reduce the T.C.R. are at a minimum and peak values will be considered. In the 2×10^{-5} torr. series the peak value of T.C.R. is 480 p.p.m./$^{\circ}$C. The structure of this film is shown by Plate (4.3). By relating it to the other photographs in the series it can be deduced that its structure lies in the linked chain region. This means that its resistivity is higher than an equivalent laminar film but its T.C.R. would be unaffected. One can now deduce its composition from the curve of T.C.R. versus composition assuming it to be homogeneous, see Fig. (5.4). The corresponding composition is 89% Ni 11% Cr. The thickness of the film is 110A$^{\circ}$ and assuming that only chromium is involved it indicates that approximately half of the

chromium atoms in the film were oxidised.

If the original undepleted film were approximately 25 atoms deep it means that ~2.5 chromium atoms were oxidised. This is equivalent to approximately one molecular layer of Cr_2O_3 involving three oxygen atoms per molecule. It is now possible to deduce the T.C.R. of thicker films as more nichrome is added by calculating the average composition at a particular thickness. The composition can never revert to normal but approaches it assymptotically. The calculated variation of T.C.R. has been plotted on Fig. 4.7. Unfortunately the fit is not very good at higher thicknesses owing to the discrepancy already noted between the T.C.R. of thick films and the value quoted by Thomas. Otherwise the curve forms a reasonable envelope of the experimental points.

Applying this now to the higher vacuum films where the peak occurs at a thickness of 150A° and has an amplitude of + 230 p.p.m./°C. This corresponds to a composition of 85% Ni and 15% Cr. Assuming the film is 37 atoms deep then ~2.2 of these atoms are involved in oxidation if they are chromium atoms. This is practically the same number as at 2×10^{-5} torr. and is therefore a very interesting result. It would appear from this that approximately the same amount of oxidation has occurred in each case. Again the curve of predicted T.C.R. values is displaced owing to the discrepancy previously mentioned. The form is still similar but the fit is not quite so

good. Considering the nature of the assumptions involved the correspondence is surprisingly good.

5.4.6 The oxidising agent

The origin of the oxidising agent must now be considered. It appears that the extent of oxidation is very similar in both cases and is rather surprisingly independent of the preparation pressure. This would suggest that the agent is a strongly chemisorbed layer of either oxygen or water on the substrate surface. Alternatively it is known that[87][88] water diffuses out of glass when it is heated. This is a very prolonged process and the rate of diffusion is proportional to the square root of the bake-out time at a particular temperature. This would certainly provide a source of water which would be independent of pressure. Since no attempt was made to standardise the time during which the substrate was heated prior to deposition the rate of issue of water would have varied and contributed to the scatter. As the oxidation process involved three atomic layers of oxygen it is unlikely that this would have been provided by a chemisorbed layer at 300°C and at 5×10^{-7} torr.[87]. It therefore seems more likely that the oxidising agent was water which was diffusing out of the glass substrate.

Using these arguments it follows that the difference in the T.C.R. maxima depends on the thicknesses at which films become

continuous or in other words at what thicknesses the segregation effect becomes apparent. This is consistent with the structure of the 7×10^{-7} torr. series which became continuous later, the effect being reminescent of the higher vacuum nickel films. One now has to reconcile the difference in structure at the two pressures with the similar extents of oxidation. This could be explained by postulating that the reduction in mobility is due to interaction between the incident gas and metal atoms rather than a substrate-atom interaction which binds the atoms more strongly to the substrate surface.

5.4.7 Electron diffraction evidence

It was hoped to reveal evidence of an oxide phase by electron diffraction. Plates (5.1) and (5.3) show the structure and its electron diffraction pattern of an 80/20 Ni-Cr film prepared at 2×10^{-5} torr. at a rate of $3A^{\circ}$/sec. The film was $250A^{\circ}$ thick and comprised small crystallites between 50 and $100A^{\circ}$ across. The electron diffraction pattern shows diffuse rings corresponding to the f.c.c. structure of 80/20 nichrome. Though it has proved impossible to print it the plate showed a very weak diffuse ring midway between rings 4 and 8 of the f.c.c. pattern.

In order to crystallise this amorphous structure the film was annealed at $700^{\circ}C$ for one hour at a pressure of 5×10^{-7} torr. Plates (5.2) and (5.4) correspond to the annealed film. It is clear

1000Å

Plate(5.1)
(as deposited)

Plate (5.2)
(annealed at 700°C)

A 250Å 80/20 Ni-Cr film prepared at a pressure of 2×10^{-5} torr., as deposited and after annealing at 700°C for 1 hour at 5×10^{-7} torr.

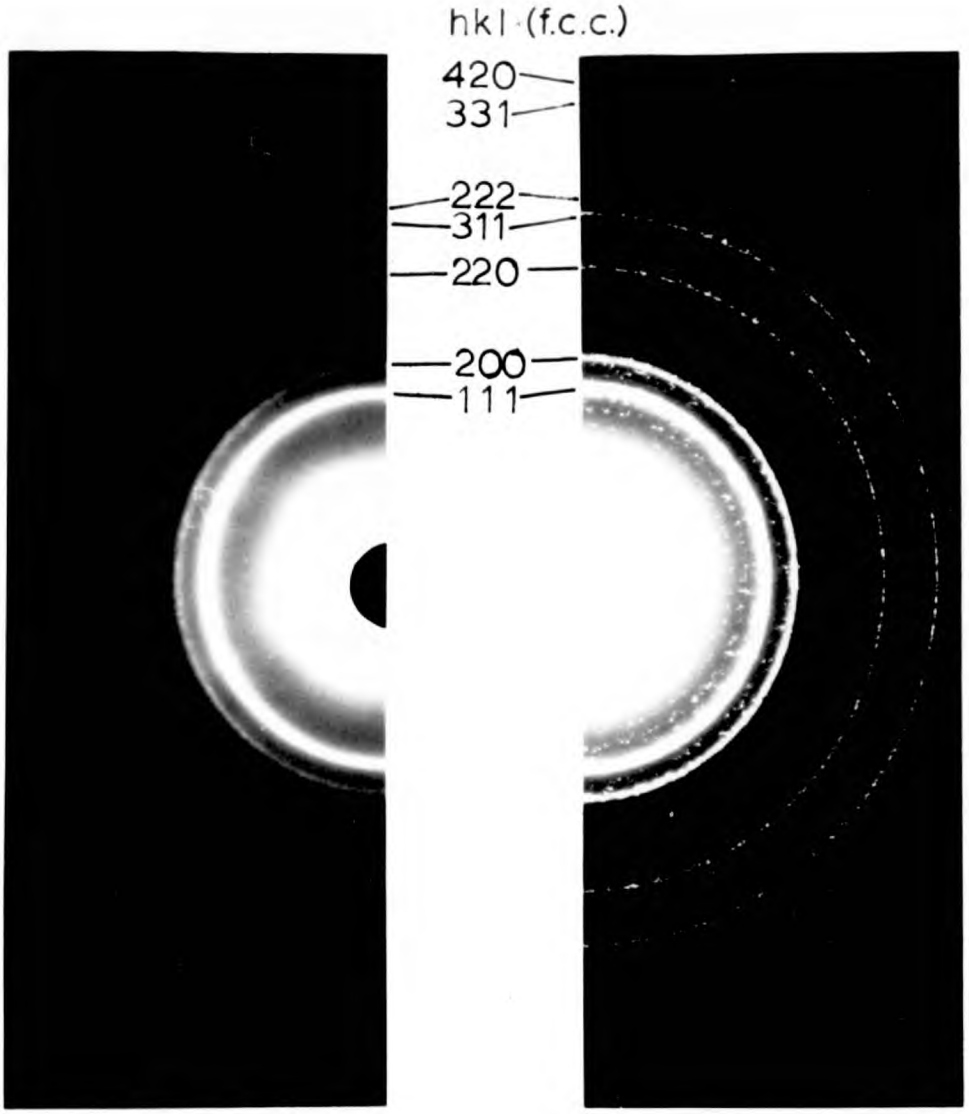

Plate(5.3)
(as deposited)

Plate(5.4)
(after annealing)

The electron diffraction patterns of the films whose structures are shown in Plates(5.1) and (5.2)
(only the visible f.c.c. lines are labelled)

that the nichrome f.c.c. phase has recrystallised to produce sharper rings and the amorphous phase has been replaced by a scatter of spots. The specimen was rephotographed while scanning the specimen to try and integrate the spots into rings. This was partially successful. The rings which resulted were broken, still very weak and difficult to index. Calibration of the microscope was achieved by coating the specimen with a 100A^{o} thick layer of aluminium to provide standard rings. The calibration photograph is not presented here but the accuracy of the plane spacings was $\pm$ 2%. An index of the lines is given in Table 5.1. Unfortunately, many of the weaker lines do not appear in Plate (5.4). The indexing was performed by projecting the original plate using a photographic enlarger.

The strongest of the extraneous lines corresponds to the 1,1,0, and 0,0,6, planes of Cr_2O_3. The only NiO lines to appear correspond to its 2,2,0, and 3,1,0, lattice planes. Often lines appear which can be attributed to either oxide and in some cases these are masked by the f.c.c. nichrome phase. There is clearly evidence of oxidation and Cr_2O_3 lines seem more prominent than those of NiO. It is very difficult to deduce that preferential oxidation of chromium has occurred or that the oxide phase lies at the film surface. The line intensities even after photographing a traversing field are very weak indicating that the oxidation is only very slight.

TABLE 5.1

Index of Plate (5.4), a diffraction pattern of an 80/20 NiCr film annealed at 700°C

d(A°)	80/20 NiCr	Cr_2O_3	NiO	Intensity	Possible components
2.95			1,1,0.		
2.66		1,0,4.			
2.51				W	Cr_2O_3
2.48		1,1,0.			
2.41			1,1,1.		
2.29				W	Cr_2O_3
2.264		0,0,6.			
2.176		1,1,3.			
2.07			2,0,0.		NiCr, Cr_2O_3, NiO
2.048	1,1,1.	2,0,2.			
2.03				VS	
1.86			2,1,0.		
1.8156		0,2,4.			
1.772	2,0,0.				NiCr
1.74				VS	
1.70			2,1,1.		
1.672		1,1,6.			
1.61				VW	Cr_2O_3
1.579		1,2,2.			

TABLE 5.1 (Continued)

d(A°)	80/20 NiCr	Cr_2C_3	NiO	Intensity	Possible components
1.50				VW	NiO
1.48			2,2,0.		
1.465		2,1,4.			Cr_2O_3
1.45				VW	
1.4314		3,0,0.			Cr_2O_3,NiO
1.40				VW	
1.39			3,0,0. 2,2,1.		
1.34				VW	NiO
1.32			3,1,0.		
1.2961		1,0,10.			
1.26			3,1,1.		NiCr,Cr_2O_3,NiO
1.25	2,2,0.				
1.24				S	
1.2398		2,2,0.			
1.07	3,1,1				NiCr
1.06				S	
1.02	2,2,2.			VW	NiCr
.886	4,0,0.				NiCr
.880				EW	

TABLE 5.1 (Continued)

d(A°)	80/20 NiCr	Cr_2O_3	NiO	Intensity	Possible components
.832			500,430	EW	NiCr,NiO
.814	3,3,1.				
.806				W	NiCr
.793	4,2,0.				NiCr
.783				W	
.723	4,2,2.				NiCr
.718				VW	
.682	5,1,1, 3,3,3.				NiCr
.673				EW	

Unfortunately, the presence of oxides was not tested in films prepared at 7×10^{-7} torr.

It is interesting to note that recent work by Glang, Holmwood and Clarke[89] on Cr.SiO cermet films has revealed the existence of a Cr_3Si phase which crystallised when the amorphous films were annealed at 400°C. This points to the possibility of its formation at the nichrome-substrate interface. If this were the case it could lead to a similar alloy disproportionation effect. Unfortunately, it would be equally difficult to identify this phase since it seems that an extremely small amount of chromium would be involved.

5.4.8 Comparison with previous work

In previous work on flash evaporated nichrome alloys Campbell and Hendry[42] had noted the tendency for thinner 80/20 films to have larger values of T.C.R. than thicker ones, in fact it was their work which led to this study. Their points corresponding to the 80/20 composition are shown for comparison in Fig. (4.7). They are in good agreement with the present results but were not sufficiently numerous to describe the peak in the region of 100A°.

A structural study by Bicknell, Blackburn, Campbell and Stirland[43] of flash evaporated Ni-Cr films led to the conclusion that the 45/55 composition films comprised two phases. A phase termed α associated with the metal film and β associated with an oxide skin. The evidence for this was two-fold. It was found that discontinuous island structure

films were coherent when they were floated off their rocksalt substrates whilst this did not occur with gold films. This was convincing evidence for a phase connecting the islands. Secondly, the as-deposited films gave very diffuse diffraction patterns which on annealing to 350°C for six hours sharpened to form the rings of an f.c.c. structure and diffuse haloes which had remained unchanged. The f.c.c. structure was termed the α phase and the amorphous structure the β phase. The α phase corresponded to a solid solution of nickel and chromium. On further annealing in the electron diffraction camera, the β phase remained unchanged upto 650°C but the grain size of the α increased. When the temperature was increased above 650°C the β phase disappeared as such and Cr_2O_3 was formed. The annealing was continued upto 750°C causing gradual oxidation of the α phase. No trace of nickel oxide was found indicating preferential oxidation. It was concluded that the film had comprised a solid solution of nickel and chromium at the solubility limit of 32% Cr, see Fig. (5.5). The remainder of the chromium was assumed to be involved in the formation of a chromium-oxygen skin phase which could be crystallised to form Cr_2O_3 at high enough temperatures.

Campbell and Hendry applied the idea of a chromium-oxygen skin to account for the anomalous electrical behaviour of their 80/20 nichrome films prepared at 10^{-4} - 10^{-5} torr. It was proposed that the T.C.R. of a film was mainly governed by the intergranular

Fig (5.5)

Phase diagram of the Ni-Cr alloy system

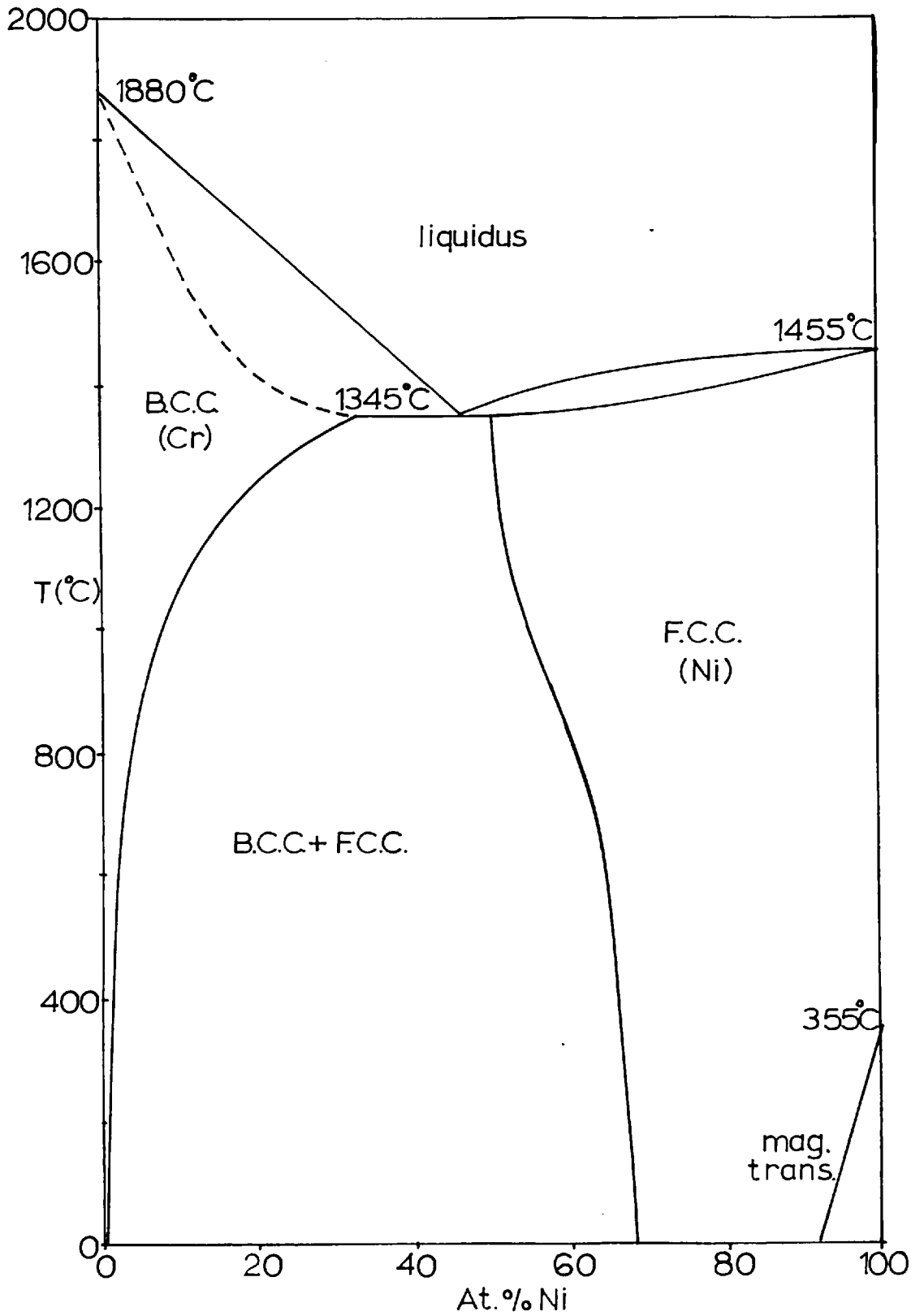

resistance and that the potential barrier height increased with temperature so causing an unusually large increase in resistance with temperature. In their model as films became thicker the number of discontinuities decreased leading to reversion to the behaviour associated with normal films.

The evidence submitted in the present study shows that unusually large values of T.C.R. occur even in continuous films and that the effect of discontinuities is a reduction in the T.C.R., so describing a maximum in the region where the film achieves continuity.

A more recent quantitative study by Bicknell[90] using radial distribution analysis has shown that the as-deposited 45/55 NiCr films contain an amorphous β phase which is now thought to be an almost amorphous chromium phase. This is the chromium which has been unable to enter the saturated solid solution, the α phase. The analysis has shown that the crystallite size of the chromium is only $8A^{\circ}$ rendering it almost amorphous, causing the diffuse haloes. It remains in this form upto $600^{\circ}C$ when it is oxidised to form Cr_2O_3. Upto this temperature no evidence of Cr-O bonding was found.

It would be impossible for such a chromium phase to exist in the 80/20 alloy because at that composition the solid solution would be far from saturated. Hence the diffuse ring reported here

cannot be acccunted for in this way. It has been shown that the crystallite size of the f.c.c. phase considerably increased on annealing to 700°C and that the diffuse ring yielded a spotty background which could be partially integrated into very weak and broken rings. These it is thought correspond to Cr_2O_3 and NiO or possibly a composite oxide phase. It is unlikely that this oxidation occurred during the annealing experiment as this was performed in a liquid nitrogen trapped system at 5×10^{-7} torr.

One cannot, however, distinguish between oxides incorporated in the film and oxide formed at its surface. However, oxide inclusions would surely increase the film resistivity above that of bulk nichrome. This was not observed in films having thicknesses above the T.C.R. peaks where agglomeration could be safely discounted. Also shown in Fig. (4.7) are values of T.C.R. for films condensed at a rate of $\sim 10 A^{\circ}$/sec. in the usual way and films prepared at similar rates after evaporating material for four minutes with the shutter closed. The purpose of this was to determine the effect of gettering the oxidising components of the vacuum before condensing the films. Though these results are far from complete the general trend is as for films deposited in the normal way at 2×10^{-5} torr. After four minutes the pressure had fallen from 2×10^{-5} torr. to 6×10^{-6} torr. Presumably this was a reduction in the partial pressure of water. These points are

consistent with the statement that the vacuum pressure during deposition has little effect on the T.C.R. of the films, only in as much as the films become continuous at different stages in their growth.

5.5 Discussion of the results on gold films

Recapitulating, the aim of the experiment was to determine the mean free paths of electrons in thin metal films from curves of $\frac{\alpha\rho}{\alpha_0\rho_0}$ plotted against thickness instead of the usual way involving curves of ρ and α versus thickness. It would have the advantage of employing films only one tenth of the thickness required in the more usual method. Films with different mean free paths were prepared by annealing them to different temperatures. Graphs of T.C.R. and resistivity have been plotted against thickness and are shown in Figs. (4.17), (4.18), (4.19) and (4.20).

Fig. (5.6) shows the corresponding curves of $\frac{\alpha\rho}{\alpha_0\rho_0}$ for the different annealing temperatures. By choosing the mean free path correctly for each series it was hoped to fit these curves to curves of the form shown in Fig. (2.13). The scattering parameter could then be deduced by comparing the experimental curve with the particular p curves. In the section on surface scattering in Chapter II it has been shown that the mean free path is approximately given by its intercept on the thickness axis x 1.2. See Fig. (2.13).

Fig (5.6)

$\frac{d\rho}{dT} / \frac{d\rho_0}{dT}$ v thickness for gold films annealed at various temperatures

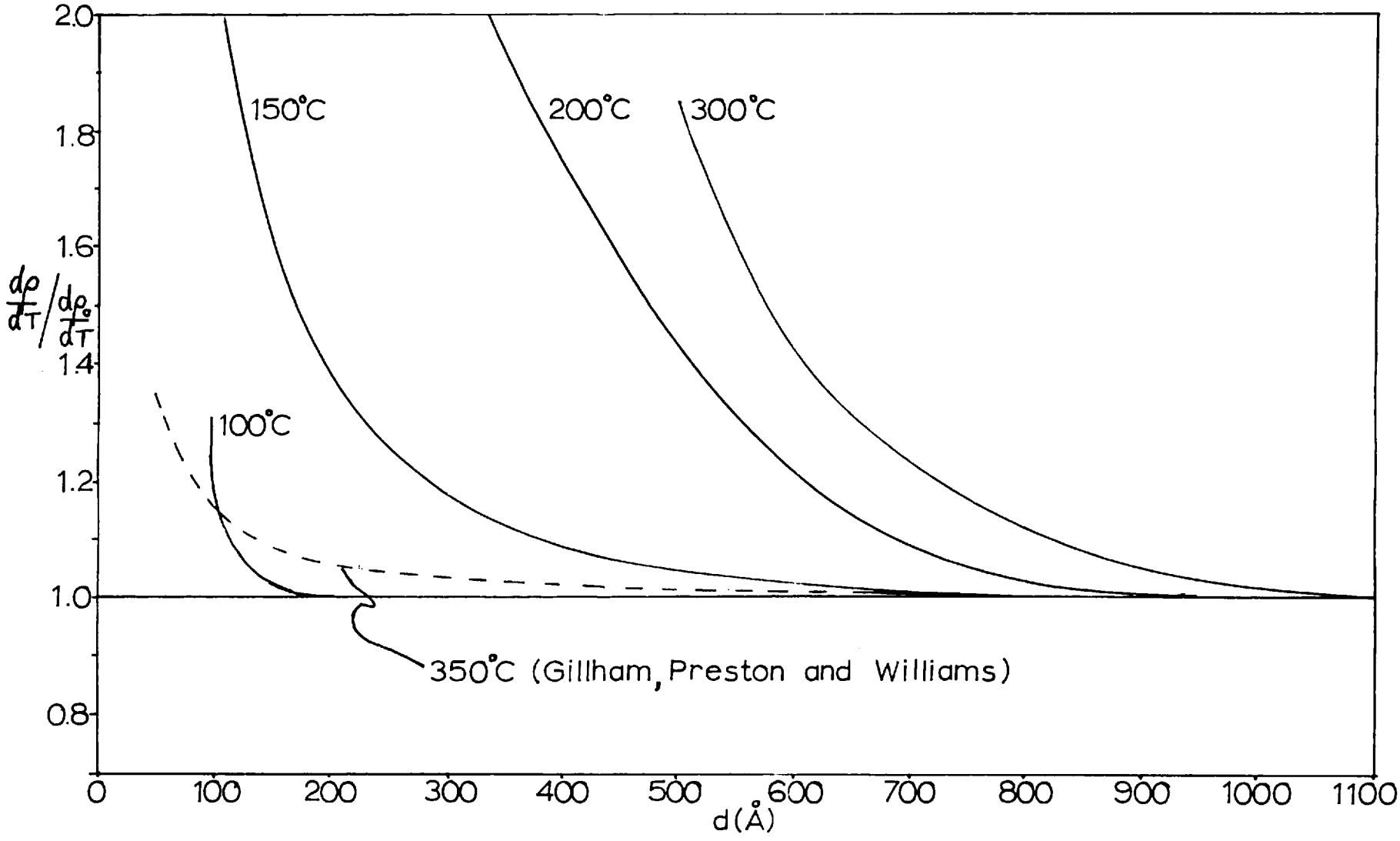

It is clear when this process is applied to the results in Fig. (5.6) that those at 300°C, 200°C and 150°C are anomalous since they would result in mean free paths of 1300A°, 1100A° and 950A° respectively. The mean free path in bulk gold is only 420A°. It is physically impossible to exceed this at room temperature since this would infer a large reduction in the lattice vibration component of resistivity.

The 100°C results yield a mean free path of 210A°. This figure is quite reasonable but it raises the possibility that the phonon spectrum of the gold film might have been modified since it corresponds to a doubling of the resistivity. The assumption that $\frac{d\rho_c}{dT}$ i.e. $\alpha_o\rho_c$ is constant might therefore not be true. Comparison shows that the $\alpha\rho$ value for the thickest film is within 10% of the bulk value. It is clear that some change has occurred. The values which are plotted have been normalised with respect to the film value since this deviation is not large.

The value of resistivity for the thickest film in the 100°C series is 5.5$\mu\Omega$-cm. The mean free path deduced from this is $\sim$160A° indicating that the figure of 210A° from the $\rho\alpha$ plot is too high. It must therefore be concluded that the experiments have failed in their original purpose. The results of Gillham, Preston and Williams who employed a similar technique are shown for comparison. These results seem to indicate a mean free path

of $800A^{o}$ which is also impossibly high.

One must now try to account for these results. Unfortunately there is no structural evidence to assist in this but it does seem likely that the films were not the plane laminae they were intended to be. Most probably the premature increases in ρ and α were due to increases of resistivity due to the film transforming into a chain structure on annealing. The curves of resistivity and T.C.R. for the $200^{o}C$ series show that α is almost constant with thickness but the resistivity has increased by a factor of ~ 5. This is certainly consistent with a meandering chain like structure. The family of curves of $\frac{\rho\alpha}{\rho_{o}\alpha_{o}}$ at the various annealing temperatures show that these deviations increase with temperature suggesting greater structural changes at the higher annealing temperatures.

There are two reasons why these changes may have occurred. In order to achieve electrical stability during measurements it was found necessary to anneal the $100^{o}C$ series for at least one hour at that temperature. Consequently, it was decided to use the same annealing time for each series of films. It is possible that this was too long particularly at the higher annealing temperatures. Also, the bismuth oxide underlayers were exposed to air before condensing the gold films. It has been suggested by March[91] that the presence of free bismuth is necessary to ensure good adhesion of gold. The reason for this is not clear but it may be

that the free bismuth forms a solid solution with the gold at the oxide gold interface and the bonding occurs between the bismuth atom and the oxygen atoms in the substrate. If the free bismuth bonds were "poisoned" with oxygen then solution with the gold would be eliminated and the adhesive effect would be lost. In retrospect it has been noted that Ennos[92] has stated that the best adhesion occurs when the bismuth oxide film is prepared in a good vacuum ($< 5 \times 10^{-5}$ torr.) and not exposed to air before coating with gold. The deviating in the results of Gillham, Preston and Williams is slight when one remembers that the results plotted were for films annealed at 350°C. Obviously much better adhesion was achieved.

If nothing else these experiments seem to substantiate the work of March and Ennos.

5.6 Conclusions

A theoretical expression has been derived for the temperature coefficient of resistance of a continuous film in which surface scattering occurs. Curves of this function for various values of p and K are provided. The function was later found to agree with that derived by Savornin[55] for the case p = 0. The experiments which were performed to demonstrate its validity experimentally failed because the films used were not laminar. However, the failure

of these experiments seems to confirm that free bismuth must be present in bismuth oxide films used as underlayers for gold films.

The theory of Neugebauer and Webb for conduction in discontinuous films has been refined. The description given here takes into account transport between island pairs other than ones formed by one charged and one neutral island. This has little effect on the predicted value of resistivity but differs markedly in the calculation of the T.C.R. It is difficult to claim agreement with experiment because of the difficulties associated with measuring island sizes and separations accurately, and the uncertainty as to the true interisland potential barrier shape. However, several films have been examined which agree more closely with this theory than that of Neugebauer and Webb.

The decrease of T.C.R. with increasing film thickness as reported by Campbell and Hendry has been confirmed in 80/20 nickel chromium films prepared at 2×10^{-5} torr. Further, on decreasing the film thickness below 100A$^{\circ}$ the films become discontinuous and the anomalously high T.C.R. fell and eventually became negative; thus describing a maximum in the T.C.R. versus thickness curve. Similar behaviour has been observed in 80/20 Ni-Cr films prepared at 7×10^{-7} torr. In this case the maximum occurred at a thickness of 150A$^{\circ}$ and its amplitude was + 250 p.p.m., half of that observed at 2×10^{-5} torr. No such behaviour was observed in nickel films

prepared under similar conditions.

The effect is thought to be due to the preferential oxidation of chromium at the film-substrate interface leaving the film nickel rich. Such a film would exhibit a T.C.R. greater than that of the original alloy. As the film becomes thicker the T.C.R. would revert to normal as the average composition tended to that of the original alloy. Analysis of the peak heights and positions suggests that the formation of only one molecular layer of Cr_2O_3 is required to produce the effect. It also indicates that the degree of oxidation is independent of the preparation pressure. For this reason it is suggested that water diffusing from the glass surface is responsible and could therefore be minimised by a stringent bake out of the substrate prior to the deposition of the film. The electron diffraction evidence suggests the presence of very small amounts of Cr_2O_3 and NiO. This model is consistent with previous structural studies of nickel chromium films and with the oxidation behaviour of bulk nickel chromium alloys.

It is worth noting that under certain conditions the T.C.R. of a discontinuous thin film might be increased positively by thermal expansion effects. In Appendix B it is shown that any increase due to this effect would only be about 50 p.p.m./^{o}C. It does not therefore afford a plausible explanation for the maxima observed.

Appendix A

The integration of the products of Fermi functions

It is necessary to evaluate functions of the form

$$I = \int_{-\infty}^{+\infty} f(E) \left[f(E-W-eV) - f(E-W+eV) \right] dE.$$

Referring energies to the Fermi level

$$I = \int_{o}^{\infty} \frac{1}{1+\exp\left(\frac{E-E_F}{KT}\right)} \left\{ \frac{1}{1+\exp\frac{(E-E_F-W-eV)}{KT}} - \frac{1}{1+\exp\frac{(E-E_F-W+eV)}{KT}} \right\} x \, dE$$

Let $\mu = \frac{E-E_F-W}{KT}$

$\therefore \frac{d\mu}{dE} = \frac{1}{KT}$

$$\therefore I = KT \int_{-\frac{E_F-W}{KT}}^{\infty} \frac{1}{1+\exp\left(\mu+\frac{W}{KT}\right)} \left\{ \frac{1}{1+\exp\left(\mu-\frac{eV}{KT}\right)} - \frac{1}{1+\exp\left(\mu+\frac{eV}{KT}\right)} \right\} d\mu$$

$$= I_1 - I_2.$$

Let $u = f\left(\mu+\frac{W}{KT}\right) f\left(\mu-\frac{eV}{KT}\right)$ and $v = \mu$

Integrating by parts

$$I_1 = KT\left[\mu f\left(\mu+\frac{W}{KT}\right) f\left(\mu-\frac{eV}{KT}\right)\right]_{-\frac{E_F-W}{KT}}^{\infty} - KT \int_{-\frac{E_F-W}{KT}}^{\infty} \mu \left[f\left(\mu+\frac{W}{KT}\right) f'\left(\mu-\frac{eV}{KT}\right) + f\left(\mu-\frac{eV}{KT}\right) f'\left(\mu+\frac{W}{KT}\right) \right] x \, d\mu.$$

Since $KT \ll E_F$ for a metal

$$f'(\mu) = \delta(\mu) \quad \text{(a delta function)}$$

and

$$I_1 = (E_F+W)\, f\left(\frac{-E_F}{KT}\right) f\left(\frac{-eV-W-E_F}{KT}\right) - \left[eVf\left(\frac{eV+W}{KT}\right) - Wf\left(\frac{-W-eV}{KT}\right)\right]$$

$\therefore$ I_2 is given by replacing $+eV$ by $-eV$.

$$I_2 = (E_F+W)\, f\left(\frac{-E_F}{KT}\right) f\left(\frac{+eV-W-E_F}{KT}\right) - \left[-eVf\left(\frac{-eV+W}{KT}\right) - Wf\left(\frac{-W+eV}{KT}\right)\right]$$

Since $eV \ll (E_F+W)$ the first terms are equal

$$\text{and } I_1-I_2 = -eV\left(\frac{2+\exp\frac{eV+W}{KT} + \exp\frac{-eV+W}{KT}}{1+\exp\frac{eV+W}{KT} + \exp\frac{-eV+W}{KT} + \exp\frac{2W}{KT}}\right)$$

$$+W\left(\frac{\exp\left(\frac{eV-W}{KT}\right) - \exp -\left(\frac{eV-W}{KT}\right)}{1+\exp^{-}\left(\frac{eV+W}{KT}\right) + \exp\frac{eV-W}{KT} + \exp\frac{-2W}{KT}}\right)$$

When $eV \ll W$

$$I_1-I_2 = -2eV\left(\frac{1+\exp {}^{W}/_{KT}}{1+2\exp\frac{W}{KT} + \exp\frac{2W}{KT}}\right)$$

For the integrals of the form

$$\int_{-\infty}^{+\infty} f(E)\, f(E-eV)\, dE = I_1(W=0) = I_3$$

Hence $I_3 - I_4 = -eV$

Also, I_5 and I_6 can be obtained from I_1 and I_2 by placing W equal to - W, giving

$$I_5 - I_6 = -2eV \frac{(1+\exp^{-W}/KT)}{(1+2\exp\frac{-W}{KT} + \exp\frac{-2W}{KT})}$$

The negative signs arise because the electron current is flowing in the direction of decreasing potential, these will be neglected.

Hence,

$$I_1 - I_2 = \frac{2eV}{1+\exp^{W}/KT}$$

$$I_3 - I_4 = eV$$

$$I_5 - I_6 = \frac{2eV}{1+\exp^{-W}/KT}$$

APPENDIX B

The effect of thermal expansion on the resistance of discontinuous films

Whilst the thermal expansion of a continuous metal film would cause a change in its resistance, the fractional change would only be of the order of the thermal coefficient of linear expansion of the film material, i.e. $\sim$ 10 p.p.m./^{o}C.

In discontinuous films the change in resistance might be expected to be greater since small changes in island separation can cause large changes of resistance, see equation 2.9, page 86. In order to calculate the change in island separation on heating, an assumption must be made about the extent to which the film expands independently of the substrate. Two cases will be considered here.

(i) Tight binding

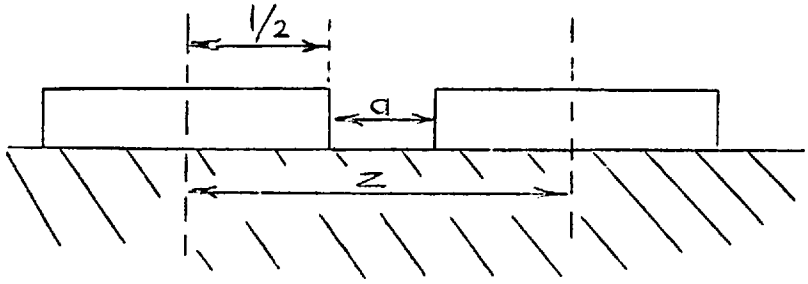

Fig. (B.1) The Expanding Islands.

In this example it will be assumed that the metal islands cannot move with respect to the substrate. Equation (2.9) can be generalised to an expression of the form

$$\rho = Aa \exp(Ba)$$

where a is the island separation and is a function of temperature T and A and B are constants.

Thus the T.C.R. due to thermal expansion is given by

$$\frac{1}{\rho} \cdot \frac{d\rho}{da} \cdot \frac{da}{dT}$$

Let this be termed α_t

$$\therefore \quad \alpha_t = \frac{(1+aB)}{a} \cdot \frac{da}{dT}$$

But $a = a'\left[1 + \beta_s (T - T') \right]$ where a' is the value of a at temperature T', say ambient, and β_s the thermal coefficient of linear expansion of the substrate (T.C.L.)

$$\therefore \quad \frac{da}{dT} = a' \beta_s$$

$$\therefore \quad \alpha_t = \frac{(1+a'B)}{a'} \cdot a' \beta_s$$

$$= \beta_s + a'.B.\beta_s$$

when $a' = 10A^{\circ}$ $a'B \sim 10$, see page 84

and $\beta_s \sim 6$ for glass

$$\alpha_t = + 66 \text{ p.p.m./}^{\circ}\text{C.}$$

It is clear that the effect on the resistance is proportional to the island separation and in typical cases α_t would be of the order of + 50 p.p.m./$^{\circ}$C.

(ii) No binding

In this example the film has complete freedom to move independently of the substrate. It will be assumed that each island is pinned at its centre so that its centre of gravity moves with the substrate.

Again

$$\alpha_t = \frac{(1+aB)}{a} \cdot \frac{da}{dT}$$

In this case the separation a is given by

$$a = z - l \quad , \quad \text{see Fig. (B.1)}$$

and $$\frac{da}{dT} = \frac{dz}{dT} - \frac{dl}{dT}$$

$$= z'\beta_s - l'\beta_f,$$

where β_f is the T.C.L. of the film.

$$\therefore \quad \alpha_t = \left(\frac{1+a'B}{a'}\right)\left(a'\beta_s + l'(\beta_s - \beta_f)\right)$$

$$= a'B\beta_s + \beta_s + \frac{l'}{a'}(\beta_s - \beta_f) + Bl'(\beta_s - \beta_f)$$

Let $l' = 200A^{\circ}$

$a' = 10A^{\circ}$

$\beta_s = 6$ p.p.m./$^{\circ}$C.

$\beta_f = 13$ p.p.m./$^{\circ}$C (for Ni)

then $\alpha_t \sim -1500$ p.p.m./$^{\circ}$C.

This value is dominated by the term $Bl'(\beta_s - \beta_f)$ so that α_t is largely governed by the island length l'.

The assumption of single pinning is unreal and l' should really be modified by a factor C, $0 \leqslant C \leqslant 1$, which depends on the extent to which the islands can expand freely. The choice of a value of C is extremely difficult but if C is taken as 0.1, α_t becomes $\sim$ - 100 p.p.m./^{o}C.

REFERENCES

1. A.C. Longden — Phys. Rev. 11, 40. (1900).
2. J.J. Thomson — Rapports presentes au Congres International de Physique (iii), 138, (1900), Paris.
3. J.J. Thomson — Proc. Camb. Phil. Soc. 11, 120, (1901).
4. Beilby — Proc. Roy. Soc. 72, 226, (1903).
5. R.W. Wood — Phil. Mag. 3, 396, (1902).
6. Maxwell-Garnett — Phil. Frans. 203 A, 385, (1904).
7. W.F.G. Swann — Phil. Mag. 28, 467, (1914).
8. R.W. Wood — Phil. Mag. 30, 300, (1915).
9. J. Frenkel — Zeit. fur Phys. 26, 117, (1924).
10. J.D. Cockcroft — Proc. Roy. Soc. A 119, 293, (1928).
11. J.P. Hirth, S.J. Hruska & G.M. Pound — Proc. Conf. on Single Crystal Films, Pennsylvania, (1963).
12. T.N. Rhodin & D. Walton — ibid.
13. A.C.B. Lovell — Proc. Roy. Soc. 157 A, 311, (1936).
14. A.C.B. Lovell & E.T.S. Appleyard — Proc. Roy. Soc. 158 A, 718, (1937).
15. K. Fuchs — Proc. Camb. Phil. Soc. 34, 100, (1938).
16. E.H. Sondheimer — Advances in Physics 1, 1, (1952).
17. M.S.P. Lucas — J. Appl. Phys. 36, 1632, (1965).
18. N. Mostevich & B. Vodar — Semiconducting materials - Butterworth, London, (1951).

REFERENCES (continued)

19. C.A. Neugebauer & M.B. Webb — J. Appl. Phys. 33, 74, (1962).

20. T.E. Hartman — J. Appl. Phys. 34, 943, (1963).

21. D.S. Herman & T.N. Rhodin — J. Appl. Phys. 37, 1594, (1966).

22. R.M. Hill — Nature No. 4953, P. 35. (1964).

23. E.J. Preston & J.S. Gillham — Proc. Phys. Soc. 65 B, 649, (1952).

24. L. Holland & G. Siddall — Vacuum 3, 375, (1953).

25. E.J. Gillham, J.S. Preston & B.E. Williams — Phil. Mag. 16, 1051,(1955).

26. J.A. Bennet — Electronic Components, September 1964, p.737.

27. D.M. Hoffmann & J. Riseman — Trans. 6th. Nat. Vac. Symp (1959).

28. K.B. Scow & R.E. Thun — Trans. 9th. Nat. Vac. Symp (1962).

29. R.M. Chapman — Vacuum 13, 213, (1963).

30. P.A. Gould — Brit. J. Appl. Phys. 16, 1481, (1965).

31. R.W. Berry & N. Schwartz — Proc. 4th. Nat. Conv. Military Electronics (1960)

32. C. Altman — Trans. 9th. Nat. Vac. Symp, 174, (1962).

REFERENCES (continued)

33. D. Gerstenberg & C.J. Calbick — J. Appl. Phys. 35, 402, (1964).

34. W. Himes, B.F. Stout & R.E. Thun. — Trans. 9th. Nat. Vac. Symp, (1962).

35. G. Siddall — A.E.I. Research Rept. No. 4890 (1951).

36. L. Holland — Vacuum 1, 23, (1951).

37. R.H. Alderson & F. Ashworth — Brit. J. Appl. Phys. 8, 205, (1957).

38. P. Huijer, W.T. Langendam & J.A. Lely — Philips Tech. Rev. 24, 144, (1962).

39. T.K. Lakshmanan — Trans. 8th. Nat. Vac. Symp, (1961).

40. G. Siddall & B.A. Probyn — Brit. J. Appl. Phys. 12, 668, (1961).

41. O. Kubachevski & B.E. Hopkins — Oxidation of Metals & Alloys (1953)

42. D.S. Campbell & B. Hendry — Brit. J. Appl. Phys. 16, 1719, (1965).

43. H. Blackburn, R.W. Bicknell, D.S. Campbell & D.J. Stirland — Microelectronics & Reliability, 3, 61, (1964).

44. R.W. Bicknell — Brit. J. Appl. Phys. 17, 775, (1966).

45. F. Bloch — Z. Physik 52, 555, (1928).

46. L. Brillouin — Wave Propagation in Periodic Structures (1946).

REFERENCES (continued)

47.	Matthiesen & Vogt	Ann. der Physik und Chem. 122, 19, (1864).
48.	A.H. Wilson	The Theory of Metals, (1953), Cambridge.
49.	A.N. Gerritsen	Handbuch der Physik XIX, (1956).
50.	C.A. Neugebauer	Trans. of 3rd. Int. Vac. Congress (1965).
51.	J.O. Linde	Ann der Physik, 15, 219, (1932).
52.	L. Nordheim	Ann der Physik, 9, 641, (1931).
53.	C.H. Johansen & J.O. Linde	Ann der Physik, 25, 331, (1936).
54.	J.G. Young & C.W. Lewis	Trans. 10th. Nat. Vac. Symp. (1963).
55.	T. Savornin	C.R. Acad. Sci. 248, 2458, (1959).
56.	D.S. Campbell	The Uses of Thin films in Physical Investigations ed. Professor J.C. Anderson, (1966), Academic Press.
57.	Mott & Sneddon	Wave mechanics and its applications (1948).
58.	R.M. Hill	Private communication (1966).
59.	J.G. Simmons	J. Appl. Phys. 34, 1793, (1963).
60.	J.C. Penley	Phys. Rev. 128, 596, (1962).
61.	F.W. Schmidlin	J. Appl. Phys. 37, 2823, (1966).
62.	M. Frohlich	Proc. Roy. Soc. A 188, 521, (1947).
63.	L. Goldstone	Rev. Sci. Inst. 35, 1265, (1964).
64.	L. Harris & B.M. Siegel	J. Appl. Phys. 19, 739, (1948).

REFERENCES (continued)

65. J.L. Richards, P.B. Hart & E.K. Muller — Single Crystal Films ed. M.H. rancombe and M. Sato (1964).

66. R. Turnell & D.S. Campbell — Private Communication (1965).

67. Corning Data Sheet — CEP 2/5M/9-62.

68. G. Hass — J. Amer. Ceram. Soc. 33, 353, (1950).

69. K.L. Chopra, L.C. Bobb & M.H. Francombe — J. Appl. Phys. 34, 1699, (1963).

70. N. Fuschillo et al. — J. Appl. Phys. 36, 575, (1965).

71. G. Siddall — Proc. Eur. Reg. Conf. on Elec. Microscopy, Delft, (1960).

72. B.I. Bertelsen — J. Appl. Phys. 33, 2026, (1962).

73. D.S. Campbell & H. Blackburn — Trans. 7th. Nat. Vac. Symp., 313, (1960).

74. N. Schwarz & R. Brown Trans. 8th. Nat. Vac. Symp., 836, (1961).

75. J.M. Watt — Private communication (1966).

76. J. Mayo — Private communication (1966).

77. J.M. Watt — B.S.I.R.A. Report No. R 322 (1964).

78. F.W. Schenkel — Electronics 38, 67, (1965).

79. T.E. Hartman, J.C. Blair & R. Bauer — J. Appl. Phys. 37, 2468, (1966).

REFERENCES (continued)

80. D.S. Campbell & B. Lewis — 13th. Nat. Vac. Symp., Contribution, TF4, (1966).

81. R.F. Adamsky & R.E. Le Blanc — Trans. 10th. Nat. Vac. Symp., 453, (1963).

82. H. Thomas — Zeit. fur Phys. 129, 219, (1951).

83. J. Jitaka & S. Miyake — Nature, 137, 457, (1936).

84. A.G. Quarrell — Nature, 145, 821, (1940).

85. B. Lustman — Iron Coal Tr. Rev., 154, 889, (1947).

86. K. Hauffe — Z. Metallk. 42, 34, (1951).

87. L. Holland, Chapman & Hall — The properties of glass surfaces (1964).

88. B. Johnson Todd — J. Appl. Phys, 26, 1238, (1955).

89. R. Glang, R.A. Holmwood & S. Clarke — 13th. Nat. Vac. Symp., Contribution 5-6 (1966).

90. R.W. Bicknell — Brit. J. Appl. Phys; 17, 775, (1966).

91. A.A.C. March — Ph.D. Dissertation, University of Cambridge, (1957).

92. A.E. Ennos — Brit. J. Appl. Phys, 8, 113, (1957).

93. H. Mayer — Structure & Properties of Thin Films, 225, (1959), Wiley.